Interactions of Polycyclic Aromatic Hydrocarbons with Mineral Surfaces

A thesis submitted to the University of Manchester for the degree of

Doctor of Philosophy

in the Faculty of Engineering and Physical Sciences

2011

Yazmina Bryant

School of Mechanical, Aerospace and Civil Engineering

Table of Contents

CHAPTER 3 Development and Optimization of a Method for the Extraction of Naphthalene in an Electrolyte Matrix

Appendices

Final word count: 48,143

Tables

Figures

Abbreviations

AFM	Atomic Force Microscopy
ATR	Attenuated Total (Internal) Reflection
BaP	Benzo[a]pyrene
BE	Binding Energy
BET	Brunauer, Emmett, and Teller
BET-SSA	Specific Surface Area after BET
BP	Boiling Point
BSA	Bovine Serum Albumin
BSI	British Standards Institute
CIS	Cool Injection System
DCDMS	Dichloro-dimethyl-siloxane
DCM	Dichloromethane
DECON 90	Surface active cleaning agent, and / or radioactive decontaminant for laboratory, medical and industrial applications (www.decon.co.uk)
DI	Direct Immersion
DIW	De-Ionised Water
DNA	Deoxyribonucleic Acid
DMDCS	Dimethyldichlorosilane
EDS	Energy Dispersive Spectra
EPA	Environmental Protection Agency
ESCA	Electron Analysis for Chemical Analysis
Fe-QS	Iron (Fe) coated Quartz Sand
FID	Flame Ionisation Detector

FTIR	Fourier Transform Infrared spectrometry
GAC	Granular Activated Carbon
GC	Gas Chromatography
GC-FID	Gas Chromatography Flame Ionisation Detector
GC-MS	Gas Chromatography-Mass Spectrometry
HCl	Hydrochloric acid
Hm	Hematite
HPLC	High Performance Liquid Chromatography
HS	Head Space
HS-SPME	Head Space Soild Phase Microextraction
ICP-AES	Inductively Coupled Plasma Atomic (optical) Emission Spectrometry
ICP-MS	Inductively Coupled Plasma Mass Spectrometry
IR	Infrared spectroscopy
LOI	Loss On Ignition
LLE	Liquid-Liquid Extraction
MCL	Maximum Contaminant Level
MP	Melting Point
MSSV	Micro Scale Sealed Vessel
MW	Molecular Weight
NMR	Nuclear Magnetic Resonance
OM	Organic Matter
OC%	Organic Carbon %
PAH	Polycyclic Aromatic Hydrocarbons
PSD	Particle Size Distribution
PDMS	Polydimethyl siloxane

pA*s	Plot of area versus time (minutes)
PHE	Phenanthrene
POP	Persistent Organic Pollutants
ppb	Parts per billion
PTFE	Polytetrafluoroethylene
PTV	Programmed Temperature Vaporisation
QS	Quartz Sand
Rpm	Revolutions per minute
RSD	Relative Standard Deviation
RSD%	Relative Standard Deviation percentage
SEM	Scan Electron Microscopy
STM	Scanning Tunneling Microscopy
SOM	Soil's Organic Matter
SPE	Solid-Phase Extraction
SPME	Solid Phase Microextraction
SSA	Specific Surface Area
STD CONC.	Standard Concentration
SUPELCO	Subsidiary company of the Sigma - Aldrich group of general chemical supplies (www.sigmaaldrich.com)
TOC	Total Organic Carbon
TOMPs	Toxic Organic Micropollutants network
UHV	Ultra High Vacuum
UNECE	United Nations Economic Commission for Europe
UV	Ultra Violet radiation
VSPME	SPME sample Volume

VWR	Distributor of chemicals and general laboratory supplies (www.vwr.com)
XPS	X-ray Photoelectron Spectroscopy
XRD	X-Ray Diffraction
XRF	X-Ray Fluorescence

Symbols

a_i	Solute's activity
A	Helmholtz energy (J)
c	Constant
C_0	Initial naphthalene concentration in the sample at the start of the reaction time (mg / ml) (t = 0)
C_s	Initial naphthalene concentration in the sample to be extracted (µg / ml)
C_{S24}	Naphthalene concentration in the sample at the end of the reaction time (t = 24) (mg / ml)
C_{min}	Concentration of naphthalene in the mineral phase after 24 hours (t = 24) (mg / ml)
f_{oc}	Organic carbon fraction
H	Enthalpy (kJ / mol)
K	Distribution constant
K_{fs}	Experimentally determined distribution constant between the fibre coating and the sample (dimensionless)
K_{hs}	Distribution constant between the headspace and the fibre coating (dimensionless, data available from literature)

K_{min}	Experimentally determined distribution constant between the mineral and the sample (dimensionless)
m_1	Combined weight of the tube and stopper
m_1	Mass of the empty crucible
m_2	Mass of the crucible plus the sample before heating
m_2	Weight of the tube, sample and stopper prior to degassing
m_3	Combined weight of the tube and sample plus stopper
m_3	Mass of the crucible plus sample after heating
M_S	Mass of sand (g)
M_S	Mass of sand retained on each sieve (g)
M_S%	Percentage of sand retained in each sieve
M_{TS}	Initial mass of sand (g)
n	Number of values in a data set
n	Mass of analyte extracted by the fibre coating whist immersed in the liquid phase (Direct Extraction)
n	Mass of naphthalene (µg) on the fibre at the end of the extraction
N_A	Avogadro's number (6.022 137 x 10^{23} molecules per mole)
n	Number of moles under specified T(K) and P(atm)
q	Charge
R	Gas constant

R^2	Quality of fit parameter (Residual value)
R%	Recovery percent
S	Slope
S	Entropy (J mol^{-1} K^{-1})
SSA_{BET}	Specific surface area (m^2 / g)
T	Temperature (K)
p_0	Gas saturation pressure (atm)
po	Nitrogen saturation pressure
p	Equilibrium pressure of a gas layer (atm)
P	Pressure
P^0_S	Partial pressure of the reference solid (solute)
P^0_L	Partial pressure of the solvent
v	Volume adsorbed at pressure p (cm^3)
V	Molecular volume
V_f	Volume of the fibre coating
V_f	Fibre volume corresponding to the polymeric PDMS coating where absorption takes place (ml)
V_h	Volume of the headspace (ml)
V_{hs}	Headspace volume

v_m	Volume of gas required to form a complete uni-molecular adsorbed layer
V_S	Sample volume (ml)
V_S	Sand volume (cm^3)
V_{STP}	Ideal gas volume at standard temperature and pressure
$\bar{x}$	Average value of a data set
x_i	Concentration of solute i
x_W	Fraction of the organic compound in the aqueous phase
Y_{INT}	Intercept
γi	Activity coefficient
γ_w	Activity coefficient of the sub cooled organic liquid at $P_L^0 = 1$ atm
γ_W	Activity coefficient
ΔG	Gibbs free energy of reaction
σ	Standard deviation
σ	Gas molecular cross sectional area (m^2)
$\sum$ LOI %	Total loss on ignition percentage
ρ_s	Specific gravity (g / cm^3)
μ_i	Chemical potential (kJ / mol) of a solute i at constant temperature T and pressure P

μ	Electric dipole moment
μ°	Standard chemical potential of the pure solute

Abstract

The toxicity and ubiquitousness of PAHs within different terrestrial environments has been an increasing cause for concern amongst environmental scientists in the last decades, in particular regarding their transport within the soil.

In an attempt to understand the role of pure inorganic phases in PAH-mobility; experiments exposing mineral soil components with low organic matter content to a PAH-representative were carried out. The systems consisted of four different mineral phases (quartz sand, hematite, iron coated quartz sand and montmorillonite) which were individually exposed to naphthalene in electrolyte solutions prepared at increasing ionic strengths ($NaNO_3$: 0.001 M; 0.01 M; 0.1 M) and pH (4.0 and 5.5). All experiments were conducted over at 24 reaction intervals and at ambient temperature conditions.

Mineral geosorbents are traditionally known to be poor PAH-scavengers; in particular when compared to organic, high surface area materials such as activated carbons. On this basis, a preliminary validation experiment (Proof of Concept Experiment) was conducted to test the sensitivity of the selected extraction method (SPME) under complete uptake (activated carbon) and very low uptake (quartz sand) conditions. By extracting and analysing the supernatant after 24 hr of exposure of both sorbents to naphthalene under identical conditions it was concluded that SPME was a feasible extraction technique, yielding good reproducibility (n=3, inter-day RSD%= 11.18%) even at very low PAH concentrations (0.2 µg / L).

The final concentration of naphthalene in the sample supernatant after 24 hours was determined by GC-FID. All samples were extracted using the Solid Phase Microextraction method developed during the Proof of Concept which allowed the rapid extraction of naphthalene in the headspace HS-SPME (extraction time = 3 minutes) using temperature control and ultrasonication as means of agitation. Each sample set included triplicates of blanks and samples as well as calibration standards (in duplicate where possible)

Out of the four minerals, only quartz sand and hematite showed a slight tendency towards naphthalene removal from solution; a finding which correlated well with increasing ionic strength. The other two minerals did not show any such trend and the results were deemed inconclusive.

In regards to the results for quartz and hematite; the detected uptake was found to be below the sensitivity of the current SPME extraction method according to the error analysis carried out by comparing the sample and blank means whilst accounting for error equal to 1σ. The overlapping of both means in the majority of the samples indicated that both averages were too close to be accurately resolved (due to very low naphthalene uptake). Modifications to the SPME method could improve the reproducibility and decrease the spread of the data; however, this measure would only guarantee higher statistical confidence (95 %) and not higher naphthalene uptake by these minerals. These observations lead to the conclusion that naphthalene was being salted out of solution rather than being removed by sorption; and under these experimental conditions it would not have been possible to detect any real PAH-mineral interaction.

In view of this outcome, a different approach was attempted in order to detect surface reactions between the minerals and naphthalene. A series of preliminary (qualitative) surface analysis (AFM, XPS and ATR-FTIR) on pre-loaded mineral specimens were carried out in air at ambient temperature conditions. No naphthalene was positively identified on the surfaces of the studied sorbents. Factors such as molecular size, sorbents characteristics (i.e. roughness, surface charge) and loading conditions impeded the detection of the target molecules. Innovative sample preparation protocols as well as controlled analytical conditions would need to be implemented and evaluated before this kind of analytical tool can be used.

The main outcome of this research work was the successful adaptation of SPME to the rapid extraction of naphthalene in electrolyte solutions at optimal and sub-optimal concentration levels; as the proof of concept preliminary experiment showed.

DECLARATION

No portion of the work referred to in this thesis has been submitted in support of an application for another degree or qualification of this or any other university or other institute of learning

COPYRIGHT STATEMENT

(i) Copyright in text of this thesis rests with the author. Copies (by any process) either in full, or of extracts, may be made **only** in accordance with instructions given by the author and lodged in the John Rylands University Library of Manchester. Details may be obtained from the Librarian. This page must form part of any such copies made. Further copies (by any process) of copies made in accordance with such instructions may not be made without the permission (in writing) of the author.

(ii) The ownership of any intellectual property rights which may be described in this thesis is vested in The University of Manchester, subject to any prior agreement to the contrary, and may not be made available for use by third parties without the written permission of the University, which will prescribe the terms and conditions of any agreement.

(iii) Further information of the conditions under which disclosures and exploitation may take place is available from the Head of School of Mechanical, Aerospace and Civil Engineering.

Acknowledgments

The School of Engineering for kindly providing the Simon Scholarship, especially Ms Beverly Knight and Michelle Ringwood,

The School of Earth Sciences for providing me with office and laboratory space, and financial support during the last stages of my PhD,

My previous supervisor Dr C Merrifield for his enthusiastic support at the beginning of my PhD and for steering me in the right direction,

My supervisor Dr William Craig for always making sure I kept on track,

My supervisor Dr R Wogelius, to whom I am forever indebted for always believing in me and supporting me. For being a great friend and Jefe,

My supervisor Dr Andrew Gize for his invaluable and dedicated training on Gas Chromatography and Organic Chemistry and for introducing me to the use of SPME,

Dr Bart van Dongen for his laboratory support and for being a great (if unusual) sounding board and for helping me de-stress with his insane remarks,

Paul Lythgow, Alastair (Trooper) Bewsher, and Dr John Waters at the Geochemistry Laboratory for all the help, support, friendship and kindness,

My colleagues, for being so tolerant and sweet to me, especially my friends Sharon, Natalie, Said, Ibrahim and Assos, for all his help

My dearest friends Gillian and John for making commuting easier for me by letting me crash at theirs during my experimental phase, thank you!!!

My Roca family, my late foster mother Mercedes (Mamin) and my brother Oscar (Manito) for giving me the best education they could afford along with a legacy of hard and honest work ,

My late mother Angela for bringing me into this world in spite of the circumstances,

My chemistry school teacher, Sister Rosa Ochoa, who inspired me to become a chemist and Prof. Eugenio Marcano for introducing me to environmental sciences

Dr Paul Bryant for his unconditional love, devotion and patience throughout all these years,

All my true friends from home, UK and all over the world, who are too many to mention here, your encouragement and support made these 7 years of my life bearable, gracias, thank you, danke!

DEDICATION

This thesis is dedicated to my little daughter Lúthien Morgana, whose smiles and love helped me keep my sanity in the last 4 and half years; I love you more than words can say Titita; esto es para ti. X

Mina

CHAPTER 1 Introduction

1.1 Polycyclic Aromatic Hydrocarbons in the Environment

The transport and fate of organic contaminants entering the soil has been the subject of intense research in the last 30 years. Amongst these pollutants, a group called Polycyclic Aromatic Hydrocarbons (PAH) has drawn considerable attention from researchers around the world due to their spread in the environment and their toxicity. Analysis of lake sediments and soil samples dating back to the industrial revolution demonstrate a link between anthropogenic activities and PAH presence in the environment (Cousins *et al.*, 1997; Wilcke, 2007).

PAH are a chemical class spanning hundreds of substituted and un-substituted organic compounds consisting of multiple aromatic rings fused together to form hydrophobic, non-polar molecules in different configurations. These hydrocarbons are also called ‘polyarenes’, ‘benzenoid’ and ‘polynuclear aromatic hydrocarbons’ in reference to the presence of several ‘benzene nuclei’ throughout the series, although these fused molecular structures often include substituting groups other than benzene. The term ‘aromatic’ has been used for a long time to designate the intense odour of some of these compounds present in organic resins and oils. However, since PAH do not comply with Huckel’s aromaticity rule (Schmid, 1995) they are not strictly aromatic in the chemical sense, but are nevertheless considered to belong to this category because of the similarities between their physicochemical properties and those of benzene.

The amount of research work studying the toxicology and health hazards of PAH on humans and animals is vast, and given how widespread these

chemicals are in all compartments of the natural environment, the study of their transport and fate is of significant importance.

PAH are chemically stable, highly resistant to degradation and can remain active in the environment for long periods of time. Even in cases where microbial degradation (in the soil) or photolytic decomposition (in the atmosphere) is possible, the resulting metabolites are not always harmless or any less hazardous. On the contrary, some PAH-derivatives have been found to be even more toxic or mobile than their parent compounds (Kiely, 1997; Moon *et al.*, 2003).

1.2 Sources of PAH

These ubiquitous pollutants are commonly found in air, water bodies, groundwater and soil which in turn makes monitoring their transport and fate a huge scientific challenge. By far the largest input of PAH originates from atmospheric emissions as a product of the incomplete combustion of fossil fuels and organic materials. PAH can be present in nature arising from volcanic eruptions, forest fires, long term geological processes (organic matter degradation during diagenesis), and biological conversion of biogenic precursors (Gerstl *et al.*, 1989). Anthropogenic sources include: wood burning in fire places, vehicle exhausts, industrial emissions, grilling, refuse incineration and cigarette smoke. Other sources which introduce PAH into the environment include: urban (asphalt) runoff (Grynkiewicz *et al.*, 2002), industrial effluents, precipitation (rain and snow), contaminated soil and waste disposal sites, diffuse and localized emissions from metallurgical processes, petroleum refineries (pyrolysis), chemical industries, power plants and vehicle exhaust

(Carlsen *et al.*, 1997). Man-made release of PAH largely exceeds the natural input and PAH levels are higher with proximity to urban and heavily populated areas particularly during the winter months, probably due to the increased use of carbon-based fuel for residential heating purposes (Prevedouros *et al.*, 2004).

In the UK the main source for PAH has been found to be particulate matter originating in road traffic exhaust although this fluctuated between seasons and depending on closeness to urban areas (Halsall *et al.*, 1994; Harrison *et al.*, 1996). Soil has been found to be the major sink for accumulated PAH in the UK. A preliminary study in the UK found that excluding contaminated sites, more than 53 thousand tonnes of PAH (expressed as the sum of 12 individual compounds) are present in the environment, predominantly within the soil (Wild and Jones, 1995). This represents great cause for concern since the lighter PAH which had been deposited or assimilated into the soil may re-evaporate during the summer months, therefore increasing the net atmospheric concentration and possibly facilitating their transport and availability.

1.3 PAH Toxicity and Health Effects

The main concern associated with PAH is their capacity to react with environmentally available chemicals and as a consequence, the products of such reactions being inherently toxic to animals, plants and humans even at very low levels (Walgraeve *et al.*, 2010).

PAH were the first organic chemicals found to cause cancer in humans and animals (Cook and Martin, 1940). PAH can enter bacteria, mammals and marine organisms, following pathways that end up in humans through the food

chain (Gerstl *et al.*, 1989; Patrolecco *et al.*, 2010). PAH have also been detected in raw as well as grilled foods from leafy plants and barbecued meats (Harvey, 1996) . Exposure to indoor smoking has been associated with cancer occurrence in humans (International Agency for Research on Cancer, 1983).

Exposure to PAH can take place either at high concentrations such as those experienced by workers in industrial scenarios or at lower levels as a more persistent form of environmental exposure. It is important to note that unlike laboratory test subjects, humans are never exposed to single PAH but to a mixture of them, and given the different properties of these chemicals, the composition of such mixtures varies with time due to changing environmental conditions. Because of this complex behaviour, some PAH such as Benzo[a]pyrene, have been selected as markers or indicators of broader PAH pollution (Rugen *et al.*, 1989; Collins *et al.*, 1991). Benzo[a]pyrene or BaP was the first PAH found to cause cancer, reproductive disorders and mutation in animals and in humans (International Agency for Research on Cancer, 1983). Its link with the causation of cancer has been monitored in the UK since the 1960s, particularly in heavily polluted working environments such as industrial chimneys, power plants, tar and coke gas factories where workers were systematically exposed to very toxic fumes. Air concentrations of BaP measured in London (1960) over a period of several years in 24-hour composite samples ranged from 4 to 46 $ng.m^{-3}$ (Hammond *et al.*, 1976; Lawther and Waller, 1978; Harvey, 1991; World Wildlife Fund, 1997).

In addition to BaP, many polycyclic aromatic hydrocarbons can undergo metabolic activation and thus become carcinogenic or promote the formation of tumours in healthy tissue (Yang and Silverman, 1988). Furthermore, some PAH

have been found to affect the development of foetuses and to cause birth defects (teratogenicity) whilst others are known to be mild skin irritants as well as cause mutations in animals (Gad and Gad, 2005) as well as phototoxcicity in specific bacterial strains (El-Alawi *et al.*, 2002; White and Claxton, 2004). Exposure to mixtures of at least 8 of the heavier PAH have been found to cause tumours in laboratory animals after exposure via ingestion, inhalation and skin contact as well as cancer in humans after long term inhalation and skin exposure (Agency for Toxic Substances and Disease Registry, 1995a).

A study in the 1970s established that on average humans accumulate 2 g of particulate matter in their lungs over a lifetime (Lewis and Coughlin, 1973). Inhalation of PAH-laden particles would seem to correlate with human carcinomas originating, amongst other body areas, in the bronchial epithelium lining of the lungs (Karahalil *et al.*, 1999). Despite these conclusions, links between PAH-exposure and the risks to humans are still very difficult to establish due to factors such as lack of records on historical long-term exposure and the use of tobacco products by the affected subjects. Nevertheless, it has been established that the atmospheric fraction presenting the highest carcinogenic potency is that containing PAH with more than 3 aromatic rings (Grimmer *et al.*, 1982). What makes PAH carcinogenic are their reactions inside target organs in the human body which turn them into different chemicals from the parent molecules and as such, capable of damaging cellular DNA. These conversion reactions are often initiated by the presence of enzymes in the affected areas.

Judging by the higher incidence of lung cancer on workers exposed to high concentrations of PAH mixtures in industrial environments (gas and coke

production) (Vu *et al.*, 2011)it could be inferred that even at low doses, particle-bound PAH are irreversibly absorbed and activated in lung tissue after repeated exposure to polluted air, and can lead to the formation of tumours (Armstrong and Gibbs, 2009). A similar outcome has been observed in animals exposed to very high single particle-bound PAH doses (Gerde *et al.*, 1991).

The lack of consistent long term data, however, and the fact that the same groups of PAH have not been monitored in standard exposure scenarios makes accurate predictions of PAH impact on humans and animals very difficult to achieve.

1.3.1 Environmental Legislation Controlling PAH

In the USA, PAH have been included in the list of the 126 EPA Priority Pollutants under the Clean Water Act (Section 307(a)(1)) (Ding *et al.*, 2005). Furthermore, up to 16 PAH are regarded as Persistent Organic Pollutants (POP) in the UNECE (United Nations Economic Commission for Europe) Protocol (UK Environment Agency, 2005). These 16 have been monitored and investigated over the past three decades in a large number of studies (Bojes and Pope, 2007; Li *et al.*, 2010). Since they are likely to be found together in the natural environment, these 16 PAH are used as indicators of broader volatile and semivolatile organic compounds pollution.

Within the European Union, PAH are regulated under the following directives: the Air Quality Framework directive (96/62/EC), the EC directive 76/464 (Pollution of the Aquatic Environment by Dangerous Substances), the Drinking Water directive 80/778/EEC. Additionally, PAH have been included in the Priority Hazardous Substances List under the Water Framework directive

and in the newest Groundwater directive (2006/118/EC), as category 4, which comprises “substances which possess carcinogenic, mutagenic or teratogenic properties in or via the aquatic environment”.

In the UK, the legislation implementing the EC directives regarding the control of PAH discharges into water bodies consists of the Surface Water Regulation and the Pollution Prevention and Control Regulations. In air, PAH are monitored under the Toxic Organic Micropollutants Network (TOMPs) in compliance with the European Water Framework directive (2000/60/EC). The Expert Panel on Air Quality Standards has designated Benzo(a)pyrene (BaP) as the marker for the presence of PAH in the UK (Expert Panel on Air Quality Standards, 1999). An annual average air concentration of 0.25 ng. m^{-3} has been recommended as the maximum for BaP in the UK whereas in the rest of Europe, a value of 1 ng. m^{-3} has been the target set by the EC under the Air Quality Daughter directive (2005/107/EC) (Meijer *et al.*, 2008).

1.4 Behaviour of Organic Molecules in Solution

This section aims to present an overview of the main physico-chemical processes involved in the dissolution and behaviour of organic molecules within the solution bulk.

1.4.1 Thermodynamics of Organic Molecules in Aqueous Environments

1.4.1.1 Chemical Potential

The driving force behind chemical reactions is the Gibbs free energy of reaction, ΔG (Stumm and Morgan, 1996). When the composition of a system varies at constant pressure and temperature, so does the system’s total energy

(Gibbs energy). The Gibbs energy increases with each mole added to the system; this increment is known as the chemical potential μ_i (kJ / mol) of a solute *i* at constant temperature T and pressure P. The chemical potential is related to the themodynamic functions of state as follows:

$$\mu_i \equiv \left[\frac{\partial G(kJ)}{\partial n_i(mol)}\right]_{T,P,n_{j\neq i}} = \left.\frac{\partial A}{\partial n_i}\right|_{P,T} + \left.\frac{P\partial V}{\partial n_i}\right|_{P,T} = \left.\frac{\partial H}{\partial n_i}\right|_{P,T} - \left.\frac{T\partial S}{\partial n_i}\right|_{P,T} \qquad (1.1)$$

$$dG = dH - TdS = dA + PdV = \Sigma n_i \mu_i \qquad (1.2)$$

$$dH = TdS + \Sigma n_i \mu_i \qquad (1.3)$$

$$dA = \Sigma n_i \mu_i - PdV \qquad (1.4)$$

The summation symbol in Equation (1.2) accounts for all the components of the system. Equation (1.1) $\partial G/n_i$ represents the rate of change in Gibbs free energy and n_i is the number of moles under specified T(K) and P(atm). The state functions included as partial derivatives on the right hand side of Equation. (1.1) are *A*, the Helmholtz energy (J); H (kJ mol^{-1}), the enthalpy; S (J mol^{-1} K^{-1}), the entropy and the variable *V* (m^3 mol^{-1}) as the molecular volume. For definitions, derivation and formulae of the state functions above please refer to the relevant bibliography (Pitzer, 1995; Stumm and Morgan, 1996; Klotz and Rosenberg, 2000).

1.4.1.2 Activity and Solubility

The activity of solute *i* in a solution is expressed in terms of the chemical potential as:

$$\mu_i = \mu^{o} + RT \ln a_i \qquad (1.5)$$

where μ^{o} represents the standard chemical potential of the pure solute and *R* the gas constant. The solute's activity a_i is related to the activity coefficient (γ_I) and concentration (x_i) of solute i. The chemical potential can be re-defined as a function of the solute molar fraction and the activity coefficient as follows:

$$\mu_i = \mu^{o} + RT \ln \gamma_i x_i \qquad (1.6)$$

The term solubility has been defined as (Schwarzenbach *et al.*, 1993) "*the abundance of the solute per unit volume in the aqueous phase when the solution is in equilibrium with the pure chemical in its actual aggregation state (gas, liquid, solid) at specified temperature and pressure*". The aqueous solubility of organic compounds determines their mobility and environmental impact within the subsoil. It can be explained in terms of the Gibb's free energy of the solute-solvent system. The molar free energy of dissolution for liquid organic compounds in water is expressed as:

$$\Delta G_S = RT \ln x_W + RT \ln \gamma_W \qquad (1.7)$$

where x_W is the fraction of the organic compound in the aqueous phase and γ_W is the activity coefficient. The last term represents the excess molar free energy resulting from solute-solvent molecular differences (such as polarity). The more "active" an organic compound is in aqueous solution, the less water-soluble it will be.

For organic *solids* dissolving in water, the corresponding equation representing the dissolution process is shown below (Schwarzenbach *et al.*, 1993; Atkins and De Paula, 2004):

$$\Delta G_s = RT\left(\ln x_w + \ln \gamma_w - \ln \frac{P_s^0}{P_L^0}\right) \quad (1.8)$$

where P^0_S is the partial pressure of the reference solid (solute) and P^0_L that of the solvent. The ratio of partial pressures accounts for the energy expenditure necessary to convert the solid into a sub cooled liquid reference state (below the solid's melting point) under ideal conditions. At equilibrium (*i.e.* $\Delta G_S = 0$) Eq (1.8) becomes:

$$x_w = \gamma_w^{-1} \cdot \frac{1}{P_L^0} \quad (1.9)$$

where γ_w is the activity coefficient of the sub cooled organic liquid at $P_L^0 = 1$ atm.

Non-polar compounds such as PAH dissolving in polar solvents such as water have positive transfer Gibbs energies and are exothermic ($H < 0$). This in turn reduces the entropy of the system ($S << 0$). Such processes require activation energy to start (*e.g.* heating or stirring to aid the dissolution of solid organics in water), but since each solute molecule is closely surrounded by the solvent, strong solute-solvent interactions are not possible. This situation describes what is known as *hydrophobicity* (Atkins and De Paula, 2004).

In the case of organic liquids, temperatures within the ambient range (0 – 35 ºC) have little effect on the compound's solubility (Schwarzenbach *et al.*, 1993). Inorganic species as co-solutes decrease the solubility of certain organics in water. This particular effect is known as "salting out" and it arises from the competition between cations such as Na^+ and Ca^{+2} and the organic molecules for niches within the water bulk (Schwarzenbach *et al.*, 1993).

1.4.1.3 Dipole Effect and Polarity

A dipole is formed by two electrical charges q^+ and q^- separated by a distance x. The vector going from q^- to q^+ is called the electric dipole moment, μ. Polar molecules have permanent dipole moments produced (amongst other factors such as chain length) by electronegativity gradients of different atoms in some molecules (i.e. HCl) in a molecular bond. Non-polar molecules on the other hand, *acquire* induced dipole moments (μ^*) as a result of disturbances generated when an electric field is applied. The induced dipole is proportional to the strength of the field and vanishes when the field is removed (Atkins and De Paula, 2004).

1.4.1.4 Resonance and Aromaticity

A molecule is resonant when it can be represented by more than one equally equivalent hybrid structure. The first organic compound known to exhibit this property was benzene. Its Kekulé structures show delocalized π electrons spread over 6 equidistant carbon atoms within a ring. The C-C bond lengths range between single and double carbon bonds; however, having resonant structures does not guarantee aromaticity.

The concept of aromaticity was first coined for benzene derivatives exhibiting a pleasant aroma; nowadays a vast number of compounds classed as aromatics are not at all pleasant to the sense of smell. The properties that make an organic compound comply with the principle of aromaticity are summarized below:

- The compound must be a cyclic hydrocarbon

- Each carbon atom in the ring must have a *p* atomic orbital
- The molecule must be planar or sp^2 hybridization

(Schmid, 1995) to allow overlap of *p* orbitals in neighbouring atoms

- It must comply with Hückel's rule of aromaticity: the number of π-electrons in *p* orbitals should sum $4n+2$; where *n* is any integer (0, 1, 2…) corresponding to the energy level (Schmid, 1995)
- All the π-electrons must fill only bonding molecular orbitals.

The last requisite follows from Hund's rule: "when orbitals of identical energy are available, electrons first occupy these singly" (Schmid, 1995).

Polycyclic aromatic compounds are resilient and very stable molecules due to the presence of delocalised π-electrons in their benzenoic components. In spite of not being strictly aromatic, they nevertheless undergo the same substitutions as benzene and present similarly large resonance energies. Additionally, the ring-hydrogens are detected in the aromatic region of NMR spectra, which in itself is irrefutable proof of aromaticity.

1.5 Behaviour of PAH within Soil

Airborne PAH are problematic given their extreme mobility due to factors such as volatility in the case of those with lower molecular weight and, in the case of heavier PAH, to the presence of solid particles (soot, dust) to which they can become attached and travel vast distances. These PAH-laden particles ultimately reach the soil in the form of precipitation or even dry deposition and once on the ground, rain run -- off and percolation will bring these contaminants

into contact with vulnerable groundwater domains (Krauss and Wilcke, 2002; Maisto *et al.*, 2006; Martuzevicius *et al.*, 2011; Schwarz *et al.*, 2011). The main problem associated with this scenario is that it could be years before any remediation scheme can successfully decontaminate the potentially affected sites. Additionally, many organic pollutants in subsoil systems move at a very slow rate through natural aquifers, and as they move through different geological strata, their transport can be retarded or accelerated depending on several factors, especially the compound's solubility (Charbeneau, 2000). Solubility, and hence polarity, is a crucial factor in the transport of organic molecules such as PAH within the soil. Organic compounds with very low solubility, or effectively insoluble, form part of a group of chemicals regarded with concern by various environmental regulative bodies (Gerstl *et al.*, 1989). The chemical composition of the soil, in particular in the absence of organic matter, plays a key role in the fate of persistent organic pollutants as is the case in several pollution scenarios where the contamination extends beyond the topsoil layers and into the deeper aquifer region (Trapido, 1999; Krauss *et al.*, 2000).

As for most other toxic organic chemicals, PAH mobility within the soil increases their potential hazards (Moon *et al.*, 2003), which is why the study of their transport within porous media has attracted so much attention over the last three decades. PAH sequestration and uptake by soil components controls their movement and this is intrinsically related to the properties of the different subsurface materials.

1.5.1 Previous Work Regarding the Role of Minerals in PAH Transport and Fate

Sorption and desorption of PAH onto soil and sediment particles is undoubtedly the most important factor affecting their subsurface mobility and fate (Schwarzenbach *et al.*, 1993; Carlsen *et al.*, 1997). The degree of sorbate-sorbent interaction is highly dependant on the sorbent characteristics. Within this context, sorbents can be broadly classified into soil materials containing a significant amount of organic carbon (i.e. high organic carbon fraction f_{oc}), and pure inorganic minerals with very low f_{oc} or no organic phases present (f_{oc} has values between 0 and 1). However, no discernible relationship between the total contents for heavier molecular weight PAH and the soil's organic matter or SOM was found by a group studying PAH distribution in UK soil; however, the lighter PAH and SOM were weakly correlated (Heywood *et al.*, 2006).

Organic carbon was shown to be largely responsible for sorption in contaminant transport experiments using sorbents with high organic carbon fraction. Factors contributing to a lesser extent were temperature, pH, ionic strength and organic co-solvents (Karickhoff *et al.*, 1979; Carlsen *et al.*, 1997; Huang and Weber W.J, 1998; Arnarson and Keil, 2000; Kim and Corapcioglu, 2002; Moon *et al.*, 2003). In a number of cases, sorption models developed on the basis on these findings presented inconsistencies such as non-linear equilibrium isotherms (Appert-Collin *et al.*, 1999; Carmo *et al.*, 2000) and irreversible sorption (Kan *et al.*, 1998). These anomalies were partly attributed to differences in the type of organic matter (OM), whose structure was further sub-classified into "glassy" (rigid) or "rubbery" (soft) (Luthy *et al.*, 1997; Middleton, 2003). This led to necessary modifications of partition models in

order to account for the multiple sorption mechanisms believed to be taking place within the system (Middleton, 2003). Given the structural complexity of the different organic matter moieties, their interaction mechanisms with PAH are still under investigation (Huang and Weber, 1997; Zhu *et al.*, 2004c).

In the case of materials with low organic carbon content (i.e. pure mineral surfaces), previously proposed partition mechanisms tended to underestimate the measured sorption coefficients (Hassett *et al.*, 1980 ; Huang and Weber W.J, 1998). It was suggested therefore that in such cases the mineral phase significantly contributed to the uptake observed because the f_{OC} was too small to account for the sorption observed. f_{oc} values reported by several researchers for low organic carbon materials range between 0.0004 and 0.00005 and are shown in Table 1.1.

The sorption of PAH on inorganic materials appears to fall into two main categories. For porous or expandable sorbents (e.g. some clays and silica gels)

Researchers	Material Source	f_{oc}
Lion et al., 1990[a]	Graded filtered sand, Columbus AFB	0.000086, 0.00036
Piatt et al.,1996[a]	Aquifer material, Bemidji, MN	0.00019
Abdul and Gibson, 1986[a]	Aquifer material,Canada	0.0002
Middleton, 2003[a]	Lower greensand, Bedfordshire, UK	0.00025, 0.000362
Schwarzenbach and Westfall, 1981[b]	Porous silica SiO_2	<0.0001
De Bryant, 2005[c]	VWR Sea sand, acid washed, calcined	0.00005

a: Middleton, 2003. Unpublished data

b: Env. Sci. & Technol. 15, (11). 1981

c: Unpublished data, 2005.

Table 1.1 f_{oc} values reported in sorption studies using low organic carbon materials.

the dominant mechanism seems to be intraparticle pores sequestration (Pignatello and Xing, 1996; Sun *et al.*, 2003). On the other hand, if the material has low porosity (e.g. α-Al_2O_3, coarse quartz sand) the interaction seems to

take place mainly within the near-surface domain, between the solution bulk and the mineral surface itself (Mader *et al.*, 1997). This approach relates to the sorbate's activity or tendency to escape the water bulk and associate with the mineral surface (hydrophobic behavior). As a result, higher activity coefficients lead to increased binding onto the surface of the mineral phase (Schwarzenbach *et al.*, 1993; Hundal *et al.*, 2001).

One research group concluded that water plays a complex role in the distribution of organic chemicals between the solution bulk and the mineral surface (Al-Abadleh and Grassian, 2003). Being a polar solvent, water is favoured above non-polar organics when competing for sorptive sites on the mineral surface. Strong interactions between water and surface hydroxyl ions re-arrange the surrounding solvent molecules differently to those in solution. This series of ordered water layers known as "vicinal water" (Drost-Hansen, 1969; Shibasaki and Fukuda, 1992; Staszczuk, 1995) extend several nanometres away from the solid and represent a more favourable sorption domain for the PAH. The thermodynamic reason is the lower energy expenditure required to accommodate sorbate molecules within the vicinal water layers (lower entropy) as compared to that in the solution bulk (higher entropy) (Schwarzenbach *et al.*, 1993; Mader *et al.*, 1997; Zhu *et al.*, 2004b).

Furthermore, Schwarzenbach and collaborators observed a direct correlation between vicinal water volume per mass unit of sorbent and a material's intraparticle porosity and surface area (Schwarzenbach *et al.*, 1993). They concluded PAH-mineral interaction may occur by means of exchange with near-surface water at very low f_{oc}, with varying results for different sorbates and sorbents (Mader *et al.*, 1997).

In the case of sorbents with surface charge or high surface area, it would be expected that these properties govern the contaminant behaviour; however, results from several researchers confirm this is not the case.

A different research group (Hundal *et al.*, 2001) reported high and linear sorption for phenanthrene (PHE) by a series of reference clays (smectites). The vicinal water approach did not explain their results, nor did they find any correlation between the low surface charge and sorption coefficient. It was concluded the sorption observed occurred due to condensation inside internal pores; a physical phenomenon. Interlayer cations influenced the formation of relatively hydrophobic sites (surface siloxane groups) and these favoured phenanthrene sorption.

Other work (Mader *et al.*, 1997) showed reversible, linear PHE sorption isotherms using pure aluminium and iron oxides and PHE concentrations up to 50% of the PAH's solubility. The nature of the mineral phase seemed to be the dominant factor in the sorption observed. Phenanthrene appeared to interact weakly and non-specifically with such sorbents.

Physisorption within internal pores has been supported by several workers as a PAH sorptive mechanism. Sorbate molecular size and sorbent tortuosity have been associated with slow PAH uptake and desorption by porous minerals such as amorphous silica (Huang *et al.*, 1996b).

Spectroscopic analysis has recently confirmed the existence of strong molecular interactions between mineral surfaces and PAH (Wang *et al.*, 2001; Zhu *et al.*, 2003; Zhu *et al.*, 2004a; Zhu *et al.*, 2004b; Zhu *et al.*, 2004c). Zhu and co-workers developed a novel approach based on nuclear magnetic resonance spectroscopy (NMR) to study sorption of polyarenes from aqueous

solutions onto silica gel and pre-saturated clays at the molecular level. Their results show strong solute-sorbent interactions between cations in the clays and π-electrons in the aromatic molecules. They concluded this was the main mechanism involved in the sorption observed, with intraparticle diffusion contributing only to a lesser extent in the PAH molecular arrangement. Their findings represent unequivocal evidence of the significant role minerals play in the subsurface mobility of PAH (Zhu *et al.*, 2003; 2004a) .

Given the different types of materials used in these studies, the literature appears to be riddled with contradictory results. The role of the different mineral surfaces remains poorly understood (Luthy *et al.*, 1997).

This thesis is the result of a multidisciplinary collaboration project between the School of Mechanical, Aerospace and Civil Engineering and the School of Earth, Atmospheric and Environmental Sciences. The findings obtained from the present study will be used in the modelling of the transport of these pollutants within natural groundwater environments when predicting their fate within aquifers.

1.6 Preparation for Analysis of PAH in Environmental Aqueous Samples

The study and analysis of PAH in environmental aqueous samples is difficult and expensive. The low aqueous solubility of PAH is a hurdle difficult to overcome when working at trace levels (sub microgram per litre). Samples are susceptible to losses to glassware and cross-contamination especially when traditional extraction approaches such as Liquid - Liquid Extraction (LLE) and

Solid-Phase Extraction (SPE) are used. These techniques are very time consuming and require large amounts of toxic organic solvents as well as tedious cleanup procedures (Handley, 1998).

1.6.1 Solid Phase Microextraction (SPME)

Separating the analytes of interest (i.e. pollutants) from the aqueous sample matrix normally requires the transfer of low polarity solutes from the aqueous phase into an organic solvent phase. The traditional methods used in organic extractions from aqueous phases are mainly liquid-liquid extraction (LLE) and solid phase extraction (SPE). These techniques present a common disadvantage: they are tedious, lengthy processes which required the use of vast a mounts of organic solvents, whose toxicity places them in several lists of environmental concern. SPME on the other hand, circumvents these disadvantages by avoiding the use of organic extractants completely and being reusable, recyclable and ultimately a non-toxic waste.

SPME was developed in 1990 by Professor Janusz Pawliszyn (Pawliszyn, 1997a) and is a fast, solvent-free sample preparation technique which combines sampling, isolation, and pre-concentration in a single step with minimal perturbation to the system. Furthermore, since SPME is a single step technique, the random errors resulting from consecutive sample transfers are significantly reduced. The simplicity of the technique and its ease of adaptation to existing analytical facilities (High Performance Liquid Chromatography (HPLC), Gas Chromatography-Mass Spectrometry (GC-MS) and Gas Chromatography-Flame Ionization Detector (GC-FID)) has played a key role in its growing acceptance for many environmental and industrial applications.

There are several advantages in using SPME over more traditional methods of extraction:

- Only small sample amounts (1 – 5 mL) required
- Less laborious and time consuming (only minutes per sample)
- No need for organic solvents
- No need for solvent disposal
- Linear response over a wide range of concentrations
- Compatible with any injectors in gas chromatographic systems
- Allows sampling of gases, liquids and solids
- Large number of environmental applications
- Can be used for on-site sampling
- Less expensive than LLE and SPE

SPME has been validated for the analysis of the 16 EPA priority pollutants in wastewater (Method 610) (SUPELCO, 1996; 1998). Additionally, SPME has been successfully used to analyse the EPA 16 PAH in laboratory, industrial and environmental aqueous samples (Zhang, 1994; Eisert and Levsen, 1996; Pawliszyn, 1997b; Doong *et al.*, 2000a; Havenga and Rohwer, 2000; Lord and Pawliszyn, 2000; Fernandez-Gonzalez *et al.*, 2007).

When compared with traditional sample preparation methodologies for the analysis of clean water, such as purge-and-trap, SPME has been found to be in very good agreement with this standard technique (Achten and Püttmann, 2000) . Additionally inter-laboratory analyses of blind samples, containing

standards of semivolatile organic compounds in pesticides mixtures, have yielded excellent precision and reproducibility values of the order of 5 % or less (Pawliszyn, 1997a).

This research work outlines the development of a fast and simple SPME sampling and extraction method specifically tailored to the rapid determination of Naphthalene in aqueous solutions after exposure to pre-treated quartz sand and granular activated carbon (GAC). Naphthalene was selected as a PAH surrogate for this study due to its lower toxicity with respect to the other PAH and its higher aqueous solubility when compared with the other 16 EPA PAH (U.S. Environmental Protection Agency, 1986; Agency for Toxic Substances and Disease Registry, 1995b). The use of these commercial sorbents with well known sorptive behaviour regarding PAH aims to illustrate the ease of use and adaptability of the technique for processes with high sample turnover, as would be the case in treatment plants using GAC (Walters and Luthy, 1984; Ania *et al.*, 2007).

1.6.2 SPME Fundamentals

Solid Phase Microextraction is based on the mass transfer of the analyte under study between multiple phases within a given system. Typically, the sampling stage is regarded as complete when a distribution equilibrium is reached between the fibre coating and the all the sample phases. At this point in time, the amount of analyte in all phases present is the same and sampling can take place anywhere in the system as long as the sampling conditions are kept constant.

The basic SPME equation for a system with a liquid matrix where no gaseous phase is present is presented below

$$n = \frac{C_0 V_f V_s K_{fs}}{K_{fs} V_f + V_s} \quad (1.10)$$

where n represents the mass of analyte extracted by the fibre coating whist immersed in the liquid phase (Direct Extraction), V_f represents the volume of the fibre coating, V_s corresponds to the sample volume, K_{fs} is the partition coefficient between the fibre and the sample bulk, and C_0 is the analyte's initial concentration in the sample. If the analyte being extracted is highly volatile it will have a much higher concentration in the headspace and it would make the extraction much faster if sampling is carried out in this phase rather than in the solution bulk. When headspace is included in the sampling vessel and after a series of practical considerations, Eq 1.10 transforms into:

$$n = \frac{C_0 V_f V_s K_{fs}}{K_{fs} V_f + K_{hs} V_{hs} + V_s} \quad (1.11)$$

where K_{hs} is the analyte's distribution coefficient between the headspace and the sample and $V_{hs}$is the headspace volume. The distribution constants and the coating volumes can be found in the available literature for several analytes or when this is not the case, the constants can be determined experimentally in the laboratory by using a combination of gas chromatographic runs and tabulated constants. The equation to be used will depend on the selected extraction mode. The full derivation of Eqs (1.10) and (1.11) can be found elsewhere (Pawliszyn, 1997a).

Although equilibrium extractions make quantification simpler and straightforward, if shorter extraction times are required, analytes can also be

extracted under pre-equilibrium conditions provided extraction parameters are kept constant. Pre-equilibrium sampling is often used in order to reduce the sampling time of highly volatile compounds on the condition that stringent controls are kept on the system's temperature and the sampling time in order to maintain acceptable margins of experimental error, typically between 5 - 15% RSD (relative standard deviation) for SPME.

In the present work, pre-equilibrium extraction was selected in order to carry out rapid extractions and to achieve a higher sample turnover whilst keeping the sampling parameters closely monitored.

A detailed description of the methodology developed is given in Chapter 3, followed by the materials and reagents employed.

1.7 Aims and Objectives

Aims:

It is expected that the systematic sorbent characterization and surface reaction monitoring at the molecular level undertaken in this research, will aid understanding and elucidation of the underlying sorption mechanisms whereby PAH interact with mineral phases.

Objectives:

- To study the sorption of Naphthalene onto thoroughly characterized materials by means of sorption experiments under different experimental conditions.

- To monitor surface PAH-mineral interactions *via* spectroscopic techniques, namely Atomic Force Microscopy, X-ray Photoelectron Microscopy and Fourier Transform Infrared spectroscopy (FTIR).

REFERENCES

Achten, C. and Püttmann, W. (2000). Determination of Methyl tert-Butyl Ether in Surface Water by Use of Solid-Phase Microextraction. Environmental Science & Technology 34(7): 1359-1364.

Agency for Toxic Substances and Disease Registry (1995a). Toxicological Profile for Polycyclic Aromatic Hydrocarbons. Atlanta, Division of Toxicology.

Agency for Toxic Substances and Disease Registry, A. (1995b). Toxicological Profile for Naphthalene (Update). U. S. D. o. H. a. H. S. Public Health Service, Atlanta, GA, USEPA.

Al-Abadleh, H. A. and Grassian, V. H. (2003). Oxide surfaces as environmental interfaces Surface Science Reports 52(3-4): 63-161.

Ania, C. O., Cabal, B., Pevida, C., Arenillas, A., Parra, J. B., Rubiera, F. and Pis, J. J. (2007). Effects of activated carbon properties on the adsorption of naphthalene from aqueous solutions. Applied Surface Science 253(13): 5741-5746.

Appert-Collin, J. C., Dridi-Dhaouadi, S., Simonnot, M. O. and Sardin, M. (1999). Nonlinear sorption of naphtalene and phenanthrene during saturated transport in natural porous media. Physics and Chemistry of the Earth, Part B: Hydrology, Oceans and Atmosphere 24(6): 543-548

Arnarson, T. S. and Keil, R. G. (2000). Mechanisms of pore water organic matter adsorption to montmorillonite. Marine Chemistry 71(3-4): 309 - 320.

Atkins, P. and De Paula, J. (2004). Atkin's Physical Chemistry. Oxford Oxford University Press. 920 pages.

Bojes, H. K. and Pope, P. G. (2007). Characterization of EPA's 16 priority pollutant polycyclic aromatic hydrocarbons (PAHs) in tank bottom solids and associated contaminated soils at oil exploration and production sites in Texas. Regulatory Toxicology and Pharmacology 47(3): 288-295.

Carlsen, L., Lassen, P., Gunnar, P. and Poulsen, M. E. (1997). Neri Technical Report No. 190: Fate of Polycyclic Aromatic Hydrocarbons in the Environment, Ministry of Environment and Energy**:** 84.

Carmo, A. M., Hundal, L. S. and Thompson, M. L. (2000). Sorption of Hydrophobic Organic Compounds by Soil Materials: Application of Unit Equivalent Freundlich Coefficients. Environmental Science and Technology 34(20): 4363-4369.

Charbeneau, R. J. (2000). Groundwater Hydraulics and Pollutant Transport. New Jersey, Prentice-Hall. 59 pages.

Cook, J. W. and Martin, R. H. (1940). Polycyclic Aromatic Hydrocarbons. Part XXIV.

Cousins, I. T., Kreibich, H., Hudson, L. E., Lead, W. A. and Jones, K. C. (1997). PAHs in soils: contemporary UK data and evidence for potential contamination problems caused by exposure of samples to laboratory air. Science of The Total Environment 203(2): 141-156.

Ding, Y. S., Trommel, J. S., Yan, Z. J., Ashley, D. and Watson, C. H. (2005). Determination of 14 Polycyclic Aromatic Hydrocarbons in Mainstream Smoke

from Domestic Cigarettes. Environmental Science and Technology 39(2): 471 - 478.

Doong, R.-a., Chang, S.-m. and Sun, Y.-c. (2000). Solid-phase microextraction for determining the distribution of sixteen US Environmental Protection Agency polycyclic aromatic hydrocarbons in water samples. Journal of Chromatography A 879(2): 177-188.

Drost-Hansen, W. (1969). Structure of Water Near Solid Interfaces. Industrial and Engineering Chemistry Research 61(11): 10-47.

Eisert, R. and Levsen, K. (1996). Review: Solid-phase Microextraction Coupled to Gas-Chromatography: A new Method for the Analysis of Organics in Water. Journal of Chromatography A 733(1-2): 143-157.

El-Alawi, Y. S., McConkey, B. J., George Dixon, D. and Greenberg, B. M. (2002). Measurement of Short- and Long-Term Toxicity of Polycyclic Aromatic Hydrocarbons Using Luminescent Bacteria. Ecotoxicology and Environmental Safety 51(1): 12-21.

Expert Panel on Air Quality Standards (1999). Polycyclic Aromatic Hydrocarbons. London, Department of the Environment, Transport and the Regions, National Assembly for Wales, Scottish Executive and Department of the Environment (Northern Ireland).

Fernandez-Gonzalez, V., Concha-Grana, E., Muniategui-Lorenzo, S. and Prada-Rodriguez, D. (2007). Solid-Phase microextraction-gas chromatography-tandem mass spectroscopy analysis of polycyclic aromatic hydrocarbons Towards the European Union water Directive 2006/0129 EC. Journal of Chromatography A 1176: 48-56.

Gad, S. C. and Gad, S. E. (2005). Polycyclic Aromatic Hydrocarbons (PAHs). Encyclopedia of Toxicology. W. Philip. New York, Elsevier**:** 513-515.

Gerde, P., Medinsky, M. A. and Bond, J. A. (1991). Particle-associated polycyclic aromatic hydrocarbons--A reappraisal of their possible role in pulmonary carcinogenesis. Toxicology and Applied Pharmacology 108(1): 1-13.

Gerstl, Z., Chen, Y., Mingelgrin, U. and Yaron, B. (1989). Toxic Organic Chemicals in Porous Media 343 pages.

Grimmer, G., Dettbarn, G., Brune, H., Deutsch-Wenzel, R. and Misfeld, J. (1982). Quantification of the carcinogenic effect of polycyclic aromatic hydrocarbons in used engine oil by topical application onto the skin of mice. International Archives of Occupational and Environmental Health 50(1): 95-100.

Grynkiewicz, M., Polkowska, Z. and Namiesnik, J. (2002). Determination of polycyclic aromatic hydrocarbons in bulk precipitation and runoff waters in an urban region (Poland). *Atmospheric Environment* **36**: 361-369.

Halsall, C. J., Coleman, P. J., Davis, B. J., Burnett, V., Waterhouse, K. S., Harding-Jones, P. and Jones, K. C. (1994). Polycyclic Aromatic Hydrocarbons in U.K. Urban Air. Environmental Science & Technology 28(13): 2380-2386.

Hammond, E. C., Selikoff, I. J., Lawther, P. L. and Seidman, H. (1976). Inhalation of Benzpyrene and Cancer in Man. Annals of the New York Academy of Sciences 271(May 28): 116-124.

Handley, A. (1998). Extraction Methods in Organic Analysis, Sheffield Academic Press Ltd. pages.

Harrison, R. M., Smith, D. J. T. and Luhana, L. (1996). Source Apportionment of Atmospheric Polycyclic Aromatic Hydrocarbons Collected from an Urban Location in Birmingham, U.K. Environmental Science & Technology 30(3): 825-832.

Harvey, R. G. (1991). Polycyclic Aromatic Hydrocarbons: Chemistry and Carcinogenicity. Cambridge, Cambridge University Press. pages.

Harvey, R. G. (1996). Polycyclic Aromatic Hydrocarbons, Wiley-VCH. pages.

Hassett, J. J., Means, J. C., Banwart, W. L., Wood, S. G., Ali, S. and Khan, A. (1980). Sorption of Dibenzothiophene by Soils and Sediments Journal of Environmental Quality 9(2): 184 -186.

Havenga, W. J. and Rohwer, E. R. (2000). The use of SPME and GC-MS for the chemical characterisation and assessment of PAH pollution in aqueous environmental samples. International Journal of Environmental Analytical Chemistry 78(3-4): 205-221.

Heywood, E., Wright, J., Wienburg, C. L., Black, H. I. J., Long, S. M., Osborn, D. and Spurgeon, D. J. (2006). Factors Influencing the National Distribution of Polycyclic Aromatic Hydrocarbons and Polychlorinated Biphenyls in British Soils. Environmental Science & Technology 40(24): 7629-7635.

Huang, W., Schlautman, M. A. and Weber, W. J. (1996). A Distributed Reactivity Model for Sorption by Soils and Sediments. 5. The Influence of

Near-Surface Characteristics in Mineral Domains. Environmental Science and Technology 30(10): 2993-3000.

Huang, W. and Weber W.J, Jr. (1998). A distributed reactivity model for sorption by soils and sediments. 11. Slow concentration-dependent sorption rates. Environmental Science and Technology 32(22): 3549.

Huang, W. and Weber, W. J. (1997). Thermodynamic Considerations in the Sorption of Organic Contaminants by Soils and Sediments. 1. The Isosteric Heat Approach and Its Application to Model Inorganic Sorbents Environmental Science and Technology 31: 3238-3249.

Hundal, L. S., Thompson, M. L., Laird, D. A. and Carmo, A. M. (2001). Sorption of Phenanthrene by Reference Smectites. Environmental Science and Technology 35(17): 3456-3461.

International Agency for Research on Cancer (1983). IARC Monographs on the Evaluation of Carcinogenic Risks to Humans. Volume 32. Polynuclear Aromatic Compounds, Part 1, Chemical, Environmental and Experimental Data. Summary of Data Reported and Evaluation, World Health Organisation, WHO. 2005.

Kan, A. T., Fu, G., Hunter, M., Chen, W., Ward, C. H. and Tomson, M. B. (1998). Irreversible sorption of neutral hydrocarbons to sediments: Experimental observations and model predictions. Environmental Science and Technology 32(7): 892-902.

Karahalil, B., Karakaya, A. E. and Burgaz, S. (1999). The micronucleus assay in exfoliated buccal cells: application to occupational exposure to polycyclic aromatic hydrocarbons. Mutation Research/Genetic Toxicology and Environmental Mutagenesis 442(1): 29-35.

Karickhoff, S. W., Brown, D. S. and Scott, T. A. (1979). Sorption of hydrophobic pollutants on natural sediments. Water Research 13(3): 241-248.

Kiely, G. (1997). Environmental Engineering, McGraw-Hill Publishing Co. 979 pages.

Kim, S. B. and Corapcioglu, M. Y. (2002). Contaminant transport in dual-porosity media with dissolved organic matter and bacteria present as mobile colloids Journal of Contaminant Hydrology 59(3 - 4): 267-289.

Klotz, I. M. and Rosenberg, R. M. (2000). Chemical Thermodynamics. Basic Theory and Methods. Canada, John Wiley & Sons. pages.

Krauss, M. and Wilcke, W. (2002). Sorption Strength of Persistent Organic Pollutants in Particle-size Fractions of Urban Soils. Soil Sci Soc Am J 66(2): 430-437.

Krauss, M., Wilcke, W. and Zech, W. (2000). Polycyclic aromatic hydrocarbons and polychlorinated biphenyls in forest soils: depth distribution as indicator of different fate. Environmental Pollution 110(1): 79-88.

Lawther, P. J. and Waller, R. E. (1978). TRENDS IN URBAN AIR-POLLUTION IN UNITED-KINGDOM IN RELATION TO LUNG-CANCER MORTALITY. Environmental Health Perspectives 22(FEB): 71-73.

Lewis, G. P. and Coughlin, L. (1973). Lung "soot" accumulation in man. Atmospheric Environment (1967) 7(12): 1249-1255.

Li, H. L., Chen, J. J., Wu, W. and Piao, X. S. (2010). Distribution of polycyclic aromatic hydrocarbons in different size fractions of soil from a coke oven plant and its relationship to organic carbon content. Journal of Hazardous Materials 176(1-3): 729-734.

Lord, H. and Pawliszyn, J. (2000). Evolution of solid-phase microextraction technology. Journal of Chromatography A 885(1-2): 153-193.

Luthy, R. G., Aiken, G. R., Brusseau, M. L., Cunningham, S. D., Gschwend, P. M., Pignatello, J. J., Reinhard, M., Traina, S. I., Weber W.J, Jr. and Westall, J. C. (1997). Sequestration of hydrophobic organic contaminants by geosorbents. Environmental Science and Technology 31(12): 3341.

Mader, B. T., Uwe-Goss, K. and Eisenreich, S. J. (1997). Sorption of Nonionic, Hydrophobic Organic Chemicals to Mineral Surfaces. Environmental Science and Technology 31(4): 1079-1086.

Maisto, G., De Nicola, F., Iovieno, P., Prati, M. V. and Alfani, A. (2006). PAHs and trace elements in volcanic urban and natural soils. Geoderma 136(1-2): 20-27.

Martuzevicius, D., Kliucininkas, L., Prasauskas, T., Krugly, E., Kauneliene, V. and Strandberg, B. (2011). Resuspension of particulate matter and PAHs from street dust. Atmospheric Environment 45(2): 310-317.

Meijer, S. N., Sweetman, A. J., Halsall, C. J. and Jones, K. C. (2008). Temporal Trends of Polycyclic Aromatic Hydrocarbons in the U.K. Atmosphere: 1991–2005. Environmental Science & Technology 42(9): 3213-3218.

Middleton, C. (2003). The Development Of A Mesoscale Contaminant Hydrogeology Column And Its Application To Environmental Organic

Systems. Department of Civil Engineering. Manchester, University of Manchester**:** 420.

Moon, J.-W., Goltz, M. N., Ahn, K.-H. and Park, J.-W. (2003). Dissolved organic matter effects on the performance of a barrier to polycyclic aromatic hydrocarbon transport by groundwater. Journal of Contaminant Hydrology 60(3-4): 307.

Patrolecco, L., Ademollo, N., Capri, S., Pagnotta, R. and Polesello, S. (2010). Occurrence of priority hazardous PAHs in water, suspended particulate matter, sediment and common eels (Anguilla anguilla) in the urban stretch of the River Tiber (Italy). Chemosphere 81(11): 1386-1392.

Pawliszyn, J. (1997a). Solid Phase Microextraction: Theory and Practice. New York, Wiley-VCH. pages.

Pawliszyn, J., Pawliszyn B. and Pawliszyn M. (1997b). Solid Phase Microextraction (SPME). The Chemical Educator 2(4).

Pignatello, J. J. and Xing, B. (1996). Mechanisms of slow sorption of organic chemicals to natural particles. Environmental Science and Technology 30(1): 1 - 8.

Pitzer, K. S. (1995). Thermodynamics. Singapore, McGraw-Hill Book Co. pages.

Prevedouros, K., Brorström-Lundén, E., J. Halsall, C., Jones, K. C., Lee, R. G. M. and Sweetman, A. J. (2004). Seasonal and long-term trends in atmospheric PAH concentrations: evidence and implications. Environmental Pollution 128(1-2): 17-27.

Schmid, G. H. (1995). Organic Chemistry McGrow Hill. pages.

Schwarz, K., Gocht, T. and Grathwohl, P. (2011). Transport of polycyclic aromatic hydrocarbons in highly vulnerable karst systems. Environmental Pollution 159(1): 133-139.

Schwarzenbach, R. P., Gschwend, P. M. and Imboden, D. M. (1993). Environmental Organic Chemistry, John Wiley & Sons Inc. 1340 pages.

Shibasaki, Y. and Fukuda, K. (1992). Aggregation states and polymerizabilities of amphiphilic monomer molecules in aqueous systems with different water contents Colloids and Surfaces 67: 195-201

Staszczuk, P. (1995). Novel studies of phase and structural transitions in bulk and vicinal water Colloids and Surfaces A: Physicochemical and Engineering Aspects 94(2-3): 213-224

Stumm, W. and Morgan, J. J. (1996). Aquatic Chemistry: Chemical Equilibria and Rates in Natural Waters, Wiley-Interscience Series of texts and Monographs. third edition. 1022 pages.

Sun, H., Tateda, M., Ike, M. and Fujita, M. (2003). Short- and long-term sorption/desorption of polycyclic aromatic hydrocarbons onto artificial solids: effects of particle and pore sizes and organic matters Water Research 37(12): 2960-2968

SUPELCO. (1996). GC Analyses of Polynuclear Aromatic Hydrocarbons. Application Note 108. Retrieved 27/06/2006.

SUPELCO. (1998). Solid Phase Microextraction of Semivolatile Compounds. Application Note 6. Retrieved 27/06/2006.

Trapido, M. (1999). Polycyclic aromatic hydrocarbons in Estonian soil: contamination and profiles. Environmental Pollution 105(1): 67-74.

U.S. Environmental Protection Agency (1986). Health and Environmental Effects Profile for Naphthalene. EPA/600/x-86/241. . E. C. a. A. Office, Office of Health and Environmental Assessment, Office of Research and Development.

UK Environment Agency, E. A. (2005). Polycyclic aromatic hydrocarbons (PAHs). Retrieved 05/07/2005, 2005, from http://www.environment-agency.gov.uk.

Walgraeve, C., Demeestere, K., Dewulf, J., Zimmermann, R. and Van Langenhove, H. (2010). Oxygenated polycyclic aromatic hydrocarbons in atmospheric particulate matter: Molecular characterization and occurrence. Atmospheric Environment 44(15): 1831-1846.

Walters, R. W. and Luthy, R. G. (1984). Equilibrium adsorption of polycyclic aromatic hydrocarbons from water onto activated carbon. Environmental Science & Technology 18(6): 395-403.

Wang, Z., Hemmer, S. L., Friedrich, D. M. and Joly, A. G. (2001). Anthracene as the Origin of the Red-Shifted Emission from Commercial Zone-Refined Phenanthrene Sorbed on Mineral Surfaces. Journal of Physical Chemistry A 105(25): 6020-6023.

White, P. A. and Claxton, L. D. (2004). Mutagens in contaminated soil: a review. Mutation Research/Reviews in Mutation Research 567(2-3): 227-345.

Wilcke, W. (2007). Global patterns of polycyclic aromatic hydrocarbons (PAHs) in soil. Geoderma 141(3-4): 157-166.

Wild, S. R. and Jones, K. C. (1995). Polynuclear aromatic hydrocarbons in the United Kingdom environment: A preliminary source inventory and budget. Environmental Pollution 88(1): 91-108.

World Wildlife Fund. (1997). Briefing on effects of PAH on the marine environment. Retrieved 17/05/2005, 2005, from http://www.wwf.org.uk/filelibrary/pdf/mu_32.pdf.

Yang, S. K. and Silverman, B. D. (1988). Polycyclic Aromatic Hydrocarbon Carcinogenesis:Structure-Activity Relationships. Boca Raton, Florida, CRC Press. pages.

Zhang, Z. Y., M.J.; Pawliszyn, J. (1994). Solid-Phase Microextraction. Analytical Chemistry 66(17): 844- 853.

Zhu, D., Herbert, B. E. and Schlautman, M. A. (2003). Molecular-level investigation of monoaromatic compound sorption to suspended soil particles by deuterium nuclear magnetic resonance. Journal of Environmental Quality 32(1): 232-239.

Zhu, D., Herbert, B. E., Schlautman, M. A. and Carraway, E. R. (2004a). Characterization of cation-pi interactions in aqueous solution using deuterium nuclear magnetic resonance spectroscopy. Journal of Environmental Quality 33(1): 276-284.

Zhu, D., Herbert, B. E., Schlautman, M. A., Carraway, E. R. and Hur, J. (2004b). Cation-pi bonding: a new perspective on the sorption of polycyclic aromatic hydrocarbons to mineral surfaces. Journal of Environmental Quality 33(4): 1322-1330.

Zhu, D., Hyun, S., Pignatello, J. J. and Lee, L. S. (2004c). Evidence for -Electron Donor-Acceptor Interactions between -Donor Aromatic Compounds and -Acceptor Sites in Soil Organic Matter through pH Effects on Sorption. Environmental Science and Technology 38(16): 4361-4368.

CHAPTER 2 Mineral Characterisation

Most of the studies concerned with the mechanisms whereby minerals affect PAH mobility have included a variety of materials or geosorbents which have been observed to influence how these chemicals behave in the environment. In general, the selection criteria employed included properties such as abundance, type of mineral, particle size, specific surface area, surface charge, exchangeable cations (in the case of clays), and intraparticle porosity. Other properties such as crystal structure, surface morphology, pore geometry and external characteristics such as surface-bound water, which is believed to compete against PAH for surface sorption sites (Drost-Hansen, 1969), were less commonly controlled.

With regards to the sorbent nature, some studies have used man-made sorbents as proxys which are not present in the environment but have industrial or environmental applications, such as silica gels (Su *et al.*, 2006), glass beads (Aksnes and Kimtys, 2004) and artificial clays such as laponite (Labbe and Reverdy, 1987) . Whilst the use of such materials makes it possible to keep the sorbent characteristics constant the selected sorbents are not representative of the natural environment. On the other hand, the literature contains many studies using natural soils (Appert-Collin *et al.*, 1999), (Carmo *et al.*, 2000), (Hwang and Cutright, 2004), in which the presence of organic matter is often not quantified nor constrained, and whose use increases the complexity of the system and the uncertainty when attempting to explain the observed results.

This study investigates the mechanism of interaction of selected PAH onto pure, homogeneous mineral surfaces. In order to understand how non-polar organic compounds react with inorganic, polar surfaces, the physical and

chemical properties of both sorbent and contaminant must be studied. An attempt has been made to proceed in a systematic manner by starting with the simplest case scenario and subsequently adding variables to the sorbate-sorbent system under study.

Section 2.1. describes the minerals chosen as model sorbents, the rationale behind their selection and their systematic characterization.

Section 2.2. explains the purpose of each analytical technique and outlines the selected laboratory protocols.

Section 2.3. presents the protocol for the modification of one of the original materials, namely quartz sand, in order to coat it with a different mineral phase (goethite).

2.1. Selected Minerals.

The selection criteria for the chosen mineral phases were based on their relative abundance in soils as well as their environmental relevance. Silica and silicates such as clays (phyllosilicates) comprise the most abundant mineral phases; therefore quartz sand (silicon dioxide, SiO_2) was selected as the simplest of the geosorbents. In addition to this, quartz sand is a very commonly used material in sorption and transport studies involving hydrophobic organic pollutants (Danzer and Grathwohl, 1998; Sluszny *et al.*, 1998; Yong-Jin and Masahiro, 2003; Chevron Cottin and Merlin, 2007) and could be useful to compare with results in cases where a similar experimental setup and the same contaminants are used.

Iron oxide (haematite, α-Fe_2O_3) was chosen due to its abundance in soils and groundwater systems as a weathering product of iron-bearing minerals (Deer *et al.*, 1972); in addition to its role as a catalyst in the remediation of PAH-contaminated soils (Nieman *et al.*, 2001; Wang *et al.*, 2009).

Clays are well known for their applications in environmental remediation schemes and their notorious contaminant transport capacity (Compere *et al.*, 2001). Expandable clays such as montmorillonite have been observed to interact with both polar and non-polar organic pollutants and have been the subject of intense research in recent years under a variety of environmental conditions (Labbe and Reverdy, 1987; Hwang and Cutright, 2004).

All minerals (except commercially pre-washed quartz sand) were obtained in their natural form and prepared according to the specifications required for each experiment. The mineral phases studied were the following:

Quartz sand. The sand was supplied by VWR (Merck Cat. No. 1077121000). The manufacturer's pre-treatment consisted of calcination at 900°C followed by acid-wash in hydrochloric acid (HCl). This process guaranteed the low levels of organic carbon required for the scheduled experiments (≤ 0.1 %) (Appelo and Postma, 1994). The precaution is based on the sequestrating effect organic moieties exert upon polyarene molecules, as is well documented in the literature (Piatt *et al.*, 1996a; Pignatello and Xing, 1996; Appert-Collin *et al.*, 1999; Carmo *et al.*, 2000; Gaboriau and Saada, 2001; Hundal *et al.*, 2001; Wefer-Roehl *et al.*, 2001; Sun *et al.*, 2003; Zhu *et al.*, 2003; Hwang and Cutright, 2004; Sabbah *et al.*, 2004; Zhu *et al.*, 2004c). The sand was used as received except where surface-bound water or excess acidity needed to be removed, or when the sand had to be ground to a fine dust.

Haematite: High purity natural Haematite was used as the representative for the iron oxide phase. Rocks from the Haile Mine in Egremont, Cumbria, were kindly supplied by Dr David Green at the Manchester Museum. The rocks were ground to a powder and then sieved to select the most abundant fraction for each experiment. No further pre-treatment or preparation was performed. The subsamples used in every experiment originated from the same rock fragment

Clay: The clay used was the expandable reference clay Texas Montmorillonite (STx-1) ordered from The Source Clay Repository at the University of Missouri, Columbia, USA. The powder was used without undergoing cationic saturation or any other form of pre-treatment. The Montmorillonite, was sieved and suspended in the background electrolyte used in each experiment.

Iron-Oxide / Fe_2O_3 coated sand: VWR quartz sand artificially coated with goethite was prepared in an attempt to compare its sorptive behaviour with that of the two individual pure minerals. The coating was carried out in the laboratory via a precipitation reaction following a protocol used by other workers which will be detailed below in Section 2.3.

2.2. Sorbent Characterisation

The characterisation of all four minerals described in Section 2.1. included the following analytical procedures:

2.2.1. Specific Gravity

The determination of the specific gravity for the materials used was only possible for the quartz sand material. In the case of the clay it was provided by the supplier and is included in Table 2.1. In the case of the natural haematite and the Fe-coated sand, it was not possible to carry out the assay due to severe constrains of the amount of material available. The values for these two mineral phases were instead obtained from the literature and are included in the table of results.

The specific gravity for quartz sand was performed following a standard method (BS 1377 - 2:1990) (British Standard Institution (BSI), 1990). The values and averaged results for a set of triplicates (sand) are shown below. The initial mass of sample used for sand was 10 g. The specific gravity for sand was calculated in g / cm^3 as indicated below:

$$\rho_S = \frac{M_S}{V_S} \tag{2.1}$$

where M_s is the mass of sand in g and V_s is the sand volume in cm^3.

2.2.2. Particle Size Distribution (PSD)

The PSD for the quartz sand was determined by sieve analysis in accordance with British Standard BS1377 (British Standard Institution (BSI), 1990). The test classifies the sand type varying from fine to coarse complying with BIS standards. The results are presented in Figure 2.1. as a grading curve. The percentage of the initial mass of sand (50 g) retained by each sieve is calculated as the average of three replicate determinations, and then plotted

against the corresponding mesh size. The mass percentage is calculated as follows:

$$M_S\% = (M_S / M_{TS}) \times 100 \quad (2.2)$$

where $M_S\%$ is the percentage of sand retained in each sieve, M_S is the mass of sand retained on each sieve in g and M_{TS} is the initial mass of sand in g.

After this analysis for quartz sand, the size fraction for all mineral phases used in the experiments thereafter was fixed at 250 - 500 μm (or anything ≥ 250 μm).

2.2.3. Specific Surface Area (SSA)

The specific surface area for the quartz sand was measured in triplicate samples using a Micrometrics Tristar (Brunauer-Emmet-Teller) BET surface area analyzer. The inert gas used as adsorbate was nitrogen. The procedure is the one followed as a standard technique in the Kinetics Laboratory of the School of Earth, Atmospheric and Environmental Sciences (SEAES) at The University of Manchester. The procedure was adapted after Morris (2004), and after the Micromeritics Tristar BET and is outlined below .

Procedure:

1. The nitrogen saturation pressure (p_o) is determined prior to the first sample run and again half way through a shift. This parameter (p_o) refers to the nitrogen's vapour pressure.
2. All tubes in the rack provided are degassed. The operating instructions, appropriate temperature and length of time required for

degassing can be found in the Micromeritics Operator's Manual (Micromeritics Ltd, 1995).

3. After degassing the tubes are allowed to cool inside the block with the stopper and the gas delivery tube in place to avoid air displacing the nitrogen inside the tube. Touching the tube body must be avoided in order to prevent burns and errors when weighing. Once the tubes reach ambient temperature the gas delivery pipeline is removed and the stopper carefully replaced to avoid air entry.

4. The combined weight (m_1) of the tube and stopper is recorded. 1 g of sample is transferred into the tube using a funnel and the stopper replaced. The weight of the tube, sample and stopper as one unit is recorded prior to degassing (m_2).

5. The sample is degassed under the same conditions as the reference tube in the heat block and is allowed to reach ambient temperature as described above (3).

6. The weight of the tube and sample plus stopper is recorded as a combined weight (m_3). The amount of dry sample is thus calculated ($m_3 - m_1$).

7. The tube is carefully inserted into the BET sample port and the sample analysed following the procedure outlined in the Micromeritics Operator's manual (Micromeritics Ltd, 1995).

The equation used to calculate the surface area of a material was originally derived by Brunauer, Emmett and Teller (Brunauer *et al.*, 1938):

$$\frac{p}{v(p_0 - p)} = \left(\frac{1}{v_m c} \right) + \left(\frac{c-1}{v_m c} \frac{p}{p_0} \right) \qquad (2.3)$$

where:

p is the equilibrium pressure of a gas layer (atm),

v is the volume adsorbed at pressure p (cm^3),

p_0 is the gas saturation pressure (atm),

v_m is the volume of gas required to form a complete uni-molecular adsorbed layer,

c is a constant.

By plotting p / v (p_0 - p) against p / p_0, the slope (S) and intercept (Y_{INT}) are obtained and used in the following equation to calculate the specific surface area (SSA_{BET}) in m^2 / g:

$$SSA_{BET} = \frac{N_A \sigma}{V_{STP}(S + Y_{INT})} \qquad (2.4)$$

where

N_A is Avogadro's number (6.022 137 x 10^{23} molecules per mole),

σ is the gas molecular cross sectional area (m^2),

V_{STP} is the ideal gas volume at standard temperature and pressure (22,414 cm^3).

The full dimensional analysis and derivation of the equation and other relationships used in the calculation of the BET surface area can be found in detail in the Data Reduction chapter of the Micromeritics Operator's Manual (Micromeritics Ltd, 1995).

2.2.4. Loss on Ignition (LOI)

The test to determine LOI yields an estimate of the levels of carbonaceous matter present in the materials under analysis; it does not discriminate between that and any water evaporation taking place. More detailed assays such as Total Organic Carbon content (see Section 2.2.5) should be carried out if the organic matter content in a sample is significant for the experimental work. The LOI test was carried out at the Analytical Geochemistry Laboratory, SEAES. The procedure comprises the determination of a sample's mass losses between laboratory temperature and 1200 °C.

Procedure:

1. 50 g of the sample are transferred to a pre- weighed porcelain crucible.
2. The crucible with the sample is placed in a pre-heated furnace at 1000 °C and kept there for two hours.
3. After cooling for one hour inside a desiccator, the crucible is reweighed and the total loss on ignition calculated as follows:

$$\Sigma LOI\% = \left(\frac{m_2 - m_3}{m_2 - m_1} \right) \times 100 \qquad (2.5)$$

where ∑LOI % equals the total loss on ignition percentage, m_1 is the mass of the empty crucible, m_2 is the mass of the crucible plus the sample before heating, m_3 is the mass of the crucible plus sample after heating; $m_2 - m_3$ represents the sample mass and $m_2 - m_1$ represents the sample mass after heating.

2.2.5. Total Organic Carbon (TOC) content

The Total Organic Carbon content of the sand was measured with a Leco Total Carbon Analyser by the Newcastle Research Group in Fossil Fuels and Environmental Geochemistry, University of Newcastle Upon Tyne, UK. Sample triplicates of 2 g were heated at > 1000 °C for 30 seconds in an induction furnace, according to the protocol followed by the Newcastle group. The results are presented in the general summary in Table 2.1.

2.2.6. X-ray Diffraction (XRD)

The identification of the mineral phases present in the sample under study was carried out *via* X-Ray diffraction (XRD) on a Philips PW 1730 X-ray generator fitted with a copper tube. The analysis was performed between 10 and 70 degrees with a step increase of 0.02 degrees. The current was set at 20 mA and the voltage at 40 kV. The detection limit calculated for this device is 5 % as mass percentage. The protocol followed is one suggested in a previous research study (Morris, 2005b).

Procedure:

1. High purity silicon internal standard (5 – 10 mg) is added to the sample (200 mg).
2. Using an agate mortar and pestle, the mixture of sand and internal standard is crushed to form a slurry with added amyl acetate.
3. This paste is smeared on a glass slide and placed under a lamp for the solvent to evaporate.

4. Once the sample on the slide has dried out, the sample is taken to the radiation chamber and the analysis conducted by a technician as specified in the laboratory's protocol (SEAES).

2.2.7. Determination of the Surface Morphology by Scan Electron Microscopy (SEM)

The surface morphology of the minerals used was analyzed by Scan Electron Microscopy (SEM) using a JEOL JSM6400 Analytical Scanning Microscope. The pictures had a resolution of 1 μm. Energy dispersion spectra were collected at 15 KeV.

The procedure involved compacting the sample (<1 g) into a grain mound at the workshop, then mounting the mound on a holder and coating it with carbon to enhance conductivity. The mound was then inserted in the chamber and the images and Energy Dispersive Spectra (EDS) taken.

2.3. Coating Protocol for Quartz Sand

The protocol followed for this procedure was an adaptation of the one used by Lai and Chen, 2001 (Lai and Chen, 2001) and is outlined below. As the sand had already been commercially pretreated it was not necessary to digest it in acid to remove interfering species prone to precipitation during the coating process. The particle size selected for coating was the same one used in every experiment and corresponds to 250 – 500 μm in order to avoid including fine particles without uniform size in the samples used.

1- An iron oxide stock solution was prepared at 0.5 M by dissolving the required amount of $Fe(NO_3)_3$ 9H2O in DIW to

prepare up to 100 ml. The solution and sand (200 g) were added to a large beaker (1 L) to which a large PTFE stirring bar was added before placing it on a magnetic stirring plate.

2- NaOH at 3.0 N was prepared on the same day and added dropwise to the iron-sand slurry whilst the pH was controlled to 2 decimal places. After large volumes of base had been added to bring the pH to the desired value of 9.5 ± 0.10; the solution continued to stir for at least 20 minutes at ambient temperature.

3- The temperature was increased to 50 ºC whilst stirring for the next 48 hours. At this point the mix had become a thick, heavy slurry and the PTFE stir bar was sanded flat on one side and was removed from the slurry.

4- The slurry was kept at 50 ºC for a further 48 hours after which it was thoroughly rinsed with DIW (26 times) until the supernatant was running clear before drying again at 50 ºC in an oven for another 96 hours. The PTFE particles were removed by flotation in the previous washes. After this the sand was stored in polystyrene sample bottles and was deemed coated and ready to use.

The coated sand was then used in the sorption experiments without further pretreatment or manipulation.

2.4. Results

The characterisation results are presented as a table with the numerical results for all minerals (table 2.1). In the case of results in the form of graphs or

pictures, these are presented separately for each mineral along with a brief description of the analysis outcome in Appendix A2.

The VWR sand is classed as fine according to the BSI classification system with particle sizes ranging between 0.15 and 0.25 mm. The grading

Assay	Units	QS	Hm	Fe-QS	Stx-1
Source	N/A	VWR	Cumbria	VWR[1]	USA[2]
PSD	(µm)	250 - 500	250 - 500	≥ 250 - 500	250 - 500
Sp. Grav.	($g.cm^{-3}$)	2.65	5.15 [4]	N/A	2.2 [2]
SSA	($m^2.\ g^{-1}$)	0.22	1.99	4.57	58.78
Main phase $_{XRD}$	N/A	SiO_2	Fe_2O_3	α-FeOOH / SiO_2	SiO_2
LOI	(%)	0.0207	< N.D.[3]	< N.D.[3]	< N.D.[3]
TOC	(OC %)	0.0046	N/A	0.0046	0.09 [4]
1- Original VWR sand coated					
2- The Clay Resource Depository, The University of Missouri					
3- Not detected					
4- J. Raman Spectrosc. 2004; 35: 480 - 485.					

Table 2.1 Mineral characterisation results.

table is presented in Appendix A2. All other materials used in the sorption experiments thereafter were sieved to obtain the same particle size (≥ 250 µm) without further PSD analysis.

The specific gravity assay was only carried out for the VWR quartz sand and not on the other minerals due to insufficient sample size (hematite and Fe-coated sand). In the case of the clay, it had already been provided by the supplier.

The lowest specific surface area obtained was for quartz sand, when compared with that corresponding to other porous sorbents used in PAH transport experiments, such as amorphous silica and expandable clays (Labbe and Reverdy, 1987; Hundal *et al.*, 2001). All particles (including fines) were

included in each analysis and the SSA obtained corresponds to all grain sizes present in the analysed sample. This SSA is still representative of the ≥ 250 μm fraction of all minerals since this particle size was the most abundant phase (> 90 %) in all cases. Table 2.1 shows the specific surface areas for the materials selected. This could potentially be a key parameter for the sorption experiments results, where it will be assessed whether or not it influences the overall naphthalene uptake from solution by the selected mineral phases. The BET surface area value accounts for the external and internal surfaces (pores).

The loss on ignition percentage for VWR sand is 0.0207 %. It agrees with the value reported by the manufacturer (0.02 %). Only one sample was analyzed. The same assay did not detect any losses for the other three materials which could be interpreted as the materials having very low organic carbon content at the selected temperature range (up to 1200 ºC).

The VWR sand has remarkably low organic carbon content. The calculated organic carbon fraction, f_{OC}, is 0.00005 (from TOC analysis). To the best knowledge of the author, this value is the lowest reported so far in studies involving the effect of organic matter on PAH transport within the soil. This characteristic makes this sand ideal for kinetic studies assessing the role of minerals on the transport of polyarenes, since solute-sorbent interactions can be attributed to a large extent to the mineral phase.

Due to severe sample size constraints it was not possible to carry out the same analysis on two of the other three minerals (namely Fe-coated sand and hematite), whose OC% values had to be estimated from the LOI test. According to the latter; the carbon fraction which would combust at the temperature range (0 º to 1200 ºC) was below the detection limit of the method (1.5 % of sample

weight). For the clay, the OC% can be found in the literature since it is a broadly used reference material (Bishop and Murad, 2004).

The XRD spectra corresponding to each mineral reflect the purity of the selected sorbents (see Appendix A2). The elemental analysis of all 4 mineral species was carried out using XRF (X-ray Fluorescence) and is presented in Appendix A2.

REFERENCES

Aksnes, D. W. and Kimtys, L. (2004). 1H and 2H NMR studies of benzene confined in porous solids: melting point depression and pore size distribution. Solid State Nuclear Magnetic Resonance 25(1-3): 146-152.

Appelo, C. A. J. and Postma, D. (1994). Geochemistry, Groundwater and Pollution. Rotterdam, Balkema. 669 pages.

Appert-Collin, J. C., Dridi-Dhaouadi, S., Simonnot, M. O. and Sardin, M. (1999). Nonlinear sorption of naphtalene and phenanthrene during saturated transport in natural porous media. Physics and Chemistry of the Earth, Part B: Hydrology, Oceans and Atmosphere 24(6): 543-548

Bishop, J. L. and Murad, E. (2004). Characterization of minerals and biogeochemical markers on Mars: A Raman and IR spectroscopic study of montmorillonite. Journal of Raman Spectroscopy 35: 480 - 486.

British Standard Institution (BSI) (1990). *Methods of test for Soils for Civil Engineering Purposes. Part 2: Classification tests. BS1377-2.* 2.

Brunauer, S., Emmett, P. H. and Teller, E. (1938). Adsorption of Gases in Multimolecular Layers. Journal of the American Chemical Society 60(2): 309.

Carmo, A. M., Hundal, L. S. and Thompson, M. L. (2000). Sorption of Hydrophobic Organic Compounds by Soil Materials: Application of Unit Equivalent Freundlich Coefficients. Environmental Science and Technology 34(20): 4363-4369.

Chevron Cottin, N. and Merlin, G. (2007). Study of pyrene biodegradation capacity in two types of solid media. Science of The Total Environment 380(1-3): 116-123.

Compere, F., Porel, G. and Delay, F. (2001). Transport and retention of clay particles in saturated porous media. Influence of ionic strength and pore velocity. Journal of Contaminant Hydrology 49(1-2): 1-21.

Danzer, J. and Grathwohl, P. (1998). Coupled transport of PAH and surfactants in natural aquifer material. Physics and Chemistry of The Earth 23(2): 237-243.

Deer, W. A., Howie, R. A. and Zussman, J. (1972). An Introduction to the Rock Forming Minerals. London, Longman Group Limited. 539 pages.

Drost-Hansen, W. (1969). Structure of Water Near Solid Interfaces. Industrial and Engineering Chemistry Research 61(11): 10-47.

Gaboriau, H. and Saada, A. (2001). Influence of heavy organic pollutants of anthropic origin on PAH retention by kaolinite. Chemosphere 44(7): 1633-1639.

Hundal, L. S., Thompson, M. L., Laird, D. A. and Carmo, A. M. (2001). Sorption of Phenanthrene by Reference Smectites. Environmental Science and Technology 35(17): 3456-3461.

Hwang, S. and Cutright, T. J. (2004). Evidence of underestimation in PAH sorption/desorption due to system nonequilibrium and interaction with soil constituents. J Environ Sci Health Part A Tox Hazard Subst Environ Eng 39(5): 1147-1162.

Labbe, P. and Reverdy, G. (1987). Adsorption Characteristics of Polycyclic Aromatic Compounds on Clays: Pyrene as Photophysical Probe on Laponite. Langmuir 4: 419-425.

Lai, C. H. and Chen, C. Y. (2001). Removal of metal ions and humic acid from water by iron-coated filter media. Chemosphere 44(5): 1177-1184.

Micromeritics Ltd (1995). Gemini 2360 Surface Area Analyzer- Operator's Manual.

Morris, P. (2005). Procedure for BET Analysis of the Surface Area Y. De Bryant. Manchester

Nieman, J. K. C., Sims, R. C., McLean, J. E., Sims, J. L. and Sorensen, D. L. (2001). Fate of pyrene in contaminated soil amended with alternate electron acceptors. Chemosphere 44(5): 1265-1271.

Piatt, J. J., Backhus, D., Capel, P. D. and Eisenreich, S. J. (1996). Temperature-Dependent Sorption of Naphthalene, Phenanthrene, and Pyrene to Low Organic Carbon Aquifer Sediments *Environmental Science and Technology* 30 (3): 751 -760.

Pignatello, J. J. and Xing, B. (1996). Mechanisms of slow sorption of organic chemicals to natural particles. Environmental Science and Technology 30(1): 1 - 8.

Sabbah, I., Rebhun, M. and Gerstl, Z. (2004). An independent prediction of the effect of dissolved organic matter on the transport of polycyclic aromatic hydrocarbons. Journal of Contaminant Hydrology 75(1-2): 55-70.

Sluszny, C., Bulatov, V. and Schechter, I. (1998). Classification and quantification of polycyclic aromatic hydrocarbons on quartz sand particles by direct Fourier transform imaging fluorescence. Analytica Chimica Acta 367(1-3): 1-10.

Su, Y. H., Zhu, Y. G., Sheng, G. and Chiou, C. T. (2006). Linear Adsorption of Nonionic Organic Compounds from Water onto Hydrophilic Minerals: Silica and Alumina. Environ. Sci. Technol. 40(22): 6949-6954.

Sun, H., Tateda, M., Ike, M. and Fujita, M. (2003). Short- and long-term sorption/desorption of polycyclic aromatic hydrocarbons onto artificial

solids: effects of particle and pore sizes and organic matters Water Research 37(12): 2960-2968

Wang, Y., Liu, C. S., Li, F. B., Liu, C. P. and Liang, J. B. (2009). Photodegradation of polycyclic aromatic hydrocarbon pyrene by iron oxide in solid phase. Journal of Hazardous Materials 162(2-3): 716-723.

Wefer-Roehl, A., Graber, E. R., Borisover, M. D., Adar, E., Nativ, R. and Ronen, Z. (2001). Sorption of organic contaminants in a fractured chalk formation. Chemosphere 44(5): 1121-1130.

Yong-Jin, K. and Masahiro, O. (2003). Leaching Characteristics of Polycyclic Aromatic Hydrocarbons (PAHs) from Spiked Sandy Soil. Chemosphere 51(5): 387-395.

Zhu, D., Herbert, B. E. and Schlautman, M. A. (2003). Molecular-level investigation of monoaromatic compound sorption to suspended soil particles by deuterium nuclear magnetic resonance. Journal of Environmental Quality 32(1): 232-239.

Zhu, D., Hyun, S., Pignatello, J. J. and Lee, L. S. (2004). Evidence for - Electron Donor-Acceptor Interactions between -Donor Aromatic Compounds and - Acceptor Sites in Soil Organic Matter through pH Effects on Sorption. Environmental Science and Technology 38(16): 4361-4368.

CHAPTER 3

Development and Optimization of a Method for the Extraction of Naphthalene in an Electrolyte Matrix

3.1. Introduction

Polycyclic Aromatic Hydrocarbons (PAH) are a chemical group whose quantitative extraction and analysis in liquid as well as solid samples has always been characterised by a tendency towards analyte losses and somewhat poor reproducibility (Bruya and Costales, 2005). Even when internal standards and standard-addition approaches are used, the extraction recoveries are not always optimal or acceptable.

The aim of the extraction step is mainly to separate the analyte of interest (i.e. pollutants) from the aqueous sample matrix. It involves the transfer of low polarity solutes from the aqueous phase into an organic solvent phase (Fifield and Kealy, 2000). The standard methods most commonly used to achieve such separations are: liquid-liquid extraction (LLE), solid phase extraction (SPE) and solid phase micro-extraction (SPME). The first and more traditional method (in all its variations) comprises the partitioning of the organic solute between the sample and an immiscible solvent (e.g. dichloromethane or DCM) using a glass separating funnel and manual shaking. Solid Phase Extraction on the other hand involves the partitioning of the solutes between the aqueous sample and a resin inside a (SPE) cartridge followed by extraction from the cartridge into a non-polar solvent (in the case of aromatic solutes). Both extraction methods, however, use large volumes of solvents which are listed as toxic substances and health hazards.

Solid Phase Micro-extraction or SPME is a fairly recent technique developed about a decade ago at the University of Waterloo in Ontario (Canada). SPME encompasses sampling and extraction in one single step therefore eliminating the need to use toxic organic solvents (such as those shown on Table 3.3) and minimizing the error associated with sample transport from the field to the laboratory. It has been referred to as 'microextraction' since the amount of solvent (sorbent volume) is small relative to the sample volume (Pawliszyn, 1997b). Given its adaptability and ease of use SPME was selected as the extraction and pre-concentration technique of choice for the samples generated in the present sorption experiments. Table 3.1 presents a comparison between the SPE and SPME extraction methodologies illustrating the reasons for choosing SPME over SPE.

This chapter describes the tailoring of SPME method to the sampling, extraction and pre-concentration of the PAH under study remaining in the supernatant of the 24 hour sorption experiments carried out with each mineral sorbent. The purpose of these experiments was to assess the capacity of the minerals to remove naphthalene from solution under given conditions by measuring how much PAH remained in the supernatant at the end of the reaction time. Section 3.2 contains a detailed description of the selected methodology. Section 3.3 covers the adaptation of SPME for the purposes described in the previous section detailing the steps of the method development. Finally, Section 3.4. consists of a description of the experiment carried out for the purposes of method validation (proof of concept experiment).

Steps	SPE	SPME
Preparation	Labelling of vials (5 per sample)	Labelling of vials (2 per sample)
	Weighting of eluant vials	
Sample pre-treatment	Requires clear samples	Samples matrix does not affect HS-SPME
Equipment Conditioning	0.5 h per sample	0.5 h (once only for new fibers)
	Requires use of organic solvents	Requires heat/high temperature
	Requires vacuum and manifold	Requires a retort clamp, stand and fiber assembly
	One SPE tube per sample	One SPME fiber for up tp 60 samples
Sampling	0.5 h per sample	3 min per sample
	Requires control of sample flowrate	Requires temperature control and ultrasonication
	Requires extra time under vacuum	End of extraction process.Sample ready for analysis
Elution of compound of interest	10 min per sample	Step not required
	Requires solvents to rinse tube	Sample ready for analysis
Eluate preparation	0.5 h -1 h per sample	Step not required
	Requires drying with Na_2SO_4	Sample ready for analysis
	Requires blowdown to constant weight	
	Requires re-dissolution in final solvent	
Analysis	10 - 20 min per sample	6.6 min per sample using manual injection
(Naphthalene only)	Normally done with autosampler	Can be done with autosampler
	Requires split injection (solvent present)	Requires splitless injection and special liner
	No special inlet device required	Specific SPME inlet guide recommended
Approximate cost per sample (£)	67.23	4.35

Table 3.1 Advantages and disadvantages of SPE and SMPE methods

3.2. SPME Technique Description

3.2.1. The SPME Device: Technical Considerations

The standard SPME assembly consists of two parts: a stainless steel support to which the fibre is glued, and a metal holder. A schematic diagram of an SPME assembly is shown below (Figure 3.4). The holder consists of a hollow needle that encases the fibre and an adjustable barrel that can be rotated to the needle depth. The fibre is made of fused silica coated with a liquid polymeric phase (for these experiments).

The plunger inside the barrel is pressed down to expose the fibre and then rotated and locked into the Z-slot to secure it in place. A photo of the dismantled SPME fibre assembly is shown in Figure 3.1.

The complete

assembly can be held above the sample or (Figure 3.2) the injector (Figure 3.3). by means of retort clamps and an inlet guide, designed specifically to hold the fibre in place at the injection ports of several GC systems.

Figure 3.1. (1) Different parts of a SPME assembly, (2) fibre inserted in needle casing, (3) fibre casing is assembled with holder and (4) assembled SPME

Figure 3.2 SPME assembly during the sampling stage.

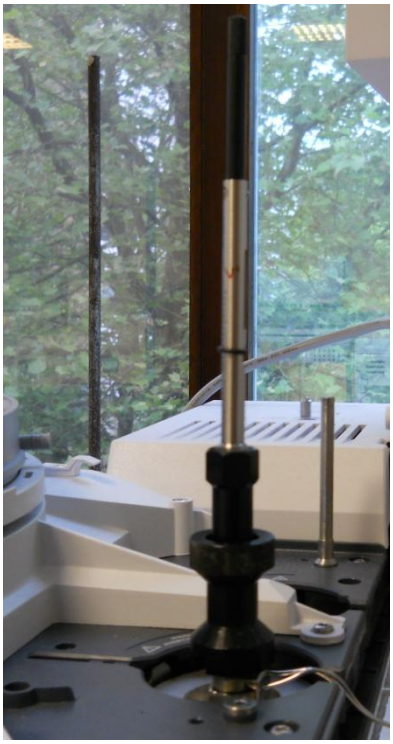

Figure 3.3 SPME assembly inside injector during the desorption stage.

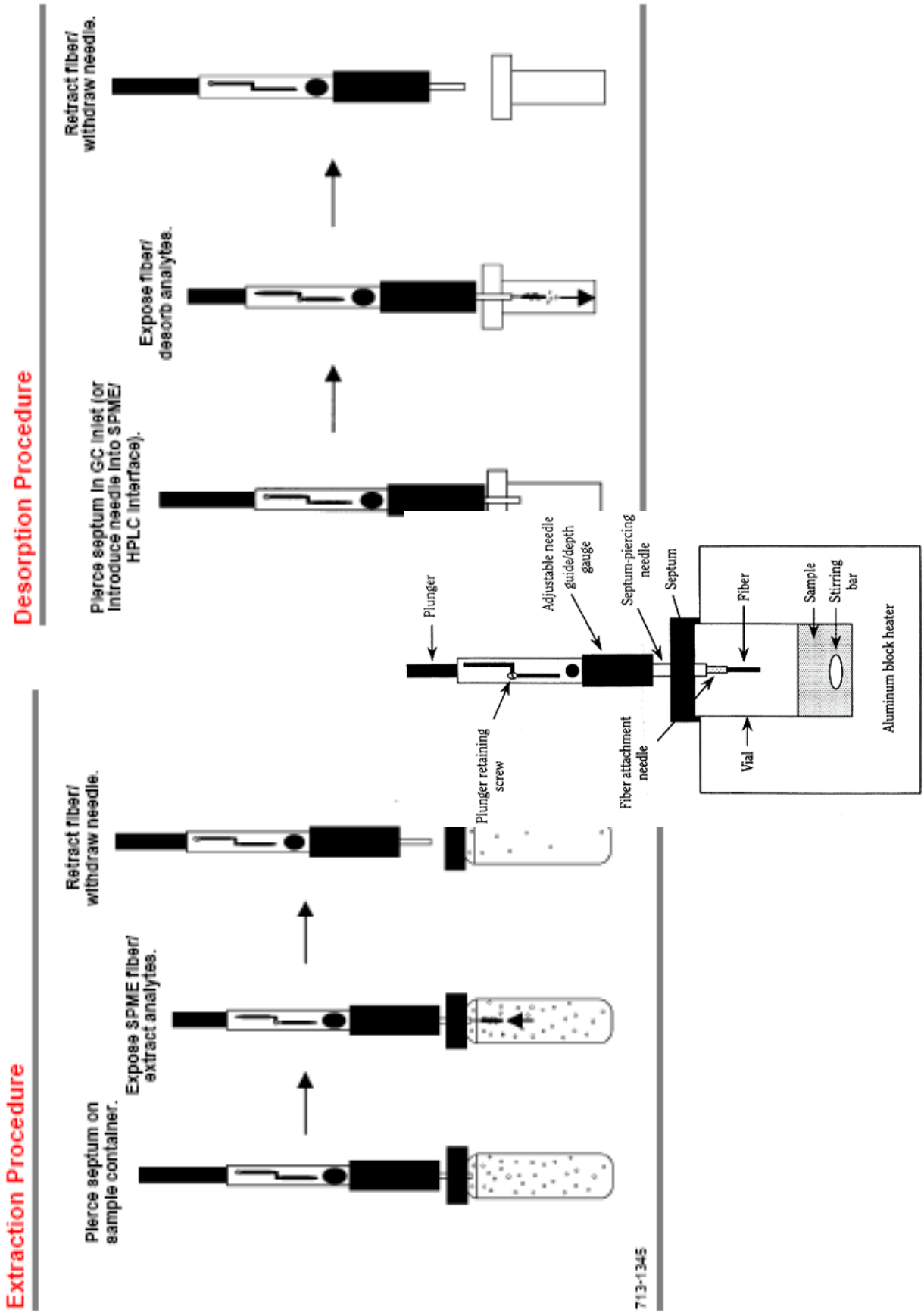

Figure 3.4. Parts of an SPME fibre assembly (SUPELCO, 2001)

Like with any other extraction method each sample extracted using SPME has an optimal set of conditions which when not taken into account could render the analysis inadequate or lead to erroneous results. These conditions will vary depending on the analytes under study and the background matrix in which these are found.

In general, the device is deceptively simple to handle, but in spite of the inherent robustness of the SPME assembly, care must be exercised to avoid touching the needle to avoid structural damage and contamination; rotating the barrel instead in order to bring the needle to the desired depth. After sampling the fibre is placed inside the heated injector of a gas chromatographer and the solutes are thermally desorbed from the exposed fibre and swept into the column with the carrier gas (helium).

When new, the fibres must be conditioned previous to first use (following manufacturer's instructions) or "desorbed" before and after every extraction step. A fibre blank should always be run before that of any samples or standards in order to ensure the fibre is not contaminated.

The SPME-sampling and extraction protocol developed for blanks, standard and samples, is described step by step in Section 3.4. The handling instructions using a manual SPME holder are outlined in Appendix A3. The extraction and GC-FID conditions are summarized below in Tables 3.3 and 3.4:

3.3. Method Development

3.3.1. Selection of Fibre Coating

The main principle in the coating selection is the chemical affinity of the analyte for the material. Properties such as volatility and polarity are the basis for the selection. Poly(dimethylsiloxane) or PDMS is a generic liquid coating commonly used in chromatographic separations as the stationary phase in capillary columns. PDMS is a non-polar phase, well suited for compounds of low to medium polarity (Pawliszyn, 1999). A number of workers have successfully used it to analyse low molecular weight PAH (Doong *et al.*, 2000b; King, 2003; Rianawati and Balasubramanian, 2009) Given the high partition coefficient between naphthalene and PDMS, the latter was the selected extraction phase.

With regards to fibre size, a 30 µm diameter represented a good compromise between the two other available sizes, namely, 7 µm (rapid sorption and desorption but very fragile fibre) and 100 µm (best analyte uptake but greater carryover between samples due to slow thermal desorption). All new fibres were conditioned following the manufacturer's guidelines, after which fibre blanks were run to ensure no contamination was already present on the fibres.

3.3.2. Sample Volume

Pawliszyn and coworkers (Pawliszyn, 1997b) estimated the minimum sample volume required for a successful mass transfer at equilibrium (Figure 3.5). The flat section of the equilibrium lines indicates a constant, maximum

uptake for a specific analyte (naphthalene), a given fibre diameter (30 µm) and the selected sampling mode (HS). According to this graph and using the

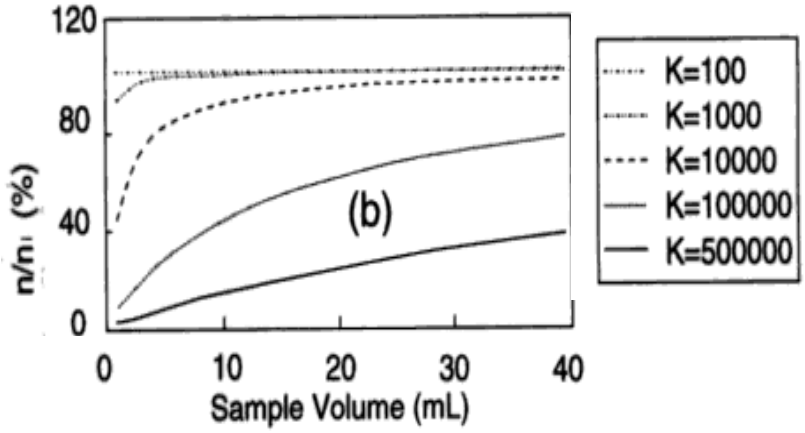

Figure 3.5 Effect of sample volume on extraction efficiency for a 30 µm fibre spanning a range of distribution constant values (K). (Adapted from Pawliszyn, 1990)

appropriate equilibrium distribution constant for naphthalene in water (K = 1000), a sampling volume of 5 mL is above the minimum required volume and therefore adequate for these experiments. Availability for vials of the required size is a common problem in laboratories and places constrains when choosing the best sampling volume but 5 ml sized samples in 10 ml vials seemed to be a good compromise. In addition, due to the flexibility of the SPME technique, the sample volume does not affect the results provided it does not go below the minimum required and is kept constant for all samples, blanks and standards.

3.3.3. Sampling Time

Several authors have reported that the typical equilibration time for naphthalene between a PDMS fibre and pure water is of the order of 1 hour

(Doong *et al.*, 2000c). This was corroborated early in this study (see Figure 3.6). In most of the studies, however, the target analytes often included more than one semivolatile PAH, which made it necessary to allow longer times in order for the system to reach equilibrium given the differences in partition coefficients of the analytes. Since the target analyte in this study was only naphthalene and in order to significantly reduce the sampling time, all samples were extracted in the pre-equilibrium mode, carefully controlling the time (5 minutes) to avoid gross errors in the reported GC-FID areas of the sample triplicates (Figure 3.6).

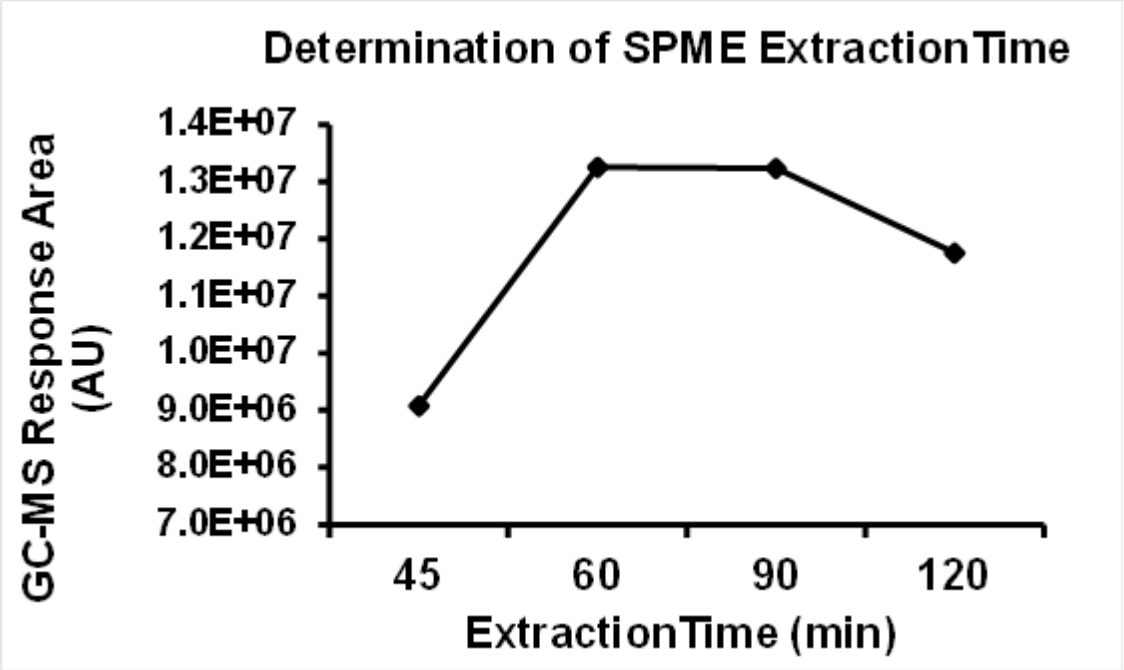

Figure 3.6 Graph showing the GC-MS area as a function of the sampling time obtained when extracting naphthalene using DI-SPME.

3.3.4. Sampling Mode: Direct Immersion or Head Space

The sampling or sample extraction can be carried out either in the gas phase above the sample (headspace sampling) or in the liquid phase (immersion sampling). Headspace extraction is adequate for solid as well as aqueous matrices. In the case of immersion sampling the fibre is exposed to the liquid sample and the solutes are transferred from the sample matrix onto the fibre coating, until an equilibrium is reached between the liquid and the polymer phase (sampling and extraction step) and as a result the fibre coating becomes saturated with the analyte (Pawliszyn, 1997b).

During the first experimental stages, all samples were extracted in the Direct Immersion mode (DI). It was immediately observed that the fibres showed significant signs of damage and breakage after approximately 25 extractions. Previous tests have shown that on average a fibre can be used normally between 40 and 50 times before it needs replacement. In these preliminary experiments this number was significantly reduced by 25 – 50% when compared to extractions in pure water and it was observed upon visual inspection that all fibres showed signs of severe damage. SEM analysis of the damaged fibres showed how the background electrolyte seemed to be damaging the polymer coating, to the point of exposing the fibre core in some cases. SEM pictures comparing a new fibre (a) to the surfaces of damaged fibres (b, c and d) are shown on Figure 3.7 below.

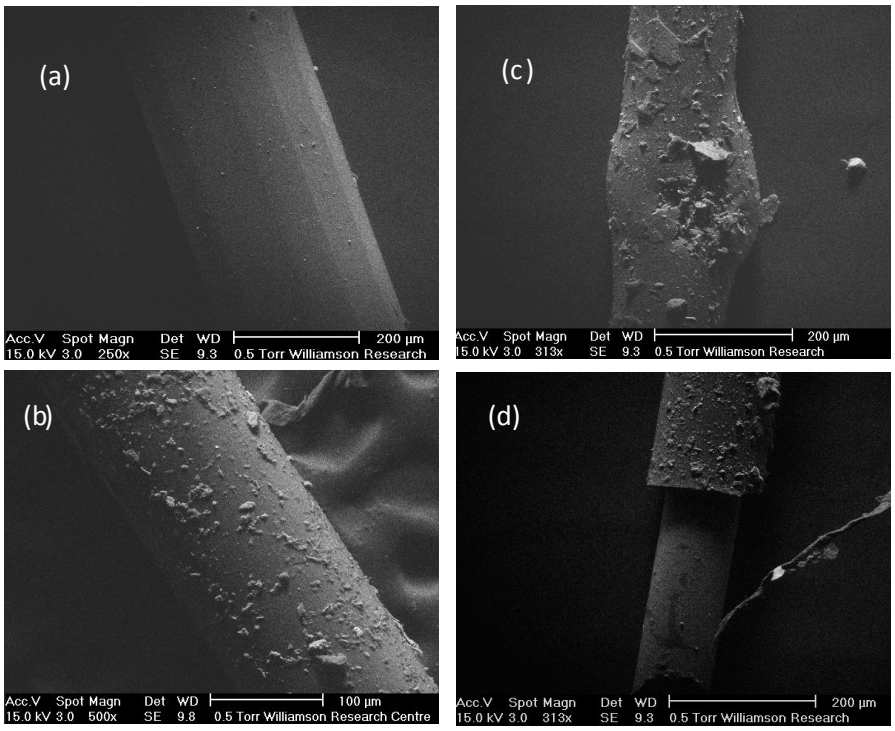

Figure 3.7 SEM pictures showing new fibre (a) and damage in different parts of the same fibre (b - d) after 25 or more extractions in DI mode.

After observing the extent of the damage to the fibres, all sampling was conducted in the headspace. Pawliszyn and co-workers recommend HS-SPME for organics with a Henry's constant of at least 90 atm. cm^3. mol^{-1}. This makes naphthalene an excellent candidate for headspace extraction with a high Henry's constant of 4500 atm. cm^3. mol^{-1}.

3.3.5 Extraction Temperature and Agitation

All extractions were performed at 40 ºC. The temperature was controlled by means of a water recirculating unit (Haake Recirculator, Model G). In order to avoid cross contamination and maximise the agitation efficiency, ultrasonic

agitation for 3 minutes was used instead of stirring bars. The samples were placed inside a custom-made hollow sample-pod (see Figure 3.8) connected to the recirculating unit via tubing and this was kept immersed inside a Grant ultrasonics bath.

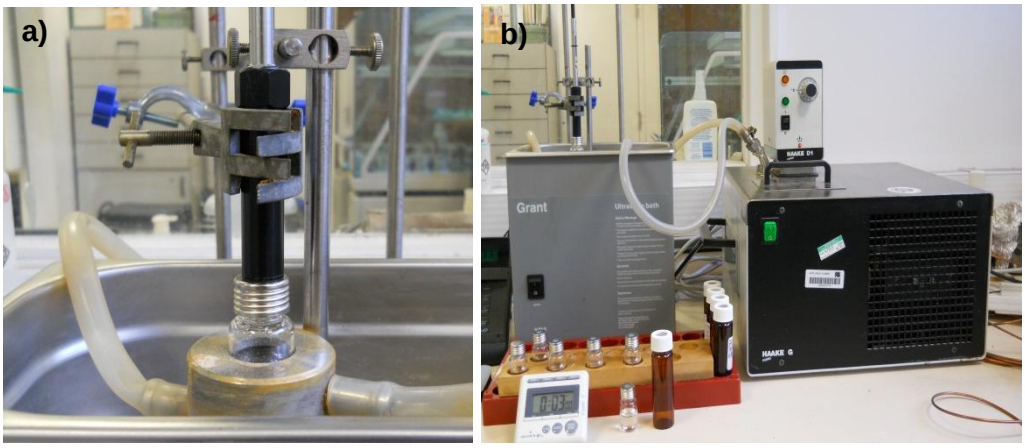

Figure 3.8 SPME extraction rig. (a) Sample pod with vial and SPME assembly, (b) ultrasonic bath (left) and recirculating unit (right).

Agitation is important as it reduces the sampling time and optimises the diffusion of analytes from the sampling phase towards the fibre coating. This increases the method's sensitivity and overall efficiency.

3.3.6. Addition of Salt

The addition of NaCl (up to concentrations of 30 % w / w) is recommended as means of increasing the analyte's partition onto the fibre and therefore lowering the limit of detection for very dilute solutions (Pawliszyn, 1999). For the purpose of the present experiments, NaCl was not added to the extraction samples at any point since naphthalene has a very high volatility (see Table 3.2) in which case the addition of salt is not necessary. The SPME extraction conditions are summarized in Table 3.2 below.

SPME Extraction Method	
Extraction	
Matrix	$NaNO_3$ 0.001 M
Method	Pre-Equil. HS
Sampling Depth	0.6 cm
Vial Location	Water jacket
Stirring	Ultrasonic bath
Temperature	40 ^{o}C
Sampling Time	3 minutes
Fiber Material	PDMS
Fiber Thickness	30 μm
DESORPTION (PTV INLET)	
Depth	3 cm
Temperature	280 ^{o}C
Time	6.6 minutes

Table 3.2 SPME extraction parameters.

3.3.7. Desorption

Immediately after extraction the fibres were inserted into a PTV (Programmed Temperature Vaporization) injection port in an Agilent 7890A GC-FID. The injector sleeve was equipped with narrow bore, CIS4 Gerstel liners made of deactivated glass (Anatune Ltd, UK). The carrier gas was helium with a linear velocity of 1 mL / minute and the injector temperature was kept constant at 280 °C. All samples were injected on splitless injection mode. The temperature of the FID detector was 320 ºC. The column was a HP-5 Agilent capillary column (30 m x 250 μm x 0.25 μm). The GC oven programme followed was: 70 ºC initially followed by 25 ºC / minute up to 160 ºC for 3 minutes. The total GC run time was 6.6 minutes. No carry-over was observed during subsequent alternate injections of 2 different fibres of the same specification. The GC-FID operational conditions are summarized in Table 3.3.

GC Apparatus: AGILENT 7890A GC SYSTEM

COLUMN	**HP5 AGILET 30 m x 250 µm x 0.25 µm**
INLET	**PTV, P = 11.799 psi**
CARRIER GAS FLOW	**1 mL / min**
MODE	**SPLITLESS**
INLET NUT	**SPME GUIDE**
SEPTA	**PRE-CORED THERMOGREEN LB-2**
EQUIL. TIME	**0.5 min**
TOTAL TIME	**6.6 min**
GC-PROGRAMME	**70 °C (0) UP TO 160 °C (3 min) AT 25 °C / min**
INJECTOR TEMP.	**280 °C**
NARROW BORE LINER	**GERSTEL DIRECT LINER CIS4 FOR PTV**
DETECTOR	**FID**
TEMPERATURE	**320 °C**
H_2	**40 psi**
AIR	**400 psi**
MAKE UP GAS	**25 psi**

Table 3.3 GC conditions for SPME desorption.

The symmetry and intensity of the chromatographic peak obtained for naphthalene with this method of extraction and analysis is shown in Figure 3.9.

3.3.8. Precision

The precision of the method was calculated using the GC-FID peak areas obtained for 10 standard dilutions prepared and extracted in identical manner, on the same day and with the same SPME fibre. These dilutions were prepared by adding the same volume of a commercial naphthalene stock solution to 10 vials with identical volumes of the same background electrolyte. The result is expressed as the relative standard deviation (RSD %) from the

mean in percentage units. It yielded values between 0.00 and 6.59 % (n = 10). The formula used to calculate the RDS % is shown as Equation 3.1. The raw data for these calculations are in Appendix A3.

$$RSD\% = \frac{\sigma}{\bar{x}} \times 100 \quad (3.1)$$

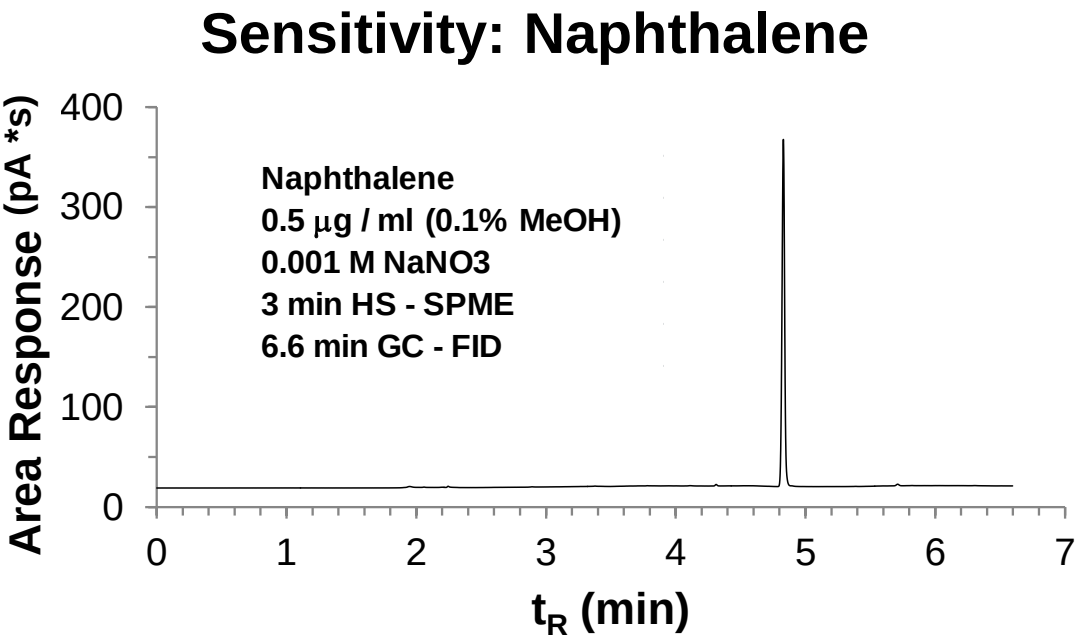

Figure 3.9 GC-FID response to a 0.5 mg / l naphthalene standard.

3.3.9. Reproducibility

The same equation was used to calculate the spread of the GC - FID areas of 10 standard dilutions prepared on different days and extracted with the same SPME method (see Appendix A3). The result represents the reproducibility or inter-day precision of the method and it varied between 5.33 and 11.18 % (n = 8). The extractions were carried out using the same set of (two) fibres throughout. This calculation was used to assess the fibres deterioration and would alert as to when a new fibre was required.

3.3.10 Linearity of the Method: GC-FID

GC-FID is well known for yielding good linearity in calibration curves spanning several orders of magnitude. This was the case for the calibration curves carried out by spiking a commercial standard into aqueous electrolyte solutions of identical composition to all samples and blanks, and extracting them using the same HS-SPME method. The linear range (correlation coefficients, R^2, between 0.9825 and 0.9983) extended 5 orders of magnitude, from 1 mg / l down to 0.0002 mg / l.

3.3.11 Limit of Detection

A calibration curve obtained with a series of very low dilutions (0.0002 – 1.0 mg / l) in electrolyte of a commercial naphthalene standard was obtained to determine the method's lower limit of detection. Serial dilution was avoided in favour of direct spiking in the case of aqueous solutions, but not in the case of the set of sub-standards in methanol. The lowest concentration at which a response ≥ 10 times the signal/noise ratio was achieved was 0.2 ppb (0.0002 mg / l, n = 2, RSD% = 0 see Appendix A3).

3.4. Method Validation: Proof of Concept

When developing a new extraction method or modifying an existing one in analytical chemistry it is customary to assess its efficiency by extracting certified standards containing the target analyte in the experimental matrix. For the purposes of the tailoring of the SPME technique to the extraction of naphthalene in electrolyte samples, a preliminary experiment denominated Proof of Concept was carried out. In this assay, a well known PAH scavenger

(granulated activated carbon, or GAC) was mixed up with quartz sand in a series of samples in order to analyse naphthalene uptake by SPME.

The capability of the method to detect very low amounts of this PAH in scenarios where removal would be complete or nearly total (depending on degree of exposure to GAC) would demonstrate the technique is appropriate for cases where the sorptive power of the selected sorbents would be much less than that of activated carbon (i.e. sorbents such as minerals with very low organic matter content).

Based on this rationale, a series of sorption experiments using a mixture of commercial activated carbon and pre-treated quartz sand were carried out in order to extract and quantify naphthalene in the remaining supernatant. The results helped to pinpoint the steps where modifications were necessary in order to increase the method's efficiency for the subsequent extraction of mineral-PAH samples. The experimental details and results are presented in the following sections.

3.4.1. Proof of Concept Experiment: Introduction

One approach to understanding the environmental fate of organic pollutants is to study a single representative contaminant. In this study, Granulated Activated Carbon F200 and pre-treated quartz sand with low organic carbon content were selected as test materials to assess the feasibility of Headspace-Solid Phase Microextraction coupled to Gas Chromatography-Flame Ionization Detector (HS – SPME - GC / FID) for the rapid analysis of a representative PAH (naphthalene) in an electrolytic solution was studied. The excellent capabilities of carbon to remove naphthalene from water are well

known, as is the characteristic low uptake of this organic exhibited by quartz sand. The experiments were designed to demonstrate the advantages of using HS-SPME in the analysis of such a widespread and representative environmental pollutant at relatively low solution concentrations (0.5 µg / ml) which emulate those typical of a complex natural system. Previously proposed extraction parameters for naphthalene in pure water were modified to encompass a background solution with different compositions. Extractions were run under pre-equilibrium conditions using mechanical agitation with pre-silanised glass-coated stir bars at ambient temperature. The extraction time was successfully reduced from 1 hour to just 5 minutes. Results are in agreement with the expected sorptive behaviour for both sorbents. The generated isotherms follow the expected trend proving that pre-equilibrium HS - SPME is very well suited for the fast and precise analysis of semivolatiles whilst avoiding lengthy extraction times. External calibration under identical conditions was carried out for quantification. Linearity was found to span at least 5 orders of magnitude (0.0002 to 1.5 ng / µl); RDS% of same-day triplicates ranged between 0.03 – 15 % and inter-day RDS% for freshly prepared identical samples extracted with the same method was 13 %.

3.4.2. Reagents and Apparatus

The electrolyte background solution (0.001 M) was prepared using $NaNO_3$ (Aldrich, A.C.S.) previously dried at 120 ºC overnight. The naphthalene standard (5000 mg / l) was purchased as a solution in methanol (Sigma Aldrich Ltd, UK). Granulated activated carbon (GAC) graded F200 was kindly supplied by Chemviron Carbon UK and was used after boiling in water, then drying in an

oven at 120 ºC overnight. The commercial quartz sand (VWR) was purchased previously washed in HCl and calcined at 900 ºC by the manufacturer. This guaranteed a mineral with very low levels of organic carbon. The properties of the sorbent materials used are outlined below on Table 3.4 along with the respective composition of the mixtures used in each experiment. The deionised water used throughout was produced by a Purelab Option - R7 / 15 water system (15 MΩ $cm^{-1,}$ Elga Water).

3.4.3. Glassware Conditioning

The reaction vials used were commercially pre-washed 15 mL SPME clear-glass vials with black phenolic screw caps and PTFE / silicon septa (Sigma Aldrich Ltd, UK). The extraction vials were clear glass, SPME 10 mL vials with magnetic screw caps and PTFE / silicon septa (Sigma Aldrich Ltd, UK). All vials were used without further conditioning except in the experiments with 100 % quartz sand when the vials were custom-silanised using dichloro-dimethyl-siloxane (DCDMS) (Sigma Aldrich Ltd, UK). This precaution was taken to avoid analyte losses to the vial walls, due to the low naphthalene uptake exhibited by this mineral.

3.4.4. Sample Preparation

Samples, blanks and standards were prepared following the same protocol. Sorbents were weighed into the vials in the proportions required for each run followed by addition of the electrolyte ($NaNO_3$, 0.001 M). When required, samples were spiked with a fixed volume of a commercial

naphthalene standard (200 or 5000 mg / l) in methanol (Sigma Aldrich Ltd, UK.). To avoid co-solvent effects in the matrix, the concentration of methanol was kept below 0.01 %.

All the vials were closed and sealed with PTFE tape, wrapped in aluminium foil and manually agitated at regular intervals for the duration of the selected reaction time. Manual agitation was used in order to avoid creating carbon and / or sand fines due to friction between the sorbents, as was the case when a mechanical shaker was used. A blank was run with each set of samples to ensure absence of cross-contamination.

SPECIFICATIONS	Quartz Sand	F200 GAC
PS (µm)	250 - 500	600 - 800
BET_{SA} (m^2/g)	0.1689	613.8008
TOC (%)	0.0048	N/A
LOI (%)	0.0207	N/A
Density (g/cm^3)	2.6321	1.4-1.5
Floating content (%)	N/A	0.1
Mixture 1	100%	0%
Mixture 2	50%	50%
Mixture 3	10%	90%
Mixture 4	0%	100%

Table 3.4 Specifications for the selected materials.

3.4.5. HS-SPME Extraction Procedure

At the end of the reaction times, identical aliquots (5 ml) of the supernatant of all triplicates were transferred to SPME extraction vials and extracted in the headspace (HS - SPME) by piercing the septa on the screw caps and exposing the fibre to the headspace for 5 minutes. Glass-coated stir bars were placed inside all extraction vials. Two stirring plates (Ika® Werke RCT Basic and Bibby Stuart) were used in tandem with equivalent rpm settings to stir the samples during extraction. To avoid the gradual increase in temperature of the vials by being in contact with the plates (which heated up

due to continuous use) the vials were held 3 mm above the plate using a retort clamp.

The fibre phase used was 30 µm Polydimethyl siloxane (PDMS) inserted in a manual holder.(Sigma Aldrich Ltd).After piercing the septum, the fibre was positioned exactly 0.6 cm into the headspace phase by downwards rotation of the needle housing. At this point the plunger was pressed and secured into the Z-slot in order to expose the fibre. The headspace was calculated as the difference between the weight of a full vial minus that of a vial filled with 5 mL of sample. The samples were extracted at room temperature. All fibres were replaced by new ones after either 50 extractions in the headspace or visible damage.

3.4.6. Results and Discussion

The results were expressed as the percentage of naphthalene removed by the sorbent mixture relative to the initial concentration of this analyte in all samples. It was calculated as the blank-normalised percentage of the ratio between the GC-FID areas obtained for the samples and those corresponding to run blanks prepared identically to the samples minus the sorbent phase. The sorption curves for all sorbents at five different reaction times are shown on Figure 3.10.

The results show how tailoring the simple, fast extraction technique of HS-SPME yielded efficiency comparable to samples extracted using traditional techniques such as the Liquid – Liquid – Extraction method (LLE) for a series of organic micropollutants (Guillot *et al.*, 2006) and the Purge and Trap / GC / MS

method for the analysis of MTBE and TBA (Stringfellow and Oh, 2005). The sorption of naphthalene by mixtures consisting mostly of activated carbon is virtually instantaneous, reaching almost complete removal with subsequent

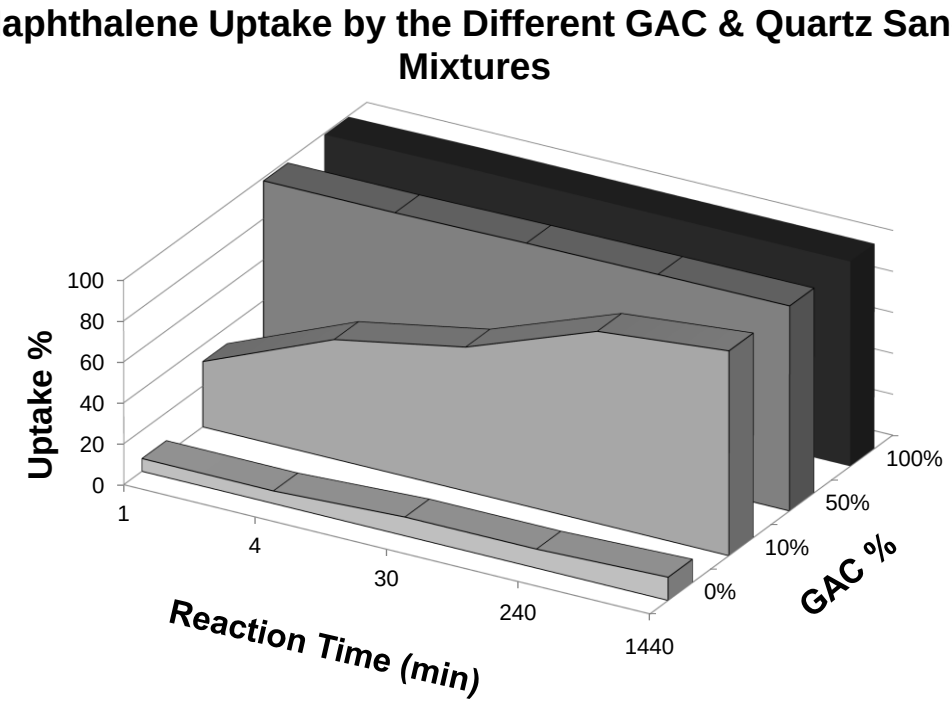

Figure 3.10 Sequential removal of naphthalene by the GAC - Quartz Sand mixtures.

increase of the contact time. On the other hand, uptake of naphthalene by quartz sand is low and increases only slowly with time. After 24 hours, when most of the naphthalene has been removed even by mixtures with only 10 %

Rxt (min)	Average Naphthalene Removal			
	100% GAC	50% GAC	10% GAC	0% GAC
1	99.42	98.48	31.90	6.24
4	100	98.52	58.30	6.09
30	100	99.31	70.28	9.09
240	100	99.71	93.64	9.20
1440	100	100	99.77	11.25

Table 3.5 Removal of naphthalene by each sorbent mixture at different reaction times.

activated carbon, the removal percentage of pure sand only reaches a maximum of 12 %. This trend agrees with previous experimental results when a tenfold increase of the amount of sand used in these experiments, and no other sorbent, only achieved a naphthalene removal of 20 % after 24 hours using continuous gentle agitation.

Direct immersion in a salt solution (0.1 M, $NaNO_3$) (compared to water alone) caused substantial damage (see detachment from needle core in Figure 3.7 (d)) to the fibres and reduced their lifetime almost by half. Subsequently, all extractions were performed in the gas phase into which naphthalene partitions well, even at ambient temperatures.

The 1-day reproducibility of standard replicates can be improved by either automation using a Combi Pal system or by keeping the extraction temperature constant. The RSD obtained (≤ 20 %) are those expected for manual sampling and have been reported by other workers (King, 2004).

The reproducibility for extractions of the same standard on different days expressed as 10-day RSD % (≤ 26 %) could improve if rigorous temperature controls are available. Extractions performed at ambient temperature can be affected to a great extent by laboratory temperature fluctuations unless temperature control is exerted.

The linearity achieved by the method is satisfactory, spanning several orders of magnitude when used in conjunction with GC - FID.

The lower detection limit reached with the present method (0.2 ppb) is the same as the EPA Maximum Contaminant Level (MCL) in drinking water (0.2 ppb) for the designated PAH representative, benzo[a]pyrene (BaP). This means

that the method can be easily be improved further in order to reach lower the detection limits within an acceptable error margin, not just for naphthalene but also for other, less soluble PAH. One such modification could be sampling in the headspace at higher than ambient extraction temperatures, which would force less volatile PAH from the solution into the gas matrix, thus reducing the sampling time and increasing the amount of analyte transferred to the SPME fibre.

3.4.7. Conclusions

An extraction system consisting of headspace Solid Phase Microextraction (HS - SPME) was tailored and modified to enable the rapid pre-concentration of naphthalene with the purpose of comparing the uptake curves to those obtained in similar experiments using traditional extraction techniques. This was attempted by exposing naphthalene in a dilute electrolyte solution to a mixture of well known sorbents, one of which (GAC) is routinely used in wastewater and water treatment.

The modification significantly improves the already effective technique by reducing the sampling time to 5 minutes (a factor of 12) and extending the lifetime of the fibres. Customary sampling and pre-concentration times in traditional extraction techniques are normally much longer (of the order of hours for naphthalene). The modification of the recommended SPME protocol for naphthalene consisted of the reduction of the sampling time by using pre-equilibrium SPME and employing a less thick fibre 30 μm (as opposed to 100 μm).

As this study shows, SPME is an accurate and fast technique for extraction and pre-concentration in systems other than pure water. Damage caused to the fibre coatings due to some environmental sample matrices can be completely avoided by sampling in the headspace.

Better precision and much lower detection limits could be achieved by using an automated sampling system, by implementing temperature control, by using sample ultrasonication instead of stirring bars and by adding NaCl to the sample aliquots to increase the analyte's mass transfer onto the fibres. The latter poses a distinctive advantage for toxic semivolatiles found at very low environmental concentrations.

The results of the experiments carried out in this work helps to illustrate how SPME is well suited for the analysis of PAH in aqueous matrices. For the last decade this method continues to grow in use and acceptance given its versatility and ease of use. SPME represents a great advantage for environmental chemists and regulatory agencies since it eliminates lengthy sample preparation steps and, if appropriate analytical parameters are selected, it can considerably greatly reduce the time needed per sample. Furthermore; since PAH are so diverse a chemical group, tailoring SPME to extract specific member of the series could represent the way forward when trying to circumvent the analytical problems so far encountered when applying more traditional extraction approaches.

It is expected that this tailored application of SPME will be appropriate when applied to the studies concerned with the interactions of other semivolatile PAH with pure mineral phases in similar matrices, including more toxic

naphthalene derivatives such as nitro and methyl-naphthalenes, as well as chlorinated phenols.

References

Doong, R., Chang, S. and Sun, Y. (2000a). Solid-phase microextraction for determining the distribution of sixteen US Environmental Protection Agency polycyclic aromatic hydrocarbons in water samples. Journal of Chromatography A 879(2): 177-188.

Doong, R. A., Chang, S. M. and Sun, Y. C. (2000b). Solid-phase microextraction and headspace solid-phase microextraction for the determination of high molecular-weight polycyclic aromatic hydrocarbons in water and soil samples. Journal of Chromatographic Science 38(12): 528-534.

Fifield, F. W. and Kealy, D. (2000). Principles and Practice of Analytical Chemistry, Blackwell Science. pages.

Guillot, S., Kelly, M. T., Fenet, H. and Larroque, M. (2006). Evaluation of solid-phase microextraction as an alternative to the official method for the analysis of organic micro-pollutants in drinking water. Journal of Chromatography A 1101(1-2): 46-52.

King, A. J., Readman, J. W. and Zhou, J. L. (2003). The Application of Solid-Phase Micro-Extraction (SPME) to the Analysis of Polycyclic Aromatic Hydrocarbons (PAHs). Environmental Geochemistry and Health 25(1): 69 - 75.

King, A. J., Readman, J. W. and Zhou, J. L. (2004). Determination of Polycyclic Aromatic Hydrocarbons in Water by Solid-Phase Microextraction-Gas

Chromatography-Mass Spectrometry. Analytica Chimica Acta 523: 259-267.

Pawliszyn, J. (1999). Applications of Solid Phase Microextraction. Bodmin, The Royal Society of Chemistry. pages.

Pawliszyn, J., Pawliszyn B. and Pawliszyn M. (1997). Solid Phase Microextraction (SPME). The Chemical Educator 2(4).

Rianawati, E. and Balasubramanian, R. (2009). Optimization and validation of solid phase micro-extraction (SPME) method for analysis of polycyclic aromatic hydrocarbons in rainwater and stormwater. Physics and Chemistry of the Earth, Parts A/B/C 34(13-16): 857-865.

Stringfellow, W. T. and Oh, K. C. (2005). Comparison of SPME Headspace Analysis to U.S. EPA Method 5030/8260B for MTBE Monitoring. Ground Water Monitoring and Remediation Volume 25 (Issue 2): 52 - 58.

SUPELCO. (2001). Solid Phase Microextraction Troubleshooting Guide. Bulletin 928. Retrieved 19/06/2006].

CHAPTER 4 Sorption Experiments

This chapter presents the sorption experiments carried out using several minerals and the selected PAH in aqueous solutions of the same electrolyte at three different concentrations.

Section 4.1 encompasses the preliminary processes carried out in preparation for each experiment, namely the required conditioning for all the glassware as well as the sorbents and sample preparation protocols.

Section 4.2 describes the set-up for the sorption experiments, where the minerals' capacity to remove naphthalene from solution under specific conditions is measured indirectly, by analysing the remaining PAH in the supernatant at the end of each reaction time.

Section 4.3 comprises a description of the selected analytical method (GC - FID), as well as the protocol followed, to obtain standard calibration curves and to analyse the samples generated.

Section 4.4 contains the calculations for all the parameters used for the purposes of quantification.

Section 4.5 presents the results from each sorption experiment as tables and plots of the appropriate parameters as a function of either ionic strength of the background solution or of the mineral phase used.

4.1 Preliminary Preparations

The experiments carried out required several stages of preparation, specifically in regards to the glassware and materials used. Each of these stages is described in detail in the following sections.

4.1.1 Glassware Conditioning

The glassware used in the experiments was conditioned following the protocol described in detail as follows (Fifield and Kealy, 2000):

All glassware was immersed in an acid bath (HNO_3 5 %) for 48 hours followed by 3 rinses with deionised water (DIW). The next stage involved immersion in DECON 90 detergent for 24 hours after which each piece is scrubbed and rinsed 3 times with tap water, followed by 3 rinses with deionised water. The glassware should be dried in the oven over aluminium paper with the exception of volumetric glassware. Upon cooling, all glassware is covered with pre-baked aluminium paper (300 °C) and stored.

4.1.2 Silanisation

Losses to the walls of vessels containing aqueous solutions of non-polar organics such as naphthalene have been reported by workers conducting similar studies (Ackerman and Hurtubise, 2000; Qian *et al.*, 2011). Since sorption of hydrophobic PAH molecules by minerals is distinctively low, all glassware needed to undergo preconditioning in order to prevent significant loss of organics by adsorption onto the vial walls. Silanization of glassware is a

standard coating procedure used for deactivating the surfaces of chromatographic columns and other related laboratory glassware. The reagent used for this purpose is dimethyldichlorosilane or DMDCS. When this chemical is put into contact with a glass surface (glass vials) it reacts by binding itself to the surface forming a permanent film. This makes the surface extremely hydrophobic and acts as a barrier which prevents exposure of potentially active sorption sites on the glassware (hydroxyl sites to the organics under study. The DMDCS molecule along with its chemical properties is shown in Table 4.1.

Dimethyldichlorosilane (DMDCS)	**$(CH_3)_2SiCl_2$**
CAS Number: 75 - 78 - 5 MW: 129.06 mol / g BP: 70℃ at 1 atm Density: 1.064 g / cm^3 Very toxic Flammable	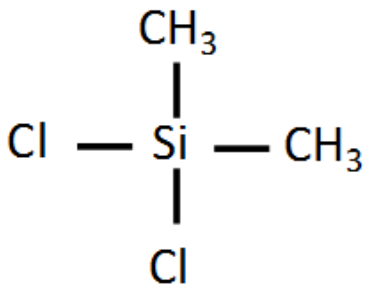

Table 4.1 Properties of silanising agent DMDCS.

The procedure for silanisation consists of soaking pre-cleaned and dried glassware in a solution of silanising agent (DMDCS) at 15 % (v / v) in toluene overnight, then rinsing twice with toluene followed by three rinses with methanol and drying at 180 ºC in the oven. The toluene rinses are required to dissolve and get rid of any un-reacted DMDCS whilst the methanol rinses wash off the toluene. All reaction and extraction vials were silanised at least one week in advance to each sorption experiment and were used straight from the oven or stored in an enclosed environment wrapped in aluminium foil (Doong and Chang, 2000).

4.2 Experimental setup

4.2.1 Reagents and Materials

Chemicals:

EPA 610 Polynuclear aromatic hydrocarbon mixture in methanol & methylene chloride (SUPELCO Cat. No. 48743)

Methanol (Pestanal; SUPELCO Cat. No. 34485)

Deionised water (DIW) (15 µS / cm)

Methylene Chloride Pestanal (SUPELCO Cat. No. 34488)

Sodium nitrate (VWR)

Quartz sand, acid-washed and calcined (Merck Cat. No. 1077121000)

Equipment:

SPME Fibre Holder for Manual Sampling (SUPELCO Cat. No. 57330-U)

PDMS fibres, 100 µm thickness, pack of 3 (SUPELCO Cat. No. 57300-U)

Hamilton syringes: 25 and 100 µL (SUPELCO Cat. No. Z109231, 20790-U)

IKA Werke RCT Hot plate/magnetic stirrer with temperature control

Stirring magnetic bars (5 cm) (SUPELCO)

Thermogreen LB-2 Septa 17 mm diameter (SUPELCO Cat. No. 23159)

Inlet Liner for SPME, 0.75 mm internal diameter (SUPELCO Cat. No. 2876601-U)

Amber Glass Vials 40 mL (SUPELCO Cat. No. 27010-U)

4.2.2 Sorbates

Commercial solutions of the PAH used were obtain from Sigma Aldrich (naphthalene Cat. No. 40053, phenanthrene Cat. No. 40079).The purpose of this research is to determine the adsorptivity of naphthalene as a representative PAH molecule onto 4 different pure mineral phases.

The reasons behind this selection include naphthalene's lower toxicity and higher aqueous solubility, which enabled the use of several concentration ranges all under its solubility limit. In addition to that; naphthalene's wide industrial use and persistence in the environment, make it ubiquitous and therefore an important target for environmental contamination studies.

Phenanthrene was included as a validation sorbate in the last set of experiments. This was done in order to compare results in terms of aqueous solubility. The properties of both PAH are shown in Table 4.2.

Properties [a]	Naphthalene	Phenanthrene
Molecular weight (g / mol)	128.17	178.18
Molecular Formula	$C_{10}H_8$	$C_{14}H_{10}$
Density (g / cm^3)	1.14	0.98
Boiling Point (℃)	218	340
Melting Point (℃)	80 - 82	98
Solubility in water (mg / l)	31.7	1.23
Flash Point (℃)	79 - 87	n / a
Vapor Pressure (mm Hg)	0.03	6.8×10^{-4}
log K_{OW} [b]	3.3	4.45
Henry's Constant (atm m^3 / mol)	3.0×10^{-4}	2.56×10^{-5}
Autoignition temperature (℃)	525	n / a
Appearance	white flaky crystals	colourless white crystals
CAS-Number	91 - 20 - 3	85 - 01 - 8
(a) Properties valid at standard conditions (25℃ and 1 atm)	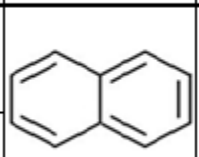	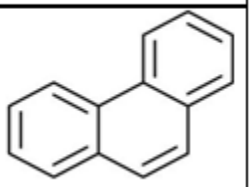
(b) Octanol / water partition coefficient		
Sources: Merck, 1989; ToxProbe by Toronto Public Health Report, 2002.		

Table 4.2 Physicochemical properties of selected PAH.

Solvents	MW (g/mol)	Formula	BP (°C)	MP (°C)	Density at 20 (°C)	S (mg/L)[a] (g/100 g)
Methanol	32	CH_3OH	65	-98	0.79	?
DCM	85	CH_2Cl_2	40	-95	1.33	1.3
Toluene	92	$C_6H_{12}CH_3$	111	-95	0.87	0.005

Adapted from "Vogel's Textbook of Practical Organic Chemistry".5th Edition
a: water solubility

Table 4.3 Properties of the selected solvents.

4.2.3 Solvents

The following solvents were used: methanol, dichloromethane (DCM) and toluene. Methanol was used as PAH-carrier (co-solvent) to aid their dissolution in the aqueous solutions. DCM and toluene were used to solvent

wash and silanise the glassware prior to use. Their properties are shown in Table 4.3.

4.2.4 Sorbents

All minerals (except commercially pre-washed quartz sand) were obtained in their natural form and prepared according to the specifications required for each experiment. The mineral phases studied were the following:

Quartz Sand. The quartz sand was supplied by VWR (Merck Cat. No. 1077121000) and was purchased as a pre-treated product. The manufacturer's pre-treatment consisted of calcination at 900 °C followed by acid-wash in hydrochloric acid (HCl). This process guaranteed the low levels of organic carbon required for the scheduled experiments. The precaution is based on the sequestrating effect organic moieties exert upon polyarene (or PAH) molecules, as is well documented in the literature (Piatt *et al.*, 1996a; Pignatello and Xing, 1996; Appert-Collin *et al.*, 1999; Carmo *et al.*, 2000; Gaboriau and Saada, 2001; Hundal *et al.*, 2001; Wefer-Roehl *et al.*, 2001; Sun *et al.*, 2003; Zhu *et al.*, 2003; Hwang and Cutright, 2004; Sabbah *et al.*, 2004; Zhu *et al.*, 2004c). The sand is used as received, except where surface-bound water or excess acidity needs to be removed, or when the sand must be ground to a fine dust.

Hematite: Natural hematite rock, from the Haile Mine in Egremont, Cumbria, was kindly supplied by Dr David Green at the Manchester Museum. The rocks were ground to a powder and then sieved to select the most abundant fraction for each experiment.

Stx-1 Montmorillonite, (The Clay Repository in Texas) was sieved and suspended in the background electrolyte used in each experiment.

Iron-Oxide / Fe_2O_3 coated sand was prepared using the 250 μm fraction of the VWR sand following a protocol suggested elsewhere (Lai and Chen, 2001)

Table 4.4 gives the physicochemical properties of the minerals used in all experiments.

Parameter	Quartz	Hematite	Fe - Quartz	Montmorillonite
Particle size	All phases between 250 - 500 μm			
Source	Pre-treated VWR	Cumbria	Coated VWR	Clay Repository
BET-SSA (sq. m / g)	0.22	1.99	4.57	58.78
Mineral Phase	SiO_2	Fe_2O_3	SiO_2 Fe_2O_3	$(Na,Ca)0.33(Al,Mg)$ $2Si_4O_{10}(OH)_2{}^{*}nH_20$

Table 4.4.Overview of the minerals used as sorbents.

4.2.5 Sorbent Preparation

The first stage in the preparation process common to all experiments is outlined in Figure 4.1. The hematite supplied by the Curator at the Manchester Museum (Dr David Green) needed to be crushed to produce grains of the desired particle size. For this purpose large crystals were firstly broken into smaller segments and then ground to a powder using the ball mill. After grinding the powder was sieved and the selected particle size (250 μm) separated for use in the experiments. A sub-sample of the mineral was analysed by XRD to determine its purity. Any mineral with less than 95 % purity was discarded and new specimens obtained. An amount of mineral powder was subsequently weighed into pre-conditioned and labelled experimental reaction vials and kept

isolated from any possible contamination until needed. The amount of mineral used in each sample set varied depending on the specific surface area determined for each mineral using the BET – N_2 method (see Chapter 2).

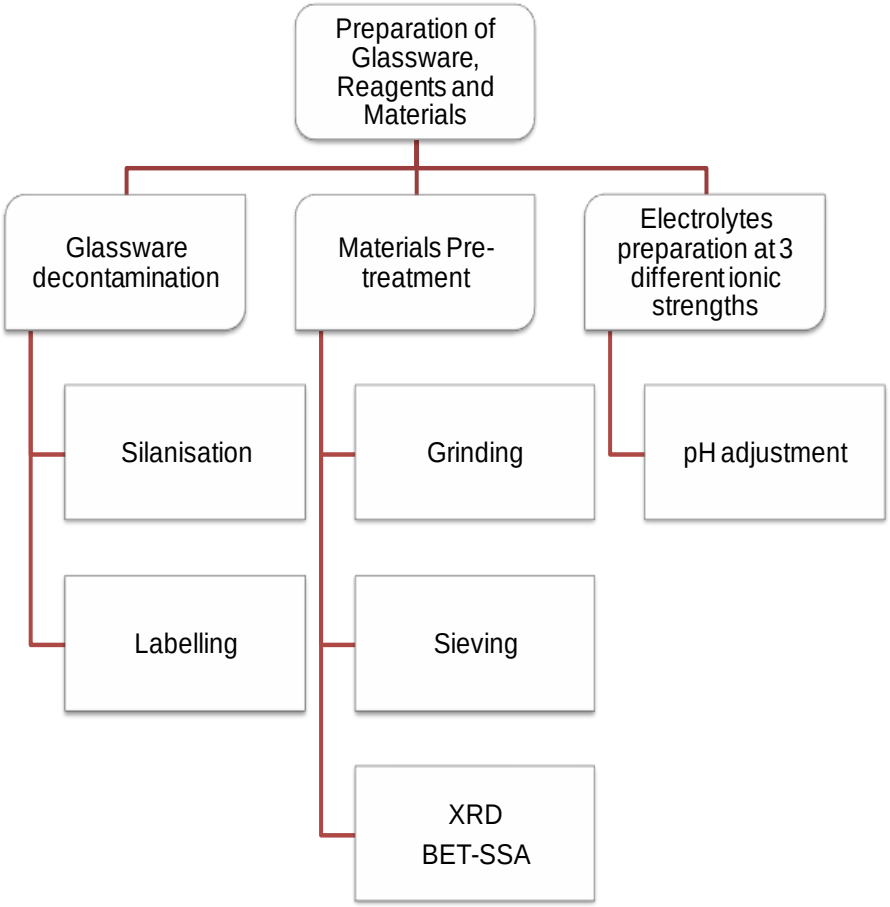

Figure 4.1 Preliminary steps in the preparation of the sorption experiments

4.2.6 Sample Preparation

A typical sample set consisted of the following vials (see Table 4.5):

Sample components	Run Blanks	Procedural Blanks	Samples	Vial Blank	Calibration Standards
Mineral	√	N/A	√	N/A	N/A
PAH-spike	N/A	√	√	N/A	√
Electrolyte	√	√	√	√	√

Table 4.5. Sample preparation.

The respective quantities of sorbent, PAH and electrolyte solution required for each sample in all experiments are shown in Appendix A4. The run blanks were used as indicators of sorbent cross-contamination by naphthalene.

Each sample set also included 3 calibration standards prepared in duplicate (or triplicates depending on the amount of vials available) at 3 different naphthalene concentrations (around the value of the initial concentration in all samples and procedural blanks). The losses blanks were used as initial concentration standards, for the purposes of uptake calculation. Vial-blanks were included every time fresh electrolyte was prepared in order to verify the electrolyte batch had not been contaminated. After several analyses it was concluded this vial was not necessary since extreme care was taken to avoid cross-contamination in the electrolyte reservoirs.

The first step in the preparation of the experimental samples was the preparation of the electrolyte background solutions for all the experiments. Fresh solutions were prepared weekly (or as required), in specially washed glass round-bottom flasks which did not undergo silanisation since there was no PAH (added only later to sample vials) present. The selected salt for the background electrolytes was $NaNO_3$ at concentrations of: 0.001, 0.01 and 0.1 M (moles per litre). The solid salt was kept in the oven at 120 ºC and was allowed to cool down inside desiccators to avoid gravimetric errors whilst weighing which could be caused by hydroscopic uptake of atmospheric water.

4.2.7 Experimental Protocol

Figure 4.2 shows the sequence followed in each experiment, starting with the sample preparation and including the stages all samples experienced until the end of the reaction time. The required amount of electrolyte was transferred to the labelled vials, after which a very small volume of PAH at the

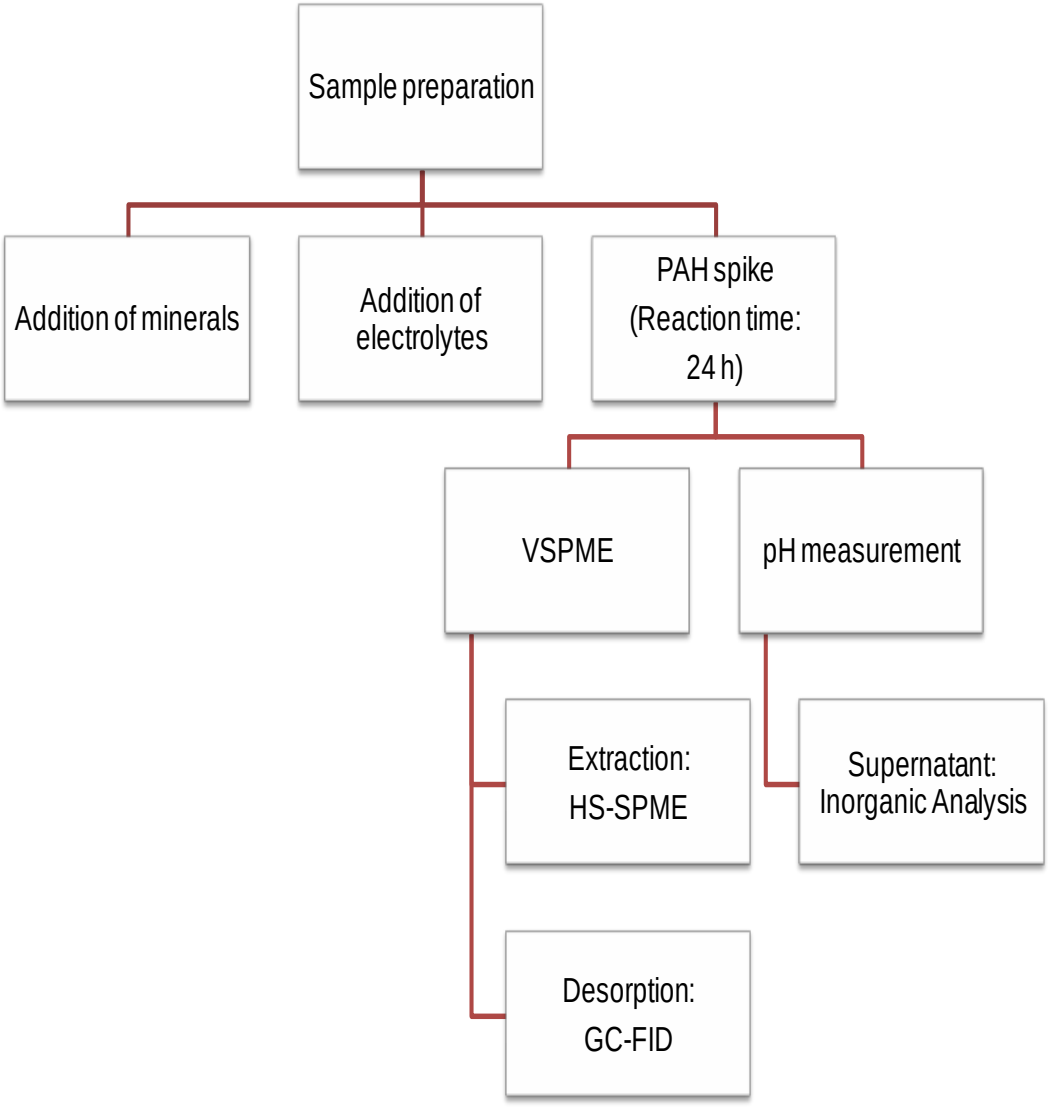

Figure 4.2 Steps of sample preparation and experimental layout

required concentration was added using a micro-syringe (spike). The amount of electrolyte and spike used was adjusted to keep the initial concentration equal in all vials. It is important to elaborate further upon the manner in which PAH were transferred to the sample vials and the volumes used.

Firstly, the PAH solutions used in this study were commercial standards in methanol at concentrations about 5 orders of magnitude higher than the target concentration in electrolytes. Naphthalene is relatively soluble in aqueous solutions (up to 30 mg / l in pure water). When attempting to dissolve non-polar organics in a very polar medium such as electrolyte solutions (fully dissociated salts) an effect called “salting out” takes place (Eisert and Levsen, 1996; Schlautman et al., 2004). This causes the aqueous solubility of the organic compound to decrease due to competition between the polar salt molecules and the non-polar organic molecules for available hydration pockets within the water bulk. When this happens, the organics are somewhat “pushed” more readily out of solution into other phases within the system. In view of this, an additional step was introduced to ensure this effect did not significantly change the amount of PAH present in the sample vials to which each mineral phase was exposed, namely: when spiking the samples, the smallest accurately measurable amount of concentrated commercial standard (called the primary stock) was transferred to each vial using calibrated micro-syringes of various sizes. The needle of the micro-syringe was immersed to a depth equal to half the length of the reaction vial, and the plunger pressed in a swift motion to release the required micro-volume of primary stock. This volume transfer was followed by the rapid withdrawal of the needle and the sealing of.the vial with the septum screw cap. PTFE tape was then wrapped around the closed cap to ensure no air left or entered the vial during the 24 hour reaction time in the

horizontal shaker. This routine procedure ensured that no major PAH losses to the atmosphere occurred and this was verified by monitoring the standard deviation of the uptake results between sample triplicates, relative to those of the sample set blanks.

Secondly, the amounts of the carrier solvent (also called co-solvent) should be high enough to aid in the organic's dissolution but not so as to interfere with the interaction between sorbent and sorbate. The use of co-solvents such as methanol to aid the analyte's dissolution in aqueous matrices has been applied by several workers studying the sorptive behavior of non-polar solutes such as PAHs. Elevated co-solvent concentrations ($x_{Cosolvent} \geq 0.1$) in aqueous systems however, are known to interfere with the sorption mechanism for the solute under study decreasing the sorption coefficients (Kookana *et al.*, 1990). This effect appears to be enhanced by non-polar solutes with higher hydrophobic surface areas and has been attributed to an increase in solubility within the ternary system (Nkedi-Kizza *et al.*, 1987; Schwarzenbach *et al.*, 1993). Different authors working with non-polar solutes in aqueous systems have used co-solvent volumetric fractions ranging from 5×10^{-4} to 2×10^{-2} (0.05 to 2 %) (Kan *et al.*, 1998; Kleineidam *et al.*, 1999; Li and Lee, 2001; Middleton, 2003; Zhou *et al.*, 2004). To avoid co-solvent interferences, a level of 0.01 % (v / v) methanol as co-solvent was used throughout all the experiments in this research work.

After the 24 hours reaction time all sample vials were removed from the horizontal shaker (operated at 140 rpm for 24 hours) and where required, the sediment was allowed to settle in order to obtain a clear supernatant. For all minerals with the exception of quartz sand (QS), centrifugation was carried out

in two consecutive stages of 30 minutes each at 3300 rpm (Environmental Laboratory centrifuge, Williamson Research Centre for Molecular Environmental Science, SEAES).

Once the SPME volume was transferred to the extraction vial, the remaining volume in the reaction glass tube was used to measure the pH of the reacted supernatant. This was conducted in the presence of the mineral phase as a sediment in the bottom of the vial. The equipment used was a pH bench meter (ORION 520) and a METLER TOLEDO INLAB 428 pH electrode. The electrode was calibrated daily with 3-point calibrations using fresh buffers at pH values of 4.00, 7.00 and 10.00 (all at ≈ 20 ºC). The remaining supernatant volume of blanks prepared at all three ionic strength were sent for ICP-MS and ICP-AES analysis of the main dissociated ions (Na^+ and Cl^-).

4.2.8 Preparation of Standard Solutions

The aqueous standard solutions were prepared as follows: A concentrated primary stock solution was purchased and diluted to the required value using reagent-grade methanol. When required this primary standard was further diluted by spiking exact volumes in the relevant solution matrix. Deionised water was used at the start of the method development (15 µS / cm, supplied by Kinetics Laboratory, School of Earth, Atmospheric and Environmental Sciences, The University of Manchester) in order to test suitability of method for the target analyte. Once the extraction method was established all samples were prepared in the electrolyte background solution required for all samples in each experiment.

4.2.9 Sample Extraction via HS-SPME

At the end of the 24 hours reaction time, identical aliquots of completely cleared supernatant (5 ml) were transferred (by weighing with an accuracy of up to 2 decimal places) to 10 ml SPME extraction vials and extracted in the headspace (HS-SPME) for 3 minutes This volume (5 ml of sample) was the designated SPME-extraction volume for all HS-SPME extractions and it was the same for blanks, standards and samples (see Figure 4.3). The extraction vials were SPME clear glass 10 ml vials assembled with aluminium septa-screw caps. In addition to washing, all vials had been previously custom-silanised. Ultrasonication at 40 ºC for 3 minutes inside a water bath was used as a source of agitation. The sample vials were inserted into a custom-made aluminium hollow sample pod (see Figure 3.8.) connected via flexible tubing to a temperature controller.

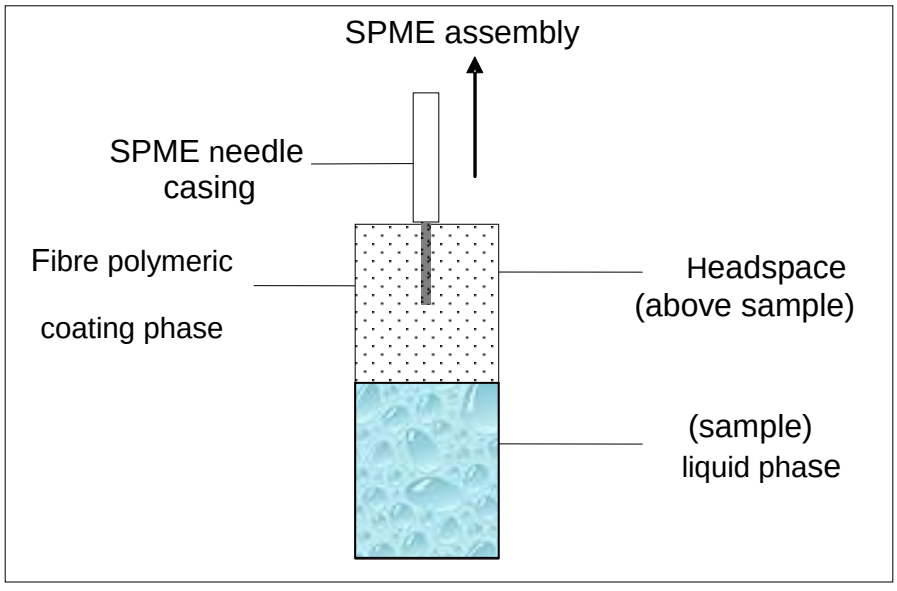

Figure 4.3 Phases present in the sampling system (SPME vial).

This rig allowed the samples to be kept at a constant temperature for the entirety of the sampling period (3 minutes). The fibre phase used was

Polydimethyl siloxane (PDMS) at 30 μm thickness inserted in a manual SPME holder. The sampling depth into the SPME vial was 0.6 cm into the headspace. The headspace was allowed to come to temperature (40 ºC) before the fibre was exposed to it, the latter being at a slightly lower temperature a few minutes after it had been removed from the injection port (at 280 ºC).The SPME extraction conditions are summarized in Table 4.6.

SPME Extraction Method	
Extraction	
Matrix	$NaNO_3$ 0.001 M
Method	Pre-Equil. HS
Sampling Depth	0.6 cm
Vial Location	Water jacket
Stirring	Ultrasonic bath
Temperature	40 ^{o}C
Sampling Time	3 minutes
Fiber Material	PDMS
Fiber Thickness	30 μm
DESORPTION (PTV INLET)	
Depth	3 cm
Temperature	280 ^{o}C
Time	6.6 minutes

Table 4.6 SPME extraction parameters.

4.3 Sample Analysis

4.3.1. Brief Introduction to Gas Chromatography

Chromatography is the most important tool for the analysis of organic compounds in aqueous matrices and is specific to organic compounds which can be vaporized. Figure 4.4 shows a diagram of a standard gas chromatography system like the one used for the analysis of the samples produced in this research work.

The process consists of a separation where the components of a sample (solutes) equilibrate between a mobile and a stationary phase as they travel through the system. The differential distribution of the solutes between these phases will result in their separation as they move (elute) through the stationary

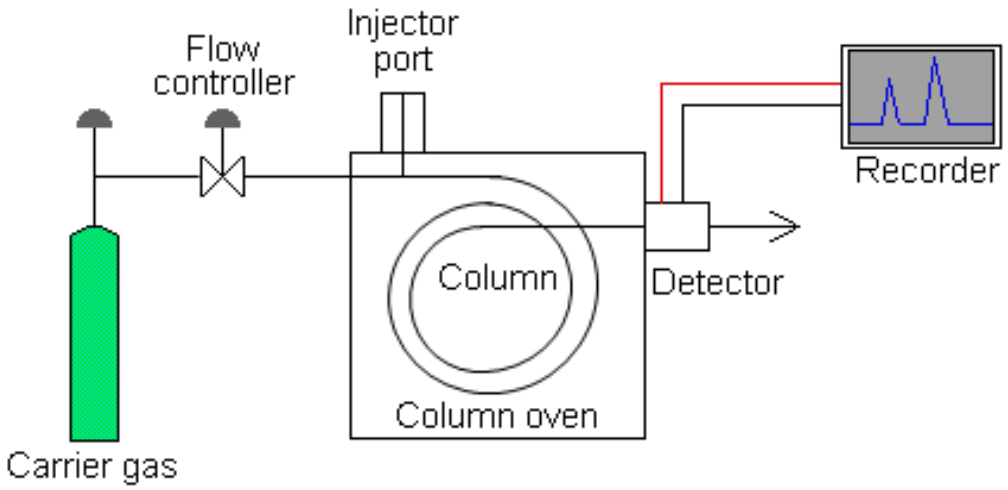

Figure 4.4 Parts of a gas chromatographic system (Sheffield Hallam University, 1998b)

phase. The rate of elution varies for each analyte and is measured in terms of the retention time (t_R) which is the time elapsed between the injection of the sample and the detection of an analyte.

An inert gas (carrier gas) is used as the mobile phase. The sample is injected through a thermally resistant septum (a rubber disk) into a heated injector and carried throughout a coiled capillary column (Willet, 1987).

The injection port is kept at a high temperature (250 – 300 °C) in order to volatilize the sample. There are several ways to introduce a sample into the injector. In the case of solid sampling devices such as SPME (solid phase micro-extraction) the samples are introduced directly into the injector where the solutes are stripped off the fibres by thermal desorption and carried into the

column. In all cases the solutes are vaporised inside a glass tube (liner) and from there swept onto the head of the capillary column inside the oven.

The main types of injector used with capillary columns are the on-column injectors and the split / splitless injector (Fowlis, 1995) of which a diagram is shown in Figure 4.5. In the split mode only a small fraction (0.1 – 10%) of the injected sample enters the column, the rest is vented to waste. (Harris, 1991). When on splitless mode, the whole sample volume/mass goes into the column. This is the preferred injection method for samples extracted by SPME since the mass of analyte extracted by these devices tends to be very small (of the order of µg) and would not require solvents as carrier.

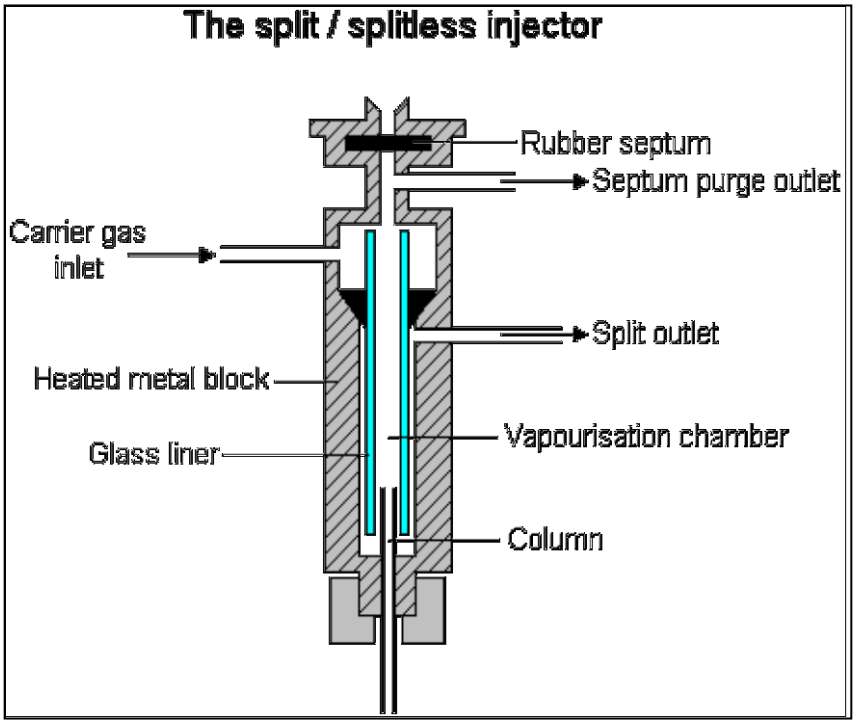

Figure 4.5 Diagram of the parts of a split / splitless injector (Sheffield Hallam University, 1998c).

The chromatographic detector used in these experiments was a Flame Ionisation Detector or FID. It is specific for organic compounds that can be ionized in a flame. A diagram of a FID detector is shown in Figure 4.6. The operating principle of ionization detectors is based on the fact that the electrical conductivity of gases is directly proportional to the concentration of charged particles within the gas. During a run, the organic compounds burning in the flame undergo pyrolysis to become ions and electrons capable of conducting electricity.

The effluent gas from the chromatographic column mixes with hydrogen and air and is burned in the flame producing CH radicals as shown in reaction (4.1):

$$CH^{\bullet} + \tfrac{1}{2}\, O_2 \rightarrow CHO^{+} + e^{-} \text{ (Harris, 1991)} \qquad (4.1)$$

These carbon radicals react with the oxygen from the air in the flame to produce CHO^{+} species. The jet forms the negative electrode of an electrolytic cell and the positive electrode, or collector, consists of a loop of wire located above the flame. The potential difference created between the insulated jet at the base of the flame and the cathode above (about 200 to 300 V) diverts the CHO^{+} radicals from the flame plasma towards the positive electrode (Fifield and Kealy, 2000) (see Figure 4.6). This current goes through a high impedance amplifier and the output signal is fed to a data acquisition system or potentiometric recorder as a plot of area (mV or pA*s) vs. elution time (minutes) (Scott, 2002).

For more in-depth information on the theory of gas chromatography the reader is referred to the references cited throughout this section, which are included in the references outlined at the end of this chapter.

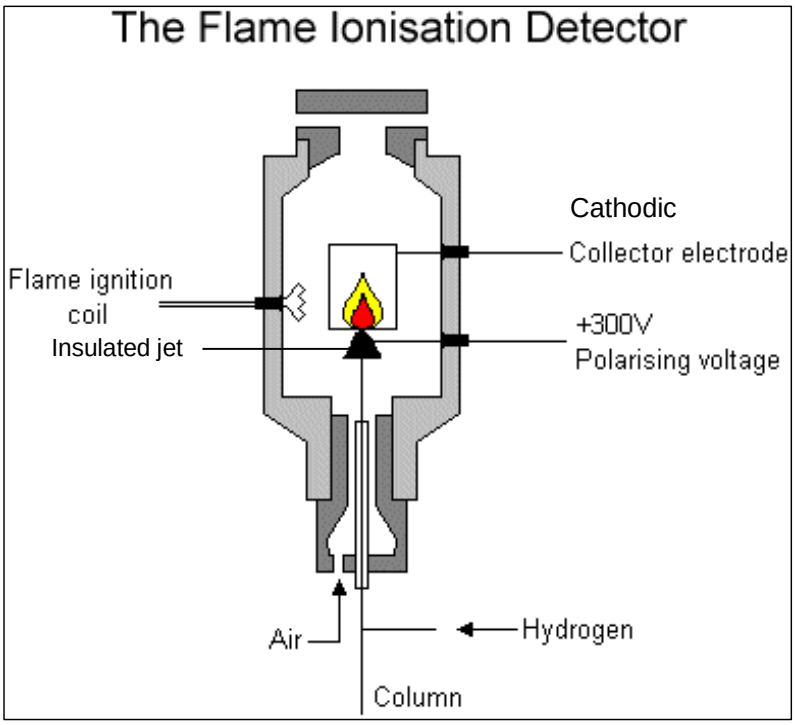

Figure 4.6 Schematic diagram of a FID detector (Sheffield Hallam University, 1998a)

4.3.2. Analytical Protocol via GC-FID

The gas chromatography system used for the analysis of the samples generated in these experiments was an Agilent 7890A (Agilent Technologies Ltd) fitted with a Flame Ionisation Detector or FID.

The PAH-laden SPME fibres were taken to the GC-FID device immediately after extraction and inserted into the injection port equipped with a special liner designed for use with SPME (Gerstel CIS-4). These liners consisted of tubes made of deactivated glass with narrow bore design to facilitate the transfer of 100 % of the sampled analyte mass from the fibre into the chromatographic column. This measure ensured no analyte losses due to volatilization as well as narrow and symmetric chromatographic peaks. The GC conditions are summarised in Table 4.7.

The depth of desorption into the injector was 3 cm and the fibre was left inside for the duration of the run (6.6 minutes).

GC SYSTEM	AGILENT 7890A GC SYSTEM
COLUMN	HP5 AGILENT; 30 m x 250 µm x 0.25 µm
INLET	PTV INJECTOR; P=11.799 PSI
CARRIER GAS FLOW	1 ml / min
MODE	SPLITLESS
INLET NUT	SPME GUIDE
SEPTA	PRE-CORED THERMOGREEN LB-2
EQUIL. TIME	0.5 min
TOTAL TIME	6.6 min
GC-PROGRAMME	70°C (0) UP TO 160°C (3 min) AT 25°C/min
INJECTOR TEMP.	280 °C
NARROW BORE LINER	GERSTEL SPME DIRECT LINER CIS4 FOR PTV
DETECTOR	FID
TEMPERATURE	320 °C
H2	40 PSI
AIR	400 PSI
MAKE UP GAS	25 PSI

Table 4.7 GC-FID analytical conditions.

At the end of each run the fibre was allowed to cool whilst another identical fibre was used to extract the next sample. In this manner the sample turnover was up to 36 samples a day including all triplicates.

No carry-over was observed during subsequent alternate injections of the 2 different fibres (see Figure 4.7). Previous external calibrations using this tandem system yielded satisfactory linearity ($R^2 \geq 0.97$).

Peak integration conditions were set to the instrument's default and therefore kept constant for all standards, blanks and samples. The system included the following analytical software: GC Chemstation Rev. B.03.02 [341], Agilent Technologies 2001 – 2008

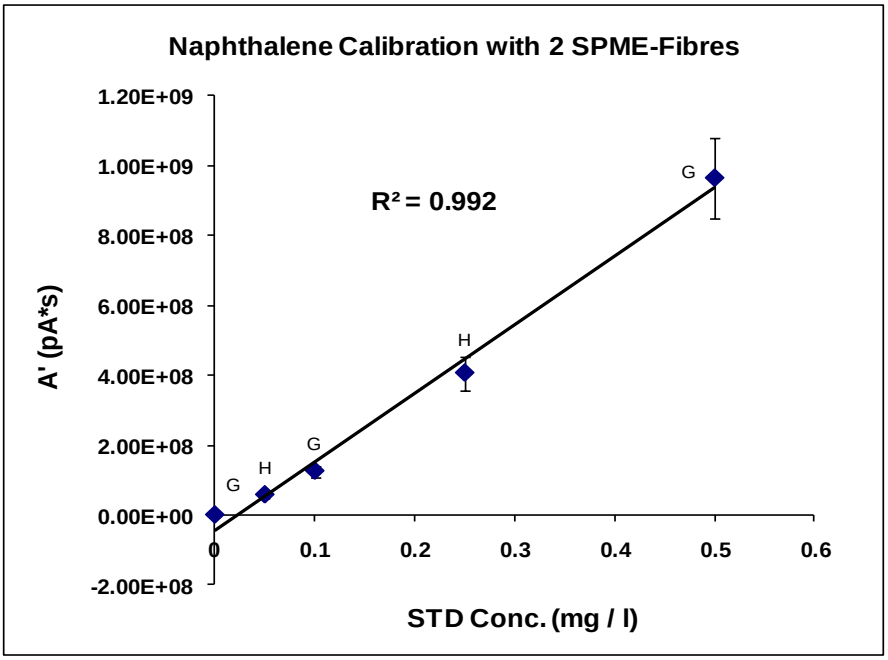

Figure 4.7 Tandem calibration for naphthalene by HS-SPME using two fibres (error bars calculated as highest intra-day RSD% for all standards and blanks).

4.3.3. Standard External Calibration

The calibration method selected for these experiments was external calibration. Commercial standards containing the analyte of interest in the desired concentration range were diluted in the same background matrix as the samples and extracted using the same SPME method. The same approach was employed in order to determine the detection limit and range of the method. Blanks with an identical matrix background and extracted under the same conditions as the standards and samples were analysed simultaneously to ensure absence of cross-contamination.

For the purpose of peak integration and quantification, GC blanks were run first thing every day in order to ensure a good chromatogram baseline,

following which SPME fibre blanks were run to guarantee the fibres were not contaminated. These preliminary steps ensured all GC runs were free of analytical interferences. The calibrations were initially carried out with up to 8 to 9 standards covering a range of several orders of magnitude above and below the initial naphthalene concentrations in all experimental samples. A typical such calibration curve is shown in Figure 4.8.

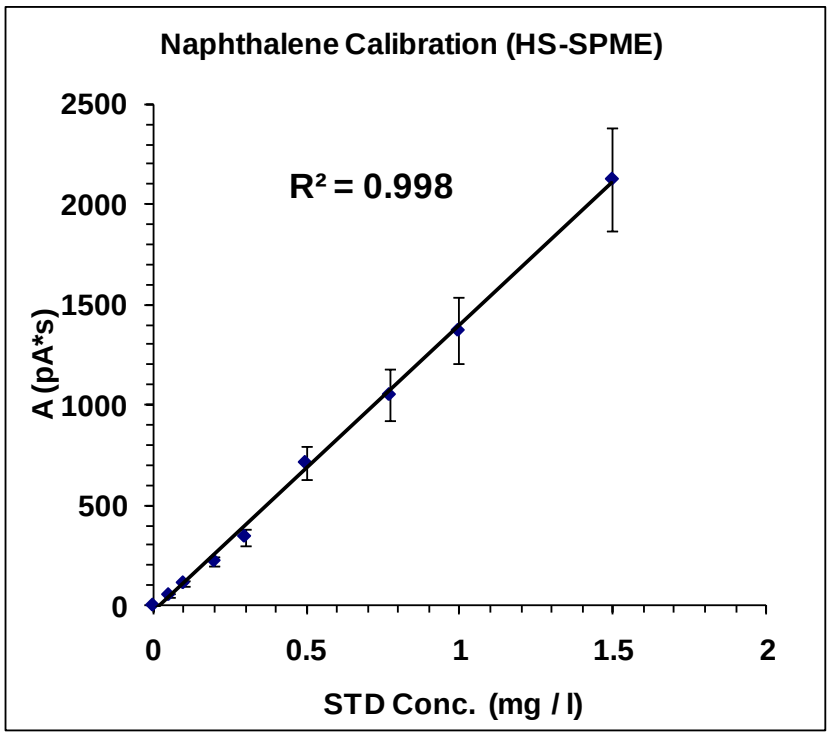

Figure 4.8 A typical naphthalene standard calibration curve extracted and analysed under the selected experimental conditions.

In order to calculate the concentration of naphthalene accurately, triplicates of 3 different standards accompanied every sample set in all experiments, undergoing identical reaction, extraction and desorption conditions together with samples and blanks. This procedure allowed the calculation of the concentration of naphthalene after 24 hours of mineral exposure by

extrapolation of the GC area obtained by each set of sample triplicates. The equation used is shown as Equation. 4.1 and is applicable if a linear response from the GC detector is assumed, which is the case for FID:

$$\frac{C_S}{A_S} = \frac{C_B}{A_B} \quad (4.1)$$

where:

Cs (mg / l) represents the unknown sample concentration at the end of the 24 hours reaction time,

A_S (mV) represents the integrated area under the GC-FID peak corresponding to the PAH under study,

C_B (mg / l) is the concentration of the losses or procedural blank (the same initial concentration in all samples),

A_B (mV) is the integrated GC-FID peak area for the same blank.

As can be seen in this equation, the 'losses' blanks included in every set of samples were used as a standard (no mineral phase present) and represented the PAH concentration at the beginning of the reaction (t = 0). This is only possible given the robust linearity exhibited by the GC-FID detectors throughout the range of PAH concentrations used in these experiments.

4.3.4. Analysis of Blind Standards

In order to test the calculation method used to work out the concentration of naphthalene in the supernatant after 24 hours, two standard dilutions of unknown concentration (blind samples) were submitted to analysis undergoing

the same extraction and desorption methods detailed in the sections above. Freshly prepared calibration standards were extracted and analysed alongside the blind sample triplicates. The concentration (Cs) of the blind samples was calculated using Equation 4.1.

The concentrations calculated for the blind samples using this method were accurate within acceptable error margins (3 – 5 %). A useful way to assess the fitness of a method for the analysis of a particular chemical is to calculate the “recovery” percentage of the analyte present in a given sample. In this case, the initial naphthalene mass had been recorded by the party providing the blind samples and the recovery % of that initial mass was calculated based on the calibration standards used. The calculation was performed in two stages:

Firstly, the equivalent concentration was calculated using the GC-FID areas and Equation. 4.1. Secondly, the recovery percent (R%) was calculated using Equation 4.2 as follows:

$$R\% = \frac{C_S}{C_t} \times 100 \qquad (4.2)$$

where:

C_S represents the unknown concentration (as in Equation 4.1.) and

C_t the theoretical concentration calculated from the dilution factor of a certified commercial naphthalene primary stock from which the blind samples have been prepared.

The primary stock used in this test was purchased from SPEX CertiPrep, and consisted of naphthalene dissolved at 1000 mg / l in methanol.

This test confirmed the feasibility of using external standards as a quantification method for all samples extracted with a modified HS-SPME method in the present experiments.

4.4. Calculations

4.4.1. Naphthalene Uptake

The results were expressed as the percentage of naphthalene removed by the sorbents relative to the initial naphthalene in the blanks, or uptake percentage (U%). All blanks were always prepared identically to the samples but did not include the sorbent phase. Each area (A) value used is the average of triplicates for all blanks and samples. The blanks represent the initial concentration at t = 0, just after the PAH-spike and before the reaction time begins. The calculation is effectively a comparison of snapshot concentrations between t = 0 and t = 24 (after 24 hours reaction time have elapsed). It shows how the concentration of naphthalene would decrease in time (24 hours) as a result of exposure to a sorbent and it is given by Equation 4.3:

$$U_{\%} = \left(\frac{A_B - A_S}{A_B} \right) \times 100\% \qquad (4.3)$$

where:

A_B represents the GC-FID response corresponding to the blank samples (or initial concentration at t = 0) and

A_S is the response corresponding to the sample at the end of the 24 hour period (at t = 24).

The GC-areas in the numerator are used as a proxy to represent the difference between the initial and the final concentrations of naphthalene in the system, or C_0 and C_{24} respectively.

The rationale behind this calculation is based on the linearity exhibited by the FID detector (see Figure 4.8) where area under the line is directly proportional to concentration. The FID responses can then be used instead of concentrations in order to estimate how much PAH has been removed from solution at the end of 24 hours.

An alternative method would be to calculate C_{24} using the standard SPME equation where the mass of naphthalene absorbed onto the fibre at the end of the extraction can be calculated. The use of external calibration using the same equation would allow to extrapolate C_{24}. This equation corresponds to a three-phase sampling system (phases: liquid sample, headspace and fibre coating) is:

$$n = \frac{C_s V_s V_f K_{fs}}{K_{fs} V_f + K_{hs} V_h + V_s} \qquad (4.4)$$

where:

n is the mass of naphthalene (µg) on the fibre at the end of the extraction,

C_s is the initial naphthalene concentration in the sample to be extracted (µg / ml),

V_S is the sample volume (ml),

V_f is the fibre volume corresponding to the polymeric PDMS coating where absorption takes place (ml),

V_h is the volume of the headspace (ml),

K_{fs} is the experimentally determined distribution constant between the fibre coating and the sample (adimensional) and

K_{hs} is the distribution constant between the headspace and the fibre coating (adimensional, data available from literature) (Pawliszyn, 1999).

This approach, however, is more complicated and time consuming since the distribution coefficient (K_{fs}) for naphthalene between the PDMS fibre coating and the sample needs to be known beforehand. Various distribution coefficients for naphthalene in deionised water have been determined by several authors (Doong and Chang, 2000; Shurmer and Pawliszyn, 2000; Niri and Pawliszyn, 2007; Ouyang *et al.*, 2008) but their values differ by as much as a factor of ten. Since the matrix used for these experiments was not deionised water (but $NaNO_3$).these coefficients are not applicable in any case. The simplification of using GC-FID responses instead of concentrations circumvents the need to apply the standard 3-phase SPME Equation (4.4).

4.4.2. PAH-Mineral Distribution Constant

For the sake of simplicity, the results are presented plotting experimentally calculated (dimensionless) PAH-mineral distribution constants (K_{min}) as a function of pH. The calculated distribution constants for each mineral used in all plots are also presented as tables for each mineral. The equations for the calculation of the distribution constants are shown as 4.5 and 4.6 below:

$$K_{min} = \frac{C_{min}}{C_{S_{24}}} \quad (4.5)$$

$$C_{min} = C_0 - C_{S_{24}} \quad (4.6)$$

where:

C_{min} is the concentration of naphthalene in the mineral phase after 24 hours (t = 24) (mg / ml),

C_0 is the initial naphthalene concentration in the sample at the start of the reaction time (mg / ml) (t = 0),

C_{24} is the naphthalene concentration in the sample at the end of the reaction time (t = 24) (mg / ml) and

K_{min} is the experimentally determined distribution constant between the mineral and the sample (dimensionless).

K_{min} is calculated under the assumption that the naphthalene has reached equilibrium with the mineral phase in the system after 24 hours have elapsed. This means that the concentration measured in the supernatant corresponds to the PAH-fraction which was not removed by the selected sorbent. The higher the value of K_{min}, the higher the naphthalene uptake by that particular sorbent.

4.4.3 Error Analysis

The distribution of the measurements about the true mean value is assumed to follow a Gaussian probability distribution function. The measurement error was calculated for each triplicate set, for the samples and blanks, at the 95 % confidence interval which corresponds to 2 standard deviations (2 σ) from the mean value. In order to be confident that there is a definite uptake of naphthalene the difference between the samples and the

blanks must be statistically significant. This is taken to be when the confidence intervals associated with each mean value from both triplicate sets do not overlap. This is expressed by the condition:

$$(\bar{x}_B - 2\sigma_B) \geq (\bar{x}_S + 2\sigma_S) \tag{4.7}$$

where

$\bar{x}_B$ is the mean value of the blank triplicate set, mg / l

σ_B is the standard deviation of the blank triplicate set, mg / l

$\bar{x}_S$ is the mean value of the sample triplicate set, mg / l

σ_S is the standard deviation of the sample triplicate set, mg / l

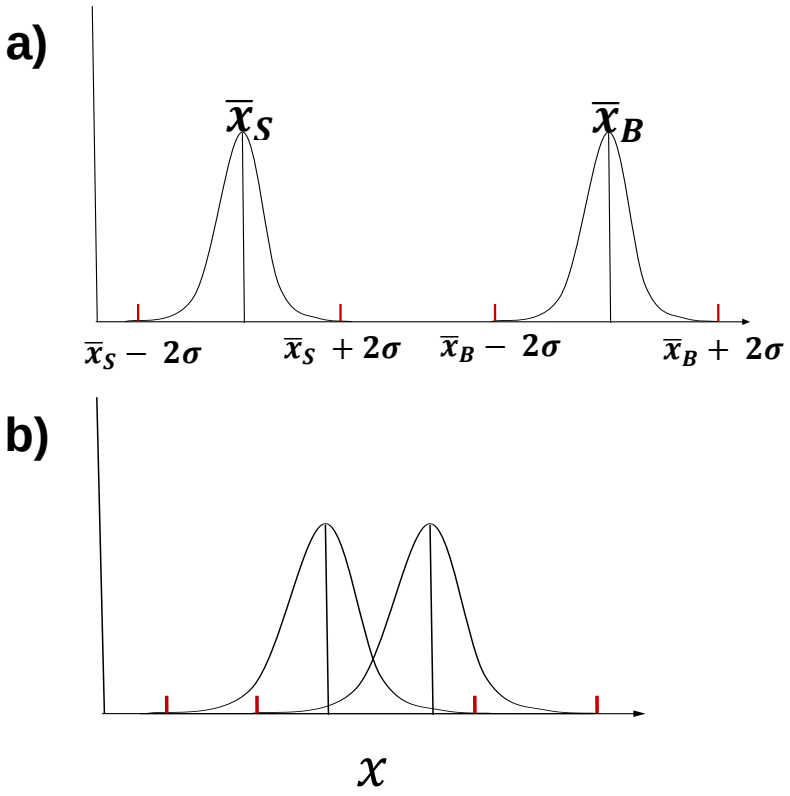

Figure 4.9 Graphic representation of condition (4.7)

The scenario in which the above criterion is satisfied is shown Figure 4.9 (a). Here, the confident intervals of both means do not overlap and both measurements are resolvable indicating sorption of naphthalene. In (b) the confidence intervals overlap and the two measurements can no longer be resolved. The latter case is observed in all experiments using quartz, hematite, montmorillonite clay and Fe-coated sand (see Tables 4.8 – 4.12).

GRANULATED ACTIVATED CARBON AND SAND TIME: 4 HOURS

GAC:SAND RATIO	0 : 100			10 : 100			50 : 50			100 : 0	
	GC AREA			GC AREA			GC AREA			GC AREA	
	Blanks	SAMPLE		Blanks	SAMPLE		Blanks	SAMPLE		Blanks	SAMPLE
1	817.359	911.655		817.359	44.919		817.359	2.583		817.359	0.000
2	886.984	763.362		886.984	66.077		886.984	3.905		886.984	0.000
3	913.000	821.022		913.000	N / A		913.000	2.435		913.000	0.000
MEAN	872.448	832.013		872.448	55.498		872.448	2.974		872.448	0.000
STDEV	49.450	74.755		49.450	14.961		49.450	0.810		49.450	0.000
HIGHER	971.347	981.523	OVERLAP	971.347	85.420		971.347	4.593		971.347	0.000
LOWER	773.549	682.503		773.549	25.576		773.549	1.355		773.549	0.000

Table 4.8 Error calculation for experiments with granulated activated carbon.

QUARTZ TIME 24 HOURS

	Exp. : QSIb			Exp. : QSIIb			Exp. : QSIIIb		
	UPTAKE % 7.043			UPTAKE % NEG.			UPTAKE % 18.016		
	GC AREA			GC AREA			GC AREA		
	Blanks	SAMPLE		Blanks	SAMPLE		Blanks	SAMPLE	
1	572.844	567.235		530.179	536.299		522.807	411.366	
2	601.646	N / A		519.339	587.702		551.327	448.952	
3	658.206	568.507		505.764	507.618		470.640	406.157	
MEAN	610.899	567.871		518.427	543.873		514.924	422.158	
STDEV	0.899	0.899		12.233	40.576		40.917	23.350	
HIGHER	612.697	569.670	OVERLAP	542.893	625.024	OVERLAP	596.758	468.858	OVERLAP
LOWER	609.100	566.073		493.962	462.721		433.090	375.459	

Table 4.9 Error calculation for experiments with quartz sand.

HEMATITE

TIME 24 HOURS

Exp. :	Hmlb		Exp. :	Hmlb		Exp. :	Hmllb	
UPTAKE %	0.359		UPTAKE %	2.711		UPTAKE %	4.643	
GC AREA			GC AREA			GC AREA		
	Blanks	SAMPLE		Blanks	SAMPLE		Blanks	SAMPLE	
1	572.844	575.492		530.179	533.260		522.807	476.719	
2	601.646	656.973		519.339	514.646		551.327	503.175	
3	658.206	593.645		505.764	465.210		470.640	493.158	
MEAN	610.899	608.703		518.427	504.372		514.924	491.018	
STDEV	43.427	42.777		12.233	35.169		40.917	13.357	
HIGHER	697.753	694.257	OVERLAP	542.893	574.711	OVERLAP	596.758	517.732	OVERLAP
LOWER	524.044	523.149		493.962	434.033		433.090	464.303	

Exp. :	Hmla		Exp. :	Hmlla		Exp. :	Hmlla	
UPTAKE %	5.003		UPTAKE %	7.874		UPTAKE %	21.274	
GC AREA			GC AREA			GC AREA		
	Blanks	SAMPLE		Blanks	SAMPLE		Blanks	SAMPLE	
1	493.952	435.596		448.784	342.703		541.345	370.087	
2	418.856	391.060		347.346	377.708		486.116	450.046	
3	407.661	427.751		362.192	346.711		566.112	434.416	
MEAN	440.157	418.136		386.107	355.707		531.191	418.183	
STDEV	46.924	23.774		54.784	19.158		40.954	42.379	
HIGHER	534.004	465.683	OVERLAP	495.676	394.024	OVERLAP	613.098	502.941	OVERLAP
LOWER	346.309	370.588		276.539	317.390		449.284	333.425	

Table 4.10 Error calculation for experiments with hematite.

Fe-QUARTZ

TIME 24 HOURS

Exp. :	Fe-QSIb		Exp. :	Fe-QSIIb		Exp. :	Fe-QSIIb	
UPTAKE %	7.198		UPTAKE %	NEG.		UPTAKE %	5.067	
GC AREA			GC AREA			GC AREA		
	Blanks	SAMPLE		Blanks	SAMPLE		Blanks	SAMPLE	
1	542.183	488.286		530.179	584.071		494.842	489.286	
2	511.787	489.927		519.339	572.695		497.441	465.464	
3	500.892	464.728		505.764	521.050		547.598	507.107	
MEAN	518.287	480.980		518.427	559.272		513.294	487.286	
STDEV	21.399	14.099		12.233	33.587		29.736	20.893	
HIGHER	561.086	509.178	OVERLAP	542.893	626.445	OVERLAP	572.767	529.073	OVERLAP
LOWER	475.488	452.782		493.962	492.098		453.821	445.499	

UPTAKE %	6.211		UPTAKE %	5.063		UPTAKE %	3.383	
Exp. :	Fe-QSIa		Exp. :	Fe-QSIIa		Exp. :	Fe-QSIIa	
GC AREA			GC AREA			GC AREA		
	Blanks	SAMPLE		Blanks	SAMPLE		Blanks	SAMPLE	
1	466.995	488.318		526.853	561.910		479.643	436.245	
2	491.430	452.845		553.250	539.198		498.331	522.847	
3	519.484	444.957		468.554	437.014		552.290	519.401	
MEAN	492.636	462.040		516.219	512.707		510.088	492.831	
STDEV	26.265	23.097		43.337	66.529		37.724	49.035	
HIGHER	545.167	508.233	OVERLAP	602.894	645.765	OVERLAP	585.535	590.901	OVERLAP
LOWER	440.106	415.847		429.544	379.649		434.641	394.761	

Table 4.11 Error calculation for experiments with Fe-coated quartz sand.

CLAY

TIME 24 HOURS

	UPTAKE % 7.099 Exp.: Mtla			UPTAKE % 5.465 Exp.: Mtlla			UPTAKE % 4.228 Exp.: Mtllla		
	GC AREA			GC AREA			GC AREA		
	Blanks	SAMPLE		Blanks	SAMPLE		Blanks	SAMPLE	
1	466.995	469.977		526.853	523.648		479.643	452.017	
2	491.430	441.423		553.250	459.288		498.331	530.166	
3	519.484	461.598		468.554	548.684		552.290	483.388	
MEAN	492.636	457.666		516.219	510.540		510.088	488.524	
STDEV	26.265	14.677		43.337	46.117		37.724	39.327	
HIGHER	545.167	487.021	OVERLAP	602.894	602.774	OVERLAP	585.535	567.178	OVERLAP
LOWER	440.106	428.311		429.544	418.305		434.641	409.869	

	UPTAKE % 2.749 Exp.: Mtlb			UPTAKE % NEG. Exp.: Mtllb			UPTAKE % 4.500 Exp.: Mtlllb		
	GC AREA			GC AREA			GC AREA		
	Blanks	SAMPLE		Blanks	SAMPLE		Blanks	SAMPLE	
1	542.183	521.164		530.179	520.111		494.842	447.369	
2	511.787	479.334		519.339	539.247		497.441	479.941	
3	500.892	511.617		505.764	N/A		547.598	543.284	
MEAN	518.287	504.038		518.427	529.679		513.294	490.198	
STDEV	21.399	21.921		12.233	13.531		29.736	48.773	
HIGHER	561.086	547.879	OVERLAP	542.893	556.742	OVERLAP	572.767	587.744	OVERLAP
LOWER	475.488	460.197		493.962	502.617		453.821	392.651	

Table 4.12 Error calculation for experiments with montmorillonite Stx-1 clay.

4.5. Results

The exposure of each mineral to naphthalene was carried out at 2 different pH values and at 3 different ionic strength concentrations of $NaNO_3$ (see Figure 4.10). The selected pH values were chosen to represent (a) an acidic environment (pH = 4.0) and (b) the natural pH value of the electrolyte dissolution in DIW (pH = 5.5 in $NaNO_3$).

Within the specified pH range the minerals would all be sufficiently far removed from their isoelectric points as can be seen in Table 4.13. This would represent a distinctive advantage when attempting to correlate their surface charge with the sorption experiments results, since the original charge of the mineral surfaces would remain constant under the specified experimental conditions. Additionally, the selected pH conditions may be considered as representing slightly different types of soil environments.

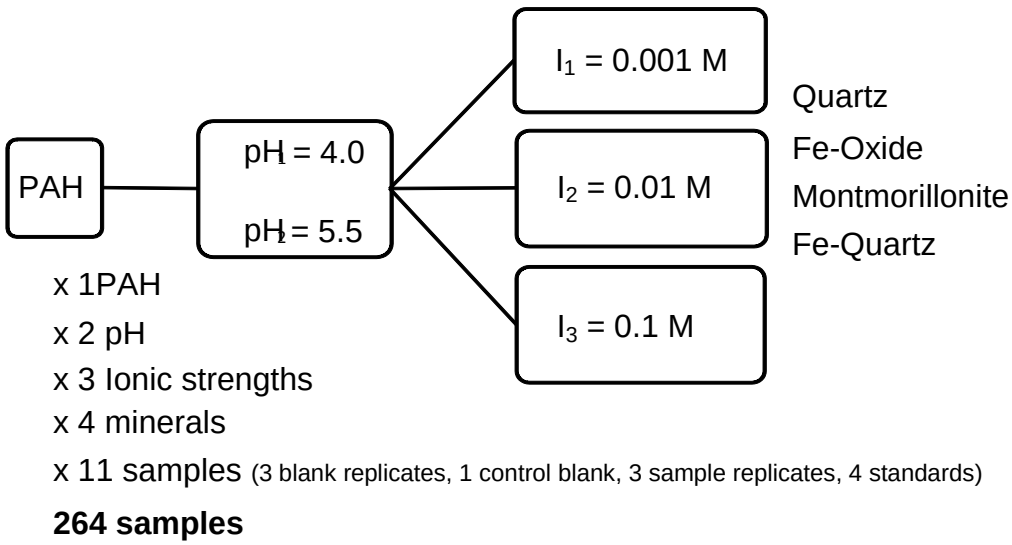

Figure 4.10 Diagram of the experimental variables

The objectives of having three different concentrations of the same electrolyte were to control the background ions present in solution and to observe whether increasing concentrations of these ions exerted any effect on the solubility of the sorbates and hence on the behaviour of the entire system.

Mineral	pH^{1}_{PZC}
Montmorillonite	< 2.5
Hematite, α-Fe_2O_3	8.5
Goethite, α-FeOOH	9.3
Quartz, SiO_2	1.5 - 3.7 [2]
[1] *Appelo & Postma, 2006*	
[2] *Fuerstenau, IUPAC ORG paper*	

Table 4.13 pH for the point of zero charge of the selected minerals (Appelo and Postma, 1994).

The results for all minerals are shown in Table 4.14. The three negative results observed at pH 4.0 and 0.01 M $NaNO_3$ corresponds to an experiment

where the losses blanks used as representative of the initial naphthalene concentration yielded a GC-FID response lower than that corresponding to the sample triplicates; and therefore the uptake calculation result is negative. This result is physically meaningless and will not be discussed further. Unfortunately it was not possible to repeat these experiments.

Kmin	**I1**		**I2**		**I3**	
$NaNO_3$, M	0.001		0.01		0.1	
Mineral / pH	4.0	5.5	4.0	5.5	4.0	5.5
QS	0.076	0.213		0.279	0.220	0.545
Hm	0.004	0.053	0.028	0.085	0.049	0.270
Fe-QS	0.078	0.066		0.053	0.053	0.035
Stx-1	0.028	0.076		0.058	0.047	0.044

Table 4.14 Summary of all sorption experiments results

All results for an individual mineral show a consistent trend with respect to the electrolyte concentration; especially at the higher pH value. The potential implications of these results are explored in the (following) discussion chapter. The graphs showing the sorptive behaviour for the individual materials used are shown in the following subsections.

4.5.1. Quartz Sand

The experiments carried out with the commercially pre-treated quartz sand are divided into two different sample groups: the samples run at pH 4.0 and those run at pH 5.5. The reason for this difference is that these samples sets were prepared, extracted and analysed under slightly different conditions. The first experiments with sand were carried out at pH 5.5, when the HS-SPME extraction process was still in the process of optimization. This set of samples was not repeated at a later stage due to financial and time constraints.

With regards to the sample preparation protocols followed at this stage, different reaction vials and different mineral masses were used and therefore (minor) volume corrections were required and applied in order to compare initial PAH concentrations (C_0, at t = 0) with the rest of the samples at all pH values. The values reported are already volume-corrected. These samples were extracted using immersion SPME (Direct Sampling) and the sampling time was 60 minutes. The raw data as well as the experimental protocols followed in these earlier experiments can be found in Appendix A4.

The calibration lines carried out with both extraction methods (at pH values 4.0 and 5.5) were found to be equally efficient since the same standardisation method and the same standard concentrations were used (external calibration). The results are therefore comparable to those obtained at pH = 4.0 and can be found in Figure 4.11.

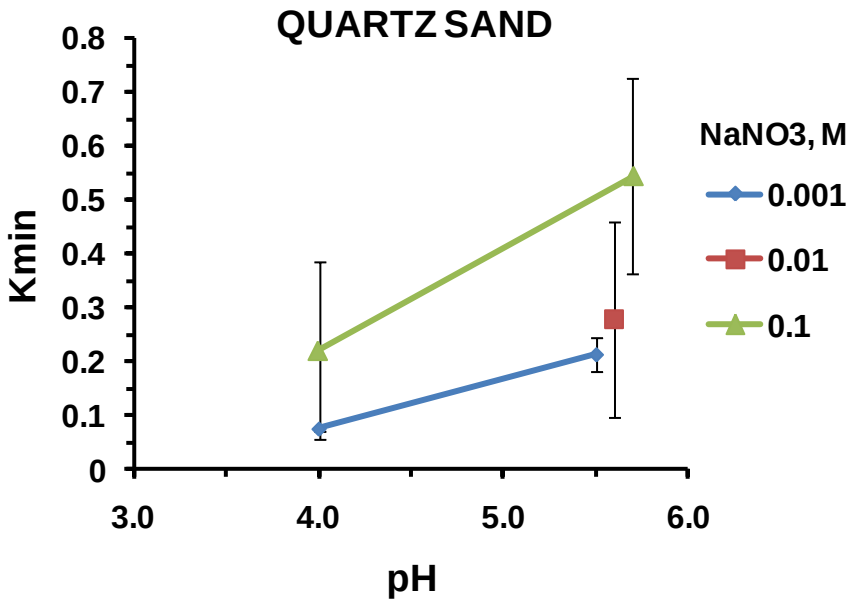

Figure 4.11Variation of K_{min} with pH and ionic strength (I1 = 0.001, I2 = 0.01, I3 = 0.1) for quartz sand. (Data points at pH 5.5 offset for clarity)

4.5.2. Hematite (α-Fe_2O_3)

The results for the sorption experiments in samples using α-Fe_2O_3 as sorbent are presented in Figure 4.12. All samples for this mineral were run, extracted and analysed in an identical manner. The results show increasing uptake with respect to ionic strength at both pH values, as is the case for quartz sand.

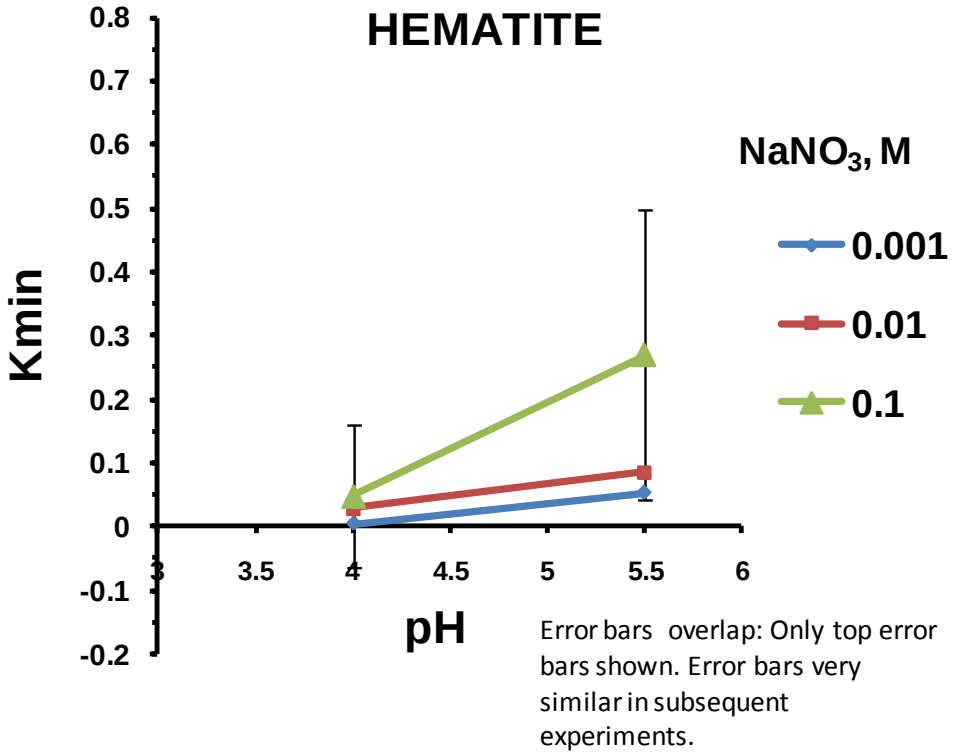

Figure 4.12 Variation of K_{min} with pH and ionic strength (I1 = 0.001, I2 = 0.01, I3 = 0.1) for hematite.

4.5.3. Montmorillonite

The sorption experiments results for the STx-1 montmorillonite are presented in Figure 4.13. Considerable difficulties were faced when trying to

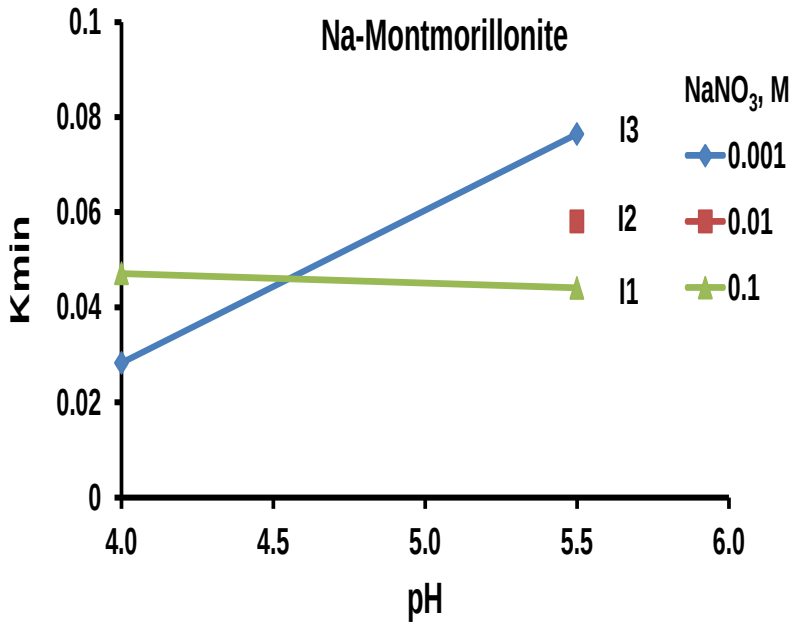

Figure 4.13 Variation of K_{min} with pH and ionic strength (I1 = 0.001, I2 = 0.01, I3 = 0.1) for montmorillonite.

obtain a clear supernatant for the samples prepared using this mineral given the colloidal nature of the material. The centrifugation step required a much longer time than for the other samples (3300 rpm for 3 hours) and since no filtration was performed, the possibility of interference from submicron colloidal particles may not be excluded. Filtration was not carried out due to concerns about severe PAH losses to filters and to the required vacuum-filtration equipment. Negative values are not included in the summary graph.

The trend for this material seems to be the opposite of that observed for the previous two minerals at high pH. Coefficient values are approximately an order of magnitude lower than for the other minerals however, and so the cryptic behaviour in this case may be a reflection of the difficulties in accurately measuring K in this system.

Clay minerals are well known to be affected by small changes in pH given their surface characteristics. The Stx-1 clay was used as received. It was selected as an example of a common natural material.and was not pre-treated (cation-saturated) prior to the experiments.

4.5.4. Fe-coated Quartz Sand

The iron-coated sand was the same sand used in the first experiments (labelled QS) was pre-conditioned in the laboratory with a coating intended to consist of a thin goethite layer. X-ray diffraction analysis of the sand post-treatment however found the coating to be amorphous.

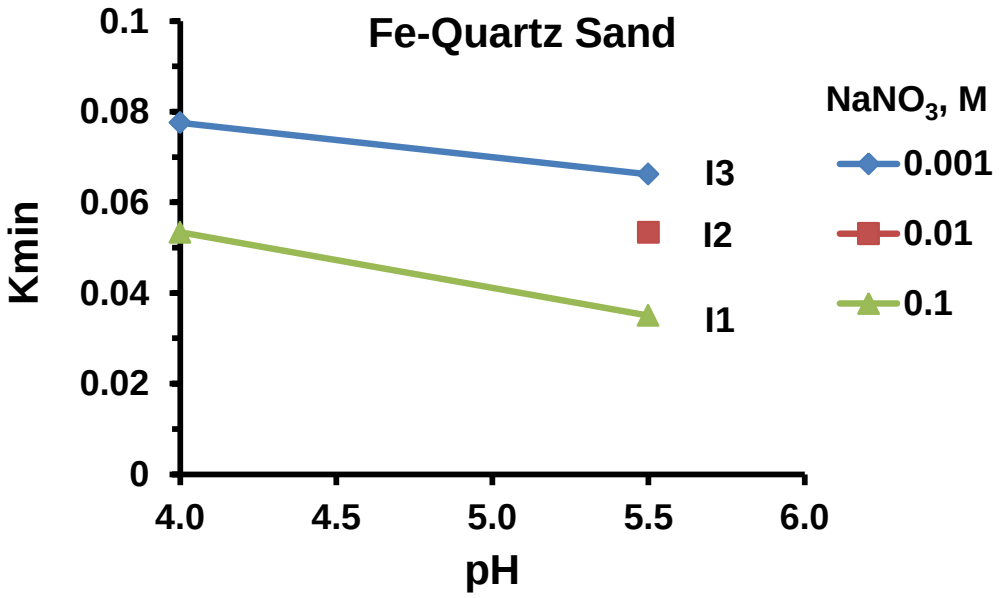

Figure 4.14 Variation of K_{min} with pH and ionic strength (I1 = 0.001, I2 = 0.01, I3 = 0.1) for the iron-coated sand.

The presence of Fe however, was corroborated using XRF analysis and the results showed that the sample consisted mostly of SiO_2 (97.528 % w / w) with Fe_2O_3 present as 1.61 % of the solid. The remainder was a mixture of

different mineral impurities (see Chapter 2). The sorption results for the coated sand are shown in Figure 4.14. The trend observed seems to be consistent for all 3 electrolyte concentrations but different from the untreated quartz and hematite results.

REFERENCES

Ackerman, A. H. and Hurtubise, R. J. (2000). The effects of adsorption of solutes on glassware and teflon in the calculation of partition coefficients for solid-phase microextraction with 1PS paper. Talanta 52(5): 853-861.

Appelo, C. A. J. and Postma, D. (1994). Geochemistry, Groundwater and Pollution. Rotterdam, Balkema. 669 pages.

Appert-Collin, J. C., Dridi-Dhaouadi, S., Simonnot, M. O. and Sardin, M. (1999). Nonlinear sorption of naphtalene and phenanthrene during saturated transport in natural porous media. Physics and Chemistry of the Earth, Part B: Hydrology, Oceans and Atmosphere 24(6): 543-548

Carmo, A. M., Hundal, L. S. and Thompson, M. L. (2000). Sorption of Hydrophobic Organic Compounds by Soil Materials: Application of Unit Equivalent Freundlich Coefficients. Environmental Science and Technology 34(20): 4363-4369.

Doong, R. a. and Chang, S. m. (2000). Determination of Distribution Coefficients of Priority Polycyclic Aromatic Hydrocarbons Using Solid-Phase Microextraction. Anal. Chem. 72(15): 3647-3652.

Eisert, R. and Levsen, K. (1996). Review: Solid-phase Microextraction Coupled to Gas-Chromatography: A new Method for the Analysis of Organics in Water. Journal of Chromatography A 733(1-2): 143-157.

Fifield, F. W. and Kealy, D. (2000). Principles and Practice of Analytical Chemistry, Blackwell Science. pages.

Fowlis, I. A. (1995). Gas Chromatography. Chichester, John Wiley and Sons. 300 pages.

Gaboriau, H. and Saada, A. (2001). Influence of heavy organic pollutants of anthropic origin on PAH retention by kaolinite. Chemosphere 44(7): 1633-1639.

Harris, D. (1991). Quantitative Chemical Analysis. New York, W. H. Freeman and Company. 3rd edition. pages.

Hundal, L. S., Thompson, M. L., Laird, D. A. and Carmo, A. M. (2001). Sorption of Phenanthrene by Reference Smectites. Environmental Science and Technology 35(17): 3456-3461.

Hwang, S. and Cutright, T. J. (2004). Evidence of underestimation in PAH sorption/desorption due to system nonequilibrium and interaction with soil constituents. J Environ Sci Health Part A Tox Hazard Subst Environ Eng 39(5): 1147-1162.

Kan, A. T., Fu, G., Hunter, M., Chen, W., Ward, C. H. and Tomson, M. B. (1998). Irreversible sorption of neutral hydrocarbons to sediments:

Experimental observations and model predictions. Environmental Science and Technology 32(7): 892-902.

Kleineidam, S., Ruegner, H., Ligouis, B. and Grathwohl, P. (1999). Organic Matter Facies and Equilibrium Sorption of Phenanthrene. Environmental Science & Technology 33: 1637-1644.

Kookana, R. S., Gerritse, R. G. and Aylmore, L. A. G. (1990). Effect of Organic Cosolvent on Adsorption and Desorption of Linuron and Simazine in Soil. Australian Journal of Soil Research 28: 717 - 725.

Lai, C. H. and Chen, C. Y. (2001). Removal of metal ions and humic acid from water by iron-coated filter media. Chemosphere 44(5): 1177-1184.

Li, N. and Lee, H. K. (2001). Assessment of Colloid Formation and Physical State Distribution of Trace Polycyclic Aromatic Hydrocarbons in Aqueous Samples. Anal. Chem. 73: 5201-5206.

Middleton, C. (2003). The Development Of A Mesoscale Contaminant Hydrogeology Column And Its Application To Environmental Organic Systems. Department of Civil Engineering. Manchester, University of Manchester**:** 420.

Niri, V. H. and Pawliszyn, J. (2007). Equilibrium in-fiber standardization method for determination of sample volume by solid phase microextraction. Analyst 132(5): 425-430.

Nkedi-Kizza, P., Rao, P. S. C. and Hornsby, A. G. (1987). Influence of Organic Cosolvents on Leaching of Hydrophobic Organic Chemicals through Soils. Environmental Science & Technology 21(11): 1107 - 1111.

Ouyang, G., Cai, J., Zhang, X., Li, H. and Pawliszyn, J. (2008). Standard-free kinetic calibration for rapid on-site analysis by solid-phase microextraction. Journal of Separation Science 31(6-7): 1167-1172.

Pawliszyn, J. (1999). Applications of Solid Phase Microextraction. Bodmin, The Royal Society of Chemistry. pages.

Piatt, J. J., Backhus, D., Capel, P. D. and Eisenreich, S. J. (1996). Temperature-Dependent Sorption of Naphthalene, Phenanthrene, and Pyrene to Low Organic Carbon Aquifer Sediments *Environmental Science and Technology* 30 (3): 751 -760.

Pignatello, J. J. and Xing, B. (1996). Mechanisms of slow sorption of organic chemicals to natural particles. Environmental Science and Technology 30(1): 1 - 8.

Qian, Y., Posch, T. and Schmidt, T. C. (2011). Sorption of polycyclic aromatic hydrocarbons (PAHs) on glass surfaces. Chemosphere 82(6): 859-865.

Sabbah, I., Rebhun, M. and Gerstl, Z. (2004). An independent prediction of the effect of dissolved organic matter on the transport of polycyclic aromatic hydrocarbons. Journal of Contaminant Hydrology 75(1-2): 55-70.

Schlautman, M. A., Yim, S., Carraway, E. R., Lee, J. H. and Herbert, B. E. (2004). Testing a surface tension-based model to predict the salting out of polycyclic aromatic hydrocarbons in model environmental solutions. Water Research 38(14-15): 3331-3339.

Schwarzenbach, R. P., Giger, W. and Grob, K. (1984). Gas Chromatography. Water Analysis. Organic Species. R. A. Minear and L. H. Keith. London, Academic Press, Inc. Ltd. 3.

Schwarzenbach, R. P., Gschwend, P. M. and Imboden, D. M. (1993). Environmental Organic Chemistry, John Wiley & Sons Inc. 1340 pages.

Scott, R. P. W. (2002). Gas Chromatographic Detectors.

Sheffield Hallam University, S. o. S. a. M. (1998a). Gas Chromatography: FID Detector. Retrieved 13/06/2006.

Sheffield Hallam University, S. o. S. a. M. (1998b). Gas Chromatography: GC system. Retrieved 12/06/06.

Sheffield Hallam University, S. o. S. a. M. (1998c). Gas Chromatography: Injectors. Retrieved 13/06/2006.

Shurmer, B. and Pawliszyn, J. (2000). Determination of Distribution Constants between a Liquid Polymeric Coating and Water by a Solid-Phase Microextraction Technique with a Flow-Through Standard Water System. Analytical Chemistry 72(15): 3660-3664.

Sun, H., Tateda, M., Ike, M. and Fujita, M. (2003). Short- and long-term sorption/desorption of polycyclic aromatic hydrocarbons onto artificial solids: effects of particle and pore sizes and organic matters Water Research 37(12): 2960-2968

Wefer-Roehl, A., Graber, E. R., Borisover, M. D., Adar, E., Nativ, R. and Ronen, Z. (2001). Sorption of organic contaminants in a fractured chalk formation. Chemosphere 44(5): 1121-1130.

Willet, J. E. (1987). Gas Chromatography, John Wiley & Sons. pages.

Zhou, Y., Liu, R. and Tang, H. (2004). Sorption interaction of phenanthrene with soil and sediment of different particle sizes and in various CaCl2 solutions. Journal of Colloid and Interface Science 270(1): 37.

Zhu, D., Herbert, B. E. and Schlautman, M. A. (2003). Molecular-level investigation of monoaromatic compound sorption to suspended soil particles by deuterium nuclear magnetic resonance. Journal of Environmental Quality 32(1): 232-239.

Zhu, D., Hyun, S., Pignatello, J. J. and Lee, L. S. (2004). Evidence for - Electron Donor-Acceptor Interactions between -Donor Aromatic Compounds and - Acceptor Sites in Soil Organic Matter through pH Effects on Sorption. Environmental Science and Technology 38(16): 4361-4368.

CHAPTER 5 Surface Analysis

"Two general rules should be remembered in surface analysis. (a) In every case it is important to understand the capabilities and limitations of the technique being used with regard to the material being studied and the information required. (b) No one technique gives the whole story."

Vickerman, "Surface Analysis: The Principal Techniques"

5.1. Surface Analysis Scope and Applications in Environmental Organic Geochemistry Studies

Since the development of electron spectroscopy in 1960 (Briggs and Seah, 1990) the surface of solids has been the subject of intense study across several disciplines (engineering, physics, chemistry, environmental sciences, mineralogy) due to the important reactions which take place at the interface between two phases at disequilibrium. The surface of a mineral may be completely different in structure and composition to the bulk crystal mainly due to the fact that the charges on surface atoms are not fully satisfied, which in turn makes their chemistry quite unique.

Surface science is therefore an exciting and rapidly growing multidimensional discipline, encompassing a range of fields from basic research to applied industrial technology. It aims to study solid surfaces at the atomic level to complement the knowledge about the bulk phase as a means to better understanding the behaviour observed at interfaces.

Surface analysis studies of the composition and geometry of the outermost layers of a solid. These techniques are capable of providing in-depth knowledge at atomic resolution with straightforward sample preparation steps. The wealth of information which can be obtained comprises: surface atomic composition, type of chemical bonding on the surface as well as detailed topology of selected surface areas showing inhomogeneities and location of atoms and specific features such as adsorbed molecules. Some surface analysis techniques can determine the electronic state of adsorbates on the surface, therefore shedding light on the type of bond that attaches them to the solid. Some techniques analyse the samples as a function of depth, whereas others are limited to the very first layers, i.e. only a few nanometres deep. and others reveal information on molecular and atomic structure (Vickerman, 1997).

5.2. Specific Advantages of Surface Analysis Techniques

The use of these innovative techniques poses several advantages to environmental scientists, amongst which are:

- the ability to study the details of environmentally important reaction pathways at the molecular or even atomic level;

- improved understanding of the nature of the reactions taking place between species at interfaces, therefore helping to explain comparable behaviour observed within bulk solution,

- accurate determination of the type of binding forces being exerted on the surface molecules,

- determination of the surface composition in very small areas (of the order of square angstroms)

Another remarkable advantage is that surface analysis techniques are often non - destructive of the substrate, which makes them an invaluable asset when dealing with small, unique or rare samples. Equally important is the fact that it is possible to carry out kinetic studies *in situ*, and in live specimens, allowing the rapid detection of reaction products as they form in a variety of scenarios.

5.3. Rationale of the Application of Surface Analysis to the Study of PAH Interactions with Mineral Surfaces

The transport and fate of PAH in the subsoil environment cannot be predicted without understanding the properties of the involved soil components. As an example, mineral phases in contaminated soil scenarios are continuously exposed to organic pollutants at the solid-liquid interface. Depending on the environmental conditions the exposed surfaces could interact with these chemicals (Appelo and Postma, 1994). Previous studies have already suggested that in the absence or near absence of organic carbon (0.1 % organic carbon has been suggested, see Chapter 1), the role of the subsurface mineral phases becomes increasingly relevant in the transport of PAH, perhaps to the extent of controlling PAH release within the soil. This study aimed to use surface analysis techniques to prove or disprove the proposed hypothesis that pure, inorganic mineral surfaces may interact with or even remove large, planar and mostly non - reactive PAH molecules from solution. The study was conducted with specific constrains on the amount of organic matter present in

the system. The specific objectives of the experiments and measurements presented in this section are:

- to find out whether any detectable chemical interaction such as adsorption took place between the PAH used and the selected mineral surfaces exposed to them in a number of different solution scenarios,

- to elucidate the most likely mode of attachment, in the case that sorption or removal from solution was observed, by which PAH managed to remain adsorbed on the mineral surface,

- to register PAH surface-deposition using enhanced imaging techniques as visual proof of surface attachment.

To the best of the author's knowledge, the application given to the surface analysis techniques used in this work have not been previously reported for similar experimental scenarios or to address the same research questions.

5.4. Limitations of Surface Analysis Techniques within the Scope of the Present Experiments

Since the surface is exposed to the environment it can accumulate dirt and contaminants as well as react with the surrounding humidity and become fundamentally different from the rest of the solid. Environmental conditions therefore greatly affect the composition and properties of the substrates under analysis. This is the reason why in some instances, a number of sample preparation or modification steps is required in order to isolate the process under study without unwanted interference from the surroundings. An example of this is the use of ultra high vacuum conditions (UHV) in order to keep the

substrate at a constant state (or unchanged) and protect a freshly exposed surface from water vapour or oxygen present in air.

As was observed during the course of the experimental work carried out; surface analysis can be severely constrained in its applicability to certain types of sample systems. Some substrates are notoriously difficult to manipulate in their natural form in which case modification steps must be undertaken; such as preliminary cleaning and coating of the surface to be analysed.

Some molecules used as potential surface adsorbates may have prohibitive dimensions and imaging them could in some instances be beyond the capability of the equipment in use. Such would be the case of small, planar molecules whose height or thickness falls below the resolution of the technique being used or the lowest irregularity or ridge on the surface being imaged. In these cases, derivatization of the compound may be the only way forward although this does not always fall within the scope of the original experiment.

5.5. Surface Analysis Techniques Employed in this Study.

The surface analytical techniques used in this study can be (broadly) divided into two main types: spectroscopic techniques: such as X-ray Photoelectron Spectroscopy (XPS) and Infrared Spectroscopy (IR); and imaging techniques such as Atomic Force Microscopy (AFM). The main difference between these two groups is how they probe the sample: whereas in the first group a beam of X--rays or infra-red light is aimed at the surface under study; in AFM the sample is scanned by an optically (or otherwise) controlled mechanical device (tip) and can produce images with exceptionally high resolution.

The fundamentals of each individual technique used as well as their scope and capability will be presented in the sections below, followed by a detailed description of materials and reagents used, the experimental setup and analytical protocols followed. Lastly, the results are presented and interpreted in light of this chapter's aims and objectives.

5.6. Atomic Force Microscopy (AFM):

5.6.1. Description

Atomic Force Microscopy or Scanning Force Microscopy, as it is also known, is a surface microscopy technique which provides information on the topography of a given area on a solid's surface. The principle behind it is the electrostatic interaction between a mobile sharp tip and the species on the surface under analysis. The intensity of this interaction as the tip is rastered over a given area is mapped as a function of its position, producing an electronic "map" or topographic image of the scanned substrate. AFM was invented by Binning and Rohrer in 1986 in order to address an experimental artefact encountered when using a similar surface microscopy technique, Scanning Tunneling Microscopy or STM. The latter is based on an application of the quantum tunnelling principle which for these purposes can be interpreted as follows: when the tip of a conductive stylus is brought into close proximity with a conductive surface and a voltage is applied; electrons travel through the vacuum gap (tunnelling current) between the two conductive materials. If this current is kept constant as the stylus moves vertically the output obtained will be equivalent to contour of the surface, mapping anything adsorbed on it. If the height is kept constant the tunnelling current or electron density can be

monitored to detect surfaces irregularities with great resolution. But there was a limitation with this approach: Binning and co-workers found that in some cases the tunnelling current was found to be too high to be of a similar order of magnitude to the interatomic forces on the surface, even at relatively low values therefore disrupting the structure being investigated (Vickerman, 1997). In addition to that, STM could not be used to image non-conductive materials as there would be no current flow.

These problems were circumvented by substituting the STM stylus for a cantilever positioned parallel to the surface and equipped with a force sensitive tip (DiNardo, 1994). This is represented in Figure 5.1 below, where the parts of an Atomic Force Microscope are depicted in a diagram. The change in scanning mechanism enabled non-conductive substrates to be analysed, since a flow of tunnelling electrons was no longer necessary.

5.6.2. AFM Operation

Atomic Force Microscopes work by rastering a cantilever with a sharp tip or needle across a selected area of the analyte's surface measuring the electrostatic interaction between the tip and the surface atoms. The cantilever is attached to piezoelectric transducers which move in response to electrical signals. The section of the cantilever just on the back of the tip is made up of a reflective material. A laser beam is directed onto this mirror and as the tip is

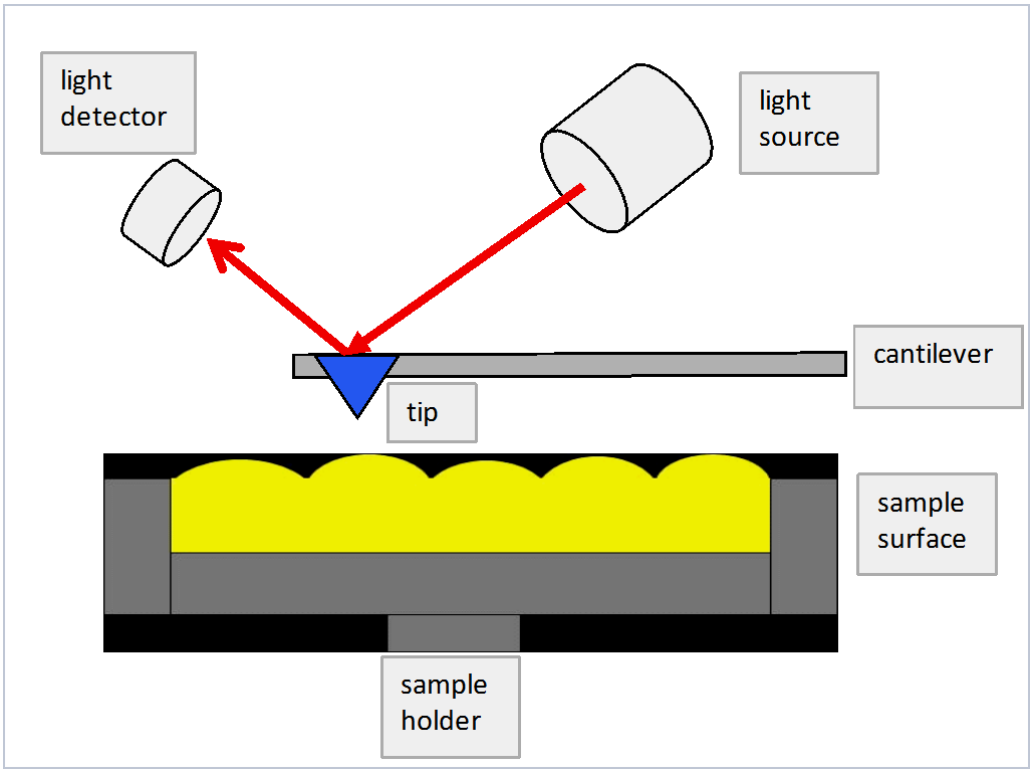

Figure 5.1 Schematic Diagram of an Atomic Force Microscope and Sample Holder.

either repelled or attracted by the surface, the cantilever deflects the laser beam towards a photodetector mounted at an angle above the sample holder. This signal is amplified and fed to a register. In this way the magnitude of cantilever deflection is used to control a piezoelectric crystal underneath the cantilever and when this signal is plotted versus the tip position an accurate topography of that section of the sample is obtained.

Any force exerted on the tip will produce a deflection of the cantilever in addition to displacement of the piezoelectric sample holder. The cantilever's response is crucial in determining the resolution of the microscope, as is the tip's design. Materials commonly used to make the tip range from plain silicon, silicon nitride (Si_3N_4) to silicon oxide or silicon doped with phosphorous/conductive materials (Nalwa, 2001).

There are four ways in which the AFM can be operated when imaging a surface:

Contact mode: If the distance between the surface atoms is small, the interatomic energy will be high and the tip will be repelled from the surface. By applying a voltage, the tip of a flexible cantilever can be made to touch the surface as it is rastered over it whilst keeping the force constant and measuring the deflections caused by the surface topography. The force applied could in cases be excessive and alter the sample's features, which makes contact mode unsuitable for soft surfaces or lightly adsorbed sorbates as they could be dragged by the tip across the scanned area.

Friction force mode: the tip touches the surface as it scans whilst a lateral force is applied to make the cantilever twist. The friction between the tip and the surface is mapped against the area scanned generating an image.

Non-contact mode: the cantilever is made to oscillate at its resonance frequency by the driving piezoelectric crystal. The amplitude of the oscillation is kept small so that the tip does not touch the surface. Depending on the surface forces and the height at which the tip hovers over the sample, this mode can be susceptible to interference by water layers on the substrate when imaging takes place in air.

Tapping mode: similarly to the non-contact mode, a very rigid cantilever is made to oscillate close to its resonance frequency when away from the surface. As the cantilever approaches the surface, the oscillation amplitude will change, depending on the characteristics of the feature. As an example: if the surface has a depression the amplitude will increase; in the case of a raised profile the amplitude will decrease. This information is used to create an image

of the surface features. This approach is the best approach for sampling in air, as the presence of a water meniscus does not affect the measurement. Additionally, it minimises damages to the substrate and any sorbates caused by the use of excessive contact force although it is not always guaranteed that it will not to some extent disturb the surface.

The samples in these experiments were scanned on tapping mode. The conditions and analytical setup are described in Section 5.6.7.

5.6.3. Information Expected from the Technique

As stated in the introduction to this chapter, the aim of using surface analysis on the mineral - PAH system selected in this study was to assess whether or not organic sequestration took place and to establish what the dominant mechanism was. The high imaging resolution of AFM was expected to provide visual confirmation of adsorbate registration on the substrates studied as well as an indirect measure of the forces interacting on reacted surfaces when compared against previous blank runs of the same substrate. Table 5.1 shows the variety of forces acting between the cantilever tip and the sample atoms which can be detected by AFM and other surface analysis techniques (Kolasinski, 2008).

5.6.4. Reagents, Materials and Equipment

The minerals used, the pre-treatment applied and the PAH adsorbates in the AFM runs are outlined below in Table 5.2. The equipment used consisted of:

Interaction	Nature	Range
Pauli exclusion	Short range/repulsive	~0.1 nm
Coulomb repulsion	Short range/repulsive	~0.1 nm
Chemical bond	Short range/attractive	~0.1 nm
van der Waals	Long range/attractive	up to 100 nm
Electrostatic	Long range/attractive or repulsive	~several 100 nm
Magnetic	Long range/attractive or repulsive	~several 100 nm
Capillary forces	Attractive	Up to 10 nm
Hydrodynamic	Very long range, damping	~10 μm

Table 5.1 Range of surface forces detectable with AFM.

- Atomic Force Microscope: Digital Instruments Nanoscope AFM.

- Tip: Phosphorous-doped silicon tip, 100 Å.

- Cantilever: length: 120 μm; width: 35 μm; thickness: 3.5 μm.

- Coating Equipment: Polaron Range Sputter Coater with a stabilised power supply and a custom-adapted chamber

- Adsorbates: diverse organic molecules

The main adsorbate was naphthalene and it was used as received from the manufacturer at two different concentrations, namely: 200 and 5000 mg / l in methanol. Sample loading took place as liquid droplets and later on as vapour deposition from sublimating neat solids. Vapour deposition was favoured over liquid as a dosing method. The other tested adsorbates were prepared from their solid form into solutions of the desired concentrations and dosed as liquid droplets onto the slides. The experimental sample preparation and dosing

details have been included in Table 5.2.

#	Substrates	Dimensions	Pre-treatment	Solvents	Chemicals	Concentration
1	SiO_2	10 x 10 x 1 mm	Polishing	Methanol (Pestanal)	Naphthalene (liquid)	5000 mg / l
2	SiO_2	10 x 10 x 1 mm	Polishing	Methanol (Pestanal)	Naphthalene (vapour deposition)	5000 mg / l
3	Muscovite	10 x 10 x 1 mm	Cleaving	Methanol (Pestanal)	Naphthalene (vapour deposition)	0.11 g
4	Muscovite	10 x 10 x 1 mm	Cleaving Au -coating	Methanol (Pestanal)	None	-
5	Muscovite	10 x 10 x 1 mm	Cleaving Au-coating Annealing	None	None	-
6	Muscovite	10 x 10 x 1 mm	Cleaving Au-coating Annealing	DIW	Bovine Serum Albumin (BSA) (liquid)	20 - 1080 mg/l
7	Muscovite	10 x 10 x 1 mm	Cleaving Au-coating Annealing	Toluene	C60	5 - 1030 mg/l

Table 5.2 Experimental materials and reagents for AFM imaging.

The thickness of the molecules to be imaged was found to play a key role in the success of AFM as imaging tool. Moreover, the contrast between the surface roughness and the size and position of the molecules attached to it will likely determine whether the cantilever tip will sense the molecule as well as the presence of adsorbates on it. Below is a schematic diagram of the naphthalene molecule depicting its molecular dimensions.

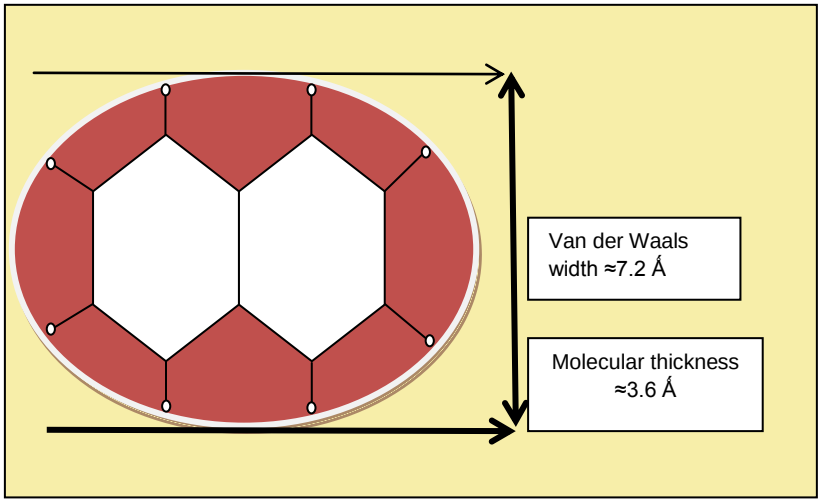

Figure 5.2 Molecular dimensions of naphthalene.

5.6.5. Sample Preparation and Pre-conditioning of Mineral Substrates:

The different mineral substrates were tested for their suitability for imaging analysis using AFM prior to loading them with organic molecules. In each case, substrate conditioning and pre-treatment was performed as required. The main conditioning step consisted of polishing the silicon dioxide slides; these were polished to an approximate thickness of 1 mm followed by solvent washes and controlled drying. Fresh exposed surfaces were obtained by cleaving in the cases of mica and graphite sheets.

5.6.6. Experimental Procedure:

After conditioning and modifying the substrates, all slides were placed on a metal plate using silver epoxy (silver dag). The samples were then placed inside the AFM chamber on a holder and kept in place by means of coil hooks on a platform made of piezoelectric materials. Microscopic lenses were then lowered down as close as possible to bring the sample into focus. Care was

taken to ensure the lenses were aimed at the centre of the slides since the edges had been touched whilst loading the substrate. The tip was focused manually as close as possible to the sample. The entire platform structure was then unlocked and the vibration controls engaged. The cantilever was made to approach the surface. The intensity of tapping (amplitude set-point) was at this point regulated to the desired value. Once the microscope was properly focused and a good signal was obtained the recording of the images would begin.

5.6.7. Analytical Conditions:

Analytical conditions differed for each test given the feasibility nature of the study. Overall, the main parameters adjusted for each substrate were:

Tip size: 100, 50 or 10 Å wide.

Mode: Tapping mode in air

Tapping force: 1.4 to 1.6 V

Area scanned: ranging from 50 nm to 500 nm

Scan rate: 0.333 Hz

Images height: 256 x 256 scan lines

Height variation (scan resolution): 0.5 nm / division

Phase: within 10 degrees in z

Amplitude variation: within 0.6 nm

Deflection: 0.07 volts

All measurements were taken under air at room temperature in air. After running blank substrates, the solids were removed from the AFM in order to dose the PAH on them. In some instances this process took several hours (up

to a day) in order to allow any liquid phase to evaporate or to permit vapour deposition of the adsorbates. Once the adsorbates had been dosed the same procedure used to image the blank substrates would be repeated and where possible, images of the PAH - or adsorbate - laden surfaces would be collected and stored for analysis. The software used to analyse the images was Nanoscope V531R1.

5.7. Results

5.7.1. AFM Preliminary Tests

Initially, attempts were made to image polished and cleaned silica wafers without any further modification. This proved to be very challenging due to severe charging when trying to approach the tip to the silica surface. At the time these preliminary experiments were carried out there were problems with the instrument's software in terms of file saving due to which photographs had to be taken of the images on the screen.

The first scan of the silica slide (≈ 10 mm^2) started with an area of 422 nm x 422 nm. Given the small size of the target molecule the scan area was reduced to 10 nm x 10 nm. Figure 5.4 is a photograph of the AFM scan imaging parameters as displayed on a computer screen. No surface features could be distinguished possibly due the substantial surface charging observed as shown on Figure 5.3.

During the acquisition of these images the tip did not track the surface very well, probably because the tip was being rejected by the surface.

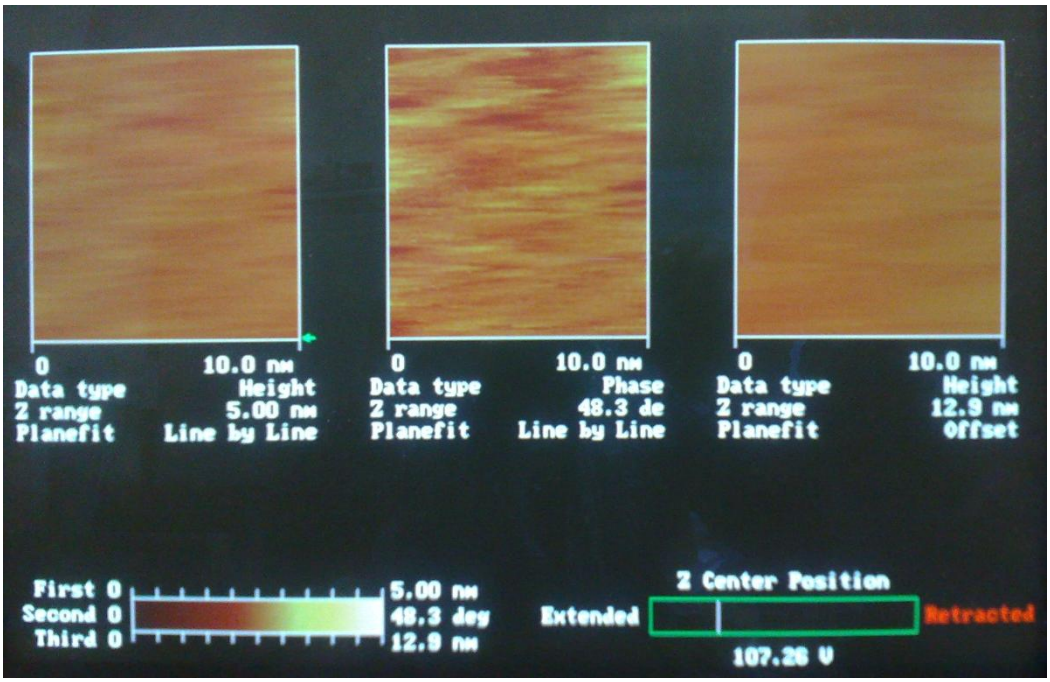

Figure 5.3 Photograph of the AFM scan of a clean, polished SiO_2 slide.

Immediately after this run, the silica slide was removed from the sample holder and a droplet of naphthalene in methanol at 5000 mg / l was transferred by touching the slide with the tip of a Pasteur pipette. The solvent was allowed (several hours) to evaporate upon which heavy crystallisation of naphthalene occurred. This was aimed to assess whether the presence of organics on the substrate affected the surface charge in any way. It was not possible to relocate the same slide area scanned in the previous run. This was a very rough surface. The surface charge in this slide appeared to have been reduced. A view of the height profile image shows no variation in the topography but the phase diagram shows much brighter spots than before as can be seen in Figure 5.4.

Subsequently the cantilever was moved to a different section of the sample (seemingly devoid of the large clusters of crystals) in order to observe any changes in the charging intensity (Figure 5.5). The charging in the cleaner

section of the same slide also appeared to be reduced, looking very similar to the clean slide prior to the loading of naphthalene (Figure 5.3).

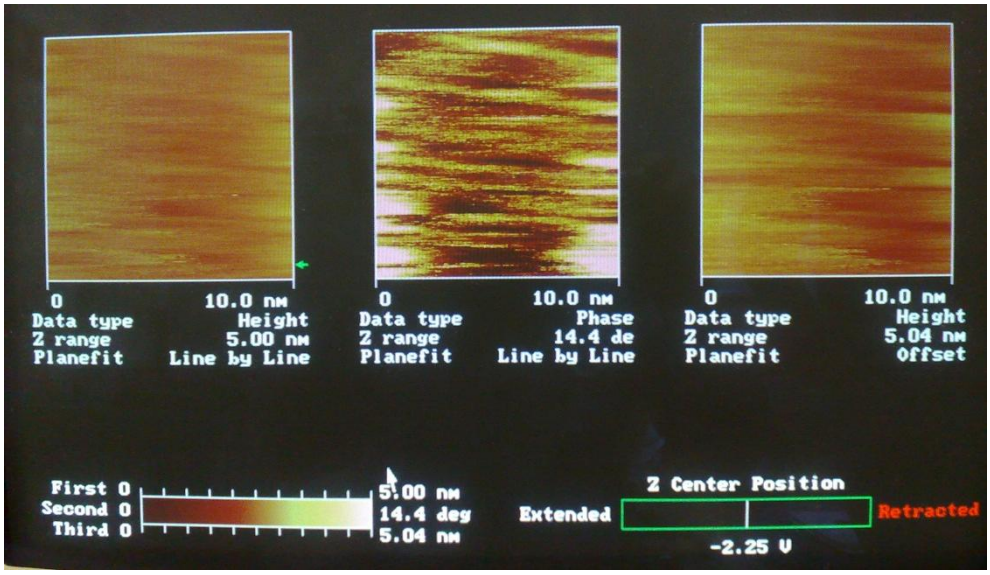

Figure 5.4 Imaging of the loaded SiO_2 slide with naphthalene crystals.

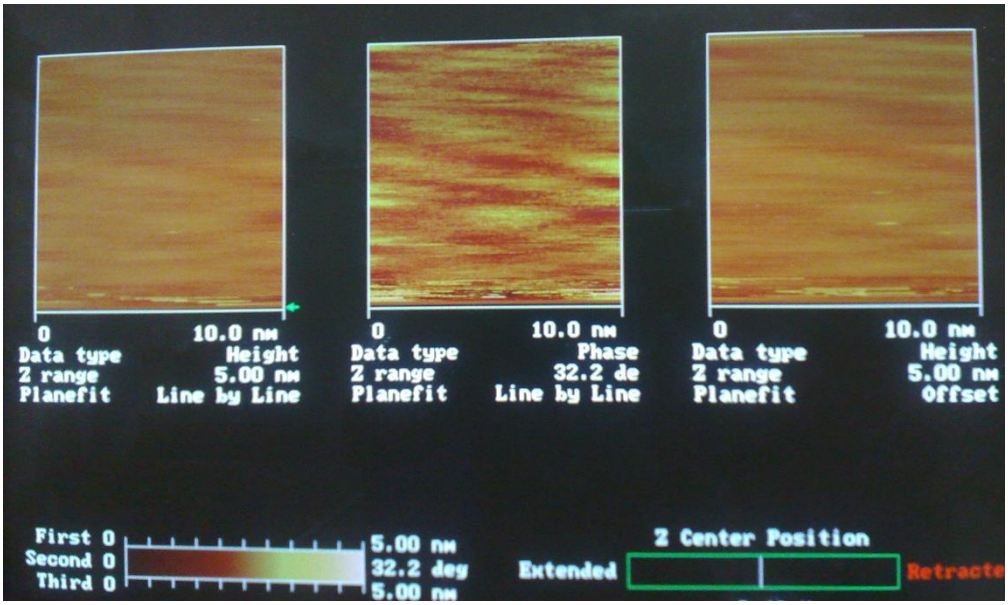

Figure 5.5 Height and phase of cleaner area.

In lieu of the naphthalene surface overload experienced when using a concentrated solution; vapour deposition was opted for as the next step in order to ensure a more uniform surface coverage. To attain this, the slide was thoroughly cleaned by leaving it overnight in DCM followed by further rinses with a series of solvents the following day (acetone, methanol and DCM). It was

then left to dry in air and then wiped with tissue (Kimberley Clark). This last step was avoided in the future as it could leave solid residue. The slide was then secured with double-sided adherent tape (whilst mounted on the AFM metal plate) underneath the septum inside the screw cap of an SPME vial (transparent glass, 10 ml volume). The vial bottom contained naphthalene crystals (0.111 g) which sublimated exposing the slide to naphthalene vapour for 24 hours. The reason for this length of exposure was to ensure large enough coverage of the surface.

The vapour treatment seemed to substantially increase the surface charging; the repulsion did not allow the tip to approach the surface close enough to acquire an image. The severe electrostatic charge repelled the tip; which would normally indicate a very clean surface (unsatisfied surface charge). Changing the imaging parameters (rastering frequency, scan rate, tapping force) had no effect on the observed results.

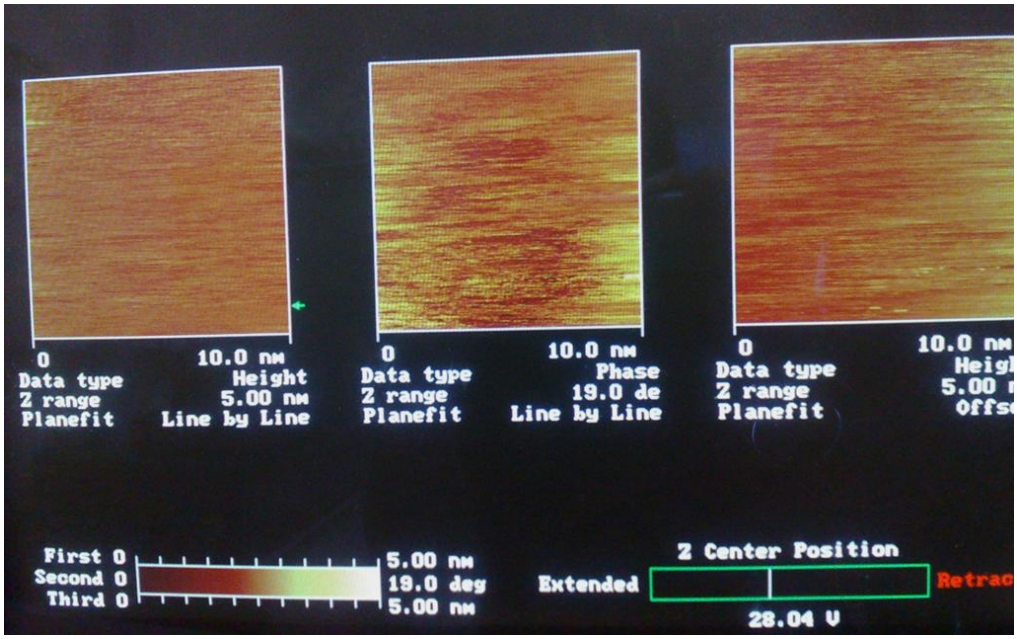

Figure 5.6 Scan corresponding to the vapour-coated SiO_2slide.

Trying to image the topography of silica in air proved to be a significant challenge, regardless of the presence of naphthalene on the substrate. Another major problem faced in regards to the SiO_2 substrate was surface roughness. The naphthalene molecule is very flat and small; exhibiting a van der Waals diameter of 7.2 Å and a thickness of 3.6 Å (Figure 5.2) (Nakhimovsky *et al.*, 1989). In order to image molecules of that size, surfaces of very flat topology would be required. The roughness of the original silica slides was found to be of the order of 30 Å (data not available), therefore a molecule of 3.6 Å height would be very hard to find on such a rough substrate.

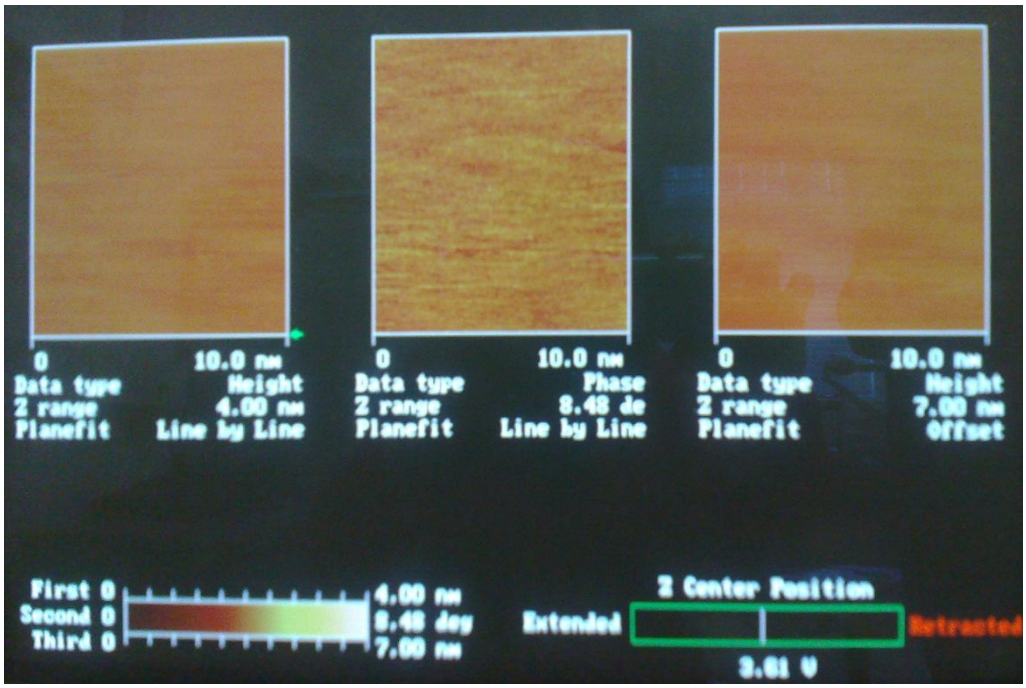

Figure 5.7 Photograph of the AFM scan of a clean muscovite slide.

As a next step, a flatter mineral surface was selected consisting of muscovite mica (average dimensions 1 cm^2) which had been cleaved and then exposed to air for a week. An area of 10 nm^2 was scanned at 0.5 nm / div and 4 nm height as shown in Figure 5.7. The surface under the microscope presented steps (photo not available) with charging similar to what was previously seen for

clean SiO_2. This surface however appears to be very much flatter as shown by the almost completely overlapping lines in the middle plot in Figure 5.8.

The same mica slide was exposed to naphthalene vapour in the same manner as for SiO_2 for 24 hours and then re-scanned). Small black clusters were observed scattered on the mica surface appearing to be little black dots of different sizes (picture not available). A large area was scanned (800 nm x 800 nm) as shown in the scope trace scan in Figure 5.9. The height and phase plots are significantly different from the naphthalene-free mica. Apparent surface features as large as 15 nm high and 160 nm wide are observed in the first trace window; whilst the second window shows a phase difference within 3 degrees (Figure 5.9).

Figure 5.8 Scope trace diagram of the clean muscovite slide.

The large features picked on the latest scan could not possibly be attributed to single naphthalene molecules but more likely to accumulated

naphthalene layers. The 24 hour exposure could have caused sequential aggregation of monolayers on top of one another, making imaging of such a surface very difficult. Lower exposure times would be required to achieve monolayer deposition and be able to infer any information regarding the interaction between the surface and the substrate. Further experiments would be necessary to confirm this.

Overall, even if a flat enough material could have been found in order to detect a 3.6 Å thick molecule as a recognizable feature on the AFM force trace, the charging experienced to a large extent with the non-conductive silica and to a lesser extent with the muscovite mica could have hindered the quality of the tracking.

Figure 5.9 Scope trace diagrams of vapour-coated mica slide.

As a drastic next step in the attempts to resolve the system and try to circumvent the charging problem, all the subsequent surfaces were Au-coated using a sputtering device. Furthermore, in order to decrease the surface roughness and ensure flatter substrates, these were flame - annealed after a

specific protocol (Elbel *et al.*, 1995). This drastic change in the methodology was aimed to gain experience in using the instrument and learn how to image the target type of molecules under ideal conditions. These processes were the last stage in the sample preparation sequence before any imaging was carried out. The images of the pre-treated materials are presented below accompanied by a table showing the experimental conditions as well as information on the system being imaged. Muscovite was sputter-coated and scanned in order to observe the effects of the pre-treatment on the quality of the surface. Figure 5.10 shows a section of the surface showing the gold coating on the freshly sputtered mica.

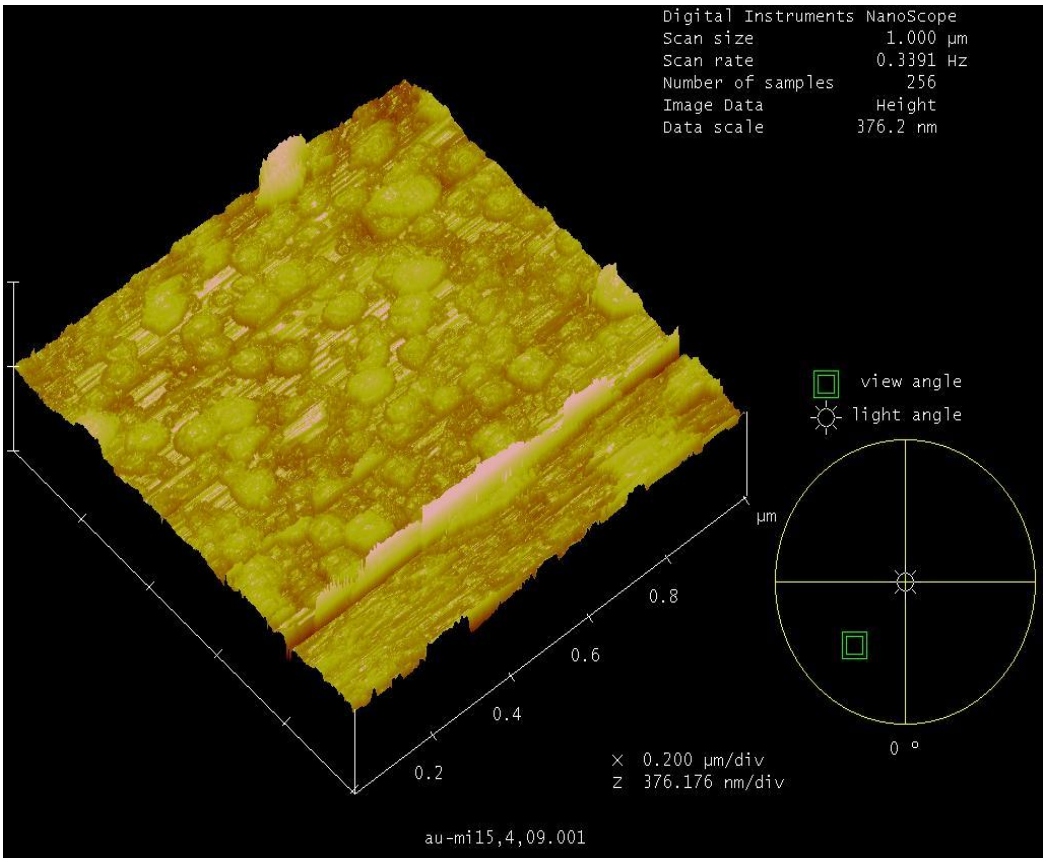

Figure 5.10 First muscovite mica slide after Au-coating.

A section analysis of the substrate is included to show the roughness of the surface (Figure 5.11). The red markers in the cross section highlighted in

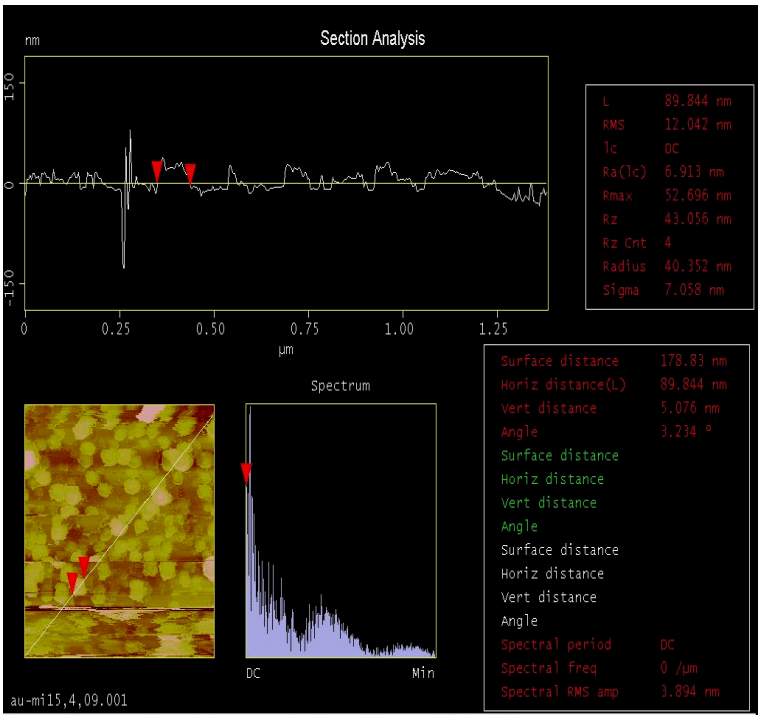

Figure 5.11 Section analysis of the first Au-coated mica slide.

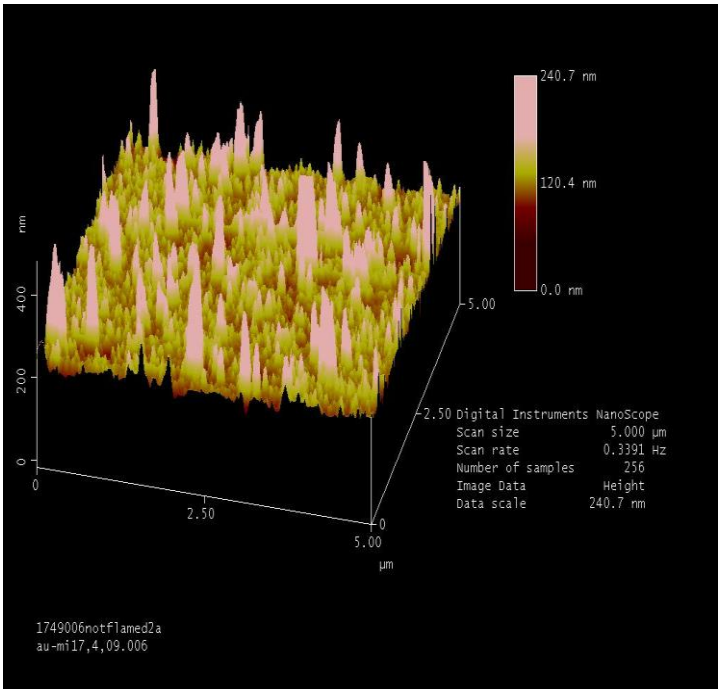

Figure 5.12 3-D surface plot of a new muscovite mica slide after coating.

Figure 5.11 shows a width (horizontal distance) of 89.844 nm (890.844 Å) and a height (vertical distance) of 5.076 nm (50.076 Å). It would be very difficult to identify naphthalene molecules in such a surface (vertical distance ≈ 3.63 Å and

horizontal distance ≈ 7 Å). Manipulating the coating parameters somewhat improved the quality of the Au layer deposition but whilst the surface charge was now satisfied, the roughness of the surfaces still represented a problem when trying to image small planar molecules such as naphthalene.

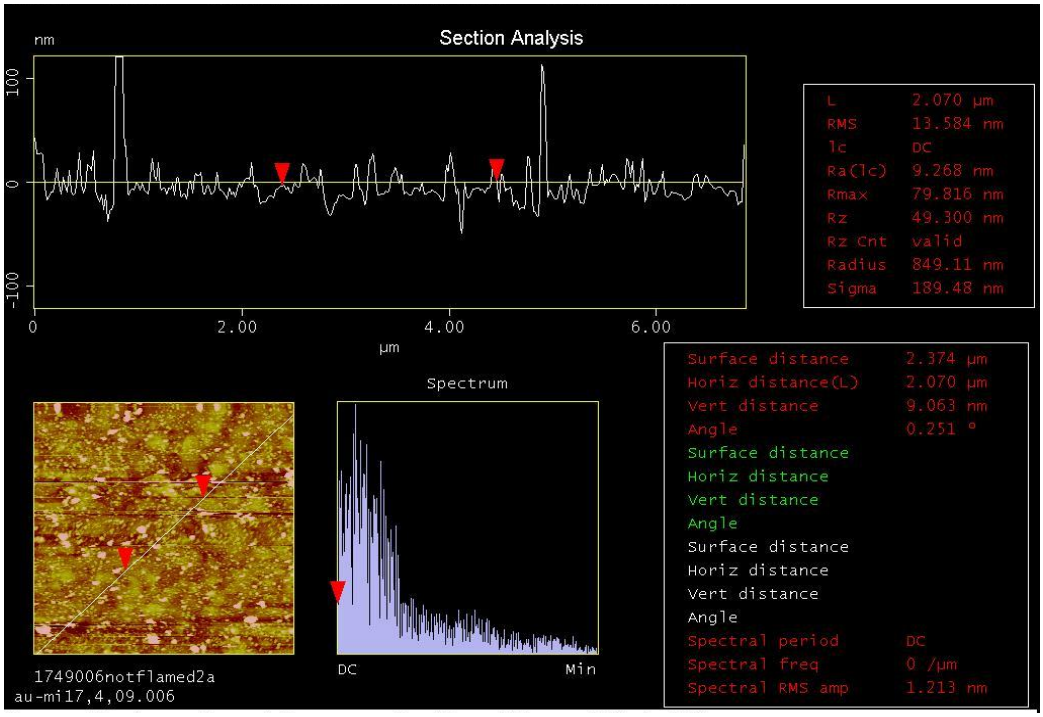

Figure 5.13 Section analysis of newly coated muscovite mica slide.

This can be appreciated in Figures 5.12 and 5.13 where a different coated mica slide was scanned and the generated images analysed.

As next step all the slides were subjected to flame annealing after a protocol followed elsewhere (Elbel *et al.*, 1995). The instructions and procedure are outlined in Appendix A5. The now flame-annealed micas are shown below in Figures 5.15 and 5.16.

Controlling the distance from and exposure to the flame was crucial in order not to overheat the gold layer. Figure 5.15 shows surface irregularities resulting from long exposure times and keeping the flame too close to the slide. Figure 5.16 presents a 3-D surface plot of a flamed slide. When compared to

the 3-D surface view of a coated slide prior to annealing (Figure 5.13) the difference in roughness can be appreciated. There are less surface irregularities although these are vertically larger than for the non-flamed slide.

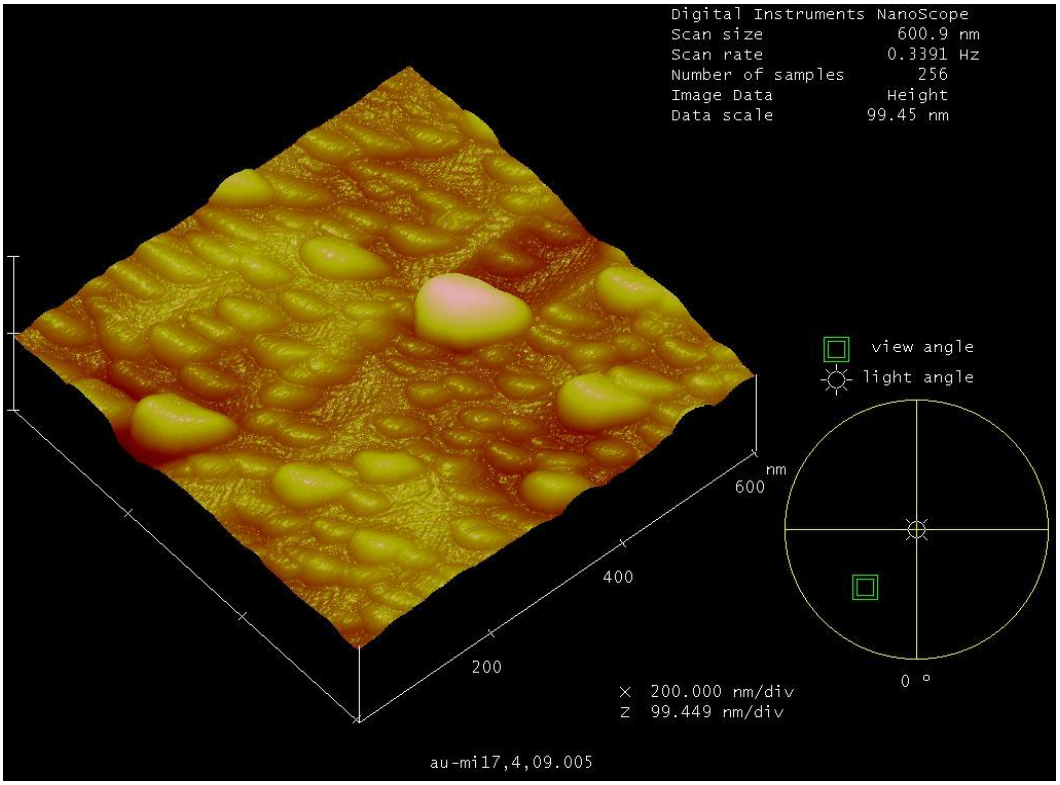

Figure 5.14 Top view of the flame-annealed muscovite surface.

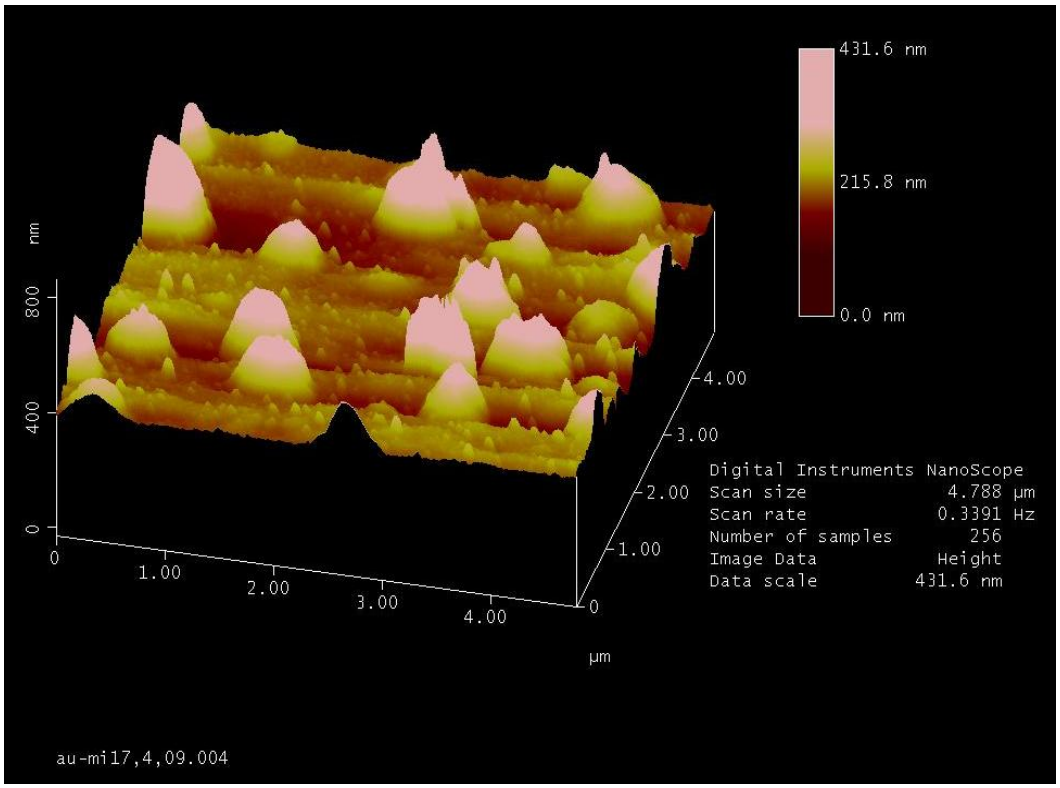

Figure 5.15 3-D surface plot of flame annealed mica.

At this point it was already evident that untreated silica slides could not be used due to charging and surface roughness. Au-coating and annealing a silica slide was therefore not attempted due to their inherently high roughness in comparison with the molecular size of naphthalene. Muscovite, on the contrary being a naturally flat material, represented a good and inexpensive choice of substrate. Once it was established that pre-treating the mica slides made them flatter and decreased the surface charge all subsequent scans were carried out in Au-coated slides after flame-annealing them.

The purpose of the following experiments was to use larger molecules on Au-coated micas as a last resort to at least learn how to image an organic molecule under ideal conditions. These would include large enough molecules to be clearly distinguished against the substrate's roughness features.

The molecules chosen for this test were: a globular protein, bovine serum albumin or BSA and a large organic molecule: C60 or Buckminster Fullerene (Bucky ball). The images in Figure 5.16 represent muscovite slides laden with C60 at different zoom sizes. The uniform coverage is the result of several dilution attempts in different solvents at different concentrations. The C60 was dissolved in toluene at the concentration specified in the table seen in Figure 5.19. This slide shows a pattern of preferential orientation similar to hexagonal patterns. The images shown in Figure 5.18 comprise the section analysis of one of the largest particles.

Bovine serum albumin or BSA was the next molecule to be imaged. Again, several dilution ratios were tried before obtaining a suitable image on the micas used. Figure 5.22 shows a zoom sequence on a BSA-laden mica slide.

Figures 5.18 to 5.20 show several views of muscovite slides covered in the same sorbate, BSA.

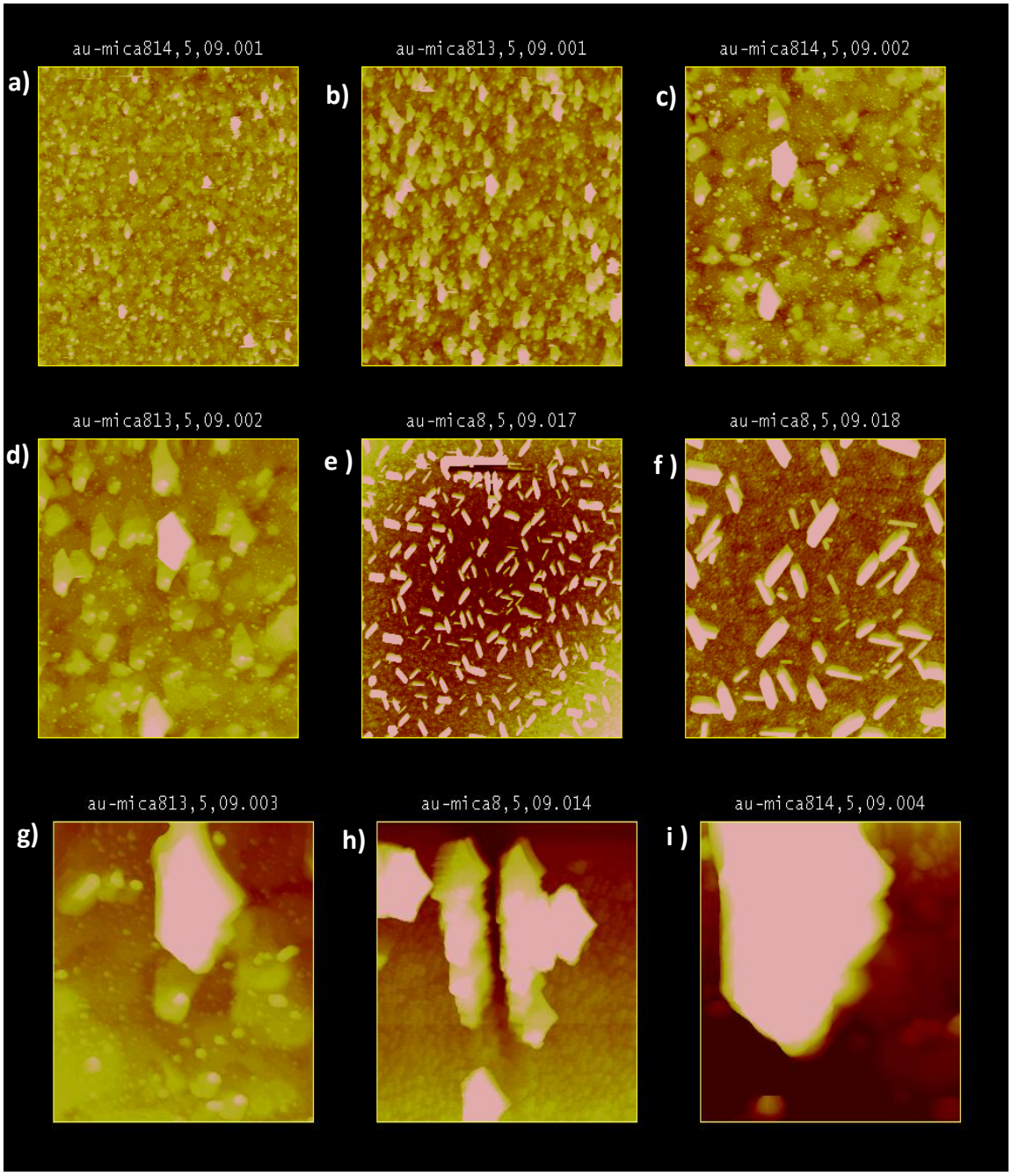

Figure 5.16 Images of C60 with progressive zooming, window widths (x axis): (a) 10.0 µm; (b) 7.57 µm; (c) 3.92 µm; (d) 2.97 µm; (e) 17.4 µm; (f) 6.81 µm; (g) 1.16 µm; (h) 2.26 µm; (i) 6.15 µm.

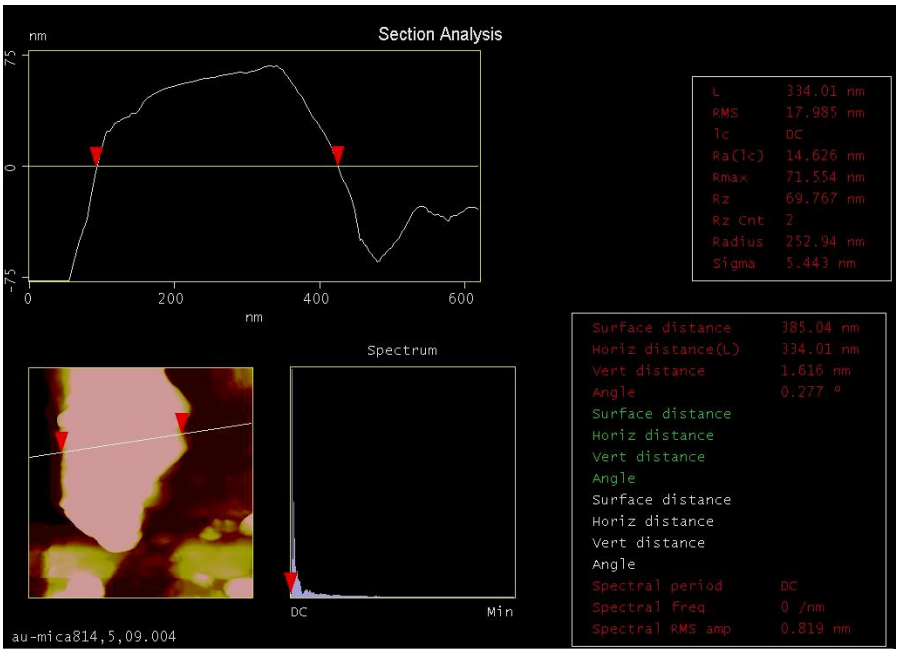

Figure 5.17 Cross-section of a large particle on the C60 covered mica.

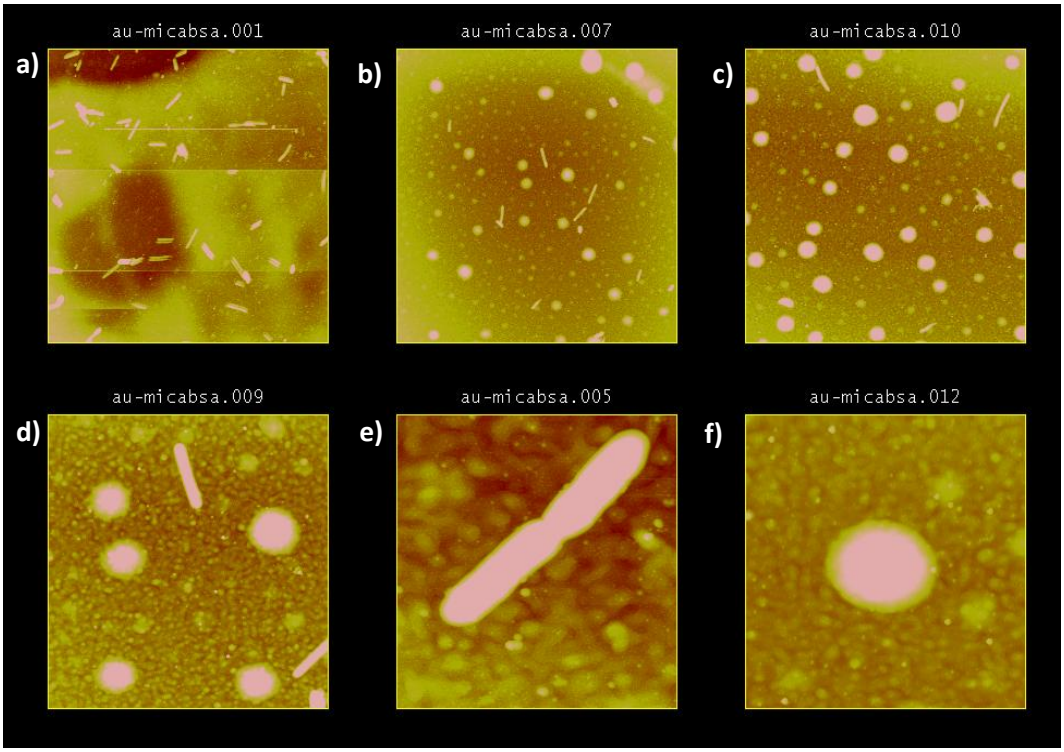

Figure 5.18 Images of BSA with progressive zooming, window widths (X-axis): (a) 40.0 µm; (b) 40.0 µm; (c) 30.0 µm; 9d) 11.9 µm; (e) 3.47 µm; (f) 6.12 µm.

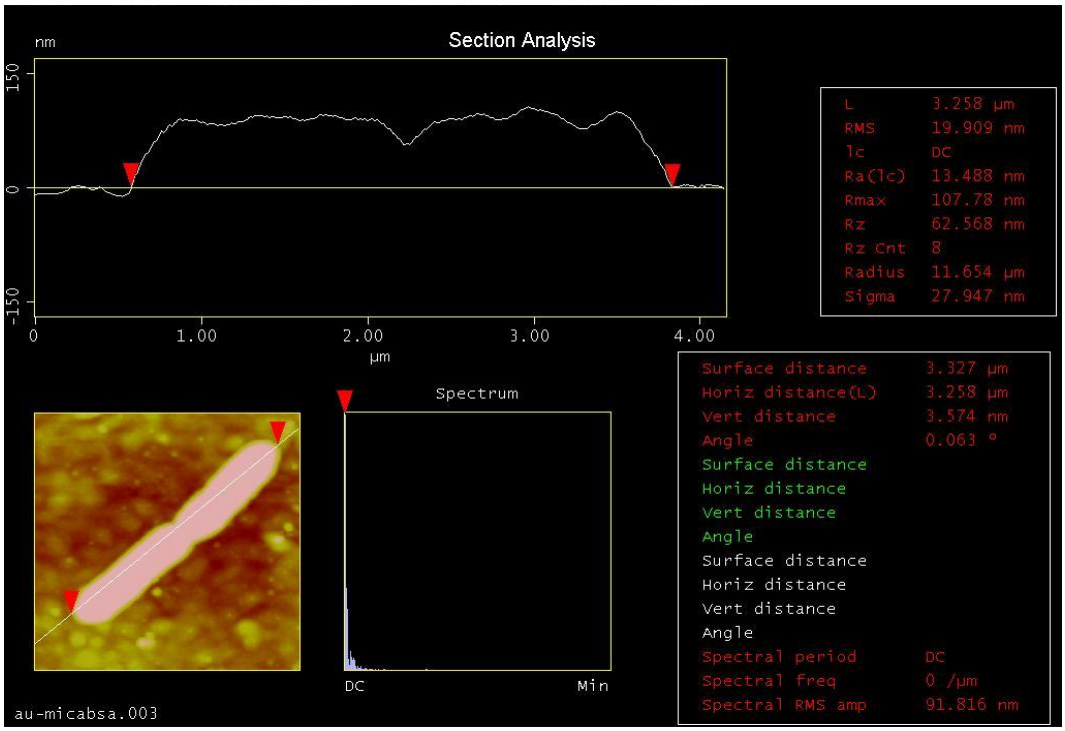

Figure 5.19 Section analysis of BSA elongated

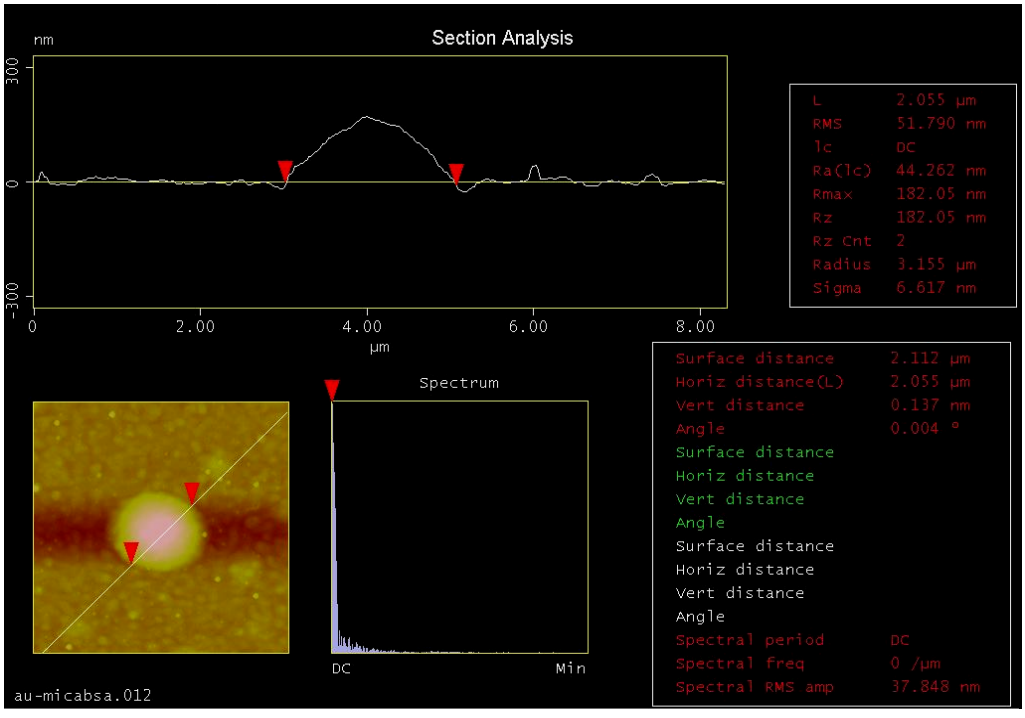

Figure 5.20 Section analysis on globular BSA particle.

5.8. X-Ray Photoelectron Spectroscopy:

After attempts to image a planar, small molecule on very rough surfaces by AFM failed to provide any confirmation of molecular interaction; the use of spectroscopic techniques instead of imaging seemed to be the next logical step in this sequence of preliminary surface analysis studies. In the context of the present experimental aims; XPS was selected in order to enable the detection of surface-bound-PAHs whilst avoiding the interference problems encountered when using AFM (mainly surface charging and roughness). In XPS these problems are circumvented due to the use of X-Ray photons instead of a cantilever tip to scan the sample surface.

Whilst previous research using XPS on similar PAH-mineral systems were not available in the literature at the time; there were other studies looking at the core structure of benzenoids such as naphthalene and other PAH in gaseous phase (Crenshaw and Banna, 1989; Minkov *et al.*, 2004). Furthermore; other workers had analysed naphthalene as an adsorbate on metal and oxide substrates under a variety of experimental conditions. The summary of the main features in the studies found to be closest to this one are presented in Table 5.3. (Tzvetkov *et al.*, 2007).

The specific objectives of attempting XPS on artificially PAH-loaded minerals were:

- to achieve unequivocal PAH identification on reacted mineral surfaces,

- to confirm that chemical reactions were taking place between the PAH and the substrates by looking at changes in chemical state and bonding of the elements previously identified on the cleaned surfaces (mainly C, O and Fe)

In lieu of the lack of previous available XPS data on the PAH-mineral system under study, a step-by-step systematic approach was used in these experiments. Several dosing protocols were attempted with different aromatic organic compounds before reliable spectra could be obtained. Additionally; all substrates were subjected to rigorous ozone and UV cleaning to avoid gross ambient-carbon contamination.

Despite these precautions, however, there was evidence of such contamination in all the carbon spectra obtained due to the levels of ambient C being much higher than the trace quantities dosed onto the surfaces under analysis. A further limitation found was that the technique was unable to discriminate sufficiently accurately between the different types of carbon chemical states. The expected aromatic peaks detected did not resolve sufficiently well even in the case of other benzenoid organics used as standards, whose polar moieties are known to attach well to the selected minerals (benzenoic acid).

The sections below comprise a description of the technique, its fundamentals, as well as the information expected and associated limitations; followed by the experimental setup used.

Authors	Substrate	Surface Analysis Technique	Results
Lukas et al., 2001	**Cu (4 4 3)**	TPD (Temperature Programmed Desorption)	Preferred adsorption along steps
	Cu (2 2 1)		Ordered monolayers on vicinal surfaces
	Cu (1 11)		
Wang et al., 2000	**Cu (1 1 1)**	2PPE (Two-photon Photoemission)	Bilayer on top of flat-lying monolayer π ring perpendicular to surface
Huang and White, 2004	**Ag (1 1 1)**	TPD (Temperature Programmed Desorption) RAIRS (Reflection Adsorption IR Spectroscopy)	Growth of naphthalene layers parallel to surface
Gland et al., 1973	**Pt (1 1 1)**	LEED (Low Energy Electron Difraction)	Temperature dependant ordered and disordered layers
Firment et al., 1976		AES (Auger Electron Spectroscopy)	Ordered layer molecule adsorbs with rings parallel to surface
Dahlgren and Hemminger, 1982		STM (Scanning Electron Microscopy)	Disordered overlayers at room temperature
Okamura et al., 2005	**Si (1 0 0) -2x1**	MIR-IRAS (IR reflection absorption spectroscopy in the Multiple Internal Reflection Geometry)	Various modes of adsorption depending on surface coverage Intermolecular interaction important at high surface coverage
Tzvekov et al., 2007	**Ag (1 0 0)**	TPD (Temperature Programmed Desorption) LEED (Low Energy Electron Difraction) XPS (X-Ray Photoelectron Spectroscopy) NEXAFS (Near Edge X-Ray Absorption Fine Structure)	Naphthalene in monolayer almost parallel to surface Molecules adopt upright orientation as film thickness increases With multilayers orientation shows temperature dependency
Reiβ et al., 2002	**TiO_2**	TPD (Temperature Programmed Desorption) XPS (X-Ray Photoelectron Spectroscopy) NEXAFS (Near Edge X-Ray Absorption Fine Structure)	Naph-oxide interaction weak vs benzene & transition metals Electrostatic interaction between PAH-ion electric field proposed Average molecular tilt angle of 24˚for adsorbed monolayer

Table 5.3. Research works studying PAH- adsorption on mineral substrates via surface analysis techniques.

5.8.1. Description:

X-Ray Photoelectron Spectroscopy or XPS; also known as Electron Spectroscopy for Chemical Analysis (ESCA) is a surface analysis technique

based on the use of a beam of X-Rays aimed at a solid surfaces in order to excite electrons within the solid's surface atoms. As a result, electrons from occupied orbitals are ejected and information on the energy, abundance and angular distribution of these photoelectrons is obtained. These parameters contribute to form a fingerprint of the elemental composition of the surface enabling accurate chemical analysis of solids and any bound adsorbates.

XPS is a direct application of the photoelectric effect discovered by Einstein in 1921. The technique which uses X-Rays as a source of radiation as it is known today was developed by Siegbahn and co-workers in Sweden (Uppsala), for which he was awarded a Nobel Prize in 1981. Other research groups simultaneously arriving to the same results but using ultraviolet light as radiation source were those led by Turner (London) and Vilesov (Leningrad) throughout the 1950's and 1960's (Vickerman, 1997)

Although X-Ray photons can penetrate deep into the solid (e.g. typically, an energy of 1000 eV can go to a depth of 10000 Å) only photoelectrons emitted from a sample depth of up to 10 nm can reach the detector before losing their kinetic energy. It is this characteristic which makes XPS inherently a surface analysis tool.

5.8.2. XPS Fundamentals

When a solid is bombarded with X-Ray photons and provided the incident energy is equal or higher than the atom's binding energy; core electrons will be emitted (photoelectrons) with an energy which will be proportional to that of the incident radiation. Core electrons have binding

energies of the same order of magnitude as X-rays and these energies are characteristic to each atom. These electrons however, do not participate in the bonding process and initially their energy is independent of the atom's electronic environment (Kolasinski, 2008).

Once a photoelectron is ejected, the initial ground state is disrupted, and a core vacancy is created in the inner orbitals. This makes the atom unstable and rearrangement of electrons from higher energy orbitals takes place in order to lower the atom's energy. This process is called "relaxation" and can include electrons from surrounding atoms (extra-atomic relaxation). After this rearrangement the atom has reached what is called the final ground state.

Both initial and final states of the atom can give rise to specific features which can be picked up in XPS spectra. The chemical shift is one of these features, and it is produced by very slight variations in the binding energies at the initial ground state. Chemical shifts are directly related to the bonding environment surrounding the atom (such as the oxidation state of a molecule) and are therefore often used as an indication of surface bonding. (Gupta and Sen, 1974; Atkins and De Paula, 2004).

Final state effects (after photoelectrons have left the atom) give rise to other identifiable spectral features, some of which are:

(1) Multiplet splitting: due to interactions of the core vacancy with unpaired electrons from outer-shell orbitals,

(2) Shake-up satellites: which arise as a result of emitted photoelectrons losing part of their kinetic energy and causing a valence electron to move into an unoccupied orbital, e.g. $\pi \rightarrow \pi^*$ transitions.

Multiplets are often seen at inorganic molecules whereas the latter feature is used in the study of aromatic molecules on solid surfaces. This kind of transition is relevant to the present experiments, since it has been suggested that it is the π orbitals of aromatic molecules which are involved in PAH-mineral surfaces bonding scenarios.

To summarize, each peak in an XPS spectrum corresponds to the binding energy of a photoelectron emitted from a specific core or inner shell atomic orbital and the intensity of the peak is directly related to the amount of the originating element present in the sample. This feature enables quantification in XPS analysis.

A comprehensive definition of all possible spectral features as well as in-depth theoretical and operational information on XPS can be found elsewhere in the cited references (Briggs and Seah, 1990).

5.8.3. XPS Operation

X-Rays Sources: The X-Rays are produced by hitting a elemental source with high energy electrons (~10 keV). This bombardment will create core holes in the target anodes which will then emit X-Rays as well as electrons. These X-Rays are aimed at the solids under study.

Typical sources are made of Al and Mg although other materials are also used, in order to obtain a wide range of energies.

Atoms/ Functional Groups	Structure	Binding Energy (eV)
Carbon: Hydrocarbon	**C-H, C-C**	285.0
Carbon: Carbonyl	**C=O**	288.0
Carbon: Alcohol, ether	**C-O-H, C-O-C**	286.5
Carbon: Acid, ester	**O-C=O**	289.0
Oxygen: carbonyl	**C=O, O-C=O**	532.2
Oxygen: alcohol, ether	**C-O-H, C-O-C**	532.8
Oxygen: ester	**C-O-C=O**	533.7

Adapted from : (Vickerman, 1997)

Table 5.4 Binding energies of some of the functional groups expected to be present in the studied samples.

When operating at at high power it is required to use a water jacket to prevent melting of the anodes. A basic representation of the XPS process is shown in Figure 5.21 below

5.8.4. Information Expected

In XPS three parameters can be measured: (1) the incidence angle for the X-ray beam, (2) the energy of the emitted photoelectron and (3) the abundance of the electrons emitted at each respective energy value. The binding energy is calculated using the Einstein equation (pg 47, Vickerman, 1997) as the result of subtracting the emitted electron's energy from the energy of the incident X-Ray

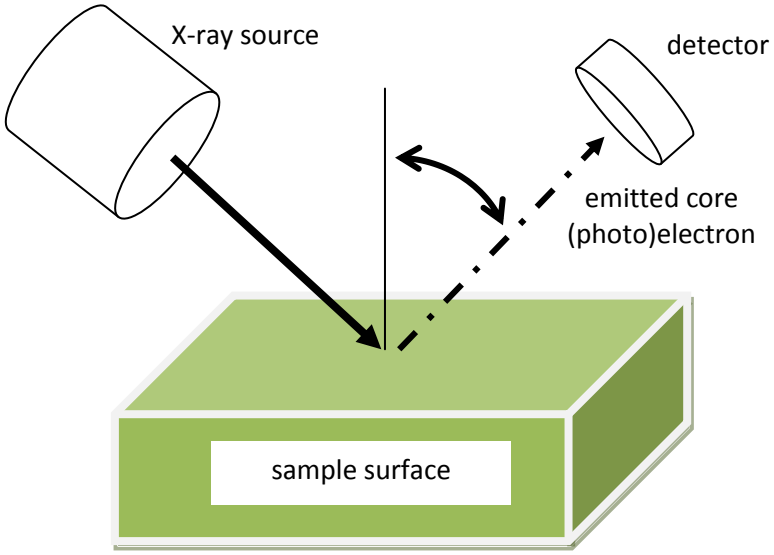

Figure 5.21 Schematic diagram of the XPS process.

photon. XPS spectra show the changes to molecular geometry caused by the loss of electrons in each orbital, depicting the molecular orbital's energy distribution and distinguishing between bonding, anti-bonding or non-bonding orbitals.

In terms of limitations; XPS can be applied to gases and solids, but is not suitable for *in-situ* study of liquid-solid or gas-solid interfaces as the incident beam may damage the surface under study depending on the depth of probing. Lastly, XPS requires ultra high vacuum (UHV) conditions in order to avoid gas collisions with the photo-emitted electrons which could prevent weakly bound molecules from being detected as they would be stripped off the surface by the strength of the vacuum. The latter would make XPS analysis unsuitable to use in the study of weakly physisorbed adsorbates.

5.8.5. Reagents and Materials

The selected mineral phases and organic molecules used in the preliminary XPS runs are presented in Table 5.4. All solvents used as PAH carriers are included as is the concentration of the dosed aromatic molecules.

5.8.6. Experimental Setup & Sample preparation

The samples for XPS analysis were prepared 24 hours prior to analysis. All samples were dosed with naphthalene and a method standard after conditioning the mineral samples via solvent cleaning (in the case of grains) or ozone cleaning (in the case of slides).

Substrates	Source	Dimensions	Pre-treatment	Solvents	Chemicals	
SiO_2	SEAES	Slides 10 mm^2	Polish UV / O_3	Cyclohexane	Benzo[e]pyrene 100 (mg / l)	N/A
SiO_2	VWR commercial sand	Grains (250 µm)	UV/O_3 Cleaning	Methanol (Pestanal)	Naphthalene (l) 200 (mg/l)	Benzoic Acid 407.9 (g/l)
Fe_2O_3	Haile Hematite, Cumia	Powder (250 µm)	UV/O_3 Cleaning	Methanol (Pestanal)	Naphthalene (l) 200 (mg/l)	Benzoic Acid 407.9 (g/l)

Table 5.5 Experimental reagents and materials used for XPS analysis.

5.8.7. Analytical Conditions and Equipment

The XPS spectra were recorded using a Kratos Axis Ultra spectrometer employing a monochromated Al Kα X-ray source and an analyser pass energy of 80 eV (wide scans) or 20 eV (narrow scans) resulting in a total energy resolution of ca. 1.2 and 0.6 eV, respectively. Uniform charge neutralisation of

the photo-emitting surface was achieved by exposing the surface to low energy electrons in a magnetic immersion lens system (Kratos Ltd.). The system base pressure was 5 x 10^{-10} mBar. Spectra were analysed by first subtracting a Shirley background and then obtaining accurate peak positions by fitting peaks using a mixed Gaussian / Lorenzian (30 / 70) line shape. During fitting, spin orbit split components were constrained to have identical line width, elemental spin orbit energy separations and theoretical spin orbital area ratios.

Quantitative analysis was achieved using theoretical Scofield elemental sensitivities and recorded spectrometer transmission functions. .All photoelectron binding energies (BE) are referenced to C1s adventitious contamination peaks set at 285 eV BE. The analyser was calibrated using elemental references; $Au4f_{7/2}$ (83.98 eV BE), $Ag3d_{5/2}$ 368.26 eV BE) and $Cu2p_{3/2}$ (932.67 eV BE).

5.8.8. Results

Two set of samples were PAH-dosed and analysed by XPS. The first sample set is shown in Table 5.5 and consists of three SiO_2 slides which were systematically dosed with solvent and a PAH, (benzo[e]pyrene). Since, at this stage a dosing protocol needed to be developed, a PAH larger and less volatile than naphthalene was chosen to be dosed in order to obtain a clear C1s signal. For identification purposes, the samples sets for each mineral were labelled as follows (see Tables 5.5 and 5.6):

(a) the mineral blank (labelled as #1)

(b) the mineral substrate plus solvent (labelled as #2)

(c) the mineral with PAH in the selected solvent (labelled as #3)

(d) the mineral with procedural blind blank (where appropriate) in the selected solvent (labelled as #4)

Sample name	Substrate	Dosing		Conc. ($\mu g \cdot cm^{-3}$)
		Solvent	PAH	
mina 1	SiO_2 slide	N/A	N/A	N/A
mina 2	SiO_2 slide	Cyclohexane	N/A	N/A
mina 3	SiO_2 slide	Cyclohexane	Benzo[e]pyrene	100

Table 5.6 Substrates and reagents used in experiment 1.

Although the results for these samples showed a shift in signal for the carbon C 1s peak and other elements identified on all slides (namely Si 2p, and O 1s) the results could not be validated due to the presence of significant carbon (C 1s) contamination on the SiO_2 blank slide (bottom peak, 'mina 1an', Figure 5.22). There should not have been any carbon present in this sample as it was a procedural blank and had not been dosed with any carbon bearing compounds. The rest of the spectra obtained for this sample set are presented in Appendix A5.

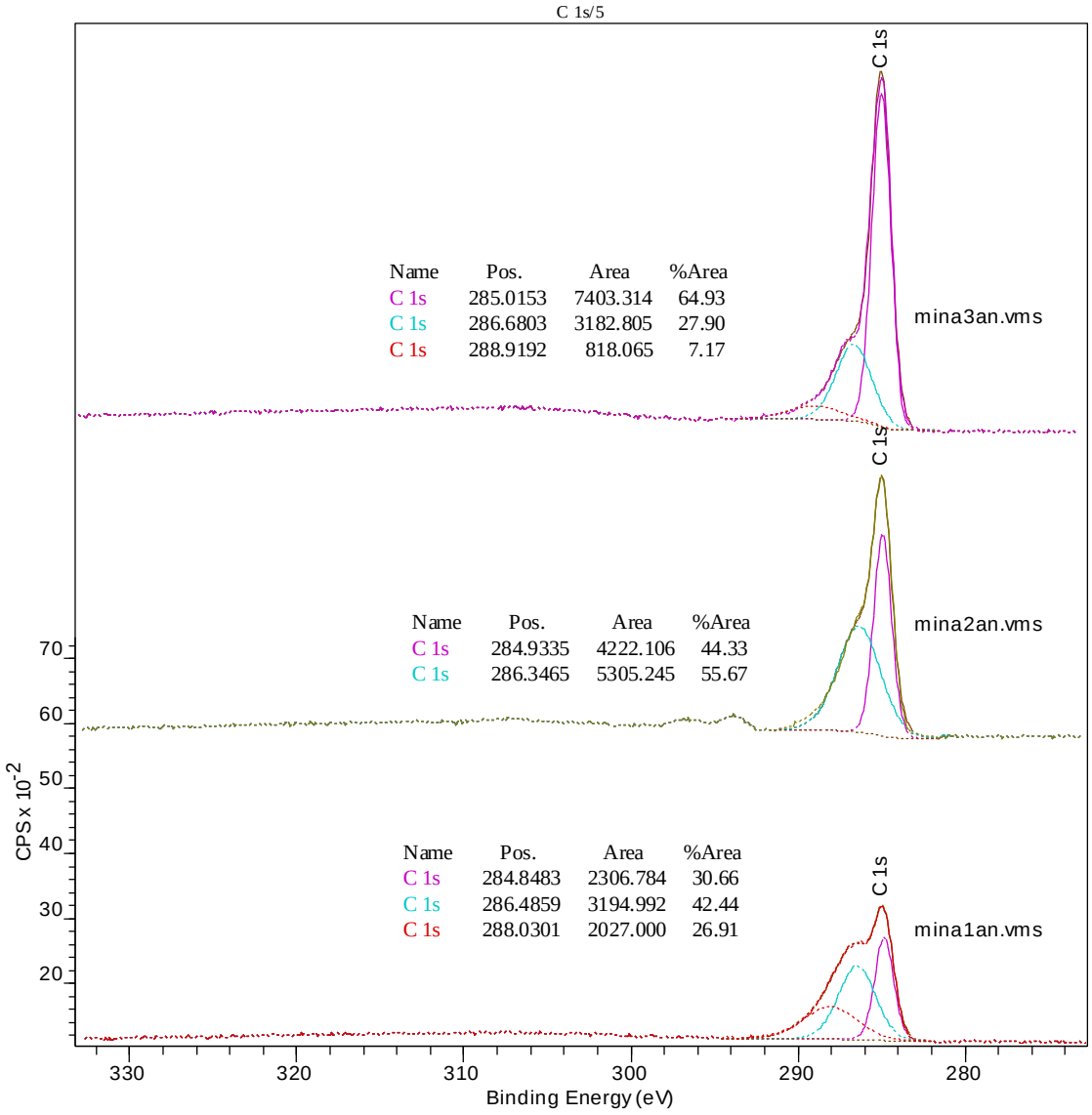

Figure 5.22 Fitted C1s peaks for B[e]pyrene on quartz slide.

The second set of samples (see Table 5.6) consisted of two different mineral substrates: quartz in the form of sand and powdered hematite. A different set of adsorbates was used for these minerals, namely: methanol as solvent, naphthalene as PAH representative and an aromatic acid (benzoic acid) as blind standard.

Sample name	Substrate	Substrate Dosing		Conc. ($\mu g \cdot cm^{-3}$)
		Solvent	PAH	
S 1	SiO_2 sand	N/A	N/A	N/A
S 2	SiO_2 sand	Methanol	N/A	N/A
S 3	SiO_2 sand	Methanol	Naphthalene	200
S 4	SiO_2 sand	Methanol	Benzoic acid	408
h 1	Fe_2O_3	N/A	N/A	N/A
h 2	Fe_2O_3	Methanol	N/A	N/A
h 3	Fe_2O_3	Methanol	Naphthalene	200
h 4	Fe_2O_3	Methanol	Benzoic acid	408

Table 5.7 Substrates and reagents used in experiment 2.

Benzoic acid was used as a blind standard in order to verify whether aromatic rings could be at all detected with the current dosing protocol. This acid is well suited for this purpose since its polar OH^- group would ensure it would stay adsorbed on the mineral substrate.

The results for these samples presented the same contamination problem with carbon (C 1s) in both substrate blanks (#1). Once again this experimental artefact rendered any possible comparison of peak position and shape between samples impossible.

In addition, since there were no changes in the C 1s, O 1s and Si 2p peaks, in the blanks (samples labelled #1) and the substrates dosed with naphthalene (samples labelled # 3) as can be seen in Figures 5.23 to 5.26. It can be inferred from this that naphthalene was not adsorbed on the surface.

Hematite :

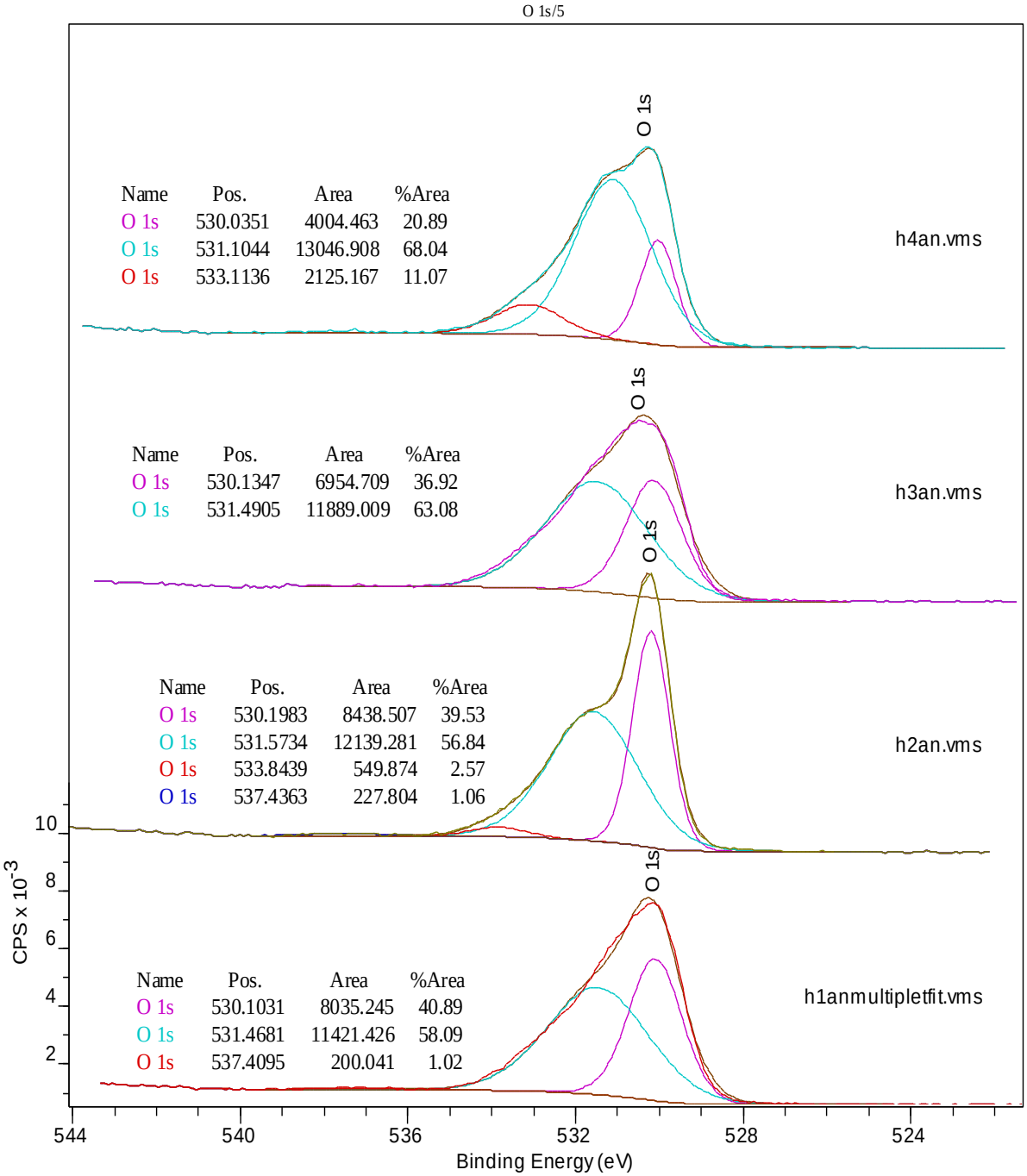

Figure 5.23 Fitted peaks for O (1s) in hematite samples.

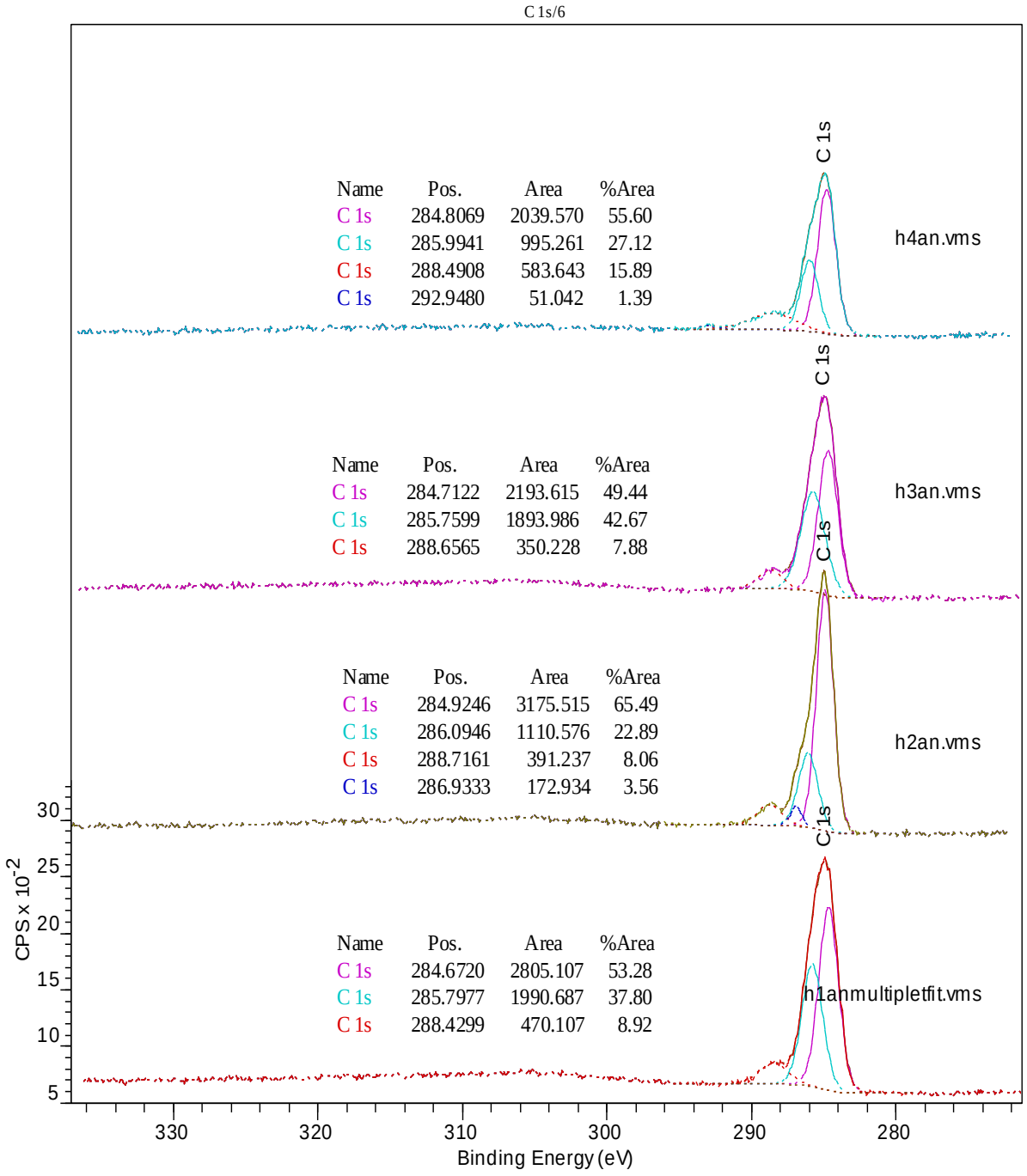

Figure 5.24 Fitted peaks for C (1s) in hematite samples.

Silica:

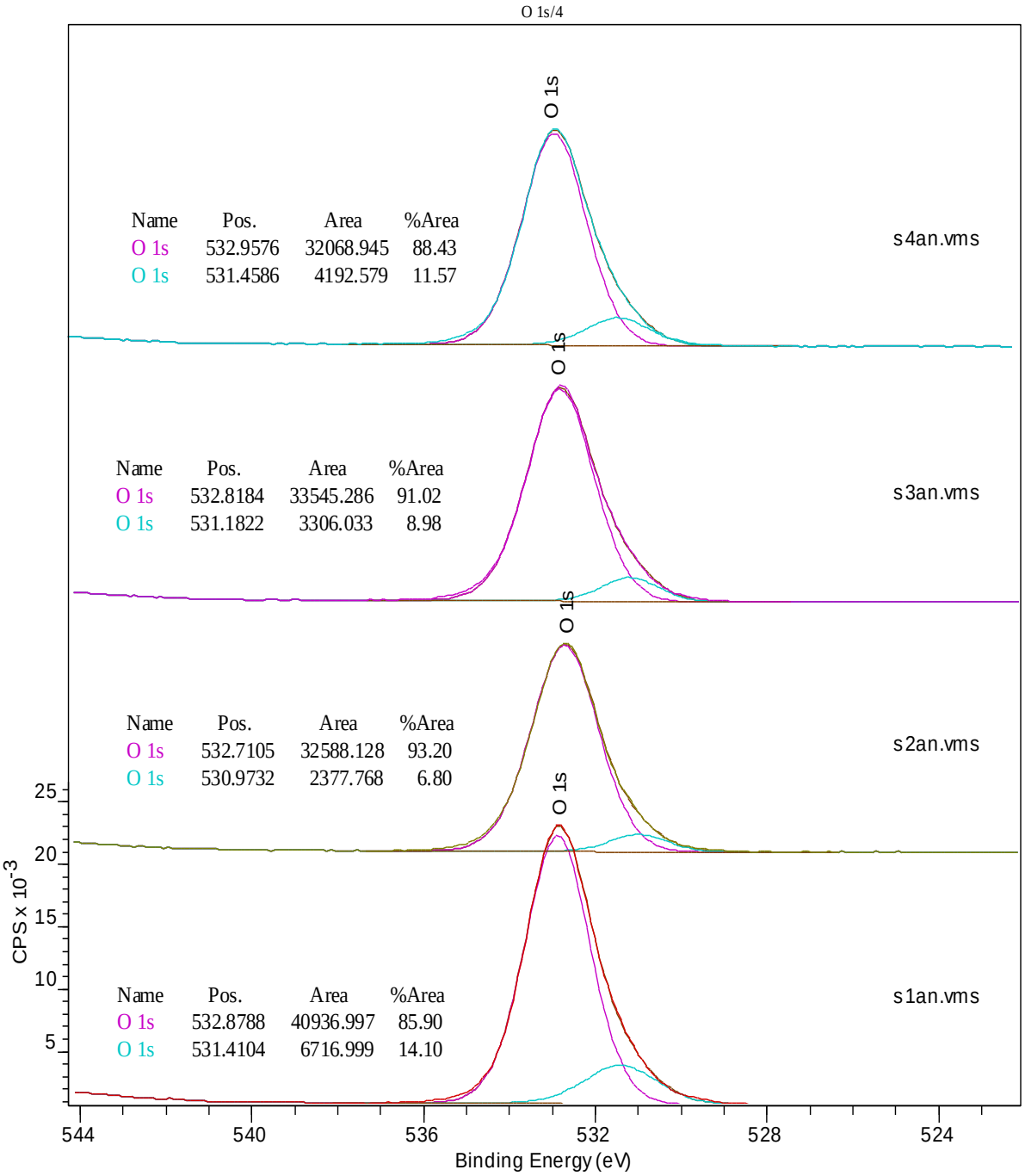

Figure 5.25 Fitted peaks for O (1s) in silica sand samples.

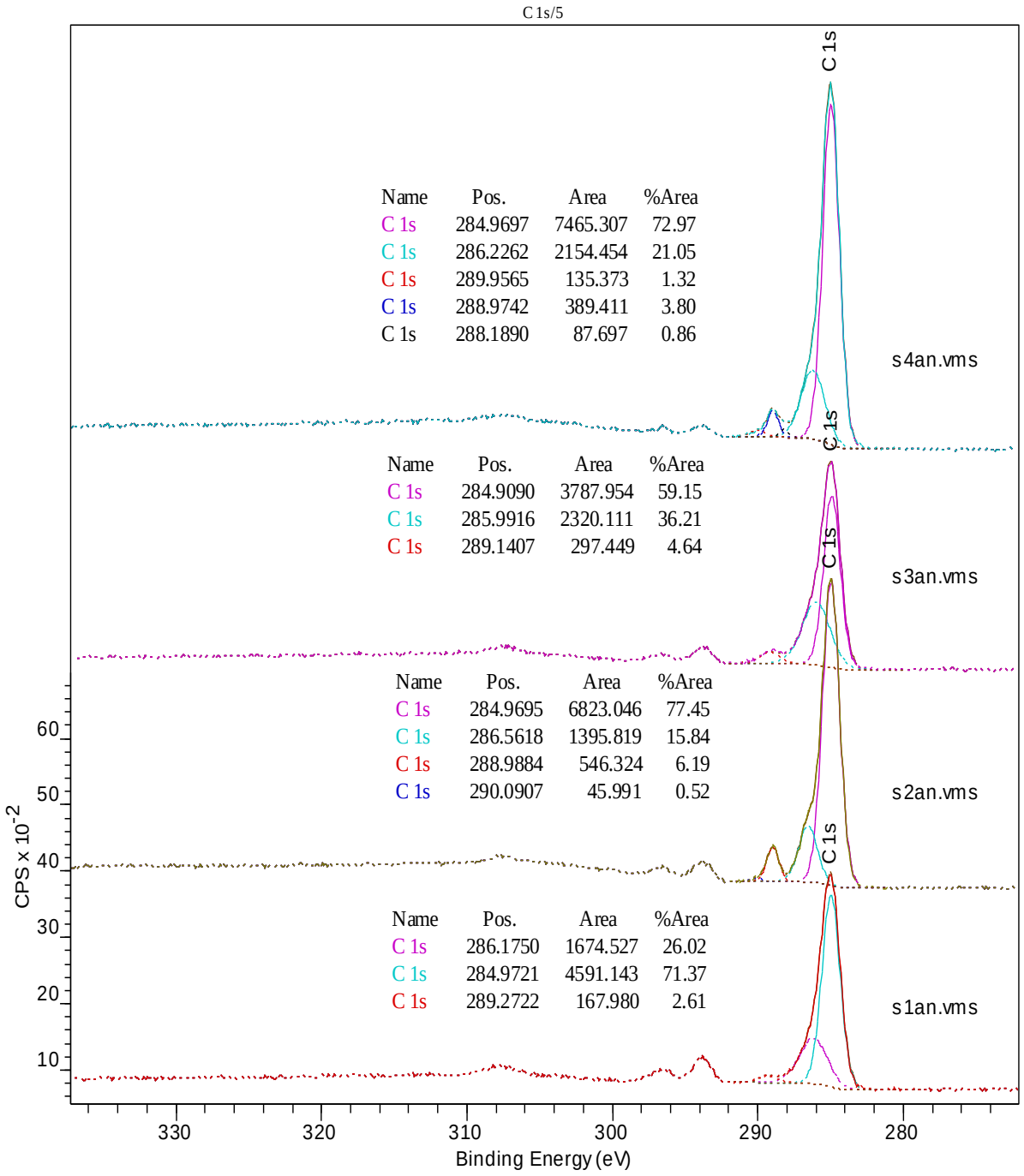

Figure 5.26 Fitted peaks for C (1s) in silica sand samples.

All other results obtained by XPS under the selected experimental and analytical conditions are presented in Appendix A5.

The next approach involved the use of functional groups identification on surfaces as an alternative to the detection of electrons, which meant less

stringent analytical controls, and less sample preparation precautions. The technique used is described in the next section.

5.9. Infrared Spectroscopy:

5.9.1. Introduction

Radiation in the infrared region of the electromagnetic spectrum (between 100 and 100,000 nm) can probe changes in the vibrational (bond) states of molecules. When molecules are bombarded with infrared (IR) radiation some of the energy is absorbed and the rest is transmitted. Depending on the energy required to excite the molecular vibrational state, IR energy will be absorbed at the corresponding wavelengths which are characteristic to specific molecular vibrational modes. An infrared spectrometer can detect this absorption and correlate intensity of the absorbed radiation as a function of wavelength therefore creating a molecular fingerprint of the functional groups and atomic arrangements in the molecules under analysis. Thus different molecules will yield IR spectra which are unique to the specific molecule. Polyatomic molecules will absorb infrared radiation at several different wavelengths due to the presence of different types of bonds, whereas diatomic molecules will have less complex vibrational spectra. It is worth noting that in order for a molecule to absorb at IR frequencies its vibrational modes must be related to a change in dipole moment. Mono-atomic symmetric molecules do not absorb infrared radiation (Atkins and De Paula, 2004).

Infrared spectroscopy is one of the greatest tools in surface science since it allows the study of almost any material under a wide range of

conditions. One of its main advantages is the fast sample analysis time (of the order of seconds per sample!) and the fact that it does not need ultra high vacuum, and hence allowing the study of systems in their natural conditions and the detection of reaction products as they form.

One of the main limitations of using IR is that certain compounds, present in the samples under study, absorb radiation in the same wavelength as the target materials. For the purposes of this study, these molecules comprise: water, NO_3^-species, and CO_2.

PAH presence can be identified using IR absorbance by looking for different absorption bands exhibited by aromatic molecules.

These, as well as the expected wavenumber range in which they would appear in the IR spectra are presented in Table 5.6 (Silverstein *et al.*, 1991).

5.9.2. FTIR Operation:

Light from an infrared source (a heat lamp) is focused towards a beamsplitter. Once inside, half of the beam is directed onto a moving mirror which reflects this part of the beam back to the splitter and from there the beam goes through the sample towards the detector. The other half of the original beam is diverted onto a fixed mirror from which it reflects back into the beamsplitter and then on towards the detector. The use of a moving mirror creates constructive or destructive interference depending on whether the two beams are in or out of phase when they recombine at the beamsplitter. These

Functional Groups	Structure	Wavenumber (cm^{-1})
Aromatic ring	**C-H Stretch**	3020-3000
	C=C Stretching	860 - 680
	C=C Bending	1600 - 1400
Hydroxyl	**O-H (alcohol)**	3625-3620
		1350-1260
		1125-1085
	O-H (water)	3710
	Water (crystals)	3600-3100
		1640-1615

Table 5.8 Absorption frequencies of Functional Groups studied

interferences are plotted as a function of mirror distance creating what is called an interferogram. Each point in the interferogram signal simultaneously contains information of every single frequency present in the original IR beam. The use of interferometers therefore enables extremely fast measurements (i.e. 25 scans per second) and sample analysis times of seconds; since all frequencies can be monitored simultaneously.

The interferometer signal is fed to a computer where it undergoes Fourier transformation in order to unravel and separate the individual frequencies and plot their intensities, generating the IR spectra as they are known. These modern infrared devices are called FTIR or Fourier Transform Infrared spectrometers.

The IR technique used in these preliminary experiments was Attenuated Total (Internal) Reflection, or ATR. In this IR operating mode the substrate is

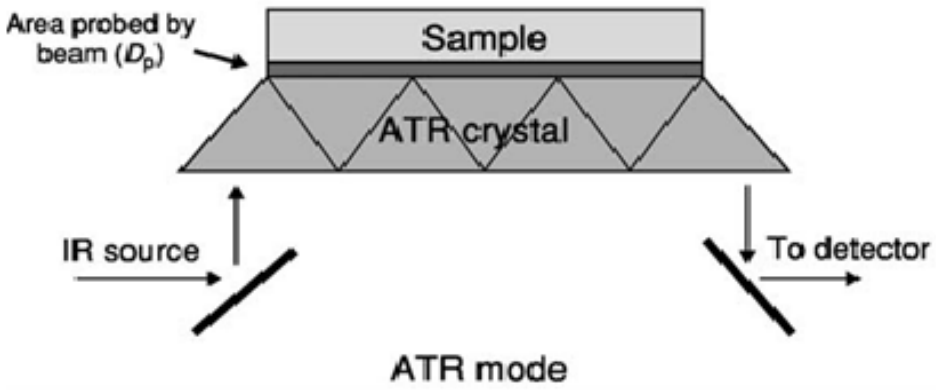

Figure 5.27 Schematic representing the parts of an ATR cell (Perkin Elmer, 2011)

pressed into intimate contact with a crystal prism manufactured of a material which should be IR-transparent in the desired wavenumber range. A diagram representing the parts of a ATR-FTIR spectrometer device is shown in Figure 5.27.

The use of ATR is based on the principle that if the incident radiation is angled correctly, by controlling the geometry of the experimental setup, then internal reflection will occur. At the point of reflection an evanescent wave is created, which will go beyond the boundaries of the prism and interact with any sample in contact to the surface of the internal reflection element.

ATR is a very versatile application of FTIR since it allows *in situ* measurements in either liquid or solid systems provided the correct accessories are in place (i.e. flow cells). It is particularly suitable for adsorption studies as a complement to bulk sorption experiments, since any changes on the surface of the adsorbent can be monitored as the reactions take place.

A detailed excerpt with the theoretical fundaments governing the application of ATR can be found in the literature.

With regards to sorption experiments, there are two general experimental approaches to ATR: (1) the sorbents under analysis can be studied in their natural form (dry solids) or suspended in the liquid phase (as a slurry), or (2) they can be deposited on the ATR element (as a thin paste) within a flow cell and the reactants then added to the system increasing their concentration in a stepwise manner. The latter approach is more systematic and likely to generate high quality spectra since by using a bigger cell, a larger number of reflections on the ATR element can be achieved, and therefore better sensitivity. Furthermore, interference from water and CO_2 IR bands can be avoided, but it does entail a fair amount of complexity in the sample preparation stage and the method protocol preparation can be very time consuming. Spectra of the sorbents prior to any loading, as well as spectra of the sorbates and medium should be collected and recorded initially; in order to enable the required background substraction at a later stage.

In our preliminary experiments, the solids under study were analysed in their natural forms (dry powders) with the exception of quartz slides; prior to and after being reacted with the contaminants. In some instances slurries were used to assess the amount of interference from water bands as well as the presence of organic solvents remaining after dosing. Lastly, attempts were made to remove all liquid phases by freeze-drying the substrates 24 hours prior to analysis. The experimental setup and the protocols followed are outlined in the section below.

5.9.3. Reagents, Materials and Equipment

Reagents:

PAH: Naphthalene and phenanthrene were purchased from Sigma Aldrich Ltd as commercial GC standards in methanol, 1 ml at 5000 and 2000 mg / l respectively.

Solvent: Methanol, Pestanal grade.

Materials: (see Table 5.9).

Equipment: all spectra were collected using a BIORAD FTS 6000 spectrometer equipped with a deuterated triglycine sulphate (DTGS) detector. The analytical conditions can be found in a protocol developed elsewhere (Charalambos Assos, 2010).

5.9.4. Experimental Setup

In all measurements, spectra of the cleaned substrates, followed by those of solvents and substrates were collected after the required background runs and prior to loading the contaminated substrates.

Substrate cleaning: All silica slides had been previously polished and on the day of the experiment were pre-cleaned with Methanol and allowed to dry prior to dosing with the PAH. Polycrystalline samples of hematite powder and quartz sand were also used in these experiments Tthese were solvent-rinsed and the solvent allowed to evaporate just before dosing.

Naphthalene and phenanthrene were dosed in two different ways: drop-wise as commercial standard solutions in methanol (see Table 5.8) or as a supersaturated electrolyte solution in which the substrates were immersed overnight.

5.9.5. Results:

The standard IR absorption spectrum for naphthalene is shown as a reference in Figure 5.28 followed by the spectra obtained with the samples under study.

The reference naphthalene spectrum in Figure 5.28 shows the diagnostic aromatic C—H out-of-plane-bending band at 900 - 675 cm^{-1}. The same band can be identified in Figures 5.29 and 5.30 where the obtained ATR spectra for naphthalene and phenanthrene respectively are shown.

#	Substrate:	Pre-treatment:	Chemicals:	Identified bands (cm^{-1}):
1	SiO_2 10 x 10 x 1 (mm)	Polishing 3xMeOH wash	Naphthalene 5000 mg/l	Water : 3333 / 1637 NO_3^-: 1390-1350
2	SiO_2 (grains)	3xMeOH wash	Naphthalene ≥30 mg/l in $NaNO_3$	1016 1162 1141
3	SiO_2 10 x 10 x 1 (mm)	Polishing 3xMeOH wash	Phenanthrene ≥1 mg/l in $NaNO_3$	2400 – 1400
4	SiO_2 10 x 10 x 1 (mm)	Polishing 3xMeOH wash	DIW	2300-1600 1632

Table 5.9 Materials and reagents used for ATR analysis.

The spectra are superimposed below for comparison. These were obtained by pressing the neat crystals to the ATR element and scanning at ambient temperature (25 scans per second). These samples were the only ones in which these PAH were successfully identified.

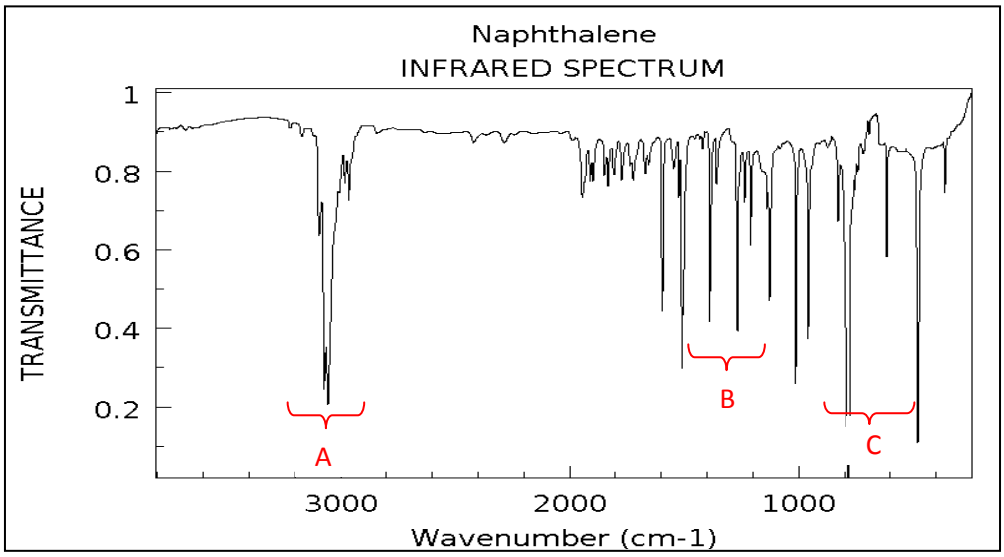

SOLUTION (10% CCl4 FOR 3800-1300, 11% CS2 FOR 1300-650, AND 10% CCl4 FOR 650-250)
Data from NIST Standard Reference Database 69
NIST Chemistry WebBook
Instrumer PERKIN-ELMER 521 (GRATING)

Figure 5.28 Infrared spectrum of naphthalene in solvent phase: A: 3100 – 3000 cm^{-1} band corresponding to C—H aromatic stretching; B: 1600 —1400 cm^{-1} corresponding to C═C ring stretch and C: 900 – 675 cm^{-1} corresponding to out-of-plane aromatic C—H bending.

PAH studied:

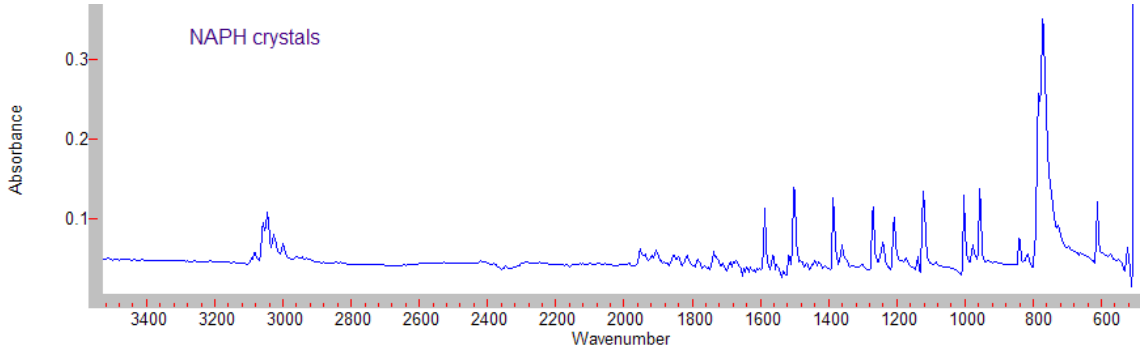

Figure 5.29 ATR spectra of pure naphthalene crystals.

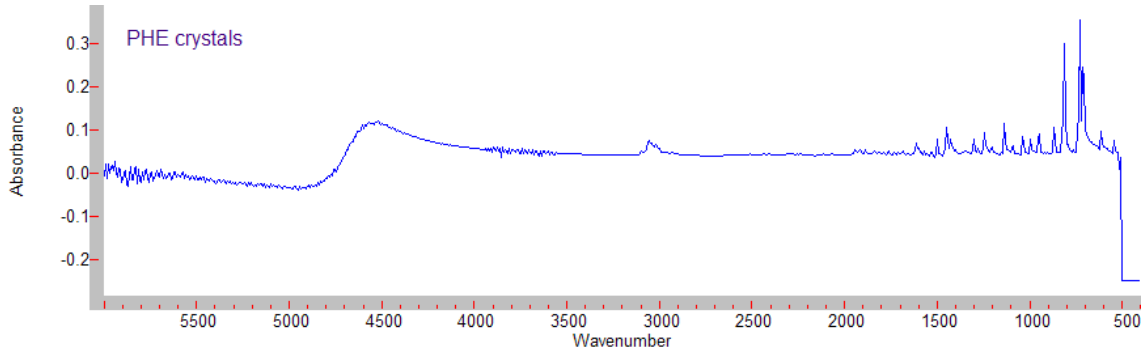

Figure 5.30 ATR spectra of pure phenanthrene crystals.

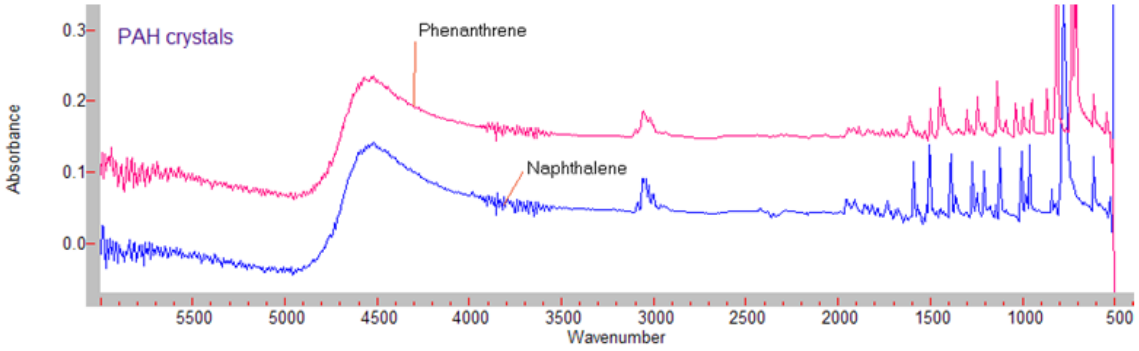

Figure 5.31 ATR spectra of both PAH in crystal form.

The following spectra show the scans obtained under the same experimental conditions for the two mineral phases used, namely quartz sand and Stx-1 montmorillonite.

Minerals:

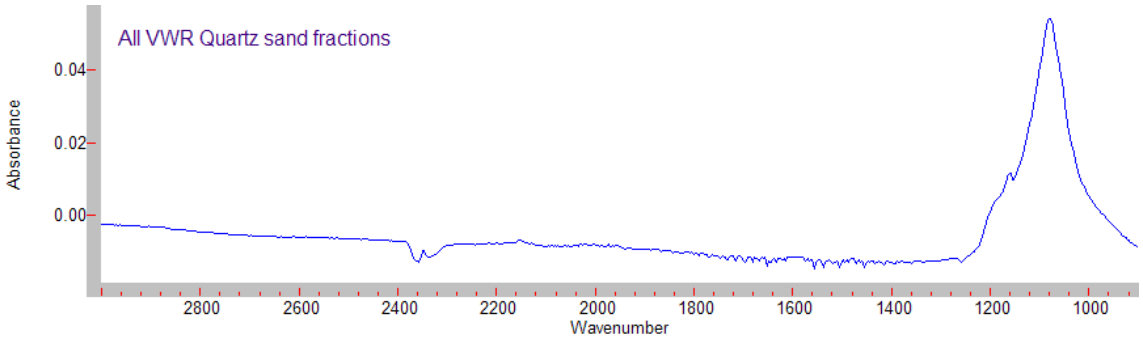

Figure 5.32 ATR spectra of all quartz sand fractions.

Figure 5.32 shows the scan of all the size fractions for SiO_2 sand. Each individual fraction showed identical spectra. These show evidence of the fine structure characteristic to silica. The next scanned substrate was the reference clay Stx-1 (montmorillonite) shown in Figure 5.33.

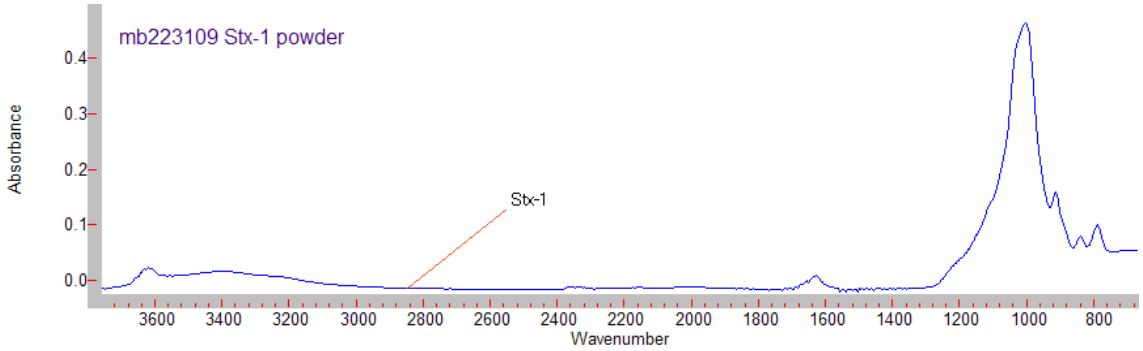

Figure 5.33 ATR spectra of montmorillonite clay, all fractions.

The spectrum shown in Figure 5.34 presents the ATR scan for plain, uncontaminated sand and superimposed on it is the resulting scan of sand pre-loaded with naphthalene. This sand sample had been exposed to the PAH for 24 hours in an aqueous electrolyte solution ($NaNO_3$, 0.001 M). The result shows negative peaks similar to those shown in Figure 5.29 between 600 and 2000 cm^{-1}.

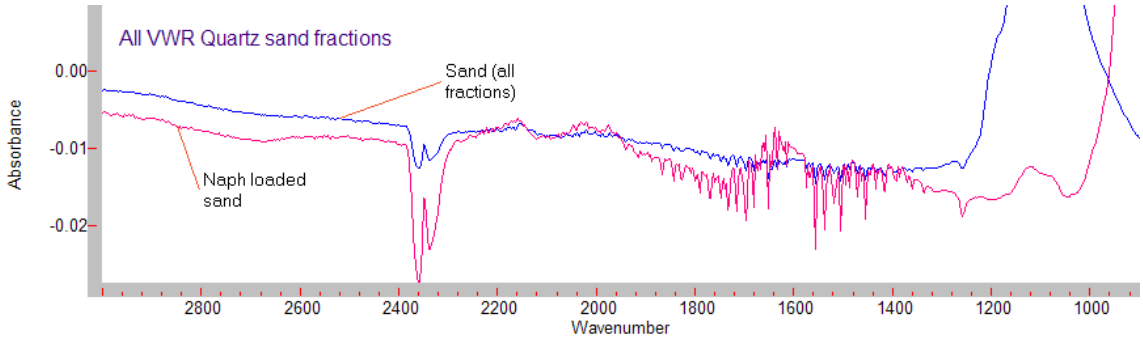

Figure 5.34 ATR spectra of negative peaks artefact when attempting to scan naphthalene-laden quartz sand

The ATR element was thoroughly washed and cleaned between scans; equally, background scans were taken and subtracted to ensure flat baselines before each new sample. In spite of these measures, negative peaks appeared every time pre-loaded samples with naphthalene were analysed. The solvent used as PAH carrier did not seem to make a difference to the appearance of the negative peaks. This became a recurrent problem and several washes needed to be carried out before even the ATR crystal would be free of contamination. Figure 5.35 shows a contaminated scan after several washes.

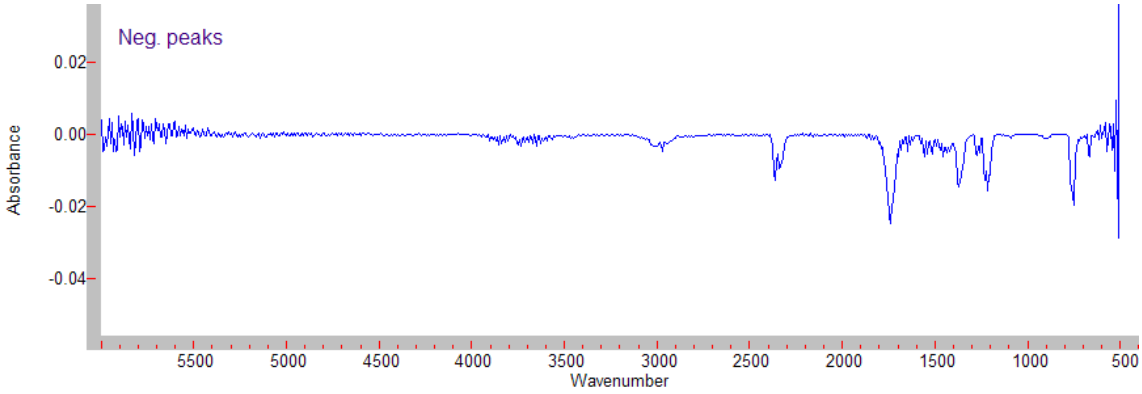

Figure 5.35 ATR spectra of negative peaks artefact on a scan with no sample loaded on the ATR crystal

Figure 5.36 shows the scan for naphthalene - loaded reference clay (Stx-1).

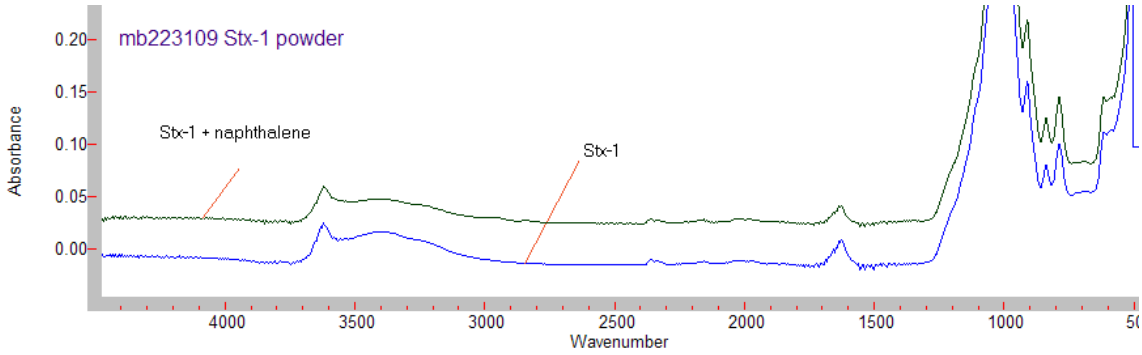

Figure 5.36 ATR spectra of naphthalene-laden montmorillonite clay.

The resulting spectrum is shown Figure 5.36 as a comparison between two superimposed spectra. The one corresponding to the PAH-loaded clay shows the C—H stretching aromatic band at 3000 $cm^{-1.}$ (very small, not visible at present scale) but does not show the diagnostic PAH bands between 600 and 900 cm^{-1}(corresponding to C—H out-of-plane-bending) as this region is dominated by bands corresponding to the montmorillonite structure.

Although presence of an aromatic band has been detected on the PAH-laden clay, the spectrum is not resolved enough to discern between a mono- or poly-aromatic hydrocarbon, therefore rendering this preliminary result inconclusive.

REFERENCES

Appelo, C. A. J. and Postma, D. (1994). Geochemistry, Groundwater and Pollution. Rotterdam, Balkema. 669 pages.

Atkins, P. and De Paula, J. (2004). Atkin's Physical Chemistry. Oxford Oxford University Press. 920 pages.

Briggs, D. and Seah, M. P. (1990). Practical Surface Analysis. Guildford, John Wiley & Sons Ltd. 420 pages.

Charalambos Assos (2010). Organic ligand complexation reactions on aluminium-bearing mineral surfaces studied by *in-situ* Multiple Internal Reflection Infrared Spectroscopy, adosrption experiments and surface complexation modelling. School of Earth, Atmospheric and Environmental Sciences. Manchester, The University of Manchester. Ph.D.**:** 260.

DiNardo, J. N. (1994). Nanoscale Characterisation of Surfaces and Interfaces. Weinheim, VCH Verlagsgesellschaft mbH. 173 pages.

Elbel, N., Behner, H. and Seggern, H. v. (1995). Preparation and characterisation of epitaxial gold films deposited on mica by direct current magnetron sputtering. J. Vac. Sci. Technol. B. 13(5).

Gupta, R. P. and Sen, S. K. (1974). Calculation of multiplet structure of core p-vacancy levels. Physical Review B 10(1): 71.

Kolasinski, K. W. (2008). Surface Science: Foundations of Catalysis and Nanoscience. Chichester, John Wiley & Sons, Ltd. 2nd edition. 496 pages.

Nakhimovsky, L. A., Lamotte, M. and Joussot-Dubien, J. (1989). Handbook of Low Temperature Electronic Spectra of Polycyclic Aromatic Hydrocarbons. Amsterdam, Elsevier. 124 pages.

Nalwa, H. S. (2001). Advances in Surface Science. San Diego, California, Academic Press. 1st edition. 454 pages.

Perkin Elmer. (2011). Technical Note on ATR-FTIR. Retrieved 20/04/2011, from http://las.perkinelmer.com/content/TechnicalInfo/TCH_FTIRATR.pdf.

Silverstein, R. M., Bassler, G. C. and Morrill, T. C. (1991). Spectrometric Identification of Organic Compounds. New York, John Wiley & Sons, Inc. 5th edition. 433 pages.

Vickerman, J. C. (1997). Surface Analysis. Chichester 462 pages.

CHAPTER 6 Overall Discussion and Conclusions

6.1. SPME Method Development

The proof of concept experiment outlined in Chapter 3 presented the results of exposing a carbon-quartz mixture system to naphthalene in an electrolyte; and the subsequent analysis of the remaining naphthalene concentration after exposure to this PAH at different reaction times. The method of analysis consisted of a novel application of SPME in the headspace after careful modification of the relevant analytical variables. The tailoring of the method followed a sequence of steps which were aimed to improve the protocols already in use by other workers (Wei and Jen, 2007; Qin *et al.*, 2009) by increasing the sample turnover under the selected conditions and with the available equipment at the time.

The results for the method's same-day repeatability show RSD% values between 1.47 and 6.59 % for 10 replicates (n = 10), which compares favourably against those reported for other research teams using state of the art equipment (Fernández-González *et al.*, 2007). Fernandez-Gonzalez and co-workers validated a method for the analysis of PAH in a variety of water samples (including groundwater) with the purpose of testing its suitability for the European Union water directive 2006 / 0129. Their setup represented ideal conditions with state-of-the art equipment which included a Combi Pal automated SPME sampling system coupled to GC-MS-MS. This instrumentation is capable of achieving excellent repeatability, remarkably low detection limits and superior chromatographic separations. The results from this team showed RSD% values between 0.5 and 5.5 % for 10 replicates (n = 10) analysed on the same day.

In the case of inter-day repeatability, where fresh replicates are prepared and analysed on different days by the same analyst; the results obtained in the present experiments (RSD % between 0.16 and 12.98 %, n = 7) are equally in good agreement with those obtained by Fernandez and co-workers (RSD% as < 14%, n = 7).

The method's limit of detection was defined as the lowest standard concentration achieving a signal at least ≥ 50 times the average background noise. In the present extractions the LOD was found to be 3 orders of magnitude higher than that found in other works in which more stringent controls on extraction conditions were exerted. This is probably due to the type of chromatographic detector used (FID as opposed to MS) as well as the higher concentrations at which the calibrating standards were prepared. Initially, no attempts were made to prepare standards below 0.2 ppb because this was already more than 2 orders of magnitude lower than the initial naphthalene concentration at which all samples and blanks were prepared. It was also observed that the final naphthalene concentrations in the supernatant were much higher than the lowest calibration standard, and therefore significantly higher than the achieved LOD. Due to these reasons and given the low naphthalene uptake exhibited by the sorbents used no further attempts to lower the LOD were carried out. However, the detection limit achieved is at least one order of magnitude lower than the annual average limit established for naphthalene in surface waters as outlined by the European Union directive 2006 / 129 proposal (2400 ng l^{-1})

Other factors which play an important role in the equipment's capability to resolve an analyte at sub-ppb levels (parts-per-billion, or µg l^{-1}) include: (1)

the use of different fibre materials (such as polyacrylate or PA), or (2) different fibre thicknesses (100, 85 or 7 µm) (Doong *et al.*, 2000b). It must be born in mind however, that increasing the recovery by changing the coating phase should be weighed against factors such as carry over and longer extraction times.

The linearity and the range obtained (R^2 between 0.9825 and 0.9983, standard concentrations between 1 mg / l and 0.0002 mg / l) are deemed satisfactory considering the high volatility of naphthalene.

Regarding the extraction temperature, some workers have reported discrepancies and experimental artefacts when using temperatures higher than ambient for the SPME extraction of naphthalene in either the liquid or the headspace phase (Fernández-González *et al.*, 2007), however, this was not observed in the experiments carried out in this research. An increase in temperature to 40 ºC led to faster extractions within acceptable error margins. Furthermore, sampling in pre-equilibrium mode permitted very fast and accurate extractions whilst avoiding analyte loss by having a closed sampling system equipped with external agitation (immersion in an ultrasonic bath). The expected rise in sample temperature (≤ 35 ºC) due to the use of ultrasound was offset by keeping the extraction time short (3 minutes) and setting the temperature controller to a higher temperature (40 ºC) than the observed increase caused by sonication during the 3 minutes extraction.

Regarding the fibre durability, this was increased by changing the sampling phase from the liquid to the headspace, which extended the usability of the SPME coating by at least 25 % (≈ 40 - 50 uses were attained before severe deterioration was evident; as opposed to only 25 - 30 uses if sampling

was done in the liquid phase). This contradicts previous work which suggests that immersion sampling should be used for non-complex matrices such as the one used in the experiments presented here (Pawliszyn, 1997a). In addition, sampling in the headspace greatly improved the reproducibility of extraction; an effect which, along with longer fibre lifetime, had been reported by other workers extracting naphthalene and other PAH in aqueous matrices (Alonso *et al.*, 2003; Lambropoulou *et al.*, 2007).

The most significant result of all this method development was the reduction in sampling time for naphthalene from 1 hour to only 3 minutes, whilst maintaining excellent reproducibility (see above) when compared to other studies using similar extraction protocols (Heiden *et al.*, 2001; King, 2004; Rianawati and Balasubramanian, 2009).

6.2. Sorption Experiments Results

Blanks (no sorbent present) and product solutions for the sorption experiments were analyzed in triplicate, and although trends were observed in terms of PAH uptake from solution, poor reproducibility in GC - FID areas for some sets of triplicates could have compromised the statistical rigour of these experiments. None of these batch sorption experiments show adsorption significant relative to the blank at the 95 % confidence limit (GC - FID areas for blank and product overlap when 2 σ errors are accounted for). However, if we accept an increased risk of making a type I error and apply 1 σ errors, then several of the experiments are consistent with measurable naphthalene uptake (at the 68 % confidence limit) but only at higher ionic strength..This suggests that the current method of extraction is not precise enough to pick up such small

naphthalene uptake (i.e. very small differences between means at these ionic strength levels). Therefore, the following discussion will briefly discuss the individual results observed for each mineral focussing only on those results that are significant. Where appropriate, possible trends will be proposed and comparisons will be drawn between the present results and those from previous works concerned with similar solute / sorbent systems.

6.2.1. Quartz sand:

Out of the 4 minerals used in this study, VWR quartz sand showed the highest uptake of naphthalene under the specified experimental conditions, with one experiment showing approximately 17 % uptake.. Furthermore, the observed increase shows a positive correlation with increasing ionic strength and pH but the calculated partition coefficients or distribution constants (Kmin) are not in agreement with the values found in the literature for quartz sands. This is to be expected since each work has employed sorbents which are fundamentally different in origin, composition or pre-treatment in a variety of experimental conditions. The majority of the previous results are therefore not directly comparable to the results in this study due to the different experimental and theoretical approaches used.

To the best of the author's knowledge, most studies dealing with PAH transport and partition into soil components have used either individual natural materials or mixtures of them; and in many cases the amount of natural organic carbon present has not been monitored nor constrained. As an example, Piatt and colleagues (Piatt *et al.*, 1996b) calculated the total distribution coefficient from batch tests data for naphthalene after spiking a mixed soil consisting of 57

% quartz, 30 % feldspar minerals, 6 % carbonate minerals and < 5 % clay minerals. These coefficients are reported for samples run at ambient temperature and after the system had reached equilibrium. The mineral contribution to the overall distribution coefficient was 0.425 %, or 0.0068 $cm^3 . g^{-1}$ (these units correspond to the solid-to-liquid ratio normalisation). But since this group used a completely different background electrolyte (Ca-HCO_3) and ran the experiments at pH = 7.7 it is not possible to make a direct comparison to their results.

Nevertheless, where similar experimental setups and materials have been employed, useful conclusions may be drawn by looking at the general trend exhibited by the PAH-mineral system under study. The work which was most closely related to the experimental conditions used in this thesis is that of Müller and co-workers (Mueller *et al.*, 2007). Here quartz was first used as a reference material and subsequently mixed with other mineral phases, all of which were exposed to 3 different PAH, namely: phenanthrene, pyrene and benzo[a]pyrene. Several batch experiments under a range of initial concentrations and reaction times were carried out in order to find the best sorption model fit for each system. This discussion will focus on those results obtained only for phenanthrene (since it is the closest one to naphthalene in aqueous solubility, molecular weight and number of benzene rings) at 24 hours reaction time and at a value for initial concentration closest to that used for naphthalene in the present study (10 % of phenanthrene's aqueous solubility).

The properties of the sorbates and sorbents used in both studies are shown in Table 6.1. The pH for the background solution used by Muller et al.

(2007) was 5.7, a value quite close to the second experimental pH selected in this study (5.5).

The results in Müller's study show no sorption of phenanthrene took place on the quartz sand used; whose organic carbon content lies below an already remarkably low detection limit (0.004 g_{OC}. Kg^{-1}). Their result seems to support the dominant role of organic matter in the sequestration of hydrophobic organic pollutants by mineral phases (Brusseau *et al.*, 1991; Pignatello and Xing, 1996; Xing, 1997).

	AUTHORS	
EXPERIMENTAL CONDITIONS	**This study, 2011**	**Müller *et al*, 2007**
REACTION TIME	24 HOURS	>120 HOURS[1]
BACKGROUND MATRIX	$NaNO_3$	$KClO_4$
PAH	Naphthalene	Phenanthrene
INITIAL CONCENTRATION	0.5 ppm[(2)]	0.112 ppm[(3)]
MINERAL	Quartz sand[4]	Quartz sand[5]
TEMPERATURE	Not controlled	Not controlled
SPECIFIC SURFACE AREA	0.22 $m^2 g^{-1}$	0.3 $m^2 g^{-1}$
O.C. (g_{OC} . Kg^{-1}_{sample})	0.048	<0.004
SORBENT / LIQUID RATIO	1:4	1:5
RESULTS	**pH = 5.5**	**pH = 5.7**
I_1 =0.001 M	*17.56%*[6]	no sorption

1- Selected apparent equilibration time for all isotherms

2- Initial concentration 1.6 % of naphthalene's aqueous solubility (~30 mg l^{-1})

3- Initial concentration 10 % of phenanthrene's aqueous solubility (~1.12 mg l^{-1})

4- Commercially pretreated: HCl wash + 900 °C calcination (24 hr)

5- Commercially pretreated: HCl wash + 800 °C calcination (24 hr)

6- Results only significant if using 1σ errors

Table 6.1 Comparison between two studies of PAH uptake by pure quartz

The results for this study shown in Table 6.1 represent the average naphthalene uptake (n = 3, see Chapter 4 for uptake calculation) on quartz sand at the indicated ionic strength and pH conditions. It must be born in mind that these numbers, however, only statistically relevant at the 68 % confidence limit. In

general, uptake was minimal and therefore difficult to resolve. Furthermore, the resolution of small changes in solute concentration was impeded by poor reproducibility of GC - FID areas of blanks and product solutions, and therefore only in a few cases where adsorption exceeded 18 % uptake could sorption data pass even a low confidence statistical test. Reasons for low amounts of adsorption will be discussed below.

In the case of quartz or silica sand, this lack (or low level) of PAH sequestration has been reported elsewhere and is consistent with the expected results from sorption experiments obtained by other workers, such as those by Huang and colleagues (Huang *et al.*, 1996b). Their study looked into phenanthrene sequestration by quartz amongst other mineral phases; using batch experiments to determine sorption coefficients normalised to the sorbent's organic matter content and surface area. Their results seemed to indicate that solution chemistry was controlling the uptake; a behaviour which becomes more relevant as the organic matter content in the mineral decreases and for which specific thresholds have been suggested. In the work by Müller *et al*. (2007), a value of log K_{OW} = 4.6 for PAH concentrations in the liquid phase < 10 % of their aqueous solubility has been proposed as a threshold beyond which short term sorption on quartz would take place. This coefficient is called the octanol-water distribution coefficient and it is widely used in estimating partition of organic molecules between organic and aqueous phases. Naphthalene's value for this parameter is 3.3; making it unlikely for this PAH to be removed by quartz sand even at the low initial concentration used in these dissertation experiments.

In this respect both studies agree and show the same trend in spite of the solutes being two different members of the PAH series. Since each result

has been arrived at using different extraction and analysis methods (SPE vs SMPE, GC - MS vs GC - FID); it could be inferred that the use of SPME for this system acted almost as an independent verification.

6.2.2. Hematite:

This oxide also exhibited naphthalene uptake, with perhaps 21 % adsorbed at pH 5.5 and high ionic strength. Results of a previous study using naphthalene and several other PAH with α-Fe_2O_3 (Mader *et al.*, 1997) showed that pH and ionic strength have no influence in their distribution constants, which were estimated from column test data. Equally, surface area and charge (including charge sign) did not seem to affect the uptake observed for this sorbent. They propose that depending on the solution pH the oxide surface could be positively charged and, in such a scenario, aromatic planar neutral molecules with high electron density clouds could form weak dipoles with the (positively charged) surface. According to surface charge values found in Mader *et al*, hematite would have been positively charged at pH = 5.5 , a value which exactly matches the second pH used in this study. If the pH of the point of zero charge for hematite is taken as pH_{pzc} = 8.5 (Appelo and Postma, 1994), the hematite would have been positive at both experimental pH values in this thesis' experiments. This could be used to explain the general tendency towards sorption observed (formation of induced-dipole between sorbates and sorbent). In spite of concluding that solution chemistry had no effect on the mineral surface and consequently on PAH uptake, the mineral distribution constant calculated by Mader's team showed a strong correlation with the PAH's

aqueous activity coefficient. This parameter is an indicator of sorbates hydrophobicity.

The possible increase in uptake with higher ionic strength observed in this study could be due to naphthalene being ‘salted-out’ of solution with increasing electrolyte concentration. In other words, the PAH appears to prefer the hematite surface over the solution phase. It has been postulated (Schwarzenbach *et al.*, 1993) that due to their weaker hydrogen-bonding capacity, HOC cannot outcompete water molecules from fully wetted inorganic hydrophilic surfaces. Instead, the neutral organic molecules are believed to partition into the near-surface domain, which depending on the solid’s surface area will consist of several monolayers of highly organised adsorbed water, effectively creating a barrier between the mineral surface and the aqueous bulk. As this interface thickens, HOC uptake will become less dependent on the solid’s chemistry and more on their own hydrophobicity.

To summarize, although it seems that in the case of non - porous oxides, the apparent HOC-sequestration mechanism is due to partitioning between vicinal water and the bulk solution, due to the limited number of studies available that take the near surface domain into account, it is not possible yet to reach a clear conclusion. Studies concerning the dynamics between non - polar organics and inorganic solid near surface domains in aqueous systems are necessary in order to ascertain whether partitioning into vicinal water is truly taking place. The apparent uptake observed for hematite in this thesis’ experiments therefore can only tentatively be attributed to an increase in hydrophobicity of naphthalene with increasing ionic strength, regardless of the

solution's pH. These observations agree with the idea that HOC uptake by oxides is weak and non-specific, and mostly dependent on solution chemistry.

6.2.3. Goethite coated quartz sand:

The goethite coated quartz sand showed a weak tendency toward naphthalene uptake in one experiment. A number of experimental artefacts associated with applying the selected coating protocol (Lai and Chen, 2001) for this mineral could have affected results with this material. The end product was not homogeneous (visual inspection) and it is believed this could have played an important role in the lack of correlation with other minerals in this and other studies (Stauffer and Macintyre, 1986). Furthermore, unlike in previous works (Lai and Chen, 2001) no crystalline layer could be identified using XRD after finalising the coating process (two coating attempts in total) and the sample had to be sent for XRF analysis. This enabled the identification of the presence of an iron oxide phase at 1.61 % w / w (SiO_2 totalled 97.528 %).

In lieu of the lack of homogeneity of the final coated product and the fact that no positive identification of crystalline goethite could be achieve by XRD; these results are rendered unusable for the purpose of comparison against other mineral phases used in this study, as well as those in other similar works and will not be discussed further.

6.2.4. Montmorillonite Reference Clay:

The reference clay showed the lowest overall tendency towards naphthalene uptake of all the minerals used in this study with no experiment

giving a resolvable quantity adsorbed. Significant uptake of phenanthrene by swelling smectites has been reported before, but the reaction conditions used differ significantly from the ones in this study (Huang *et al.*, 1996a; Hundal *et al.*, 2001; Zhu *et al.*, 2004b; Mueller *et al.*, 2007). In these studies, the average exposure time to phenanthrene in batch tests at which equilibrium was ensured ranged from 72 hours to 21 days. In contrast, phase separation problems encountered in the present work prompted the use of very large centrifugation periods (2 – 4 hours) at the operational limit of the available centrifuge's capability (2400 rpm) which in turn made it necessary to considerably shorten the reaction times (≤ 20 hr). This could have had a detrimental effect on the overall uptake rate expected from such materials given the average time required by the clay to reach equilibrium within the system.

Moreover, different saturating cations were observed to exert a remarkable influence on the sorption of phenanthrene; particularly soft, weakly hydrated cations such as Ag^{+}, Cs^{+} and K^{+} which appeared to increase phenanthrene sequestration whilst harder, strongly hydrated cations such as Na^{+} and Mg^{+2} had the opposite effect. Furthermore, when Ca^{+2} was used as the saturating cation for montmorillonite a higher phenanthrene sorption than that observed for the same clay saturated with Na^{+} and K^{+} was reported. The authors explain this effect as Ca^{+2} triggering the re-arrangement of the clay structure in a way which allowed the phenanthrene molecule to preferentially enter the clay's interlayer driven from the bulk solution by hydrophobicity.

In this research, the same reference clay was suspended in Na^{+} solutions of different molarities but was not pre-saturated with this or any other metal; nor was it allowed to equilibrate in the background electrolytes before

adding naphthalene and starting the reaction times. It must be noted that the uptake trend shown by this sorbent appeared to decrease with increased Na^+ concentration in the background electrolyte. This could be interpreted as competition between the cation and the PAH for sorption sites on the smectite interlayer. As postulated in the work by Huang *et al* the increasingly higher Na^+ density and consequently the higher vicinal water density on the surface could have prevented the planar, neutral naphthalene molecule from accessing available active sites on the clay.

Previous studies also report pH having a significant influence on the sorptive potential of montmorillonite. Zhu, Herbert and co-workers embarked in spectroscopic molecular probing of mineral surfaces in order to understand the dynamics behind their experimental results and find a mechanism to match the sorption models suggested by others. In addition to batch tests they used deuterium nuclear magnetic resonance (D^2NMR) and used a parameter called "quadrupolar splitting" to detect changes in molecular orientation of deuterated solvents in solution ranging from benzene to alcohols and water. The full theoretical treatment for this concept falls beyond the scope of this discussion and is available elsewhere (Zhu *et al.*, 2004a; Zhu *et al.*, 2004c). Higher values for quadrupolar splitting showed direct correlation with higher uptake on the mineral surface due to cation-π interactions between planar aromatic molecules and cation-saturated mineral surfaces. The sorbates used were naphthalene, phenanthrene, pyrene and 1, 2, 4, 5-tetrachlorobenzene.The Ag^+- saturated montmorillonite (Stx-1) showed the highest phenanthrene uptake, and Na^+-montmorillonite the lowest. This is an example of how softer, weakly hydrated cations make the clay's surface more accessible for PAH. Furthermore, D^2-

benzene sorption increased with lower clay to solution ratio (1:200 as opposed to 1:1000) and higher solution pH (pH = 9.0).

In this dissertation's experimental work, pH readings taken from the run blanks at the beginning and the end of the 24 hour reaction period (mineral and background electrolyte, no PAH) showed the solution's pH always returned to that of the Stx-1 suspensions (~ 7.4). This value is below the pH range at which sorption of benzene by Na-montmorillonite is reported by Müller *et al* (9.0 – 11.0).

A further difference between the author's work and that of others cited here is the lack of pre-treatment to remove amorphous iron or organic matter since the goal of the experiments was to use solely natural materials with the exception of quartz sand, which had undergone pre-treatment.

These comparisons between experimental details help to explain the apparent lack of sorption observed for a sorbent known to be an effective PAH scavenger from solution, as is the case for this reference clay (Stx-1). It also helps to illustrate how in spite of controlling up to three key experimental variables (OC %, ionic strength and pH), more than one mechanism seems to be at play and it would therefore be unwise to try and fit a universal explanation or mathematical model to fit all PAH-clay mineral scenarios.

This type of smectite appears to reach equilibrium with the system only after a minimum of 72 hours and its sorptive capacity seems to be closely related to the individual sorbate's characteristics as well as to surface and solution chemistry. On that basis it can be concluded that the behaviour observed for this particular reference clay in this research is in agreement with the general trend observed in the literature.

To summarize, the behaviour observed in these experiments involving inorganic surfaces and neutral hydrophobic (compounds under the condition of organic matter content ~f_{oc} < 0.01 (Schwarzenbach *et al.*, 1993)) fall into two main categories:

- Solution chemistry: PAH is being salted out of solution by increasing concentrations of electrolyte in the case of quartz and hematite

- Sorbent surface chemistry: naphthalene uptake may decrease as the amount of hard cations adsorbed onto the surface of Stx-1 montmorillonite increases.

Although naphthalene hydrophobicity is almost guaranteed to have contributed to the observed behaviour, its contribution to the overall trend cannot be assessed without comparison against other PAH in the same experimental systems.

The sensitivity of the method can be improved in order to be able to better detect PAH sequestration by the employed minerals. Better separation between the sample and control means can be achieved by taking a series of steps aimed to improve the experimental design, such as:

- Increasing the solid-to-liquid ratio in all the sample replicates to ensure sufficient sorption active sites are available to the PAH in solution,

- Increasing the samples reaction times to allow the system to completely reach equilibrium or steady state prior to and after spiking

with PAH, especially in the case of swelling clay minerals and sorbents with high porosity or capacity for surface cation exchange,

- Using a wide range of initial PAH-concentrations in order to assess whether this factor influences the sorbents' removal capacity.

These measures would in principle reduce the spread of the data, and by improving the precision of the method, the mean sample and control distributions would no longer overlap. Human error can also be minimised, i.e. by implementing automated SPME sampling and extraction (Combi Pal system). This step would enable accurate time and temperature control as well as consistent sampling depth; whilst providing inbuilt agitation and ensuring problem-free injections into the designated desorption port.

6.3. Surface Analysis

Techniques for sample preparation and analysis in bulk solutions are inherently different from surface analysis methods and although useful, they provide little or no information concerning the molecular configuration or mode of binding at the inorganic surface.

The preliminary nature of the surfaces analysis assays carried out in this work do not allow us to make definite conclusions even in those few cases where detection was possible. Moreover; the lack of data from comparable studies reinforces the need for further experimental work before any sorption mechanism can be proposed on the basis of these observations. As a result, the data presented in the following sections will focus on potential implications in regards to the trends observed in the sorption experimental data.

6.3.1. AFM

Atomic Force Microscopy (AFM) was used in a feasibility study in order to attempt to visualize the naphthalene as an adsorbate on a series of mineral substrates. No previous studies have been found in which the same kind of system had been used, and therefore laboratory protocols and analytical methods had to be devised and developed without any previous basis.

The technique proved to be very challenging and inadequate for the selected systems at the desired resolution. The apparently ‘negative ‘results obtained could signify that:

- there is either no adsorption taking place between naphthalene and all the substrates scanned, namely: silicon oxide slides, muscovite slides and the Au-coated versions of the latter substrate and this would be the reason why it was never detected;

- or that the goals of the experiment were beyond the limit of the microscope’s capabilities because the PAH used is too planar and too small to be detected. There are constrains as to the minimum size adsorbates can be in order to be sensed by the AFM cantilever tips; they must be larger than the largest irregularities or inhomogeneities present on the surface or they will not be picked up. The latter assumption could have been the case here.

These were preliminary measurements and were aimed to identify the presence of adsorbed PAH molecules on slides made of the minerals used as sorbents in previous sorption tests. Several instrumentation and protocol problems were encountered along the way: software problems when attempting to save files during a scan (images could not be saved for as long a period as 8

months); severe charging prevented successful scans and substrate roughness did not allow the use of unmodified original scheduled substrates. These inconveniences led to a drastic change in methodology and although every effort was made to focus on naphthalene as the substrate of choice, larger model adsorbates had to be used in order to at least develop a protocol and gain experience using the AFM instrument. After experiencing such amount of difficulties in imaging even the larger molecules on the desired substrates (several dosing methodologies and concentrations had to be tested) it was concluded that time would be better spent in attempting to use a different surface analysis technique.

6.3.2. XPS:

The objectives of using X-ray photoelectron spectroscopy in this research work were:

- to identify the presence of aromatic molecules (PAH) on the pre-loaded minerals within a controlled environment and at known concentrations

- to go beyond imaging and try to detect the presence of any electrons originating from bonding orbitals in either the adsorbate or mineral substrates in order to find irrefutable proof of chemical bonding

- to detect any surface changes on the substrates upon PAH-loading as evidence of chemisorption or adsorption in the system

Although XPS is a suitable analytical technique for the identification of surface organic molecules; however, no presence of polycyclic aromatics was detected in the minerals analysed under the specified experimental conditions.

It is possible that the ultra-high vacuum conditions required for analysis could have disrupted the system to such an extent that any planar, weakly sorbed PAH molecules would have been ripped away from the mineral surface. This outcome would seem to support the physisorption hypothesis suggested by the work of Mader and colleagues (Mader *et al.*, 1997). Furthermore, if physisorption is the dominant mechanism at play XPS would not be the most appropriate analytical tool to use since any evidence of surface interactions would be destroyed due to the required vacuum conditions.

Equally, the lack of temperature control on the sample platform could have played a crucial role in the observed outcome, as PAH have been detected in previous works which used XPS but under controlled loading temperatures.

After attempts to image a planar, small molecule on very rough surfaces failed to provide any confirmation of molecular chemisorption, analysis by XPS seemed to be the next logical step in the surface analysis studies. Using spectroscopic techniques instead of imaging circumvented two big problems encountered whilst using AFM, namely: surface charging and roughness; since the sample was no longer probed with a mechanical tip. In spite of these advantages, however, and of all the precautions taken during the systematic sample preparation protocol, the initial objectives of the use of XPS were not met, possibly due to aggressive analytical conditions and sample cross-contamination.

The presence of these carbon peaks in procedural blanks does not allow us to interpret the data in an conclusive manner, in spite of the significant shifts observed in the binding energies for O 1s (i.e. oxygen from hydroxyl and silanol

groups) as well as Si 2p (in the case of quartz) in some of the analysed samples.

6.3.3. ATR-FTIR

Preliminary FTIR studies were attempted in this study in order to detect molecular adsorption of PAH on mineral surfaces by identifying absorption bands corresponding to functional groups characteristic of pi-cation bonding.on the mineral surfaces under analysis.

ATR - FTIR analysis was applied to a series of mineral-PAH sample systems in a variety of loading scenarios. The resulting surface spectra do not show unambiguous presence of PAH or any other aromatic derivatives. Furthermore the date cannot be interpreted with accuracy due to the presence of negative peaks and water interference.

Solvent evaporation at ambient temperature was such that it was impossible to collect PAH spectra without encountering negative peaks; which in turn hindered the potential identification of PAH-mineral surface species.

Another detrimental factor is the fact that the protocols followed for loading the PAH onto the sample substrates may not have been the best suited for this particular system given the volatile nature of the pollutants under study.

It was therefore concluded that the best approach would have been *in situ* IR experiments within a controlled environment (i.e. controlled temperature and sorbate deposition coating) such as that presented in the work by Morris and Wogelius, 2005 (Morris, 2005a). The preparation and testing of this and

other experimental setup required for such an approach, however, would have been prohibitive within the time frame allocated to these preliminary tests.

REFERENCES

Achten, C. and Püttmann, W. (2000). Determination of Methyl tert-Butyl Ether in Surface Water by Use of Solid-Phase Microextraction. Environmental Science & Technology 34(7): 1359-1364.

Ackerman, A. H. and Hurtubise, R. J. (2000). The effects of adsorption of solutes on glassware and teflon in the calculation of partition coefficients for solid-phase microextraction with 1PS paper. Talanta 52(5): 853-861.

Agency for Toxic Substances and Disease Registry (1995a). Toxicological Profile for Polycyclic Aromatic Hydrocarbons. Atlanta, Division of Toxicology.

Agency for Toxic Substances and Disease Registry, A. (1995b). Toxicological Profile for Naphthalene (Update). U. S. D. o. H. a. H. S. Public Health Service, Atlanta, GA, USEPA.

Aksnes, D. W. and Kimtys, L. (2004). 1H and 2H NMR studies of benzene confined in porous solids: melting point depression and pore size distribution. Solid State Nuclear Magnetic Resonance 25(1-3): 146-152.

Al-Abadleh, H. A. and Grassian, V. H. (2003). Oxide surfaces as environmental interfaces Surface Science Reports 52(3-4): 63-161.

Alonso, A., Fernández-Torroba, M., Tena, M. and Pons, B. (2003). Development and validation of a solid-phase microextraction method for the analysis of volatile organic compounds in groundwater samples. Chromatographia 57(5): 369-378.

Ania, C. O., Cabal, B., Pevida, C., Arenillas, A., Parra, J. B., Rubiera, F. and Pis, J. J. (2007). Effects of activated carbon properties on the adsorption of naphthalene from aqueous solutions. Applied Surface Science 253(13): 5741-5746.

Appelo, C. A. J. and Postma, D. (1994). Geochemistry, Groundwater and Pollution. Rotterdam, Balkema. 669 pages.

Appert-Collin, J. C., Dridi-Dhaouadi, S., Simonnot, M. O. and Sardin, M. (1999). Nonlinear sorption of naphtalene and phenanthrene during saturated transport in natural porous media. Physics and Chemistry of the Earth, Part B: Hydrology, Oceans and Atmosphere 24(6): 543-548

Armstrong, B. G. and Gibbs, G. (2009). Exposure–response relationship between lung cancer and polycyclic aromatic hydrocarbons (PAHs). Occupational and Environmental Medicine 66(11): 740-746.

Arnarson, T. S. and Keil, R. G. (2000). Mechanisms of pore water organic matter adsorption to montmorillonite. Marine Chemistry 71(3-4): 309 - 320.

Atkins, P. and De Paula, J. (2004). Atkin's Physical Chemistry. Oxford Oxford University Press. 920 pages.

Bishop, J. L. and Murad, E. (2004). Characterization of minerals and biogeochemical markers on Mars: A Raman and IR spectroscopic study of montmorillonite. Journal of Raman Spectroscopy 35: 480 - 486.

Bojes, H. K. and Pope, P. G. (2007). Characterization of EPA's 16 priority pollutant polycyclic aromatic hydrocarbons (PAHs) in tank bottom solids and associated contaminated soils

at oil exploration and production sites in Texas. Regulatory Toxicology and Pharmacology 47(3): 288-295.

Briggs, D. and Seah, M. P. (1990). Practical Surface Analysis. Guildford, John Wiley & Sons Ltd. 420 pages.

British Standard Institution (BSI) (1990). *Methods of test for Soils for Civil Engineering Purposes. Part 2: Classification tests. BS1377-2.* 2.

Brunauer, S., Emmett, P. H. and Teller, E. (1938). Adsorption of Gases in Multimolecular Layers. Journal of the American Chemical Society 60(2): 309.

Brusseau, M. L., Jessup, R. E. and Rao, P. S. C. (1991). Nonequilibrium sorption of organic chemicals: elucidation of rate-limiting processes. Environmental Science & Technology 25(1): 134-142.

Bruya, J. E. and Costales, M. (2005). Discussion of the Error Associated with Polycyclic Aromatic Hydrocarbon (PAH) Analyses. Environmental Forensics 6(2): 175-185.

Carlsen, L., Lassen, P., Gunnar, P. and Poulsen, M. E. (1997). Neri Technical Report No. 190: Fate of Polycyclic Aromatic Hydrocarbons in the Environment, Ministry of Environment and Energy**:** 84.

Carmo, A. M., Hundal, L. S. and Thompson, M. L. (2000). Sorption of Hydrophobic Organic Compounds by Soil Materials: Application of Unit Equivalent Freundlich Coefficients. Environmental Science and Technology 34(20): 4363-4369.

Charalambos Assos (2010). Organic ligand complexation reactions on aluminium-bearing mineral surfaces studied by *in-situ* Multiple Internal Reflection Infrared Spectroscopy, adosrption experiments and surface complexation modelling. School of Earth, Atmospheric and Environmental Sciences. Manchester, The University of Manchester. Ph.D.**:** 260.

Charbeneau, R. J. (2000). Groundwater Hydraulics and Pollutant Transport. New Jersey, Prentice-Hall. 59 pages.

Chevron Cottin, N. and Merlin, G. (2007). Study of pyrene biodegradation capacity in two types of solid media. Science of The Total Environment 380(1-3): 116-123.

Collins, J. F., Brown, J. P., Dawson, S. V. and Marty, M. A. (1991). Risk assessment for benzo[a]pyrene. Regulatory Toxicology and Pharmacology 13(2): 170-184.

Compere, F., Porel, G. and Delay, F. (2001). Transport and retention of clay particles in saturated porous media. Influence of ionic strength and pore velocity. Journal of Contaminant Hydrology 49(1-2): 1-21.

Cook, J. W. and Martin, R. H. (1940). Polycyclic Aromatic Hydrocarbons. Part XXIV.

Cousins, I. T., Kreibich, H., Hudson, L. E., Lead, W. A. and Jones, K. C. (1997). PAHs in soils: contemporary UK data and evidence for potential contamination problems caused by exposure of samples to laboratory air. Science of The Total Environment 203(2): 141-156.

Crenshaw, M. L. and Banna, M. S. (1989). A study of C1s binding energies in some gaseous polycyclic aromatic hydrocarbons. Journal of Electron Spectroscopy and Related Phenomena 48(1): 179-185.

Danzer, J. and Grathwohl, P. (1998). Coupled transport of PAH and surfactants in natural aquifer material. Physics and Chemistry of The Earth 23(2): 237-243.

Deer, W. A., Howie, R. A. and Zussman, J. (1972). An Introduction to the Rock Forming Minerals. London, Longman Group Limited. 539 pages.

DiNardo, J. N. (1994). Nanoscale Characterisation of Surfaces and Interfaces. Weinheim, VCH Verlagsgesellschaft mbH. 173 pages.

Ding, Y. S., Trommel, J. S., Yan, Z. J., Ashley, D. and Watson, C. H. (2005). Determination of 14 Polycyclic Aromatic Hydrocarbons in Mainstream Smoke from Domestic Cigarettes. Environmental Science and Technology 39(2): 471 - 478.

Doong, R.-a., Chang, S.-m. and Sun, Y.-c. (2000a). Solid-phase microextraction for determining the distribution of sixteen US Environmental Protection Agency polycyclic aromatic hydrocarbons in water samples. Journal of Chromatography A 879(2): 177-188.

Doong, R., Chang, S. and Sun, Y. (2000b). Solid-phase microextraction for determining the distribution of sixteen US Environmental Protection Agency polycyclic aromatic hydrocarbons in water samples. Journal of Chromatography A 879(2): 177-188.

Doong, R. a. and Chang, S. m. (2000). Determination of Distribution Coefficients of Priority Polycyclic Aromatic Hydrocarbons Using Solid-Phase Microextraction. Anal. Chem. 72(15): 3647-3652.

Doong, R. A., Chang, S. M. and Sun, Y. C. (2000c). Solid-phase microextraction and headspace solid-phase microextraction for the determination of high molecular-weight polycyclic aromatic hydrocarbons in water and soil samples. Journal of Chromatographic Science 38(12): 528-534.

Drost-Hansen, W. (1969). Structure of Water Near Solid Interfaces. Industrial and Engineering Chemistry Research 61(11): 10-47.

Eisert, R. and Levsen, K. (1996). Review: Solid-phase Microextraction Coupled to Gas-Chromatography: A new Method for the Analysis of Organics in Water. Journal of Chromatography A 733(1-2): 143-157.

El-Alawi, Y. S., McConkey, B. J., George Dixon, D. and Greenberg, B. M. (2002). Measurement of Short- and Long-Term Toxicity of Polycyclic Aromatic Hydrocarbons Using Luminescent Bacteria. Ecotoxicology and Environmental Safety 51(1): 12-21.

Elbel, N., Behner, H. and Seggern, H. v. (1995). Preparation and characterisation of epitaxial gold films deposited on mica by direct current magnetron sputtering. J. Vac. Sci. Technol. B. 13(5).

Expert Panel on Air Quality Standards (1999). Polycyclic Aromatic Hydrocarbons. London, Department of the Environment, Transport and the Regions, National Assembly for Wales, Scottish Executive and Department of the Environment (Northern Ireland).

Fernández-González, V., Concha-Graña, E., Muniategui-Lorenzo, S., López-Mahía, P. and Prada-Rodríguez, D. (2007). Solid-phase microextraction-gas chromatographic-tandem mass

spectrometric analysis of polycyclic aromatic hydrocarbons: Towards the European Union water directive 2006/0129 EC. Journal of Chromatography A 1176(1-2): 48-56.

Fernandez-Gonzalez, V., Concha-Grana, E., Muniategui-Lorenzo, S. and Prada-Rodriguez, D. (2007). Solid-Phase microextraction-gas chromatography-tandem mass spectroscopy analysis of polycyclic aromatic hydrocarbons Towards the European Union water Directive 2006/0129 EC. Journal of Chromatography A 1176: 48-56.

Fifield, F. W. and Kealy, D. (2000). Principles and Practice of Analytical Chemistry, Blackwell Science. pages.

Fowlis, I. A. (1995). Gas Chromatography. Chichester, John Wiley and Sons. 300 pages.

Gaboriau, H. and Saada, A. (2001). Influence of heavy organic pollutants of anthropic origin on PAH retention by kaolinite. Chemosphere 44(7): 1633-1639.

Gad, S. C. and Gad, S. E. (2005). Polycyclic Aromatic Hydrocarbons (PAHs). Encyclopedia of Toxicology. W. Philip. New York, Elsevier**:** 513-515.

Gerde, P., Medinsky, M. A. and Bond, J. A. (1991). Particle-associated polycyclic aromatic hydrocarbons--A reappraisal of their possible role in pulmonary carcinogenesis. Toxicology and Applied Pharmacology 108(1): 1-13.

Gerstl, Z., Chen, Y., Mingelgrin, U. and Yaron, B. (1989). Toxic Organic Chemicals in Porous Media 343 pages.

Grimmer, G., Dettbarn, G., Brune, H., Deutsch-Wenzel, R. and Misfeld, J. (1982). Quantification of the carcinogenic effect of polycyclic aromatic hydrocarbons in used engine oil by topical application onto the skin of mice. International Archives of Occupational and Environmental Health 50(1): 95-100.

Grynkiewicz, M., Polkowska, Z. and Namiesnik, J. (2002). Determination of polycyclic aromatic hydrocarbons in bulk precipitation and runoff waters in an urban region (Poland). *Atmospheric Environment* **36**: 361-369.

Guillot, S., Kelly, M. T., Fenet, H. and Larroque, M. (2006). Evaluation of solid-phase microextraction as an alternative to the official method for the analysis of organic micro-pollutants in drinking water. Journal of Chromatography A 1101(1-2): 46-52.

Gupta, R. P. and Sen, S. K. (1974). Calculation of multiplet structure of core p-vacancy levels. Physical Review B 10(1): 71.

Halsall, C. J., Coleman, P. J., Davis, B. J., Burnett, V., Waterhouse, K. S., Harding-Jones, P. and Jones, K. C. (1994). Polycyclic Aromatic Hydrocarbons in U.K. Urban Air. Environmental Science & Technology 28(13): 2380-2386.

Hammond, E. C., Selikoff, I. J., Lawther, P. L. and Seidman, H. (1976). Inhalation of Benzpyrene and Cancer in Man. Annals of the New York Academy of Sciences 271(May 28): 116-124.

Handley, A. (1998). Extraction Methods in Organic Analysis, Sheffield Academic Press Ltd. pages.

Harris, D. (1991). Quantitative Chemical Analysis. New York, W. H. Freeman and Company. 3rd edition. pages.

Harrison, R. M., Smith, D. J. T. and Luhana, L. (1996). Source Apportionment of Atmospheric Polycyclic Aromatic Hydrocarbons Collected from an Urban Location in Birmingham, U.K. Environmental Science & Technology 30(3): 825-832.

Harvey, R. G. (1991). Polycyclic Aromatic Hydrocarbons: Chemistry and Carcinogenicity. Cambridge, Cambridge University Press. pages.

Harvey, R. G. (1996). Polycyclic Aromatic Hydrocarbons, Wiley-VCH. pages.

Hassett, J. J., Means, J. C., Banwart, W. L., Wood, S. G., Ali, S. and Khan, A. (1980). Sorption of Dibenzothiophene by Soils and Sediments Journal of Environmental Quality 9(2): 184 - 186.

Havenga, W. J. and Rohwer, E. R. (2000). The use of SPME and GC-MS for the chemical characterisation and assessment of PAH pollution in aqueous environmental samples. International Journal of Environmental Analytical Chemistry 78(3-4): 205-221.

Heiden, A. C., Hoffmann, A. and Kolahgar, B. (2001). Comparison of the Sensitivity of Solid Phase MicroExtraction (SPME) and Stir Bar Sorptive Extraction (SBSE) for the Determination of Polycyclic Aromatic Hydrocarbons (PAHs) in Water and Soil Samples. Muelheim an der Ruhr, Germany, Gerstel-Global Analytical Solutions.

Heywood, E., Wright, J., Wienburg, C. L., Black, H. I. J., Long, S. M., Osborn, D. and Spurgeon, D. J. (2006). Factors Influencing the National Distribution of Polycyclic Aromatic Hydrocarbons and Polychlorinated Biphenyls in British Soils. Environmental Science & Technology 40(24): 7629-7635.

Huang, W., Schlautman, M. A. and Weber, W. J. (1996a). A Distributed Reactivity Model for Sorption by Soils and Sediments. 5. The Influence of Near-Surface Characteristics in Mineral Domains. Environmental Science & Technology 30(10): 2993-3000.

Huang, W., Schlautman, M. A. and Weber, W. J. (1996b). A Distributed Reactivity Model for Sorption by Soils and Sediments. 5. The Influence of Near-Surface Characteristics in Mineral Domains. Environmental Science and Technology 30(10): 2993-3000.

Huang, W. and Weber W.J, Jr. (1998). A distributed reactivity model for sorption by soils and sediments. 11. Slow concentration-dependent sorption rates. Environmental Science and Technology 32(22): 3549.

Huang, W. and Weber, W. J. (1997). Thermodynamic Considerations in the Sorption of Organic Contaminants by Soils and Sediments. 1. The Isosteric Heat Approach and Its Application to Model Inorganic Sorbents Environmental Science and Technology 31: 3238-3249.

Hundal, L. S., Thompson, M. L., Laird, D. A. and Carmo, A. M. (2001). Sorption of Phenanthrene by Reference Smectites. Environmental Science and Technology 35(17): 3456-3461.

Hwang, S. and Cutright, T. J. (2004). Evidence of underestimation in PAH sorption/desorption due to system nonequilibrium and interaction with soil constituents. J Environ Sci Health Part A Tox Hazard Subst Environ Eng 39(5): 1147-1162.

International Agency for Research on Cancer (1983). IARC Monographs on the Evaluation of Carcinogenic Risks to Humans. Volume 32. Polynuclear Aromatic Compounds, Part 1, Chemical, Environmental and Experimental Data. Summary of Data Reported and Evaluation, World Health Organisation, WHO. 2005.

Kan, A. T., Fu, G., Hunter, M., Chen, W., Ward, C. H. and Tomson, M. B. (1998). Irreversible sorption of neutral hydrocarbons to sediments: Experimental observations and model predictions. Environmental Science and Technology 32(7): 892-902.

Karahalil, B., Karakaya, A. E. and Burgaz, S. (1999). The micronucleus assay in exfoliated buccal cells: application to occupational exposure to polycyclic aromatic hydrocarbons. Mutation Research/Genetic Toxicology and Environmental Mutagenesis 442(1): 29-35.

Karickhoff, S. W., Brown, D. S. and Scott, T. A. (1979). Sorption of hydrophobic pollutants on natural sediments. Water Research 13(3): 241-248.

Kiely, G. (1997). Environmental Engineering, McGraw-Hill Publishing Co. 979 pages.

Kim, S. B. and Corapcioglu, M. Y. (2002). Contaminant transport in dual-porosity media with dissolved organic matter and bacteria present as mobile colloids Journal of Contaminant Hydrology 59(3 - 4): 267-289.

King, A. J., Readman, J. W. and Zhou, J. L. (2003). The Application of Solid-Phase Micro-Extraction (SPME) to the Analysis of Polycyclic Aromatic Hydrocarbons (PAHs). Environmental Geochemistry and Health 25(1): 69 - 75.

King, A. J., Readman, J. W. and Zhou, J. L. (2004). Determination of Polycyclic Aromatic Hydrocarbons in Water by Solid-Phase Microextraction-Gas Chromatography-Mass Spectrometry. Analytica Chimica Acta 523: 259-267.

Kleineidam, S., Ruegner, H., Ligouis, B. and Grathwohl, P. (1999). Organic Matter Facies and Equilibrium Sorption of Phenanthrene. Environmental Science & Technology 33: 1637-1644.

Klotz, I. M. and Rosenberg, R. M. (2000). Chemical Thermodynamics. Basic Theory and Methods. Canada, John Wiley & Sons. pages.

Kolasinski, K. W. (2008). Surface Science: Foundations of Catalysis and Nanoscience. Chichester, John Wiley & Sons, Ltd. 2nd edition. 496 pages.

Kookana, R. S., Gerritse, R. G. and Aylmore, L. A. G. (1990). Effect of Organic Cosolvent on Adsorption and Desorption of Linuron and Simazine in Soil. Australian Journal of Soil Research 28: 717 - 725.

Krauss, M. and Wilcke, W. (2002). Sorption Strength of Persistent Organic Pollutants in Particle-size Fractions of Urban Soils. Soil Sci Soc Am J 66(2): 430-437.

Krauss, M., Wilcke, W. and Zech, W. (2000). Polycyclic aromatic hydrocarbons and polychlorinated biphenyls in forest soils: depth distribution as indicator of different fate. Environmental Pollution 110(1): 79-88.

Labbe, P. and Reverdy, G. (1987). Adsorption Characteristics of Polycyclic Aromatic Compounds on Clays: Pyrene as Photophysical Probe on Laponite. Langmuir 4: 419-425.

Lai, C. H. and Chen, C. Y. (2001). Removal of metal ions and humic acid from water by iron-coated filter media. Chemosphere 44(5): 1177-1184.

Lambropoulou, D. A., Konstantinou, I. K. and Albanis, T. A. (2007). Recent developments in headspace microextraction techniques for the analysis of environmental contaminants in different matrices. Journal of Chromatography A 1152(1-2): 70-96.

Lawther, P. J. and Waller, R. E. (1978). TRENDS IN URBAN AIR-POLLUTION IN UNITED-KINGDOM IN RELATION TO LUNG-CANCER MORTALITY. Environmental Health Perspectives 22(FEB): 71-73.

Lewis, G. P. and Coughlin, L. (1973). Lung "soot" accumulation in man. Atmospheric Environment (1967) 7(12): 1249-1255.

Li, H. L., Chen, J. J., Wu, W. and Piao, X. S. (2010). Distribution of polycyclic aromatic hydrocarbons in different size fractions of soil from a coke oven plant and its relationship to organic carbon content. Journal of Hazardous Materials 176(1-3): 729-734.

Li, N. and Lee, H. K. (2001). Assessment of Colloid Formation and Physical State Distribution of Trace Polycyclic Aromatic Hydrocarbons in Aqueous Samples. Anal. Chem. 73: 5201-5206.

Lord, H. and Pawliszyn, J. (2000). Evolution of solid-phase microextraction technology. Journal of Chromatography A 885(1-2): 153-193.

Luthy, R. G., Aiken, G. R., Brusseau, M. L., Cunningham, S. D., Gschwend, P. M., Pignatello, J. J., Reinhard, M., Traina, S. I., Weber W.J, Jr. and Westall, J. C. (1997). Sequestration of hydrophobic organic contaminants by geosorbents. Environmental Science and Technology 31(12): 3341.

Mader, B. T., Uwe-Goss, K. and Eisenreich, S. J. (1997). Sorption of Nonionic, Hydrophobic Organic Chemicals to Mineral Surfaces. Environmental Science and Technology 31(4): 1079-1086.

Maisto, G., De Nicola, F., Iovieno, P., Prati, M. V. and Alfani, A. (2006). PAHs and trace elements in volcanic urban and natural soils. Geoderma 136(1-2): 20-27.

Martuzevicius, D., Kliucininkas, L., Prasauskas, T., Krugly, E., Kauneliene, V. and Strandberg, B. (2011). Resuspension of particulate matter and PAHs from street dust. Atmospheric Environment 45(2): 310-317.

Meijer, S. N., Sweetman, A. J., Halsall, C. J. and Jones, K. C. (2008). Temporal Trends of Polycyclic Aromatic Hydrocarbons in the U.K. Atmosphere: 1991–2005. Environmental Science & Technology 42(9): 3213-3218.

Micromeritics Ltd (1995). Gemini 2360 Surface Area Analyzer- Operator's Manual.

Middleton, C. (2003). The Development Of A Mesoscale Contaminant Hydrogeology Column And Its Application To Environmental Organic Systems. Department of Civil Engineering. Manchester, University of Manchester**:** 420.

Minkov, I., Gel'mukhanov, F., Friedlein, R., Osikowicz, W., Suess, C., Ohrwall, G., Sorensen, S. L., Braun, S., Murdey, R., Salaneck, W. R. and Agren, H. (2004). Core excitations of naphthalene: Vibrational structure versus chemical shifts. The Journal of Chemical Physics 121(12): 5733-5739.

Moon, J.-W., Goltz, M. N., Ahn, K.-H. and Park, J.-W. (2003). Dissolved organic matter effects on the performance of a barrier to polycyclic aromatic hydrocarbon transport by groundwater. Journal of Contaminant Hydrology 60(3-4): 307.

Morris, P. (2005a). Ligand-surface complexation at mineral-water interfaces studied *via in-situ* Multiple Internal Reflection Infrarred Spectroscopy, X-ray Scattering techniques, and Surface Titrations. School of Earth, Atmospheric and Environmental Sciences (SEAES). Manchester, The University of Manchester. Ph.D.**:** 180.

Morris, P. (2005b). Procedure for BET Analysis of the Surface Area Y. De Bryant. Manchester

Mueller, S., Totsche, K. U. and Kogel-Knabner, I. (2007). Sorption of polycyclic aromatic hydrocarbons to mineral surfaces. European Journal of Soil Science 58(4): 918-931.

Nakhimovsky, L. A., Lamotte, M. and Joussot-Dubien, J. (1989). Handbook of Low Temperature Electronic Spectra of Polycyclic Aromatic Hydrocarbons. Amsterdam, Elsevier. 124 pages.

Nalwa, H. S. (2001). Advances in Surface Science. San Diego, California, Academic Press. 1st edition. 454 pages.

Nieman, J. K. C., Sims, R. C., McLean, J. E., Sims, J. L. and Sorensen, D. L. (2001). Fate of pyrene in contaminated soil amended with alternate electron acceptors. Chemosphere 44(5): 1265-1271.

Niri, V. H. and Pawliszyn, J. (2007). Equilibrium in-fiber standardization method for determination of sample volume by solid phase microextraction. Analyst 132(5): 425-430.

Nkedi-Kizza, P., Rao, P. S. C. and Hornsby, A. G. (1987). Influence of Organic Cosolvents on Leaching of Hydrophobic Organic Chemicals through Soils. Environmental Science & Technology 21(11): 1107 - 1111.

Ouyang, G., Cai, J., Zhang, X., Li, H. and Pawliszyn, J. (2008). Standard-free kinetic calibration for rapid on-site analysis by solid-phase microextraction. Journal of Separation Science 31(6-7): 1167-1172.

Patrolecco, L., Ademollo, N., Capri, S., Pagnotta, R. and Polesello, S. (2010). Occurrence of priority hazardous PAHs in water, suspended particulate matter, sediment and common eels (Anguilla anguilla) in the urban stretch of the River Tiber (Italy). Chemosphere 81(11): 1386-1392.

Pawliszyn, J. (1997a). Solid Phase Microextraction: Theory and Practice. New York, Wiley-VCH. pages.

Pawliszyn, J. (1999). Applications of Solid Phase Microextraction. Bodmin, The Royal Society of Chemistry. pages.

Pawliszyn, J., Pawliszyn B. and Pawliszyn M. (1997b). Solid Phase Microextraction (SPME). The Chemical Educator 2(4).

Perkin Elmer. (2011). Technical Note on ATR-FTIR. Retrieved 20/04/2011, from http://las.perkinelmer.com/content/TechnicalInfo/TCH_FTIRATR.pdf.

Piatt, J. J., Backhus, D., Capel, P. D. and Eisenreich, S. J. (1996a). Temperature-Dependent Sorption of Naphthalene, Phenanthrene, and Pyrene to Low Organic Carbon Aquifer Sediments *Environmental Science and Technology* 30 (3): 751 -760.

Piatt, J. J., Backhus, D. A., Capel, P. D. and Eisenreich, S. J. (1996b). Temperature-Dependent Sorption of Naphthalene, Phenanthrene, and Pyrene to Low Organic Carbon Aquifer Sediments. Environmental Science & Technology 30(3): 751-760.

Pignatello, J. J. and Xing, B. (1996). Mechanisms of slow sorption of organic chemicals to natural particles. Environmental Science and Technology 30(1): 1 - 8.

Pitzer, K. S. (1995). Thermodynamics. Singapore, McGraw-Hill Book Co. pages.

Prevedouros, K., Brorström-Lundén, E., J. Halsall, C., Jones, K. C., Lee, R. G. M. and Sweetman, A. J. (2004). Seasonal and long-term trends in atmospheric PAH concentrations: evidence and implications. Environmental Pollution 128(1-2): 17-27.

Qian, Y., Posch, T. and Schmidt, T. C. (2011). Sorption of polycyclic aromatic hydrocarbons (PAHs) on glass surfaces. Chemosphere 82(6): 859-865.

Qin, Z., Bragg, L., Ouyang, G., Niri, V. H. and Pawliszyn, J. (2009). Solid-phase microextraction under controlled agitation conditions for rapid on-site sampling of organic pollutants in water. Journal of Chromatography A 1216(42): 6979-6985.

Rianawati, E. and Balasubramanian, R. (2009). Optimization and validation of solid phase micro-extraction (SPME) method for analysis of polycyclic aromatic hydrocarbons in rainwater and stormwater. Physics and Chemistry of the Earth, Parts A/B/C 34(13-16): 857-865.

Rugen, P. J., Stern, C. D. and Lamm, S. H. (1989). Comparative carcinogenicity of the PAHs as a basis for acceptable exposure levels (AELs) in drinking water. Regulatory Toxicology and Pharmacology 9(3): 273-283.

Sabbah, I., Rebhun, M. and Gerstl, Z. (2004). An independent prediction of the effect of dissolved organic matter on the transport of polycyclic aromatic hydrocarbons. Journal of Contaminant Hydrology 75(1-2): 55-70.

Schmid, G. H. (1995). Organic Chemistry McGrow Hill. pages.

Schwarz, K., Gocht, T. and Grathwohl, P. (2011). Transport of polycyclic aromatic hydrocarbons in highly vulnerable karst systems. Environmental Pollution 159(1): 133-139.

Schwarzenbach, R. P., Gschwend, P. M. and Imboden, D. M. (1993). Environmental Organic Chemistry, John Wiley & Sons Inc. 1340 pages.

Scott, R. P. W. (2002). Gas Chromatographic Detectors.

Sheffield Hallam University, S. o. S. a. M. (1998a). Gas Chromatography: FID Detector. Retrieved 13/06/2006.

Sheffield Hallam University, S. o. S. a. M. (1998b). Gas Chromatography: GC system. Retrieved 12/06/06.

Sheffield Hallam University, S. o. S. a. M. (1998c). Gas Chromatography: Injectors. Retrieved 13/06/2006.

Shibasaki, Y. and Fukuda, K. (1992). Aggregation states and polymerizabilities of amphiphilic monomer molecules in aqueous systems with different water contents Colloids and Surfaces 67: 195-201

Shurmer, B. and Pawliszyn, J. (2000). Determination of Distribution Constants between a Liquid Polymeric Coating and Water by a Solid-Phase Microextraction Technique with a Flow-Through Standard Water System. Analytical Chemistry 72(15): 3660-3664.

Silverstein, R. M., Bassler, G. C. and Morrill, T. C. (1991). Spectrometric Identification of Organic Compounds. New York, John Wiley & Sons, Inc. 5th edition. 433 pages.

Sluszny, C., Bulatov, V. and Schechter, I. (1998). Classification and quantification of polycyclic aromatic hydrocarbons on quartz sand particles by direct Fourier transform imaging fluorescence. Analytica Chimica Acta 367(1-3): 1-10.

Staszczuk, P. (1995). Novel studies of phase and structural transitions in bulk and vicinal water Colloids and Surfaces A: Physicochemical and Engineering Aspects 94(2-3): 213-224

Stauffer, T. B. and Macintyre, W. G. (1986). Sorption of low-polarity organic compounds on oxide minerals and aquifer material. Environmental Toxicology and Chemistry 5(11): 949-955.

Stringfellow, W. T. and Oh, K. C. (2005). Comparison of SPME Headspace Analysis to U.S. EPA Method 5030/8260B for MTBE Monitoring. Ground Water Monitoring and Remediation Volume 25 (Issue 2): 52 - 58.

Stumm, W. and Morgan, J. J. (1996). Aquatic Chemistry: Chemical Equilibria and Rates in Natural Waters, Wiley-Interscience Series of texts and Monographs. third edition. 1022 pages.

Su, Y. H., Zhu, Y. G., Sheng, G. and Chiou, C. T. (2006). Linear Adsorption of Nonionic Organic Compounds from Water onto Hydrophilic Minerals: Silica and Alumina. Environ. Sci. Technol. 40(22): 6949-6954.

Sun, H., Tateda, M., Ike, M. and Fujita, M. (2003). Short- and long-term sorption/desorption of polycyclic aromatic hydrocarbons onto artificial solids: effects of particle and pore sizes and organic matters Water Research 37(12): 2960-2968

SUPELCO. (1996). GC Analyses of Polynuclear Aromatic Hydrocarbons. Application Note 108. Retrieved 27/06/2006.

SUPELCO. (2001). Solid Phase Microextraction Troubleshooting Guide. Bulletin 928. Retrieved 19/06/2006].

SUPELCO. (1998). Solid Phase Microextraction of Semivolatile Compounds. Application Note 6. Retrieved 27/06/2006.

Trapido, M. (1999). Polycyclic aromatic hydrocarbons in Estonian soil: contamination and profiles. Environmental Pollution 105(1): 67-74.

Tzvetkov, G., Schmidt, N., Strunskus, T., Wöll, C. and Fink, R. (2007). Molecular adsorption and growth of naphthalene films on Ag(1 0 0). Surface Science 601(9): 2089-2094.

U.S. Environmental Protection Agency (1986). Health and Environmental Effects Profile for Naphthalene. EPA/600/x-86/241. . E. C. a. A. Office, Office of Health and Environmental Assessment, Office of Research and Development.

UK Environment Agency, E. A. (2005). Polycyclic aromatic hydrocarbons (PAHs). Retrieved 05/07/2005, 2005, from http://www.environment-agency.gov.uk.

Vickerman, J. C. (1997). Surface Analysis. Chichester 462 pages.

Vu, V.-T., Lee, B.-K., Kim, J.-T., Lee, C.-H. and Kim, I.-H. (2011). Assessment of carcinogenic risk due to inhalation of polycyclic aromatic hydrocarbons in PM10 from an industrial city: A Korean case-study. Journal of Hazardous Materials 189(1-2): 349-356.

Walgraeve, C., Demeestere, K., Dewulf, J., Zimmermann, R. and Van Langenhove, H. (2010). Oxygenated polycyclic aromatic hydrocarbons in atmospheric particulate matter: Molecular characterization and occurrence. Atmospheric Environment 44(15): 1831-1846.

Walters, R. W. and Luthy, R. G. (1984). Equilibrium adsorption of polycyclic aromatic hydrocarbons from water onto activated carbon. Environmental Science & Technology 18(6): 395-403.

Wang, Y., Liu, C. S., Li, F. B., Liu, C. P. and Liang, J. B. (2009). Photodegradation of polycyclic aromatic hydrocarbon pyrene by iron oxide in solid phase. Journal of Hazardous Materials 162(2-3): 716-723.

Wang, Z., Hemmer, S. L., Friedrich, D. M. and Joly, A. G. (2001). Anthracene as the Origin of the Red-Shifted Emission from Commercial Zone-Refined Phenanthrene Sorbed on Mineral Surfaces. Journal of Physical Chemistry A 105(25): 6020-6023.

Wefer-Roehl, A., Graber, E. R., Borisover, M. D., Adar, E., Nativ, R. and Ronen, Z. (2001). Sorption of organic contaminants in a fractured chalk formation. Chemosphere 44(5): 1121-1130.

Wei, M.-C. and Jen, J.-F. (2007). Determination of polycyclic aromatic hydrocarbons in aqueous samples by microwave assisted headspace solid-phase microextraction and gas chromatography/flame ionization detection. Talanta 72(4): 1269-1274.

White, P. A. and Claxton, L. D. (2004). Mutagens in contaminated soil: a review. Mutation Research/Reviews in Mutation Research 567(2-3): 227-345.

Wilcke, W. (2007). Global patterns of polycyclic aromatic hydrocarbons (PAHs) in soil. Geoderma 141(3-4): 157-166.

Wild, S. R. and Jones, K. C. (1995). Polynuclear aromatic hydrocarbons in the United Kingdom environment: A preliminary source inventory and budget. Environmental Pollution 88(1): 91-108.

Willet, J. E. (1987). Gas Chromatography, John Wiley & Sons. pages.

World Wildlife Fund. (1997). Briefing on effects of PAH on the marine environment. Retrieved 17/05/2005, 2005, from http://www.wwf.org.uk/filelibrary/pdf/mu_32.pdf.

Xing, B. (1997). The effect of the quality of soil organic matter on sorption of naphthalene. Chemosphere 35(3): 633-642.

Yang, S. K. and Silverman, B. D. (1988). Polycyclic Aromatic Hydrocarbon Carcinogenesis:Structure-Activity Relationships. Boca Raton, Florida, CRC Press. pages.

Yong-Jin, K. and Masahiro, O. (2003). Leaching Characteristics of Polycyclic Aromatic Hydrocarbons (PAHs) from Spiked Sandy Soil. Chemosphere 51(5): 387-395.

Zhang, Z. Y., M.J.; Pawliszyn, J. (1994). Solid-Phase Microextraction. Analytical Chemistry 66(17): 844- 853.

Zhou, Y., Liu, R. and Tang, H. (2004). Sorption interaction of phenanthrene with soil and sediment of different particle sizes and in various CaCl2 solutions. Journal of Colloid and Interface Science 270(1): 37.

Zhu, D., Herbert, B. E. and Schlautman, M. A. (2003). Molecular-level investigation of monoaromatic compound sorption to suspended soil particles by deuterium nuclear magnetic resonance. Journal of Environmental Quality 32(1): 232-239.

Zhu, D., Herbert, B. E., Schlautman, M. A. and Carraway, E. R. (2004a). Characterization of cation-pi interactions in aqueous solution using deuterium nuclear magnetic resonance spectroscopy. Journal of Environmental Quality 33(1): 276-284.

Zhu, D., Herbert, B. E., Schlautman, M. A., Carraway, E. R. and Hur, J. (2004b). Cation-pi bonding: a new perspective on the sorption of polycyclic aromatic hydrocarbons to mineral surfaces. Journal of Environmental Quality 33(4): 1322-1330.

Zhu, D., Hyun, S., Pignatello, J. J. and Lee, L. S. (2004c). Evidence for - Electron Donor-Acceptor Interactions between -Donor Aromatic Compounds and -Acceptor Sites in Soil Organic Matter through pH Effects on Sorption. Environmental Science and Technology 38(16): 4361-4368.

APPENDICES

Appendix A2

A 2.1 Particle Size Distribution Analysis

Determination of the Particle Size Distribution (PSD)

SIEVES: Dry sieves (small) set from the Kinetics Lab. Earth Sciences.

Test #: SSVWR1/SSVWR2/SSVWR3
Date: 16/02/2005
Sand name: VWR
Pretreatment: drying in oven at 110°C since 09/02/05

Test	Mesh size (µm)	Sieve weight W1(g)	W2(g)	W retained sand	Retained %	Passing %
SSVWR1	250.00	121.04	147.46	26.42	52.73	47.27
	150.00	119.43	141.64	22.21	44.33	2.93
	75.00	115.63	117.08	1.45	2.89	0.04
	45.00	116.13	116.15	0.02	0.04	0.00
	0.00	89.84	89.84	0.00	0.00	0.00
		Weight of total dried sample:	Ws (g)=	50.10	100.00	
SSVWR2	250.00	121.04	141.80	20.76	41.45	58.55
	150.00	119.43	145.92	26.49	52.90	5.65
	75.00	115.63	118.38	2.75	5.49	0.16
	45.00	116.13	116.21	0.08	0.16	0.00
	0.00	89.84	89.84	0.00	0.00	0.00
		Weight of total dried sample:	Ws (g)=	50.08	100.00	
SSVWR3	250.00	121.04	140.55	19.51	38.98	61.02
	150.00	119.43	146.15	26.72	53.39	7.63
	75.00	115.63	119.31	3.68	7.35	0.28
	45.00	116.13	116.27	0.14	0.28	0.00
	0.00	89.84	89.84	0.00	0.00	0.00
		Weight of total dried sample:	Ws (g)=	50.05	100.00	

Size (mm)	Mean Weight retained (g)	Retained %	Passing %
0.5	0	0	100
0.250	22.230	44.392	55.608
0.150	25.140	50.203	5.405
0.075	2.627	5.245	0.160
0.045	0.080	0.160	0.000
0.000	0.000	0.000	0.000
	50.077		

Size (mm)	ean Weight retained	Retained %	Passing %
0.5	0	0	100
0.25	22.23	44.39193237	55.60806763
0.15	25.14	50.20302203	5.405045597
0.075	2.626666667	5.245290554	0.159755042
0.045	0.08	0.159755042	0
0	0	0	0

VWR sand	Retained %		
Mesh size (µm	Test 1	Test 2	Test 3
75	2.89	5.49	7.35
45	0.04	0.16	0.28

VWR

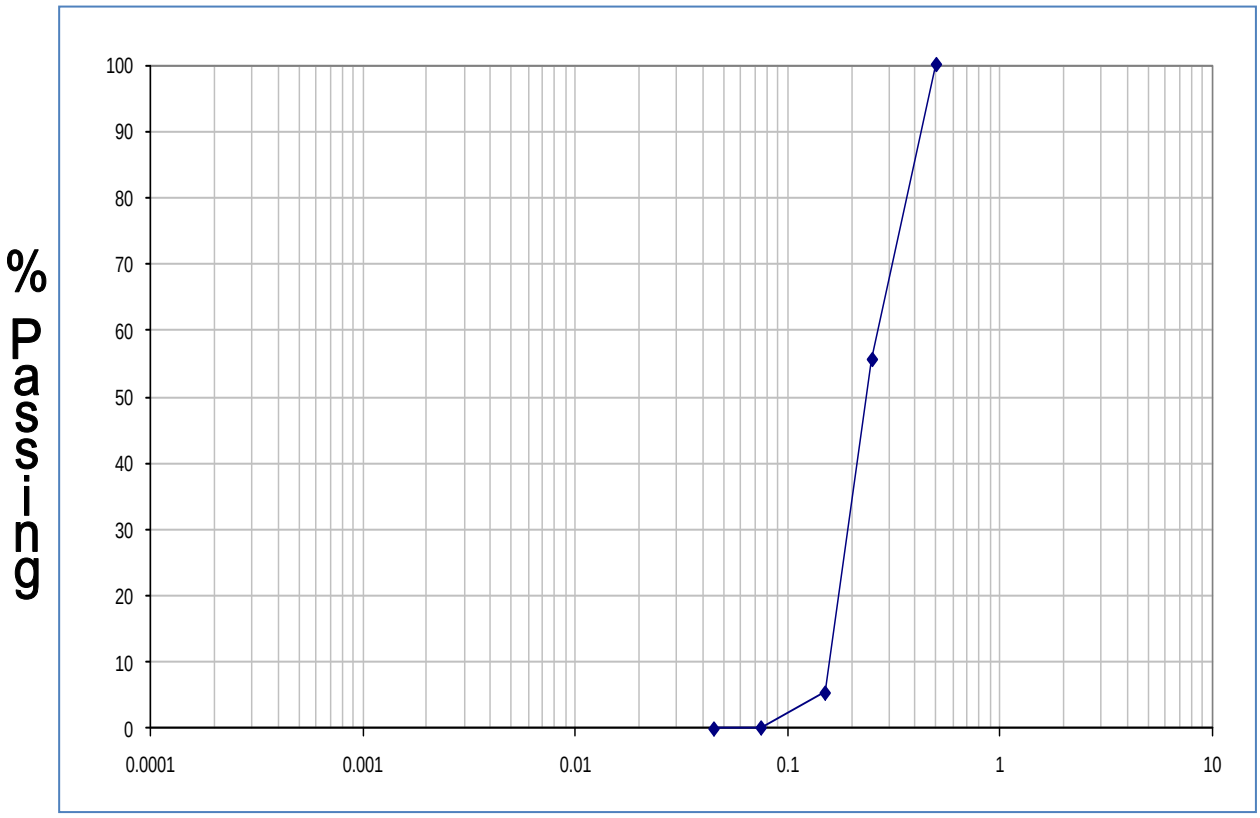
% Passing
100
90
80
70
60
50
40
30
20
10
0
0.0001
0.001
0.01
0.1
1
10
Particle size (mm)

A2.2 X-ray Diffraction Results (XRD)

sand

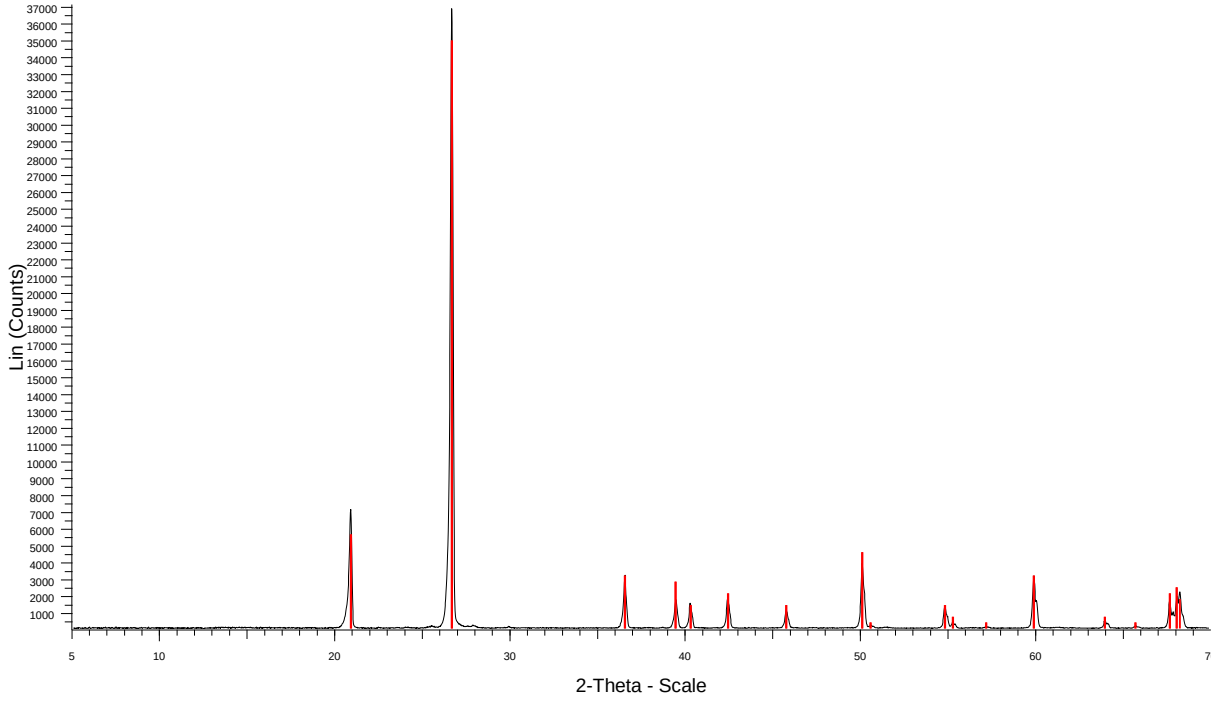

coated sand

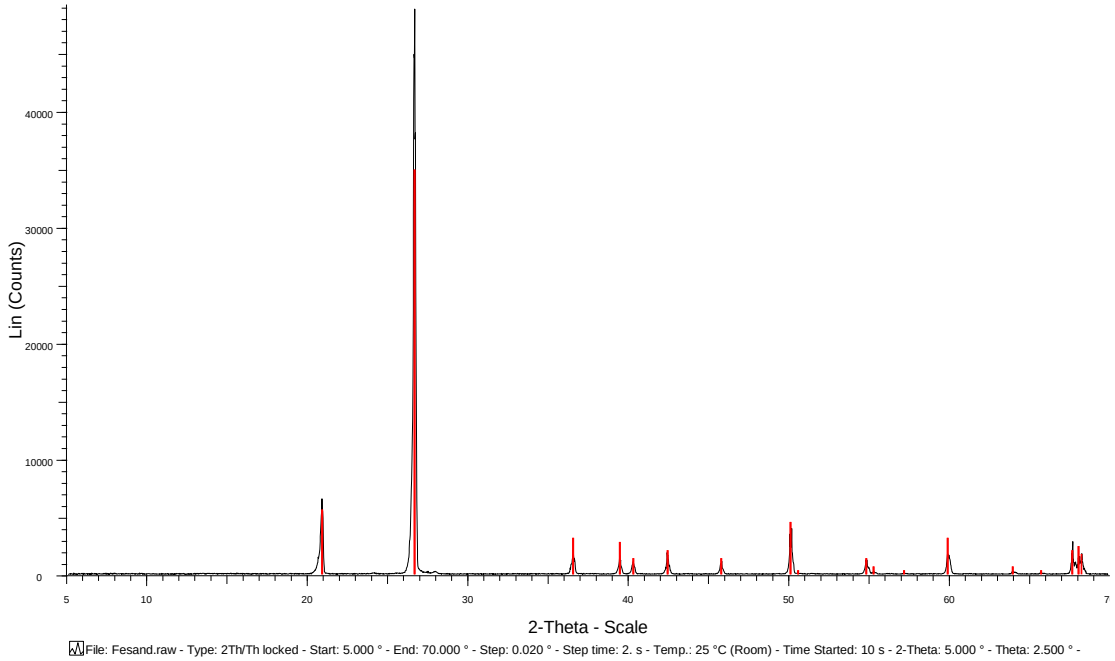

hematite

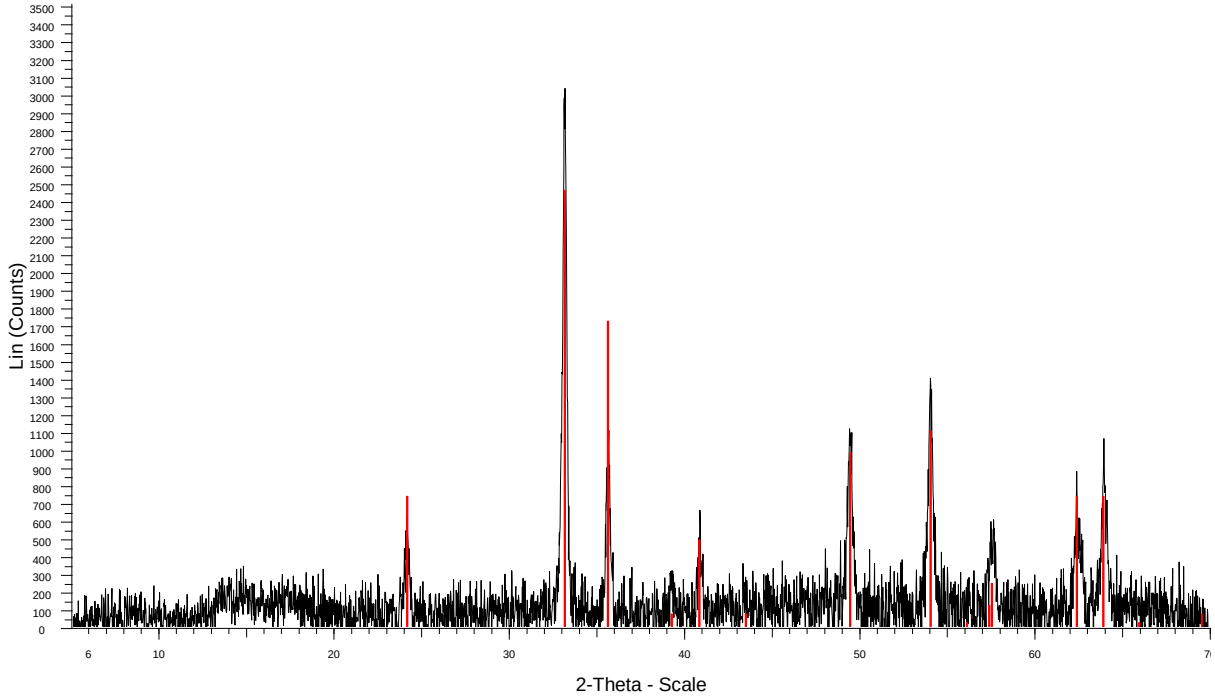

File: hematite.raw - Type: 2Th/Th locked - Start: 5.000 ° - End: 70.000 ° - Step: 0.020 ° - Step time: 4. s - Temp.: 25 °C (Room) - Time Started: 6538 s - 2-Theta: 5.000 ° - Theta: 2.500
Operations: Background 0.257,1.000 | Import
00-033-0664 (*) - Hematite, syn - Fe2O3 - Y: 35.49 % - d x by: 1. - WL: 1.5406 - Rhombo.H.axes - a 5.03560 - b 5.03560 - c 13.74890 - alpha 90.000 - beta 90.000 - gamma 120.000 -

montmorillonite

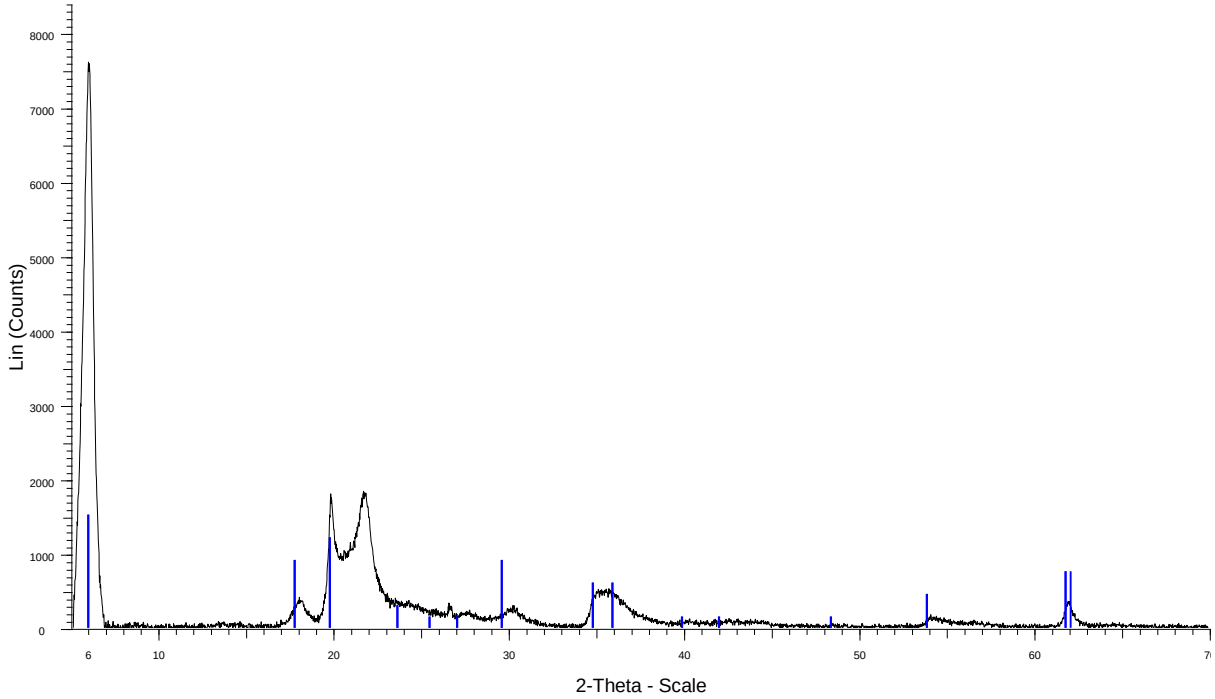

File: mont.raw - Type: 2Th/Th locked - Start: 5.000 ° - End: 70.000 ° - Step: 0.020 ° - Step time: 2. s - Temp.: 25 °C (Room) - Time Started: 10 s - 2-Theta: 5.000 ° - Theta: 2.500 ° - Chi
Operations: Background 0.046,1.000 | Import
00-013-0135 (N) - Montmorillonite-15A - Ca0.2(Al,Mg)2Si4O10(OH)2·4H2O - Y: 14.74 % - d x by: 1. - WL: 1.5406 - Hexagonal - a 5.16900 - b 5.16900 - c 15.02000 - alpha 90.000 - be

A2.3. SEM and EDS Results

A2.3.1. Hematite:

Energy Dispersive Spectrum for natural hematite mineral

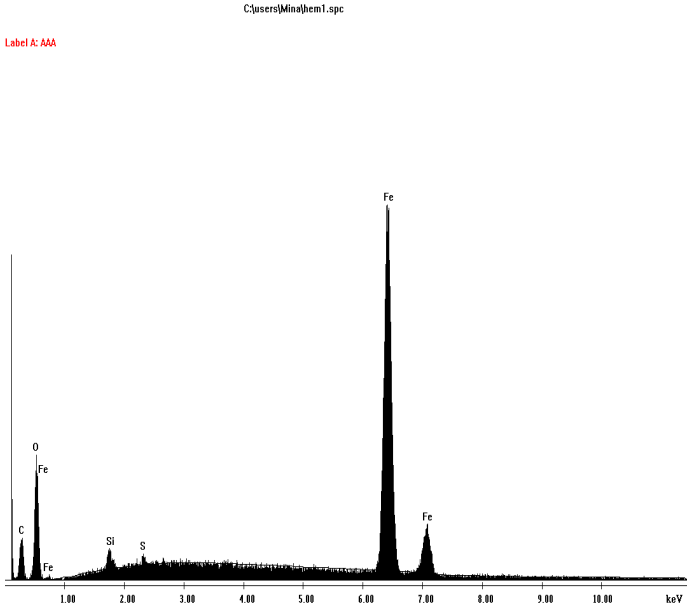

Scan Electron Microscopy (SEM) Images of Hematite

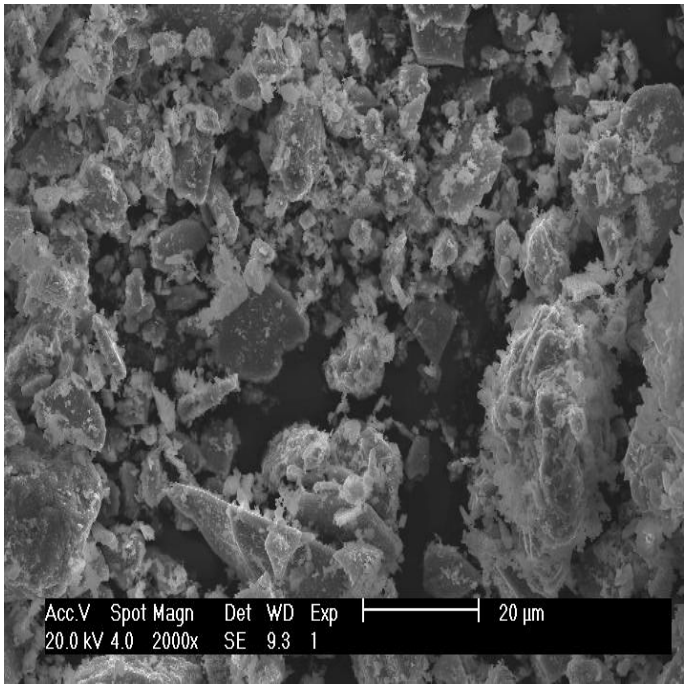

H-1

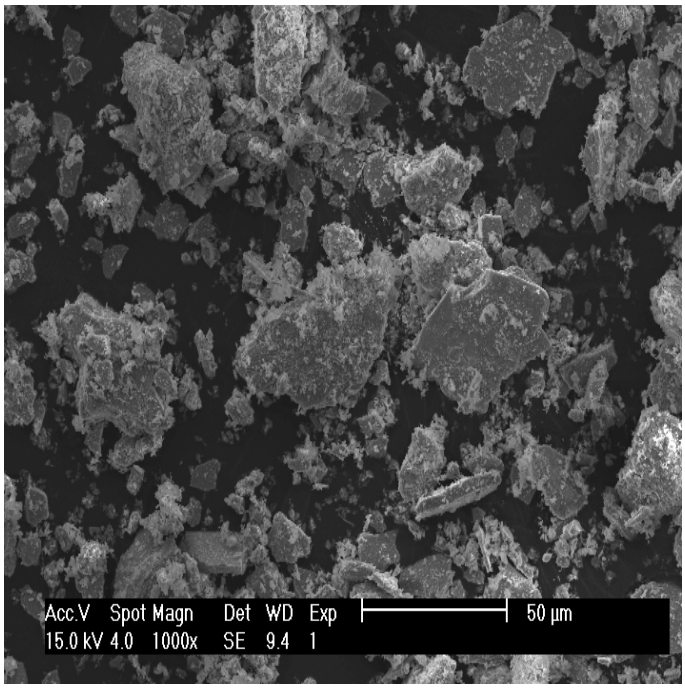
Acc.V Spot Magn Det WD Exp 50 µm
15.0 kV 4.0 1000x SE 9.4 1

H-2

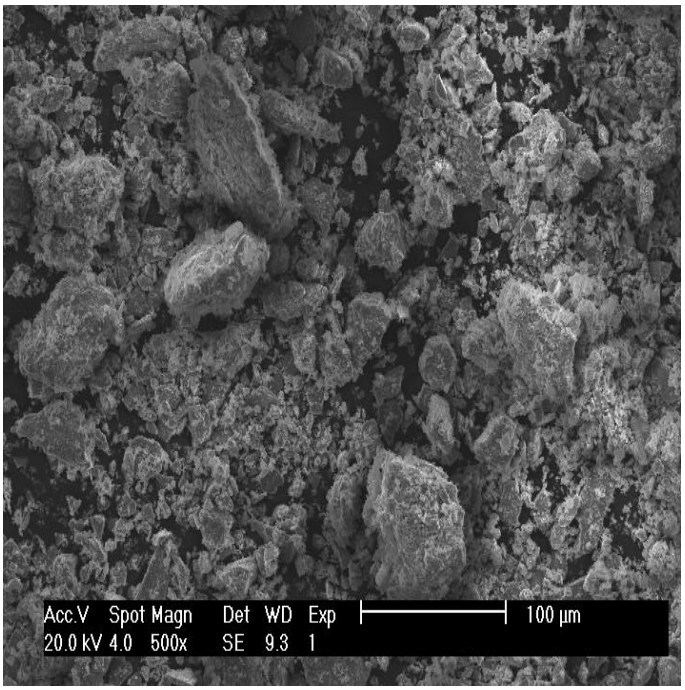
Acc.V Spot Magn Det WD Exp 100 µm
20.0 kV 4.0 500x SE 9.3 1

H-3.

Energy Dispersive Spectrum for quartz sand

A2.3.2. Quartz Sand

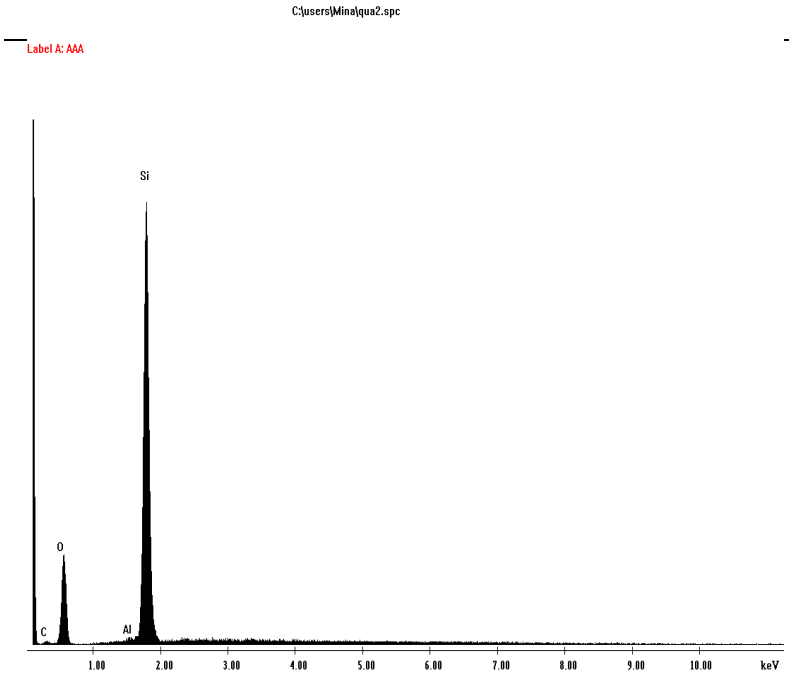

Scan Electron Microscopy (SEM) Images of Quartz Sand

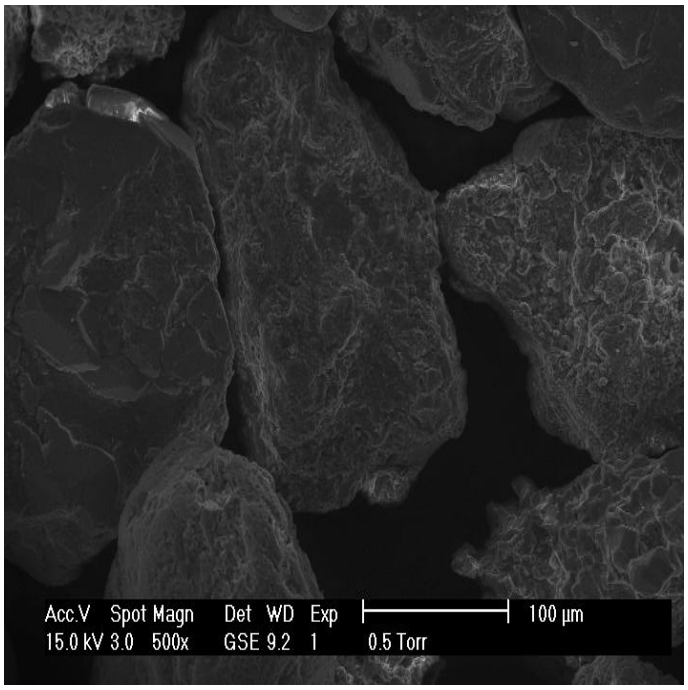

QS-1

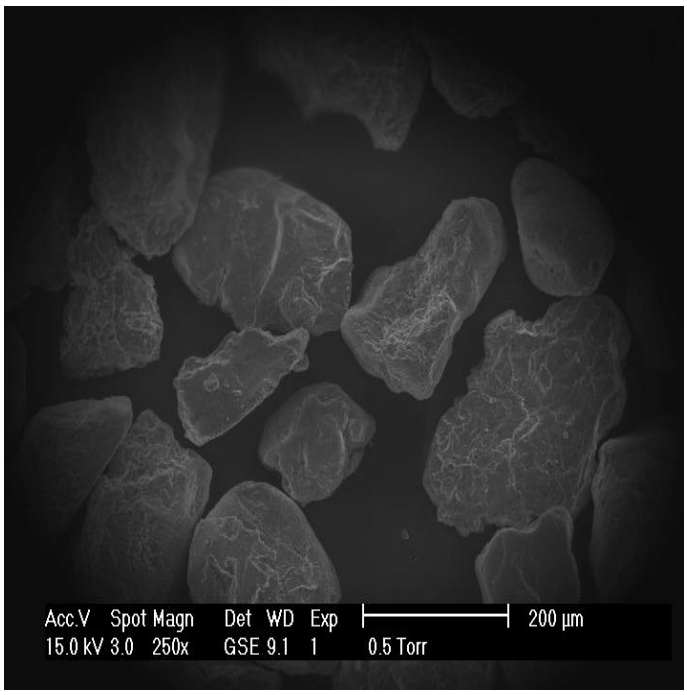
Acc.V Spot Magn Det WD Exp 200 µm
15.0 kV 3.0 250x GSE 9.1 1 0.5 Torr

QS-2

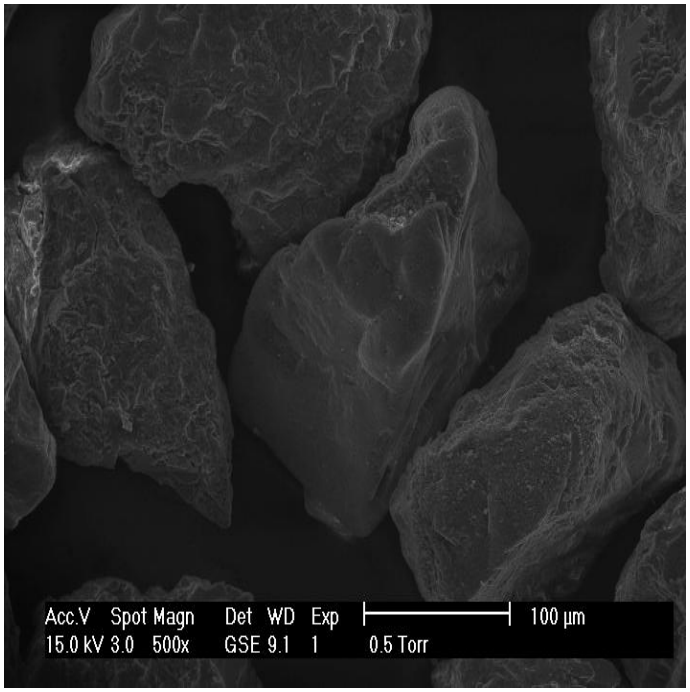
Acc.V Spot Magn Det WD Exp 100 µm
15.0 kV 3.0 500x GSE 9.1 1 0.5 Torr

QS-3

Energy Dispersive Spectrum for Stx-1 Montmorillonite

A2.3.3. Stx-1

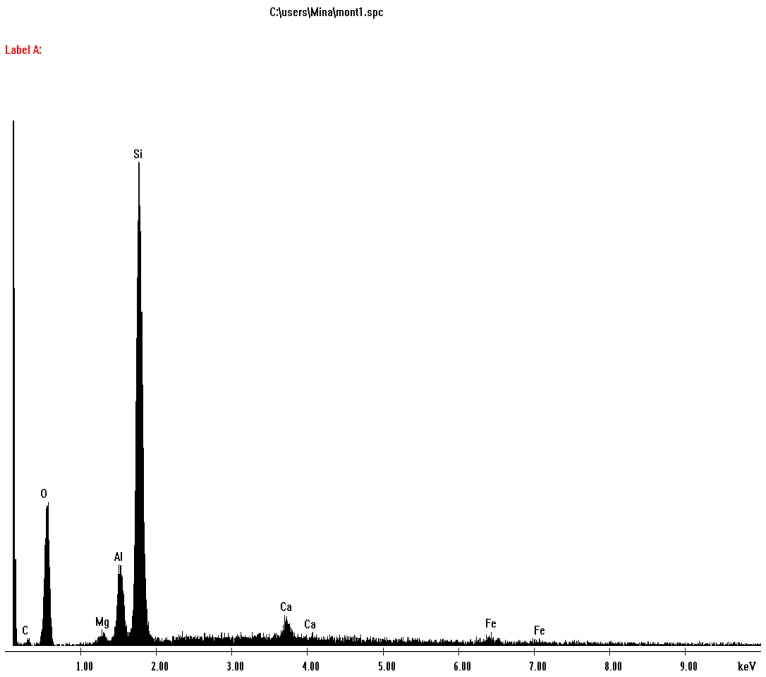

Scan Electron Microscopy (SEM) Images of Montmorillonite

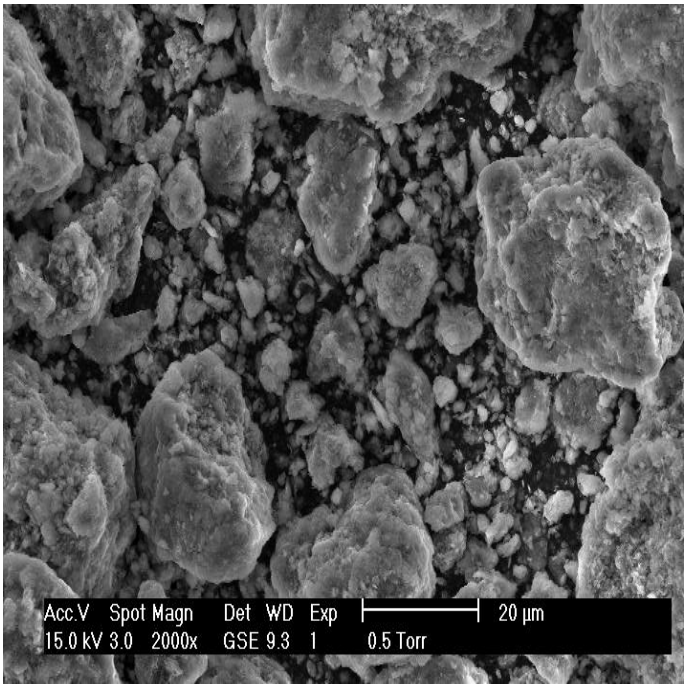

Mt-1

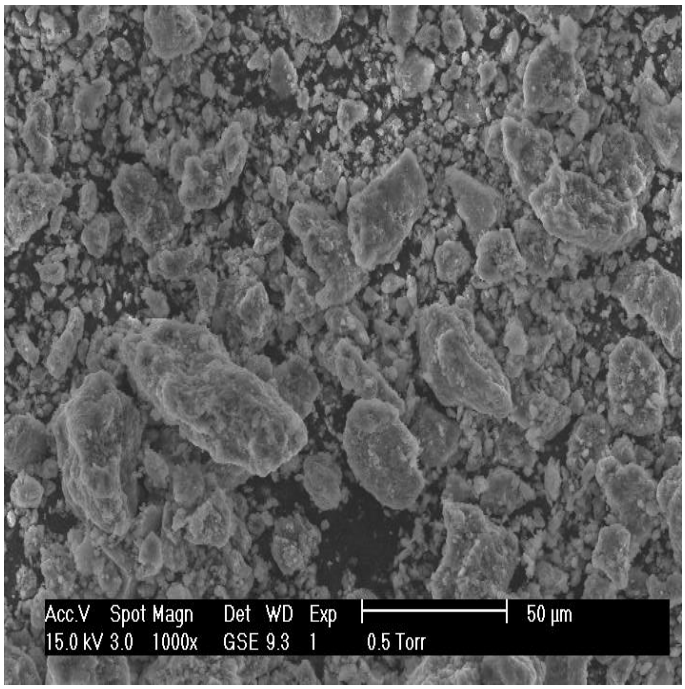
Acc.V Spot Magn Det WD Exp 50 µm
15.0 kV 3.0 1000x GSE 9.3 1 0.5 Torr

Mt-2

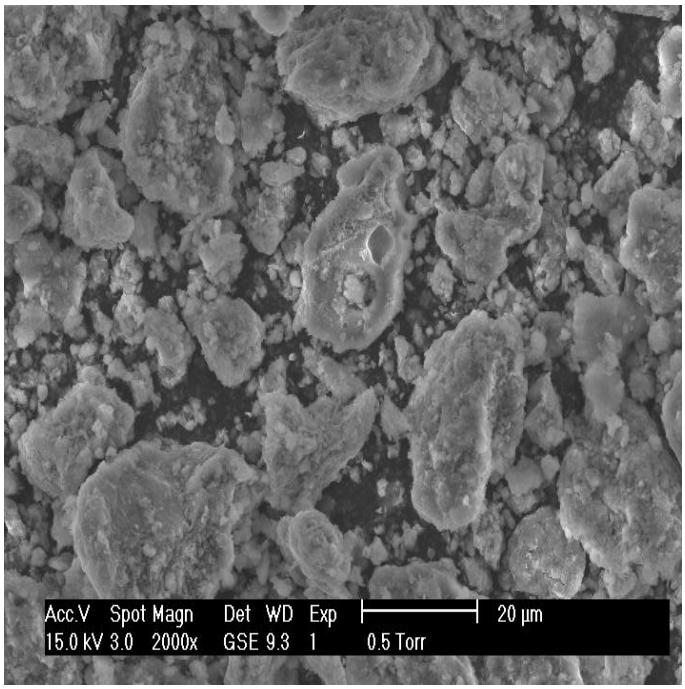
Acc.V Spot Magn Det WD Exp 20 µm
15.0 kV 3.0 2000x GSE 9.3 1 0.5 Torr

Mt-3

Scan Electron Microscopy (SEM) Images of Fe-coated Sand

A2.3.4. Fe-coated quartz sand

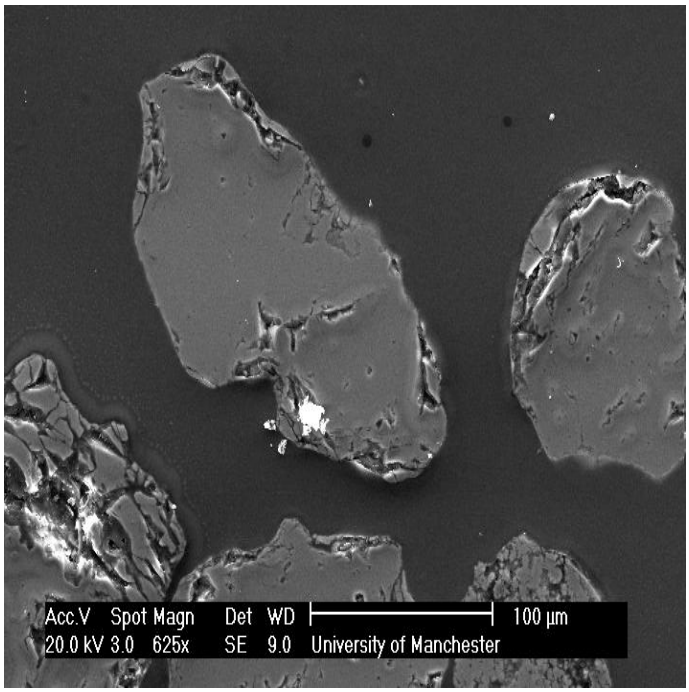

Fe-QS-1 (QS=quartz sand)

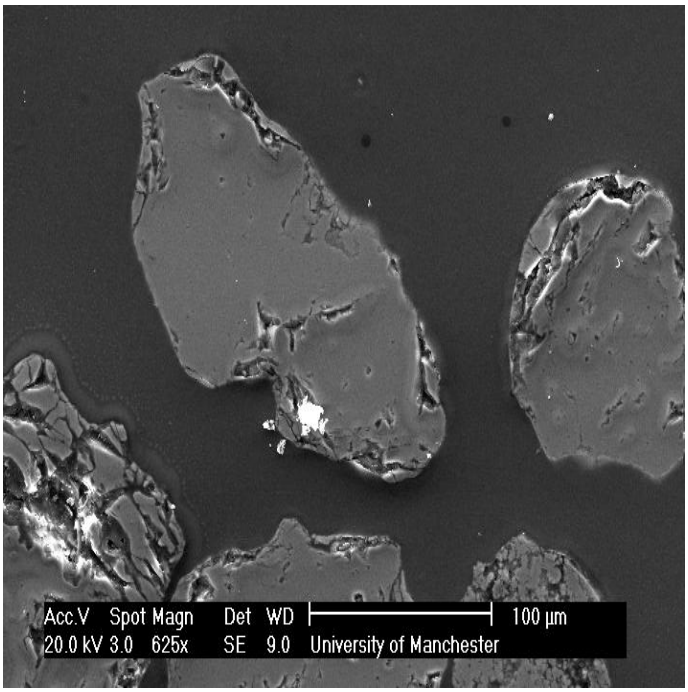

Fe-QS-2

A2.4. Elemental Analysis by X-ray Fluorescence (XRF)

A2.4.1. Quartz Sand

These results quantify the elemental impurities bound onto the sand surface. The sample acid extract (HCl) turned yellow due to the presence of iron in the sample, the second element highest in concentration. The most abundant element found was aluminium, its concentration was above the detection limit for the dilution ratio used (1:20). The results agree with the impurities found in the SEM images and EDS spectra. Silicon was not detected because the sample pre-treatment with HCl only washed the sand surface leaving the Si and O lattice intact.

Element	Conc.(µg /g sand)	SD	%RSD
Li	0.019	0.013	1.348
Be	0.001	0.001	0.994
B	0.042	0.006	0.305
Na	0.867	1.236	2.851
Mg	5.042	1.485	0.589
Al	>D.L.	N/A	N/A
Ca	1.295	0.077	0.118
Sc	0.027	0.015	1.137
Ti	0.119	0.367	6.170
V	0.043	0.171	7.918
Cr	0.173	0.012	0.142
Mn	0.323	0.106	0.657
Fe	13.138	0.233	0.035
Co	0.016	0.010	1.229
Ni	0.112	0.072	1.293
Cu	0.012	0.126	21.560
Zn	0.299	0.248	1.654
Ga	0.091	0.010	0.227
Ge	0.002	0.000	0.217
As	0.210	0.032	0.309
Se	0.059	0.414	13.970
Rb	0.284	0.022	0.158
Sr	4.050	0.882	0.436
Y	0.062	0.003	0.102
Zr	0.090	0.004	0.097
Nb	<D.L.	N/A	N/A
Mo	0.007	0.013	3.987
Ru	0.000	0.001	29.850
Rh	0.000	0.000	0.500
Pd	0.003	0.001	0.941
Ag	<D.L.	N/A	N/A
Cd	0.000	0.021	180.900

Element	Conc.(µg /g sand)	SD	%RSD
Sn	0.004	0.010	5.399
Sb	0.003	0.001	0.742
Te	0.000	0.014	86.330
Cs	0.039	0.005	0.262
Ba	4.330	0.742	0.343
La	1.258	0.164	0.260
Ce	1.704	0.244	0.286
Pr	0.245	0.098	0.804
Nd	0.881	0.101	0.228
Sm	0.123	0.020	0.329
Eu	0.021	0.024	2.220
Gd	0.068	0.026	0.772
Tb	0.006	0.001	0.464
Dy	0.019	0.003	0.269
Ho	0.003	0.001	0.481
Er	0.008	0.007	1.825
Tm	0.002	0.002	2.957
Yb	0.005	0.007	2.609
Lu	0.002	0.001	0.674
Hf	0.005	0.008	0.000
Ta	<D.L.	N/A	N/A
W	0.006	0.008	2.671
Re	0.000	0.000	0.826
Os	<D.L.	N/A	N/A
Pt	0.000	0.003	143.200
Au	<D.L.	N/A	N/A
Hg	<D.L.	N/A	N/A
Tl	0.003	0.005	3.066
Pb	0.072	0.112	3.095
Bi	0.001	0.004	13.140
Th	0.063	0.012	0.011
U	0.019	0.011	1.178

Elemental composition of VWR sand surface

Appendix A3.

A.3.1. Headspace-SPME Calibrations

Calibration

Type: External
Date: 19.06.08
Analyte: Naphthalene
Stock: 5000 mg/L, SUPELCO

SPME
Extraction: HS- Pre-equilibrium
Temp.: 0.3°C
Time:
Depth:

Desorption:
3 cm inside injection port @250°C
5 min desorption
GC-MS: FISONS 8000
Column: DB-17 MS, 30 m, 0.25 mm, 0.25µm.
SIM mode at m/z=128
GC Programme:
Initial oven temp. 100 °C
T2= 160°C (hold for 3 min)

STD Preparation

C1(ppm)	V1 (µL)	C2 (ppm)	V2 (mL)
5000	1	1	5
5000	2	2	5
5000	3	3	5
5000	4	4	5
5000	5	5	5

C2 (ppm)	t_R (min)	Area	Height
0	-	0	0
1	4.75	12622	3378
2	4.76	28124	8214
3	4.78	39891	11702
4	4.79	53485	16065
5	4.74	79013	23235
6	4.74	82281	24030

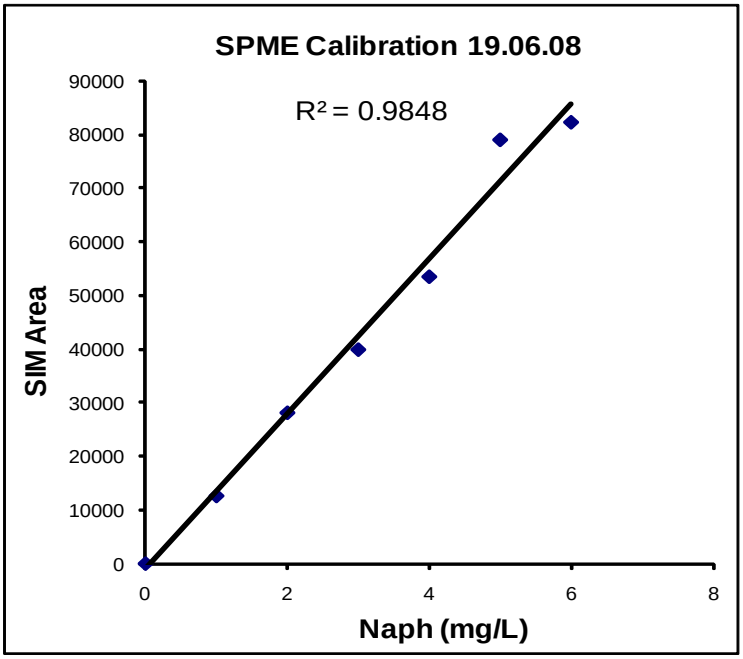

CALIBRATION IN THE HEADSPACE

DATE	SAMPLE	Vs (µL)	Vstock (µl)	Cstock (ppm)	Cs (ppm)	Syringe
23.7.9	B1	5027	1	5000	0.9946	1 µL
23.7.9	C1	5011	1.5	5000	1.4967	5 µL
23.7.9	D1	5063.2	0.78	5000	0.7703	1 µL
23.7.9	E1	5035.5	0.5	5000	0.4965	1 µL
23.7.9	F1	5019.1	7.5	200	0.29885	10 µL
23.7.9	G1	5011.9	5	200	0.1995	5 µL
23.7.9	H1	5028.1	2.5	200	0.099	5 µL
23.7.9	I1	5044.7	1.3	200	0.0515	5 µL
23.7.9	J1	5048.4	0	N/A	0	N/A

DATE	SAMPLE	Cs (ppm)	A_{FID} (pA*s)
23.7.9	C1	1.4967	2125.37207
23.7.9	B1	0.9946	1371.0606
23.7.9	D1	0.7703	1050.44531
23.7.9	E1	0.4965	711.96332
23.7.9	F1	0.29885	343.10104
23.7.9	G1	0.1995	221.30109
23.7.9	H1	0.099	111.15895
23.7.9	I1	0.0515	51.94458
23.7.9	J1	0	0

SPME EXTRACTION	
DATE	23.07.2009
MATRIX	NaNO3 0.001 M
METHOD	Headspace
FIBRE DEPTH	0.6 cm
STIRRING	3mm above plate
TEMPERATURE	ambient
TIME	5 minutes
DESORPTION (PTV INLET)	
DEPTH	3 cm
TEMPERATURE	280 °C
TIME	5 minutes
FIBRE MATERIAL	PDMS
FIBRE THICKNESS	30 µm

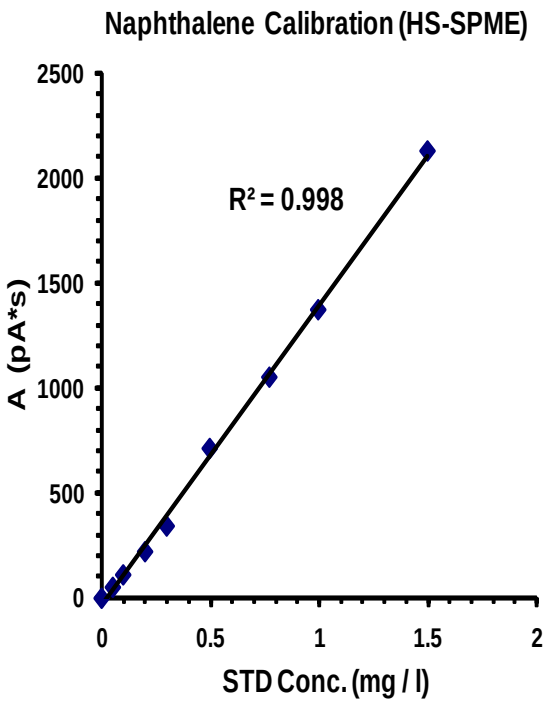

A3.2: Raw Data used in the Calculation of Precision and Reproducibility :

Same-day measurements for precision RSD %:

t_R=4.2 min 0.001M NaNO3

n	Co (mg/l)	A_{FID} (pA*s)
1	0.5	490.60
2	0.5	473.80
3	0.5	432.70
4	0.5	494.26
5	0.5	493.00
6	0.5	422.00
7	0.5	447.20
8	0.5	484.90
9	0.5	476.02
10	0.5	523.67
	Mean :	473.81
	σ :	31.21
	%R.S.D.:	6.59

SPME time=3 min
SPME depth in HS=0.6 cm
SPME temp. =40 °C
Sample volume=5 ml
Agitation technique= ultrasonics for 3 min
Fibre= PDMS 30 µm
Fibre used : U
HS= 51 % of vial total volume
pH=5.5

n	Co (mg/l)	A_{FID} (pA*s)	Mean :	σ :	%R.S.D.:
1	0.0002	1.90E-01	1.90E-01	0	0.0000
2		1.90E-01			
1	0.0003	3.30E-01	3.35E-01	0.007071	0.7071
2		3.40E-01			
1	0.0004	5.80E-01	5.25E-01	0.077782	5.8000
2		4.70E-01			

Different-day measurements for reproducibility RSD %:

n	Co (mg/l)	A_{FID} (pA*s)	Daily triplicates:	
1	0.5	467.00	**Mean :**	492.64
2	0.5	491.43	**σ :**	26.27
3	0.5	519.48	**%R.S.D.:**	5.33
1	0.5	493.95	**Mean :**	440.16
2	0.5	418.86	**σ :**	46.92
3	0.5	407.66	**%R.S.D.:**	10.66
1	0.5	561.910	**Mean :**	550.554
2	0.5	539.198	**σ :**	16.06002
3	0.5	outlier	**%R.S.D.:**	2.917066
	Mean	487.44		
all days, n=8	**σ :**	54.5059008		
	%R.S.D.:	11.1821708		

EXPERIMENTAL CONDITIONS

REACTION TIME	24 HOURS
SHAKER SETTINGS	140 orbital shaker
BACKGROUND MATRIX	*(0.001 - 0.1) M NaNO3*
CONTAMINANT	NAPHTHALENE
MATERIAL	*N/A*
INITIAL CONCENTRATION	*0.5 ppm*
TEMPERATURE	40 degrees
pH	N/A
SORBENT MASS	*1*
BET SSA (m^2/g)	N/A
LIQUID PHASE VOLUME	40 mL
SORBENT/LIQUID RATIO	N/A
VIALS	40mL, AMBER;CLEANED & SILANISED
SPME MODE	HEADSPACE
SAMPLING DEPTH	0.6 cm FOR 3 min
DESORPTION DEPTH	3 cm
AGITATION	Ultrasound

Relative Standard Deviation % of Different Blanks (Controls) at 3 Ionic Strength Values (as $NaNO_3$) calculated the same day and on different days

I.S.	Date	A_{FID} (pA*s)	FIBRE	MINERAL	MEAN A (pA*s)	
0.001	27.05.09	468.14	K	B	495.81	*DAY MEAN*
0.001	27.05.09	521.37	K	B	26.68	*DAY-σ*
0.001	27.05.09	497.91	K	B	5.38	*DAY - RSD%*
0.001	02.06.09	539.66	K	H	532.34	*DAY MEAN*
0.001	02.06.09	545.05	N	H	17.55	*DAY-σ*
0.001	02.06.09	512.32	N	H	***3.30***	*DAY - RSD%*
0.01	03.06.09	533.16	N	B	533.16	*DAY MEAN*
0.01	03.06.09	579.14	N	B	30.47	*DAY-σ*
0.01	03.06.09	590.78	N	B	5.72	*DAY - RSD%*
0.10	04.06.09	563.62	N	B	590.13	*DAY MEAN*
0.10	04.06.09	629.28	N	B	34.60	*DAY-σ*
0.10	04.06.09	577.50	N	B	5.86	*DAY - RSD%*

I.S.	MEAN	STDDEV	RSD%
0.001 M	265.05	**28.43**	10.73
0.01 M	533.16	**30.47**	5.72
0.1 M	590.13	**34.60**	5.86

APPENDIX 4: SORPTION EXPERIMENTS RAW DATA

A4.1. QUARTZ SAND, pH = 4.0

DATE	SAMPLE	Mineral	M_S (g)	$C_{E\pm}$ (M)	$V_{E\pm}$ (µL)	pH_1	T °C	V_{Spike} (µL)	C_o (mg/L)	t_{START}	t_{END}	pH_2	T °C	V_{SPME} (g)	t_R (min)	A_{GC-FID} (pA*s)	Average
17.3.10	RBQSIb	Quartz Sand Run Blank	10.0011	0.001	38000	4	19	0	0.00	14:33	14:33	5.54	19.6	5.0	-	-	
17.3.10	QSIb-1	Quartz Sand Triplicate 1	9.9994	0.001	38000	4	19	3.8	0.50	14:41	14:43	5.39	19.6	5.0	4.849	567.23535	567.871215
17.3.10	QSIb-2	Quartz Sand Triplicate 2	10.0000	0.001	38000	4	19	3.8	0.50	14:48	14:44	5.17	19.6	5.0	4.823	45.21670	
17.3.10	QSIb-3	Quartz Sand Triplicate 3	10.0006	0.001	38000	4	19	3.8	0.50	14:54	14:53	5.26	19.6	5.0	4.843	568.50708	
17.3.10	BlkIb-1	BLANK	0.0000	0.001	40000	4	19	4	0.50	15:04	14:25	4.86	19.6	5.0	4.846	572.84381	610.89860
17.3.10	BlkIb-2	BLANK	0.0000	0.001	40000	4	19	4	0.50	15:28	14:29	4.36	19.6	5.0	4.840	601.64551	
17.3.10	BlkIb-3	BLANK	0.0000	0.001	40000	4	19	4	0.50	15:21	14:30	4.74	19.6	5.0	4.843	658.20648	

DATE	SAMPLE	Mineral	M_S (g)	$C_{E\pm}$ (M)	$V_{E\pm}$ (µL)	pH_1	T °C	V_{Spike} (µL)	C_o (mg/L)	t_{START}	t_{END}	pH_2	T °C	V_{SPME} (g)	t_R (min)	A_{GC-FID} (pA*s)	Average
29.04.10	LBIIb-1	BLANK	0.0000	0.01	40000	4	20.4	4	0.5000	13:34	13:54	3.83	18.8	5.012	4.837	530.179	518.427
29.04.10	LBIIb-2	BLANK	0.0000	0.01	40008	4	20.4	4	0.4999	13:45	14:01			5.013	4.828	519.339	
29.04.10	LBIIb-3	BLANK	0.0000	0.01	40001	4	20.4	4	0.5000	14:04	14:12			5.013	4.848	505.764	
29.04.10	RBQSIIb	Quartz Sand Run Blank	n/a	n/a	n/a	n/a	n/a	n/a	n/a	n/a	n/a	n/a	n/a	n/a	n/a	n/a	n/a
29.04.10	QSIIb-1	Quartz Sand Triplicate 1	10.0080	0.01	38002	4	20.4	3.8	0.5000	13:47	14:03	4.64	18.8	5.006	4.84	536.29852	543.873
29.04.10	QSIIb-2	Quartz Sand Triplicate 2	10.0000	0.01	38004	4	20.4	3.8	0.4999	13:50	14:05	4.6	18.8	5.002	4.834	587.7019	
29.04.10	QSIIb-3	Quartz Sand Triplicate 3	10.0050	0.01	38006	4	20.4	3.8	0.4999	13:52	14:07	4.63	18.8	5.003	4.834	507.61801	

DATE	SAMPLE	Mineral	M_S (g)	$C_{E\pm}$ (M)	$V_{E\pm}$ (µL)	pH_1	T °C	V_{Spike} (µL)	C_o (mg/L)	t_{START}	t_{END}	pH_2	T °C	V_{SPME} (g)	t_R (min)	A_{GC-FID} (pA*s)	Average
24.3.10	LBIIIb-1	BLANK	0.0000	0.1	40000	4.03	20	4	0.5	12:24	12:15	4.06	21.3	5	4.855	522.8071	514.9245
24.3.10	LBIIIb-2	BLANK	0.0000	0.1	40000	4.03	20	4	0.5	12:27	12:16	4.05	21.3	5	4.849	551.3267	
24.3.10	LBIIIb-3	BLANK	0.0000	0.1	40000	4.03	20	4	0.5	12:30	12:17	4.09	21.3	5	4.845	470.6397	
24.3.10	STDIIIb-1A	Std 0.125 A	0.0000	0.1	40000	4.03	20	1	0.125	11:53	11:50	4.05	21.3	5	4.848	103.4849	
24.3.10	STDIIIb-2A	Std 0.25 A	0.0000	0.1	40000	4.03	20	2	0.25	12:17	11:55	4.04	21.3	5	4.841	274.2474	
24.3.10	STDIIIb-3A	Std 0.375 A	0.0000	0.1	40000	4.03	20	3	0.375	12:19	11:56	4.04	21.3	5	4.847	390.3479	
24.3.10	RBQSIIIb	Quartz Sand Run Blank	10.0000	0.1	38000	4.03	20	0	0	12:35	12:37	4.36	21.3	5	-	-	422.158263
24.3.10	QSIIIb-1	Quartz Sand Triplicate 1	10.0000	0.1	38000	4.03	20	3.8	0.5	12:45	12:50	4.33	21.3	5	4.846	411.3658	
24.3.10	QSIIIb-2	Quartz Sand Triplicate 2	10.0000	0.1	38000	4.03	20	3.8	0.5	12:42	12:41	4.4	21.3	5	4.835	448.9521	
24.3.10	QSIIIb-3	Quartz Sand Triplicate 3	10.0000	0.1	38000	4.03	20	3.8	0.5	12:50	12:52	4.32	21.3	5	4.845	406.1568	

A4.2. QUARTZ SAND, pH=5.5

DATE	SAMPLE	Mineral	M_S (g)	$C_{E\pm}$ (M)	$V_{E\pm}$ (µL)	pH_1	T °C	V_{Spike} (µL)	C_o (mg/L)	t_{START}	t_{END}	pH_2	T °C	V_{SPME} (mL)	t_R (min)	A_{GC-MS}	Corrected A	Average
16.03.09	25 PURPLE ®	LOSSES BLANK 1	0.0000	0.001	39300	N/A	N/A	3.93	0.50	12:09	12:09	N/A	N/A	10.024		5532247.00	6146941.111	6146941.11
16.03.09	6 PURPLE*	Quartz Sand Run Blank	10.017	0.001	35000	N/A	N/A	0	0	13:53	13:53	N/A	N/A	10		2651		N/A
16.03.09	7 PURPLE*	Quartz Sand Triplicate 1	10.013	0.001	36000	N/A	N/A	4	0.56	14:46	14:46	N/A	N/A	10		5014892		5067729
16.03.09	8 PURPLE*	Quartz Sand Triplicate 2	10.061	0.001	36000	N/A	N/A	4	0.56	14:52	14:52	N/A	N/A	10		5120566		

DATE	SAMPLE	Mineral	M_S (g)	$C_{E\pm}$ (M)	$V_{E\pm}$ (µL)	pH_1	T °C	V_{Spike} (µL)	C_o (mg/L)	t_{START}	t_{END}	pH_2	T °C	V_{SPME} (mL)	t_R (min)	A_{GC-MS}	Corrected A	Average
18.03.09	12 PURPLE	LOSSES BLANK 1	0.0000	0.01	39500	N/A	N/A	4	0.51	14:03	14:03	N/A	N/A	10.011		6265037	6874137.819	6874137.82
18.03.09	13 PURPLE	Quartz Sand Run Blank	10.031	0.01	36000	N/A	N/A	0	0	14:09	14:20	N/A	N/A	10.029		3293		N/A
18.03.09	14 PURPLE	Quartz Sand Triplicate 1	10.037	0.01	36000	N/A	N/A	4	0.56	14:04	14:04	N/A	N/A	10.015		5676602		5375216.5
18.03.09	15 PURPLE	Quartz Sand Triplicate 2	10.056	0.01	36000	N/A	N/A	4	0.56	14:10	14:15	N/A	N/A	10.036		5073831		

DATE	SAMPLE	Mineral	M_S (g)	$C_{E\pm}$ (M)	$V_{E\pm}$ (µL)	pH_1	T °C	V_{Spike} (µL)	C_o (mg/L)	t_{START}	t_{END}	pH_2	T °C	V_{SPME} (mL)	t_R (min)	A_{GC-MS}	Corrected A	Average
19.03.09	16 PURPLE	LOSSES BLANK 1	0.0000	0.1	39500	N/A	N/A	4	0.51	13:02	13:02	N/A	N/A	10.029		6475274	7104814.528	7477317.59
19.03.09	17 PURPLE	Quartz Sand Run Blank	10.005	0.1	35900	N/A	N/A	0	0	13:05	13:05	N/A	N/A	10.03		3245		N/A
19.03.09	18 PURPLE	Quartz Sand Triplicate 1	10.057	0.1	35900	N/A	N/A	4	0.56	13:43	13:43	N/A	N/A	10.003		3788043		4839711.5
19.03.09	19 PURPLE	Quartz Sand Triplicate 2	10.014	0.1	35900	N/A	N/A	4	0.56	13:46	13:46	N/A	N/A	10.028		5891380		

A4.3. HEMATITE, pH=4.0

DATE	SAMPLE	Mineral	M_S (g)	$C_{E\pm}$ (M)	$V_{E\pm}$ (µL)	pH_1	T °C	V_{Spike} (µL)	C_o (mg/L)	t_{START}	t_{END}	pH_2	T °C	V_{SPME} (g)	t_R (min)	$A_{GC\text{-}FID}$ (pA*s)	Average
17.3.10	Run Blk Ib	Hematite (Florence Mine)	1.0007	0.001	40000	4	19	0	0.00	14:00	14:23	4.95	19.6	5.0	4.840	4.31071	
17.3.10	HmIb-1	Hematite (Florence Mine)	1.0009	0.001	40000	4	19	4	0.50	14:13	14:15	5.3	19.6	5.0	4.846	575.49158	608.70333
17.3.10	HmIb-2	Hematite (Florence Mine)	1.0001	0.001	40000	4	19	4	0.50	14:17	14:18	5.28	19.6	5.0	4.849	656.97314	
17.3.10	HmIb-3	Hematite (Florence Mine)	1.0006	0.001	40000	4	19	4	0.50	14:22	14:20	5.29	19.6	5.0	4.846	593.64526	
17.3.10	BlkIb-1	BLANK	0.0000	0.001	40000	4	19	4	0.50	15:04	14:25	4.86	19.6	5.0	4.846	572.84381	610.89860
17.3.10	BlkIb-2	BLANK	0.0000	0.001	40000	4	19	4	0.50	15:28	14:29	4.36	19.6	5.0	4.840	601.64551	
17.3.10	BlkIb-3	BLANK	0.0000	0.001	40000	4	19	4	0.50	15:21	14:30	4.74	19.6	5.0	4.843	658.20648	
17.3.10	STDI b 1A	Std 0.125 A	0.0000	0.001	40000	4	19	1	0.125	15:25	14:35	4.17	19.6	5.0	4.847	142.96284	139.98129
17.3.10	STDI b 1B	Std 0.125 B	0.0000	0.001	40000	4	19	1	0.125	15:26	14:36	4.16	19.6	5.0	4.848	136.99974	
17.3.10	STDI b 2 A	Std 0.25 A	0.0000	0.001	40000	4	19	2	0.250	15:27	14:37	4.24	19.6	5.0	4.837	300.24542	297.85758
17.3.10	STDI b 2B	Std 0.25 B	0.0000	0.001	40000	4	19	2	0.250	15:28	14:38	4.28	19.6	5.0	4.841	295.46973	
17.3.10	STDI b 3A	Std 0.375 A	0.0000	0.001	40000	4	19	3	0.375	15:30	14:40	4.22	19.6	5.0	4.847	460.75717	455.86336
17.3.10	STDI b 3B	Std 0.375 B	0.0000	0.001	40000	4	19	3	0.375	15:31	14:41	4.37	19.6	5.0	4.847	450.96954	

DATE	SAMPLE	Mineral	M_S (g)	$C_{E\pm}$ (M)	$V_{E\pm}$ (µL)	pH_1	T °C	V_{Spike} (µL)	C_o (mg/L)	t_{START}	t_{END}	pH_2	T °C	V_{SPME} (g)	t_R (min)	$A_{GC\text{-}FID}$ (pA*s)	Average
	Run Blk IIb	Quartz Sand Run Blank	n/a	n/a	n/a	n/a	n/a	n/a	n/a	n/a	n/a	n/a	n/a	n/a	n/a	n/a	n/a
29.04.10	HmIIb-1	Quartz Sand Triplicate 1	1.000	0.01	40017	4	20.4	4	0.4998	11:45	11:57	4.61	18.8	5.004	4.843	533.260	504.372
29.04.10	HmIIb-2	Quartz Sand Triplicate 2	1.000	0.01	40002	4	20.4	4	0.5000	11:41	11:59	4.63	18.8	5.002	4.834	514.646	
29.04.10	HmIIb-3	Quartz Sand Triplicate 3	1.001	0.01	40005	4	20.4	4	0.4999	11:36	12:00	4.6	18.8	5.001	4.845	465.210	
29.04.10	LBIIb-1	BLANK	0.0000	0.01	40000	4	20.4	4	0.5000	13:34	13:54	3.83	18.8	5.012	4.837	530.179	518.427
29.04.10	LBIIb-2	BLANK	0.0000	0.01	40008	4	20.4	4	0.4999	13:45	14:01			5.013	4.828	519.339	
29.04.10	LBIIb-3	BLANK	0.0000	0.01	40001	4	20.4	4	0.5000	14:04	14:12			5.013	4.848	505.764	

DATE	SAMPLE	Mineral	M_S (g)	$C_{E\pm}$ (M)	$V_{E\pm}$ (µL)	pH_1	T °C	V_{Spike} (µL)	C_o (mg/L)	t_{START}	t_{END}	pH_2	T °C	V_{SPME} (g)	t_R (min)	$A_{GC\text{-}FID}$ (pA*s)	Average
24.3.10	Run Blk IIIb	Hematite (Florence Mine)	1.0000	0.1	40000	4.03	20	0	0	12:54	12:54	4.59	21.3	5	4.830	4.2385	491.01774
24.3.10	HmIIIb-1	Hematite (Florence Mine)	1.0000	0.1	40000	4.03	20	4	0.5	13:03	13:04	4.61	21.3	5	4.848	476.7195	
24.3.10	HmIIIb-2	Hematite (Florence Mine)	1.0002	0.1	40000	4.03	20	4	0.5	13:09	13:17	4.66	21.3	5	4.845	503.1754	
24.3.10	HmIIIb-3	Hematite (Florence Mine)	1.0000	0.1	40000	4.03	20	4	0.5	13:18	13:20	4.6	21.3	5	4.850	493.1584	514.92449
24.3.10	LBIIIb-1	BLANK	0.0000	0.1	40000	4.03	20	4	0.5	12:24	12:15	4.06	21.3	5	4.855	522.8071	
24.3.10	LBIIIb-2	BLANK	0.0000	0.1	40000	4.03	20	4	0.5	12:27	12:16	4.05	21.3	5	4.849	551.3267	
24.3.10	LBIIIb-3	BLANK	0.0000	0.1	40000	4.03	20	4	0.5	12:30	12:17	4.09	21.3	5	4.845	470.6397	
24.3.10	STDIIIb-1A	Std 0.125 A	0.0000	0.1	40000	4.03	20	1	0.125	11:53	11:50	4.05	21.3	5	4.848	103.4849	
24.3.10	STDIIIb-2A	Std 0.25 A	0.0000	0.1	40000	4.03	20	2	0.25	12:17	11:55	4.04	21.3	5	4.841	274.2474	
24.3.10	STDIIIb-3A	Std 0.375 A	0.0000	0.1	40000	4.03	20	3	0.375	12:19	11:56	4.04	21.3	5	4.847	390.3479	

A4.4. HEMATITE, pH=5.5

DATE	SAMPLE	Mineral	M_S (g)	$C_{E\pm}$ (M)	$V_{E\pm}$ (µL)	pH_1	T °C	V_{Spike} (µL)	C_o (mg/L)	t_{START}	t_{END}	pH_2	T °C	V_{SPME} (g)	t_R (min)	$A_{GC\text{-}FID}$ (pA*s)	Average
28.10.09	Run Blk Ia	Hematite (Florence Mine)	1.0000	0.001	40000	N/A	N/A	0	0.00	11:00	11:00	6.1	25	5.016			
28.10.09	HmIa-1	Hematite (Florence Mine)	1.0000	0.001	40000	N/A	N/A	4	0.50	11:30	11:31	5.41	25	5.005	4.225	435.596	418.1357733
28.10.09	HmIa-2	Hematite (Florence Mine)	1.0002	0.001	40000	N/A	N/A	4	0.50	11:38	11:38	5.48	25	5.019	4.222	391.060	
28.10.09	HmIa-3	Hematite (Florence Mine)	1.0000	0.001	40000	N/A	N/A	4	0.50	11:45	11:45	5.4	25	5.001	4.225	427.751	
28.10.09	BlkIa-1	BLANK	0.0000	0.001	40000	N/A	N/A	4	0.50	11:34	12:05	5.25	25	5.007	4.224	493.952	440.1565133
28.10.09	BlkIa-2	BLANK	0.0000	0.001	40000	N/A	N/A	4	0.50	11:42	12:07	n/a	n/a	5.01	4.223	418.856	
28.10.09	BlkIa-3	BLANK	0.0000	0.001	40000	N/A	N/A	4	0.50	11:48	12:10	n/a	n/a	5.009	4.226	407.661	
28.10.09	STD 1A	Std 0.125 A	0.0000	0.001	40000	N/A	N/A	1	0.125	15:10	15:10	n/a	n/a	5.00	4.221	88.222	99.74278667
28.10.09	STD 1B	Std 0.125 B	0.0000	0.001	40000	N/A	N/A	1	0.125	15:13	15:13	n/a	n/a	5.00	4.222	92.989	
28.10.09	STD 1C	Std 0.125 C	0.0000	0.001	40000	N/A	N/A	1	0.125	15:16	15:16	n/a	n/a	5.00	4.239	118.017	
28.10.09	STD 2 A	Std 0.25 A	0.0000	0.001	40000	N/A	N/A	2	0.250	15:19	15:19	n/a	n/a	5.00	4.221	234.698	242.08565
28.10.09	STD 2B	Std 0.25 B	0.0000	0.001	40000	N/A	N/A	2	0.250	15:22	15:22	n/a	n/a	5.00	4.223	273.009	
28.10.09	STD 2C	Std 0.25 C	0.0000	0.001	40000	N/A	N/A	2	0.250	15:24	15:24	n/a	n/a	5.00	4.222	218.551	
28.10.09	STD 3A	Std 0.375 A	0.0000	0.001	40000	N/A	N/A	3	0.375	15:27	15:27	n/a	n/a	5.00	4.234	343.058	368.5637833
28.10.09	STD 3B	Std 0.375 B	0.0000	0.001	40000	N/A	N/A	3	0.375	15:30	15:30	n/a	n/a	5.00	4.225	412.387	
28.10.09	STD 3C	Std 0.375 C	0.0000	0.001	40000	N/A	N/A	3	0.375	15:34	15:34	n/a	n/a	5.00	4.223	350.247	

DATE	SAMPLE	Mineral	M_S (g)	$C_{E\pm}$ (M)	$V_{E\pm}$ (µL)	pH_1	T °C	V_{Spike} (µL)	C_o (mg/L)	t_{START}	t_{END}	pH_2	T °C	V_{SPME} (g)	t_R (min)	$A_{GC\text{-}FID}$ (pA*s)	Average
04.02.10	Run Blk IIa	Hematite (Florence Mine)	1.0000	0.01	40000	5.44	17.3	0	0.00	11:52	11:48	5.65	23.20	5	4.807	10.02.2010	
04.02.11	HmIIa-1	Hematite (Florence Mine)	1.0000	0.01	40000	5.38	15.8	4	0.50	11:54	11:54	5.73	23.20	5	4.838	342.70251	355.7072233
04.02.12	HmIIa-2	Hematite (Florence Mine)	1.0002	0.01	40000	5.33	15.6	4	0.50	12:10	12:10	5.66	23.20	5	4.822	377.70804	
04.02.13	HmIIa-3	Hematite (Florence Mine)	1.0000	0.01	40000	5.23	15.5	4	0.50	12:16	12:16	5.78	22.80	5	4.838	346.71112	
04.02.14	BlkIIa-1	L.S. BLANK II 1	0.0000	0.01	40000	N/A	N/A	4	0.50	12:18	13:26	5.49	22.30	5	4.841	448.78363	386.1074167
04.02.15	BlkIIa-2	L.S. BLANK II 2	0.0000	0.01	40000	N/A	N/A	4	0.50	12:22	13:27	5.61	21.70	5	4.838	347.34636	
04.02.16	BlkIIa-3	L.S. BLANK II 3	0.0000	0.01	40000	N/A	N/A	4	0.50	12:24	13:29	5.43	22.00	5	4.837	**362.19226**	
04.02.17	HSTDII1A	Std 0.125 A	0.0000	0.01	40000	N/A	N/A	1	0.125	12:36	13:30	5.39	23.30	5	4.833	117.556	116.578
04.02.18	HSTDII1B	Std 0.125 B	0.0000	0.01	40000	N/A	N/A	1	0.125	12:39	13:33	5.36	23.30	5	4.834	115.600	
04.02.20	HSTDII 2 A	Std 0.25 A	0.0000	0.01	40000	N/A	N/A	2	0.250	12:40	13:34	5.46	21.80	5	4.833	201.997	209.041
04.02.21	HSTDII 2B	Std 0.25 B	0.0000	0.01	40000	N/A	N/A	2	0.250	12:42	13:35	5.5	22.10	5	4.833	216.085	
04.02.23	HSTDII 3A	Std 0.375 A	0.0000	0.01	40000	N/A	N/A	3	0.375	12:46	13:36	5.73	22.20	5	4.834	352.095	368.374
04.02.24	HSTDII 3B	Std 0.375 B	0.0000	0.01	40000	N/A	N/A	3	0.375	12:49	13:38	5.75	22.20	5	4.835	384.654	

DATE	SAMPLE	Mineral	M_S (g)	$C_{E\pm}$ (M)	$V_{E\pm}$ (µL)	pH_1	T °C	V_{Spike} (µL)	C_o (mg/L)	t_{START}	t_{END}	pH_2	T °C	V_{SPME} (g)	t_R (min)	$A_{GC\text{-}FID}$ (pA*s)	Average
09.02.10	Run Blk IIIa	Hematite (Haile)	1.0000	0.1	40000	5.67	18.8	0	0.00	15:13	15:12	6.34	19.2	5	4.803	3.02914	
09.02.11	HmIIIa-1	Hematite (Haile)	1.0000	0.1	40000	5.6	18.8	4	0.50	14:40	14:54	6.25	19.2	5	4.83	370.0873	418.1831
09.02.12	HmIIIa-2	Hematite (Haile)	1.0002	0.1	40000	5.64	18.8	4	0.50	14:44	14:56	5.95	19.2	5	4.826	450.04562	
09.02.13	HmIIIa-3	Hematite (Haile)	1.0000	0.1	40000	5.65	18.8	4	0.50	14:46	14:57	5.93	19.2	5	4.829	434.41638	
09.02.14	BlkIIIa-1	BLANK	0.0000	0.1	40000	N/A	N/A	4	0.50	14:49	14:59	5.91	19.2	5	4.831	541.34454	531.1908233
09.02.15	BlkIIIa-2	BLANK	0.0000	0.1	40000	N/A	N/A	4	0.50	14:52	15:01	5.83	19.2	5	4.83	486.1155	
09.02.16	BlkIIIa-3	BLANK	0.0000	0.1	40000	N/A	N/A	4	0.50	14:53	15:03	5.95	19.2	5	4.832	566.11243	
09.02.17	HSTDIII 1A	Std 0.125 A	0.0000	0.1	40000	N/A	N/A	1	0.125	14:55	15:05	7.49	19.2	5	4.825	102.95214	
09.02.18	HSTDIII 1B	Std 0.125 B	0.0000	0.1	40000	N/A	N/A	1	0.125	14:57	15:06	7.8	19.2	5	4.825	118.54837	
09.02.19	HSTDIII 2 A	Std 0.25 A	0.0000	0.1	40000	N/A	N/A	2	0.250	14:58	15:08	6.27	19.2	5	4.826	240.99506	
09.02.20	HSTDIII 2B	Std 0.25 B	0.0000	0.1	40000	N/A	N/A	2	0.250	15:01	15:09	6.26	19.2	5	4.825	234.61798	
09.02.21	HSTDIII 3A	Std 0.375 A	0.0000	0.1	40000	N/A	N/A	3	0.375	15:03	15:11	6	19.2	5	4.827	355.65298	
09.02.22	HSTDIII 3B	Std 0.375 B	0.0000	0.1	40000	N/A	N/A	3	0.375	15:04	15:12	5.84	19.2	5	4.825	356.71912	

A4.5. Fe-QS, pH=4.0

DATE	SAMPLE	Mineral	M_S (g)	$C_{E\pm}$ (M)	$V_{E\pm}$ (µL)	pH_1	T °C	V_{Spike} (µL)	C_o (mg/L)	t_{START}	t_{END}	pH_2	T °C	V_{SPME} (g)	t_R (min)	$A_{GC\text{-}FID}$ (pA*s)	Average
28.04.10	Run Blk FeQSIb	Fe-coated QS	N/A	N/A	N/A	N/A	N/A	N/A	N/A	N/A	N/A	N/A	N/A	N/A	N/A	N/A	N/A
28.04.10	FeQSIb-1	Fe-coated QS	5.00	0.001	40000	4.00	20.4	4	0.50	15:35	15:39	6.72	20.4	5.004	4.839	488.28598	480.98016
28.04.10	FeQSIb-2	Fe-coated QS	5.00	0.001	40000	4.00	20.4	4	0.50	15:37	15:41	6.53	20.4	5.010	4.836	489.92676	
28.04.10	FeQSIb-3	Fe-coated QS	5.00	0.001	40010	4.00	20.4	4	0.50	15:39	15:43	6.56	20.4	5.000	4.835	464.72775	
28.04.10	LBFeQSIb-1	BLANK	0.0000	0.001	40007	4.00	20.4	4	0.50	15:32	15:37	4.13	20.4	5.015	4.842	542.18317	518.28725
28.04.10	LBFeQSIb-2	BLANK	0.0000	0.001	40006	4.00	20.4	4	0.50	15:41	15:45	4.21	20.4	5.018	4.8119	511.78677	
28.04.10	LBFeQSIb-3	BLANK	0.0000	0.001	40030	4.00	20.4	4	0.50	15:50	15:54	4.15	20.4	5.014	4.838	500.89182	

DATE	SAMPLE	Mineral	M_S (g)	$C_{E\pm}$ (M)	$V_{E\pm}$ (µL)	pH_1	T °C	V_{Spike} (µL)	C_o (mg/L)	t_{START}	t_{END}	pH_2	T °C	V_{SPME} (g)	t_R (min)	$A_{GC\text{-}FID}$ (pA*s)	Average
29.04.10	Run Blk FeQSIIb	Fe-coated QS	N/A	N/A	N/A	N/A	N/A	N/A	N/A	N/A	N/A	N/A	N/A	N/A	N/A	N/A	N/A
29.04.10	FeQSIIb-1	Fe-coated QS	5.00	0.01	40000	4.00	20.4	4	0.50	13:36	13:56	5.85	18.8	5.006	4.83	584.07123	559.27179
29.04.10	FeQSIIb-2	Fe-coated QS	5.00	0.01	40000	4.00	20.4	4	0.50	13:39	13:57	5.95	18.8	5.002	4.845	572.69464	
29.04.10	FeQSIIb-3	Fe-coated QS	5.00	0.01	40000	4.00	20.4	4	0.50	13:42	13:59	6.03	18.8	5.000	4.838	521.04950	
29.04.10	LBFeQSIIb-1	BLANK	0.0000	0.01	40000	4.00	20.4	4	0.50	13:34	13:54	3.83	18.8	5.012	4.837	530.17872	518.42734
29.04.10	LBFeQSIIb-2	BLANK	0.0000	0.01	40008	4.00	20.4	4	0.50	13:45	14:01			5.013	4.828	519.33887	
29.04.10	LBFeQSIIb-3	BLANK	0.0000	0.01	40001	4.00	20.4	4	0.50	14:04	14:12			5.013	4.848	505.76443	

DATE	SAMPLE	Mineral	M_S (g)	$C_{E\pm}$ (M)	$V_{E\pm}$ (µL)	pH_1	T °C	V_{Spike} (µL)	C_o (mg/L)	t_{START}	t_{END}	pH_2	T °C	V_{SPME} (g)	t_R (min)	$A_{GC\text{-}FID}$ (pA*s)	Average
29.04.10	Run Blk FeQSIIIb	Fe-coated QS	N/A	N/A	N/A	N/A	N/A	N/A	N/A	N/A	N/A	N/A	N/A	N/A	N/A	N/A	N/A
29.04.10	FeQSIIIb-1	Fe-coated QS	5.00	0.1	40018	4.01	20.6	4.00	0.5	11:07	11:10	6.55	18.8	5.008	4.851	489.28592	487.28558
29.04.10	FeQSIIIb-2	Fe-coated QS	5.00	0.1	40007	4.01	20.6	4.00	0.5	11:10	11:12	6.43	18.8	5.002	4.845	465.46387	
29.04.10	FeQSIIIb-3	Fe-coated QS	5.00	0.1	40010	4.01	20.6	4.00	0.5	11:12	11:13	6.29	18.8	5.002	4.858	507.10696	
29.04.10	LBFeQSIIIb-1	BLANK	0.0000	0.1	40001	4.01	20.6	4.00	0.5	11:04	11:08	N/A	N/A	5.006	4.84	**547.598**	513.29377
29.04.10	LBFeQSIIIb-2	BLANK	0.0000	0.1	40004	4.01	20.6	4.00	0.5	11:15	11:15	N/A	N/A	5.010	4.836	**494.8424**	
29.04.10	LBFeQSIIIb-3	BLANK	0.0000	0.1	40005	4.01	20.6	4.00	0.5	11:24	11:26	N/A	N/A	5.008	4.837	**497.4412**	

A4.6. Fe-QS, pH=5.5

DATE	SAMPLE	Mineral	M_S (g)	$C_{E\pm}$ (M)	$V_{E\pm}$ (µL)	pH_1	T °C	V_{Spike} (µL)	C_o (mg/L)	t_{START}	t_{END}	pH_2	T °C	V_{SPME} (g)	t_R (min)	$A_{GC\text{-}FID}$ (pA*s)	Average
21.04.10	Run Blk FeQSIa	Fe-coated QS	N/A	N/A	N/A	N/A	N/A	N/A	N/A	N/A	N/A	N/A	N/A	N/A	N/A	N/A	N/A
21.04.10	FeQSIa-1	Fe-coated QS	5.0000	0.001	40000	5.58	20	4	0.50	14:06	14:06	6.6	20.00	5.00	4.853	488.31784	462.040
21.04.10	FeQSIa-2	Fe-coated QS	5.0000	0.001	40000	5.58	20	4	0.50	14:12	14:14	6.83	20.00	5.00	4.868	452.84482	
21.04.10	FeQSIa-3	Fe-coated QS	5.0000	0.001	40000	5.58	20	4	0.50	14:17	14:21	6.78	20.00	5.00	4.852	444.95718	
21.04.10	LBFeQSIa-1	BLANK	0.0000	0.001	40000	5.58	20	4	0.50	14:20	14:04	5.49	20.00	5.00	4.853	466.99518	492.636
21.04.10	LBFeQSIa-2	BLANK	0.0000	0.001	40000	5.58	20	4	0.50	14:25	14:24	6.19	20.00	5.00	4.485	491.42999	
21.04.10	LBFeQSIa-3	BLANK	0.0000	0.001	40000	5.58	20	4	0.50	14:29	14:36	5.95	20.00	5.00	4.848	519.48425	

DATE	SAMPLE	Mineral	M_S (g)	$C_{E\pm}$ (M)	$V_{E\pm}$ (µL)	pH_1	T °C	V_{Spike} (µL)	C_o (mg/L)	t_{START}	t_{END}	pH_2	T °C	V_{SPME} (g)	t_R (min)	$A_{GC\text{-}FID}$ (pA*s)	Average
22.04.10	Run Blk FeQSIIa	Fe-coated QS	N/A	N/A	N/A	N/A	N/A	N/A	N/A	N/A	N/A	N/A	N/A	N/A	N/A	N/A	N/A
22.04.10	FeQSIIa-1	Fe-coated QS	5.0000	0.01	40000	5.49	20.2	4	0.50	14:11	14:17	6.60	21.00	5.00	4.549	561.910	512.707
22.04.10	FeQSIIa-2	Fe-coated QS	5.0000	0.01	40000	5.49	20.2	4	0.50	14:18	14:18	6.60	21.00	5.00	4.849	539.198	
22.04.10	FeQSIIa-3	Fe-coated QS	5.0000	0.01	40000	5.49	20.2	4	0.50	14:27	14:29	6.62	21.00	5.00	4.849	437.014	
22.04.10	LBFeQSIIa-1	BLANK	0.0000	0.01	40000	5.49	20.2	4	0.50	14:31	14:33	5.77	21.00	5.00	N/A	N/A	540.0512
22.04.10	LBFeQSIIa-2	BLANK	0.0000	0.01	40000	5.49	20.2	4	0.50	14:41	14:40	5.82	21.00	5.00	4.844	526.8529	
22.04.10	LBFeQSIIa-3	BLANK	0.0000	0.01	40000	5.49	20.2	4	0.50	14:56	14:59	5.96	21.00	5.009	4.844	553.2496	

DATE	SAMPLE	Mineral	M_S (g)	$C_{E\pm}$ (M)	$V_{E\pm}$ (µL)	pH_1	T °C	V_{Spike} (µL)	C_o (mg/L)	t_{START}	t_{END}	pH_2	T °C	V_{SPME} (g)	t_R (min)	$A_{GC\text{-}FID}$ (pA*s)	Average
27.04.10	Run Blk FeQSIIIa	Fe-coated QS	N/A	N/A	N/A	N/A	N/A	N/A	N/A	N/A	N/A	N/A	N/A	N/A	N/A	N/A	N/A
27.04.10	FeQSIIIa-1	Fe-coated QS	5.0000	0.1	40030	5.65	20.8	4	0.50	11:44	11:50	6.64	19.4	5.014	4.847	436.24536	492.831
27.04.10	FeQSIIIa-2	Fe-coated QS	5.0000	0.1	40020	5.65	20.8	4	0.50	11:48	11:52	6.66	19.4	5.013	4.842	522.84711	
27.04.10	FeQSIIIa-3	Fe-coated QS	5.0000	0.1	40005	5.65	20.8	4	0.50	11:51	11:54	6.68	19.4	5.012	4.828	519.40085	
27.04.10	LBFeQSIIIa-1	BLANK	0.0000	0.1	40022	5.65	20.8	4	0.50	11:38	11:57	5.65	19.4	5.005	4.85	479.64288	510.0880
27.04.10	LBFeQSIIIa-2	BLANK	0.0000	0.1	40028	5.65	20.8	4	0.50	12:08	13:32	5.79	19.4	5.008	4.844	498.33099	
27.04.10	LBFeQSIIIa-3	BLANK	0.0000	0.1	40006	5.65	20.8	4	0.50	11:54	11:59			5.000	4.844	552.29010	

A4.7.Stx-1 (montmorillonite clay), pH=4.0

DATE	SAMPLE	Mineral	M_S (g)	$C_{E\pm}$ (M)	$V_{E\pm}$ (µL)	pH_1	T °C	V_{Spike} (µL)	C_o (mg/L)	t_{START}	t_{END}	pH_2	T °C	V_{SPME} (g)	t_R (min)	A_{GC-FID} (pA*s)	Average
28.4.10	Run Blk MtIb	N/A	N/A	N/A	N/A	N/A	N/A	N/A	N/A	N/A	N/A	N/A	N/A	N/A	N/A	N/A	N/A
28.4.10	MtIb-1	STx-1	1.0006	0.001	40001	4	20.4	4	0.50	15:43	15:48	7.95	20.4	5.006	4.841	521.16394	504.03819
28.4.10	MtIb-2	STx-1	1.0001	0.001	40015	4	20.4	4	0.50	15:45	15:50	7.94	20.4	5.002	4.849	479.33389	
28.4.10	MtIb-3	STx-1	1.0007	0.001	40012	4	20.4	4	0.50	15:48	15:52	7.91	20.4	5.006	4.838	511.61673	
28.4.10	LBMtIb-1	BLANK	0.0000	0.001	40007	4	20.4	4	0.50	15:32	15:37	4.13	20.4	5.015	4.842	542.18317	518.28725
28.4.10	LBMtIb-2	BLANK	0.0000	0.001	40006	4	20.4	4	0.50	15:41	15:45	4.21	20.4	5.018	4.8119	511.78677	r
28.4.10	LBMtIb-3	BLANK	0.0000	0.001	40030	4	20.4	4	0.50	15:50	15:54	4.15	20.4	5.014	4.838	500.89182	r

DATE	SAMPLE	Mineral	M_S (g)	$C_{E\pm}$ (M)	$V_{E\pm}$ (µL)	pH_1	T °C	V_{Spike} (µL)	C_o (mg/L)	t_{START}	t_{END}	pH_2	T °C	V_{SPME} (g)	t_R (min)	A_{GC-FID} (pA*s)	Average
29.4.10	Run Blk MtIIb	STx-1	N/A	N/A	N/A	N/A	N/A	N/A	N/A	N/A	N/A	N/A	N/A	N/A	N/A	N/A	N/A
29.4.10	MtIIb-1	STx-1	1.0000	0.01	40000	4	20.4	4	0.50	13:55	broken	N/A	N/A	N/A	N/A	N/A	N/A
29.4.10	MtIIb-2	STx-1	0.9996	0.01	40000	4	20.4	4	0.50	13:58	14:08	7.39	18.8	5.0100	4.845	520.11115	529.84569
29.4.10	MtIIb-3	STx-1	0.9998	0.01	40000	4	20.4	4	0.50	14:00	14:10	7.5	18.8	5.0070	4.834	539.24719	
29.4.10	LBMtIIb-1	BLANK	0.0000	0.01	40000	4	20.4	4	0.50	13:34	13:54	3.83	18.8	5.012	4.837	530.17872	518.42734
29.4.10	LBMtIIb-2	BLANK	0.0000	0.01	40008	4	20.4	4	0.50	13:45	14:01			5.013	4.828	519.33887	
29.4.10	LBMtIIb-3	BLANK	0.0000	0.01	40001	4	20.4	4	0.50	14:04	14:12			5.013	4.848	505.76443	

DATE	SAMPLE	Mineral	M_S (g)	$C_{E\pm}$ (M)	$V_{E\pm}$ (µL)	pH_1	T °C	V_{Spike} (µL)	C_o (mg/L)	t_{START}	t_{END}	pH_2	T °C	V_{SPME} (g)	t_R (min)	A_{GC-FID} (pA*s)	Average
29.04.10	Run Blk MtIIIb	STx-1	N/A	N/A	N/A	N/A	N/A	N/A	N/A	N/A	N/A	N/A	N/A	N/A	N/A	N/A	
29.04.10	MtIIIb-1	STx-1	1.0002	0.1	40003	4.01	20.6	4	0.5	11:07	11:10	7.32	18.8	5.008	4.838	447.3686	490.19764
29.04.10	MtIIIb-2	STx-1	1.0003	0.1	40002	4.01	20.6	4	0.5	11:21	11:23	7.31	18.8	5.009	4.834	479.9406	
29.04.10	MtIIIb-3	STx-1	1.0004	0.1	40207	4.01	20.6	4	0.5	11:24	11:24	7.35	18.8	5.001	4.842	543.2837	
29.04.10	LBMtIIIb-1	BLANK	0.0000	0.1	40001	4.01	20.6	4	0.5	11:04	11:08	N/A	N/A	5.006	4.84	**547.598**	513.29377
29.04.10	LBMtIIIb-2	BLANK	0.0000	0.1	40004	4.01	20.6	4	0.5	11:15	11:15	N/A	N/A	5.01	4.836	**494.8424**	
29.04.10	LBMtIIIb-3	BLANK	0.0000	0.1	40005	4.01	20.6	4	0.5	11:24	11:26	N/A	N/A	5.008	4.837	**497.4412**	

A4.8. Stx-1 (montmorillonite clay), pH=5.5

DATE	SAMPLE	Mineral	M_S (g)	$C_{E\pm}$ (M)	$V_{E\pm}$ (µL)	pH_1	T °C	V_{Spike} (µL)	C_o (mg/L)	t_{START}	t_{END}	pH_2	T °C	V_{SPME} (g)	t_R (min)	$A_{GC\text{-}FID}$ (pA*s)	Average
21.04.10	Run Blk Mtla	STx-1	N/A	N/A	N/A	N/A	N/A	N/A	N/A	N/A	N/A	N/A	N/A	N/A	N/A	N/A	N/A
21.04.10	Mtla-1	STx-1	0.9999	0.001	40000	5.5	20	4	0.50	14:36	14:37	7.85	20.00	5.00	4.858	469.977	457.666
21.04.10	Mtla-2	STx-1	1.0009	0.001	40000	5.5	20	4	0.50	14:41	14:43	7.9	20.00	5.00	4.845	441.423	
21.04.10	Mtla-3	STx-1	1.0004	0.001	40000	5.5	20	4	0.50	14:49	14:48	7.99	20.00	5.00	4.852	461.598	
21.04.10	LBMtla-1	BLANK	0.0000	0.001	40000	5.5	20	4	0.50	14:20	14:04	5.49	20.00	5.00	4.853	466.99518	492.636
21.04.10	LBMtla-2	BLANK	0.0000	0.001	40000	5.5	20	4	0.50	14:25	14:24	6.19	20.00	5.00	4.485	491.42999	
21.04.10	LBMtla-3	BLANK	0.0000	0.001	40000	5.5	20	4	0.50	14:29	14:36	5.95	20.00	5.00	4.848	519.48425	

DATE	SAMPLE	Mineral	M_S (g)	$C_{E\pm}$ (M)	$V_{E\pm}$ (µL)	pH_1	T °C	V_{Spike} (µL)	C_o (mg/L)	t_{START}	t_{END}	pH_2	T °C	V_{SPME} (g)	t_R (min)	$A_{GC\text{-}FID}$ (pA*s)	Average
22.4.10	Run Blk MtIIa	STx-1	N/A	N/A	N/A	N/A	N/A	N/A	N/A	N/A	N/A	N/A	N/A	N/A	N/A	N/A	N/A
22.4.10	MtIIa-1	STx-1	0.9999	0.01	40000	5.49	20.2	4	0.50	14:34	14:42	7.56	21.0	5.0	4.846	523.6475	510.540
22.4.10	MtIIa-2	STx-1	1.0000	0.01	40000	5.49	20.2	4	0.50	14:46	14:43	7.76	21.0	5.0	4.847	459.2875	
22.4.10	MtIIa-3	STx-1	1.0004	0.01	40000	5.49	20.2	4	0.50	14:53	14:57	7.77	21.0	5.0	4.843	548.6838	
22.4.10	LBMtIIa-1	BLANK	0.0000	0.01	40000	5.49	20.2	4	0.50	14:31	14:33	5.77	21.0	5.0	4.843	N/A	540.0512
22.4.10	LBMtIIa-2	BLANK	0.0000	0.01	40000	5.49	20.2	4	0.50	14:41	14:40	5.82	21.0	5.0	4.844	526.8529	
22.4.10	LBMtIIa-3	BLANK	0.0000	0.01	40000	5.49	20.2	4	0.50	14:56	14:59	5.96	21.0	5.009	4.844	553.2496	

DATE	SAMPLE	Mineral	M_S (g)	$C_{E\pm}$ (M)	$V_{E\pm}$ (µL)	pH_1	T °C	V_{Spike} (µL)	C_o (mg/L)	t_{START}	t_{END}	pH_2	T °C	V_{SPME} (g)	t_R (min)	$A_{GC\text{-}FID}$ (pA*s)	Average
27.04.10	Run Blk MtIIIa	STx-1	N/A	N/A	N/A	N/A	N/A	N/A	N/A	N/A	N/A	N/A	N/A	N/A	N/A	N/A	
27.04.10	MtIIIa-1	STx-1	1.0000	0.1	40000	5.65	20.8	4	0.50	11:57	13:30	7.5	20.4	5.014	4.86	452.0166	488.5236
27.04.10	MtIIIa-2	STx-1	1.0007	0.1	40026	5.65	20.8	4	0.50	12:00	13:35	7.52	20.4	5.009	4.845	530.1663	
27.04.10	MtIIIa-3	STx-1	1.0004	0.1	40022	5.65	20.8	4	0.50	12:04	13:38	7.51	20.4	5.016	4.845	483.3879	
27.04.10	LBMtIIIa-1	BLANK	0.0000	0.1	40022	5.65	20.8	4	0.50	11:38	11:57	5.65	19.4	5.005	4.85	**479.643**	510.0880
27.04.10	LBMtIIIa-2	BLANK	0.0000	0.1	40020	5.65	20.8	4	0.50	12:08	13:32	5.79	19.4	5.008	4.844	**498.331**	
27.04.10	LBMtIIIa-3	BLANK	0.0000	0.1	40006	5.65	20.8	4	0.50	11:54	11:59			5.000	4.844	**552.290**	

APPENDIX 5. SURFACE ANALYSIS RESULTS

A5. 1. XPS additional spectra.

QUARTZ SLIDE

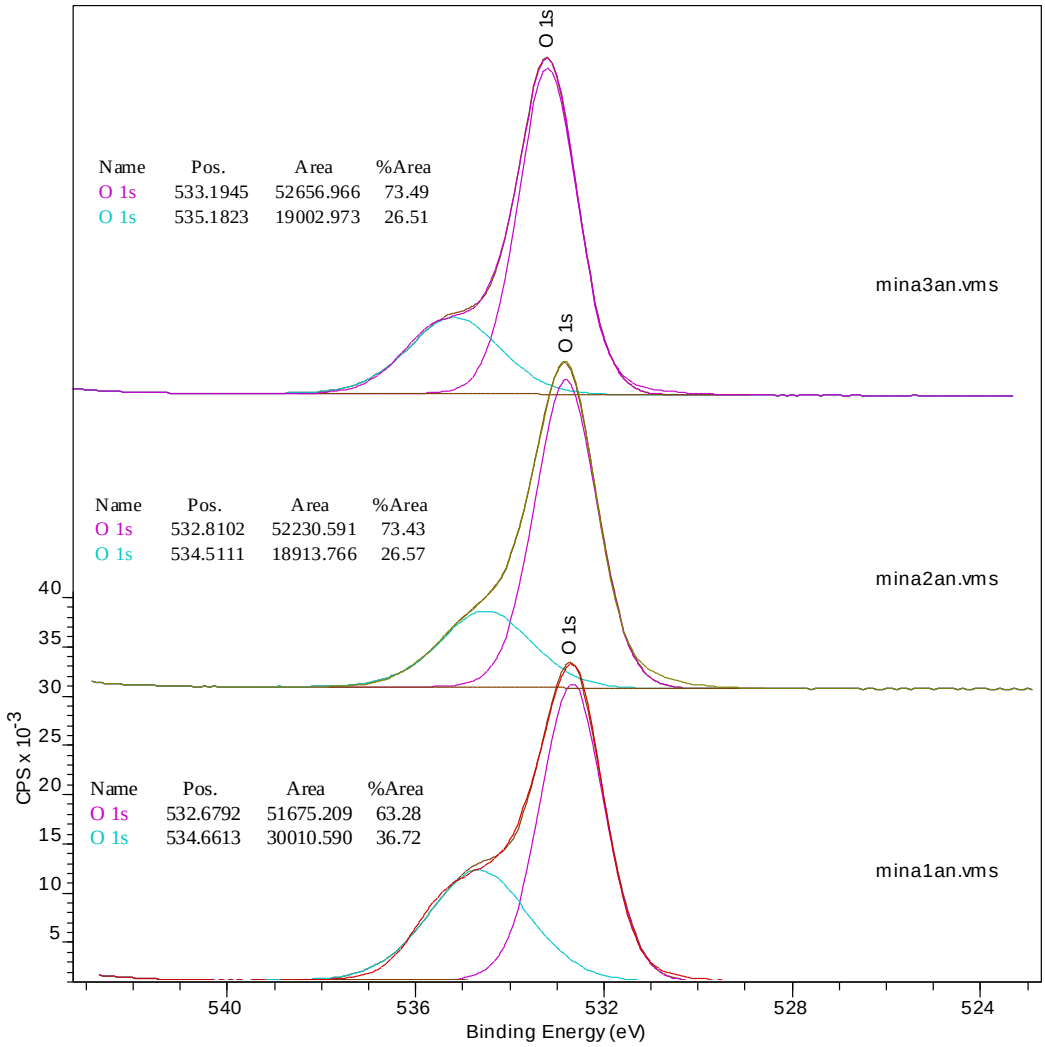

A5.1.1. Fitted O1s peaks for b[e]pyrene on quartz slides.

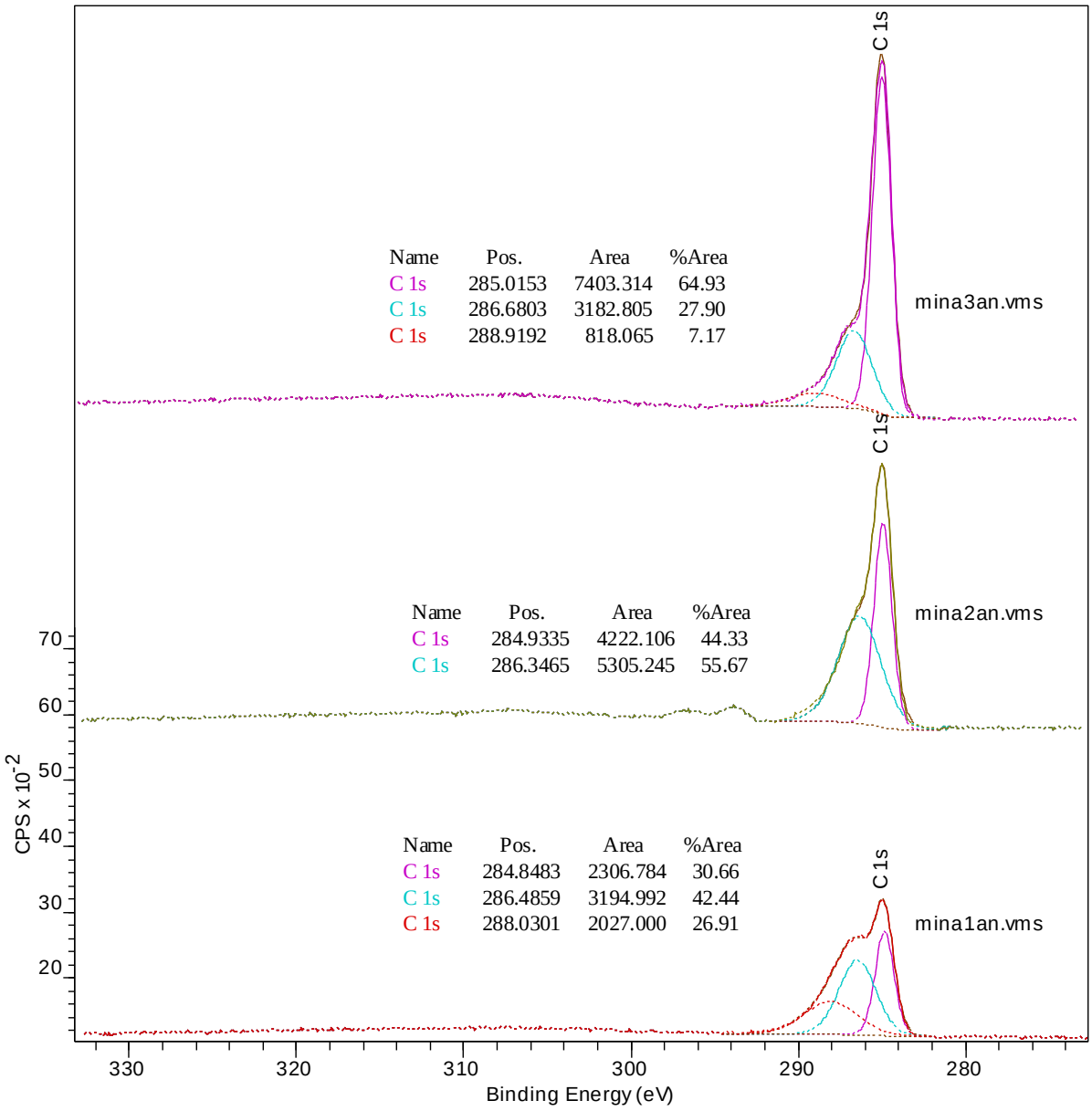

A5.1.2. Fitted C1s peaks for B[e]pyrene on quartz slide.

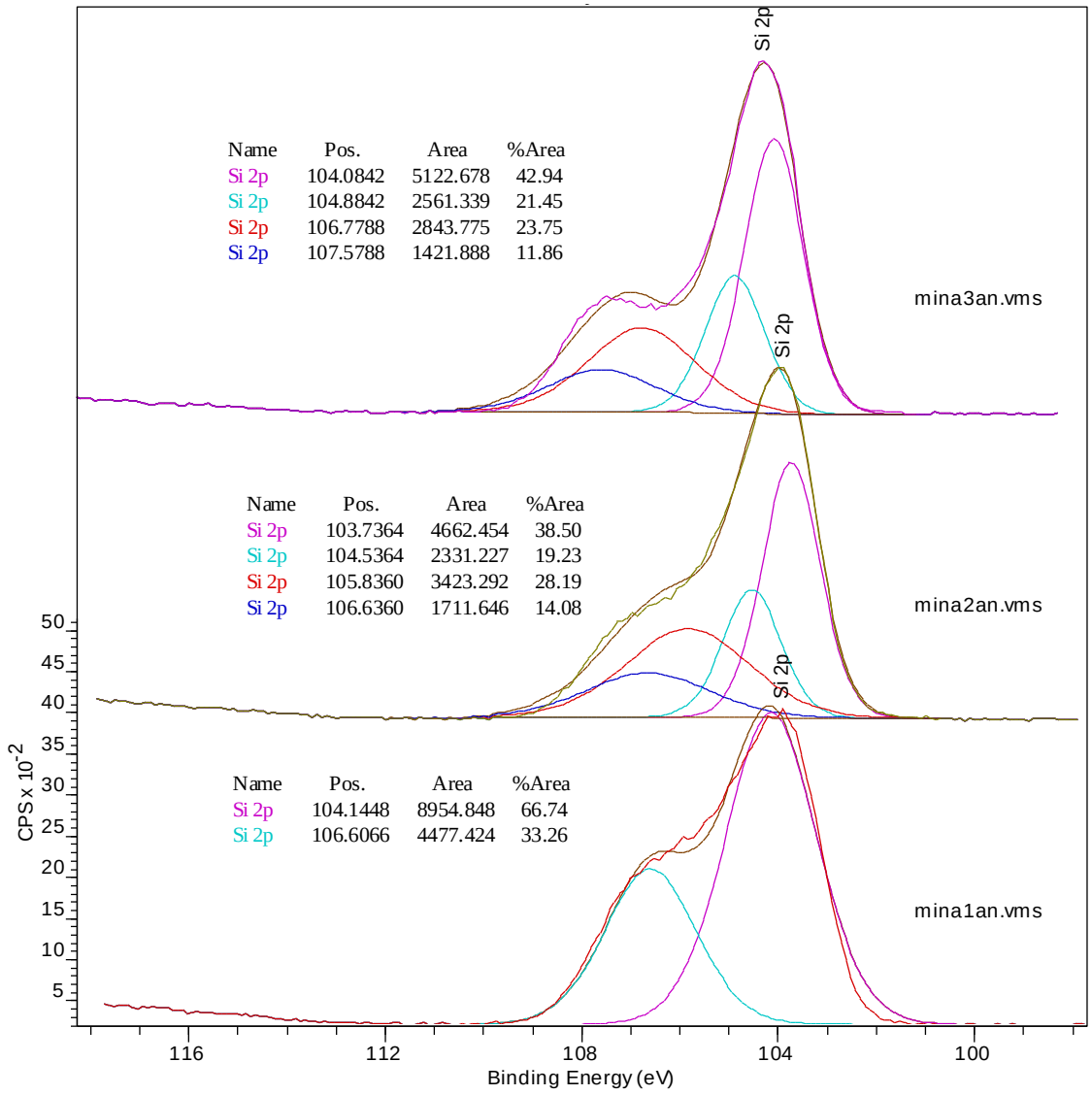

A5.1.3. Fitted Si 2p peaks for B[e]pyrene on quartz slide.

HEMATITE POWDER

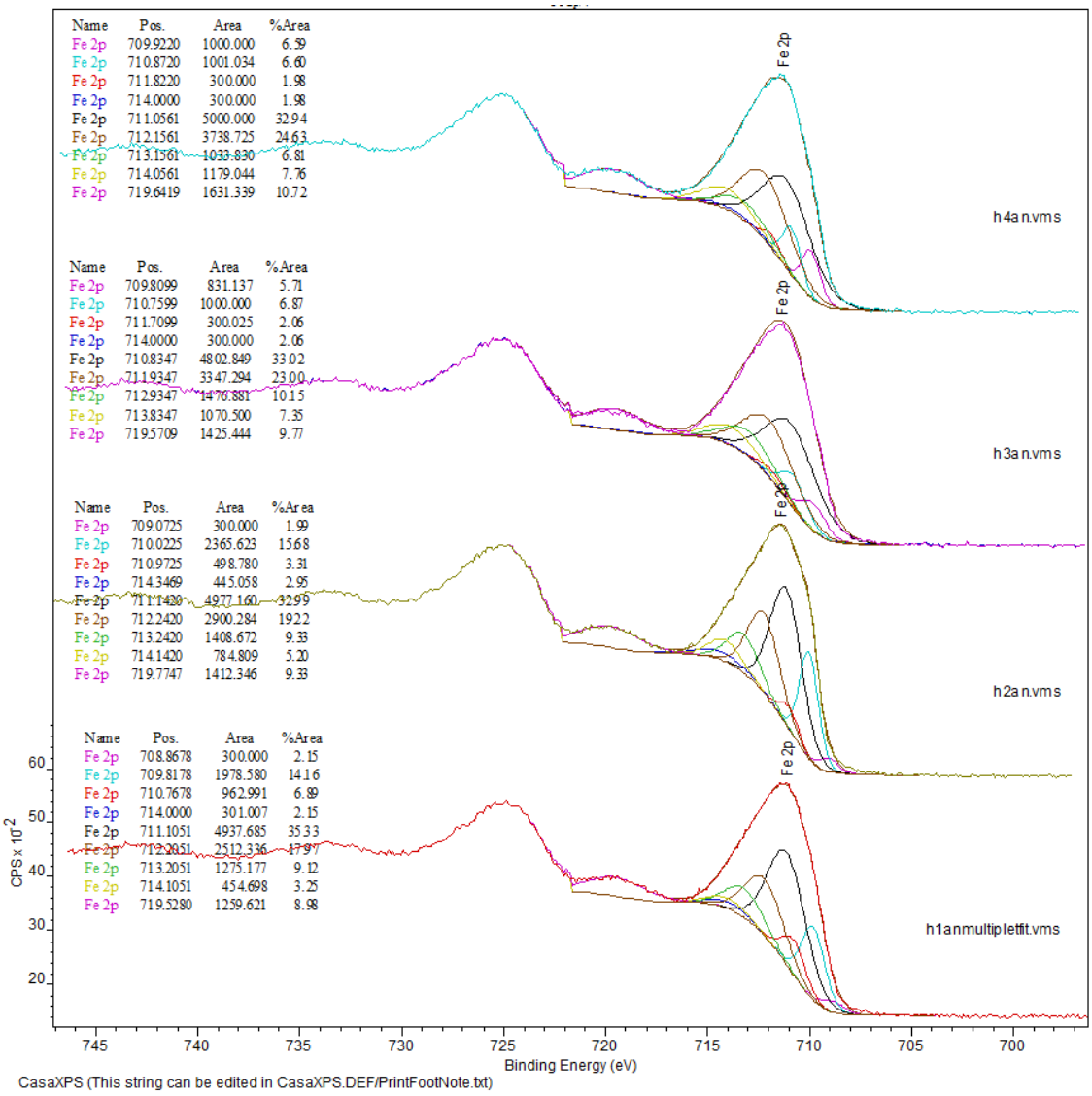

A5.1.4. Fitted peaks for Fe (2p) in hematite samples.

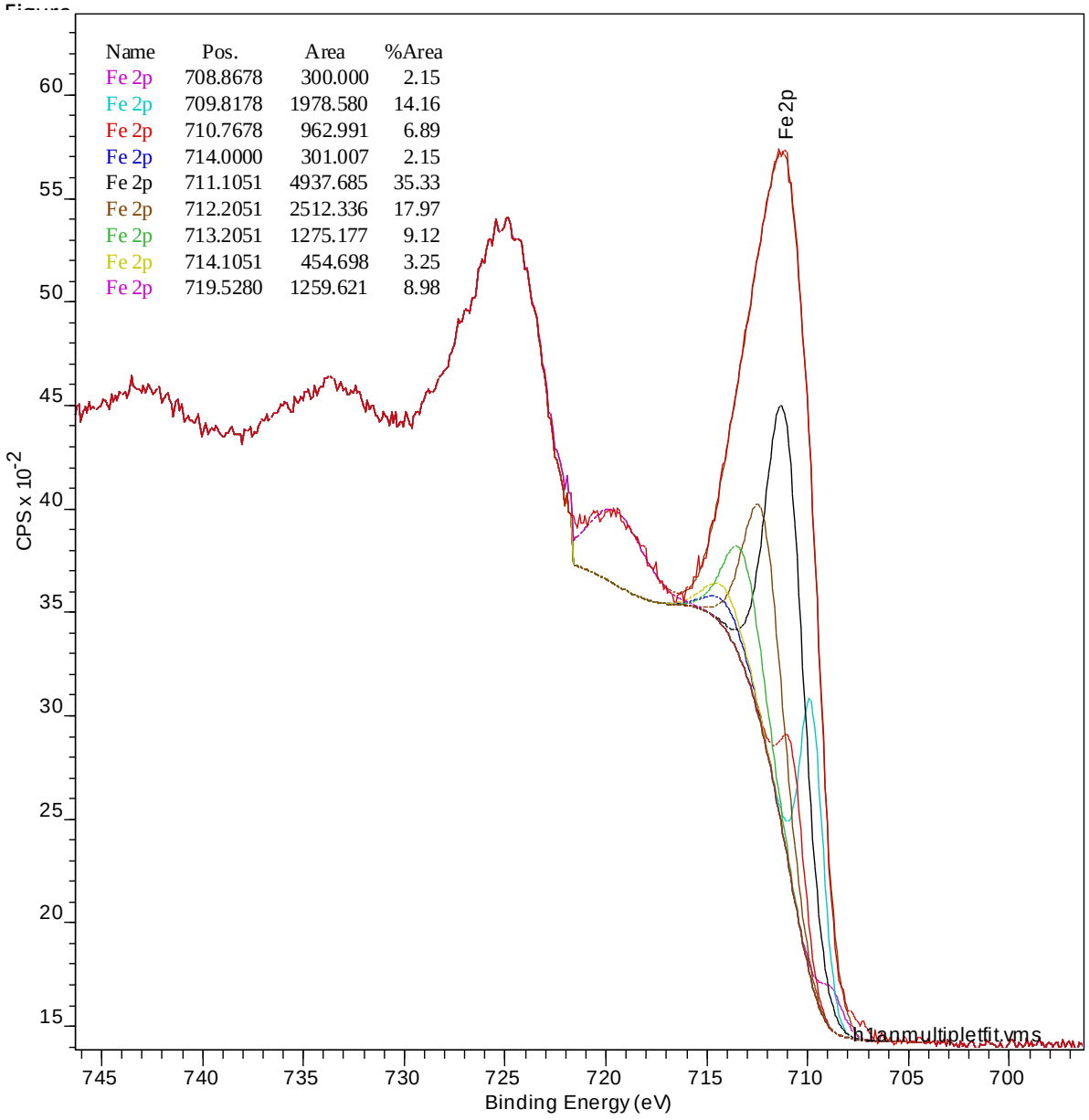

A5.1.5. Fitted peaks for Fe (2p) in hematite.

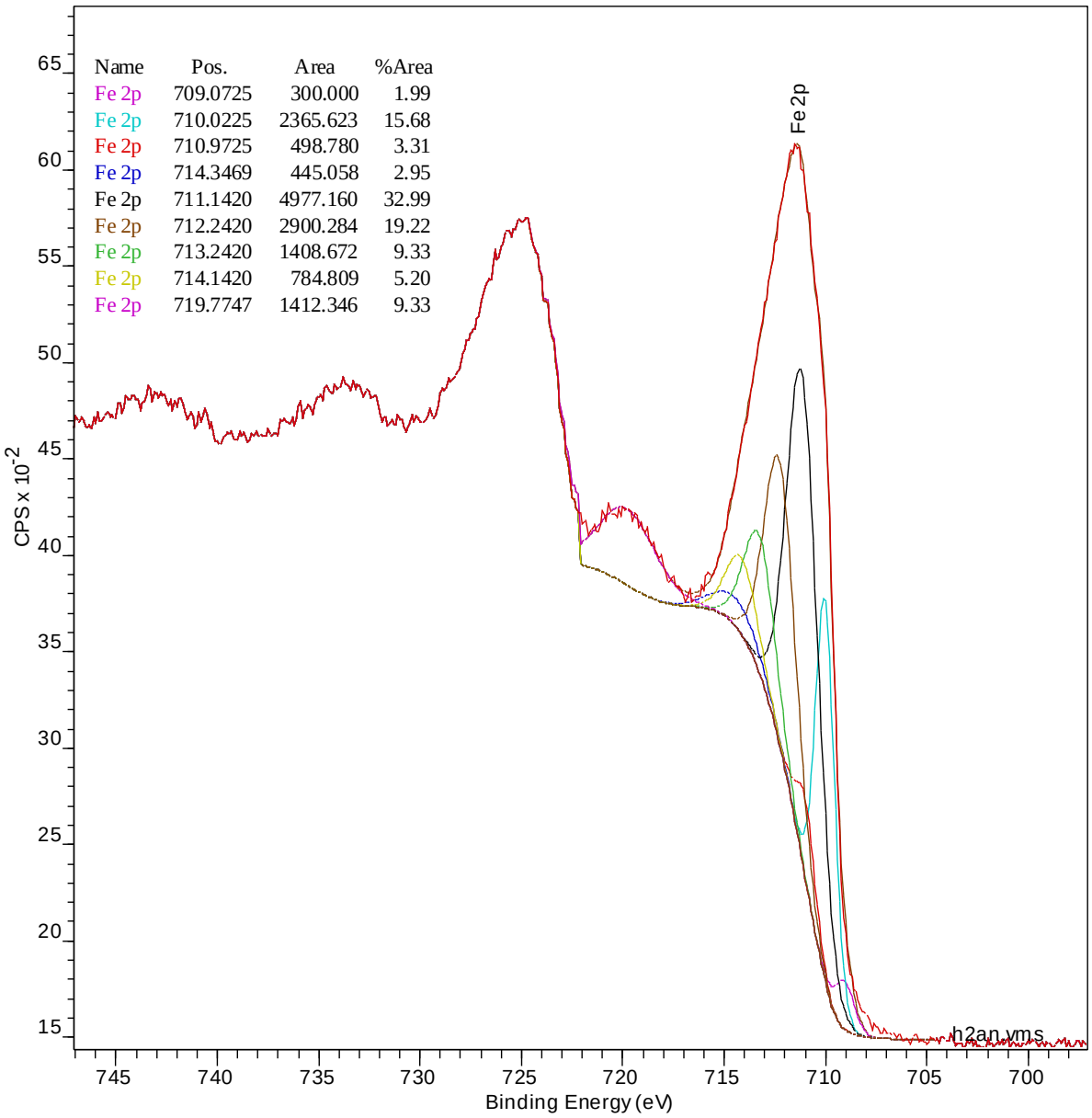

A5.1.6. Fitted peaks for Fe (2p) in hematite with methanol.

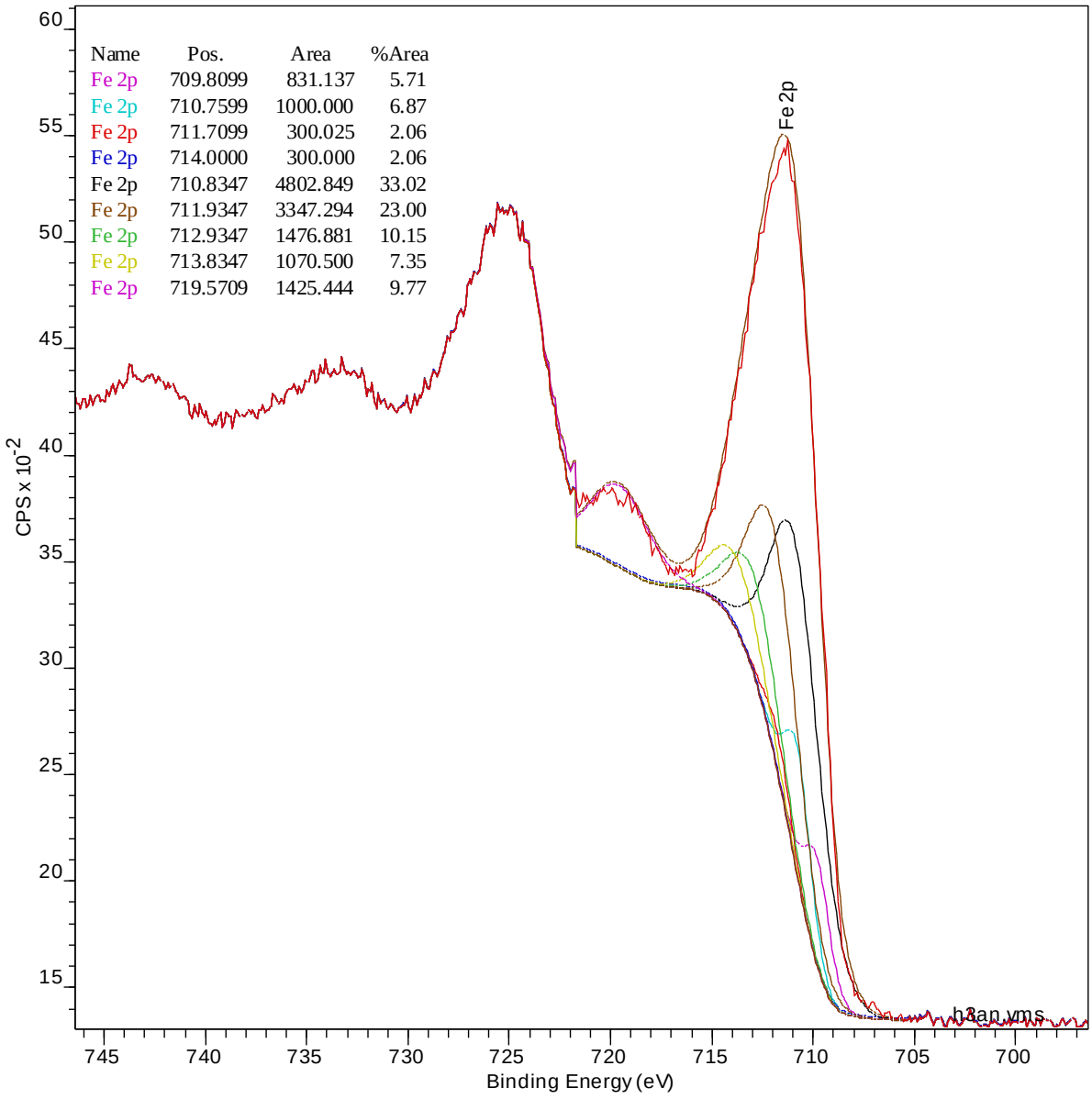

A5.1.7. Fitted peaks for Fe (2p) in hematite with naphthalene in methanol.

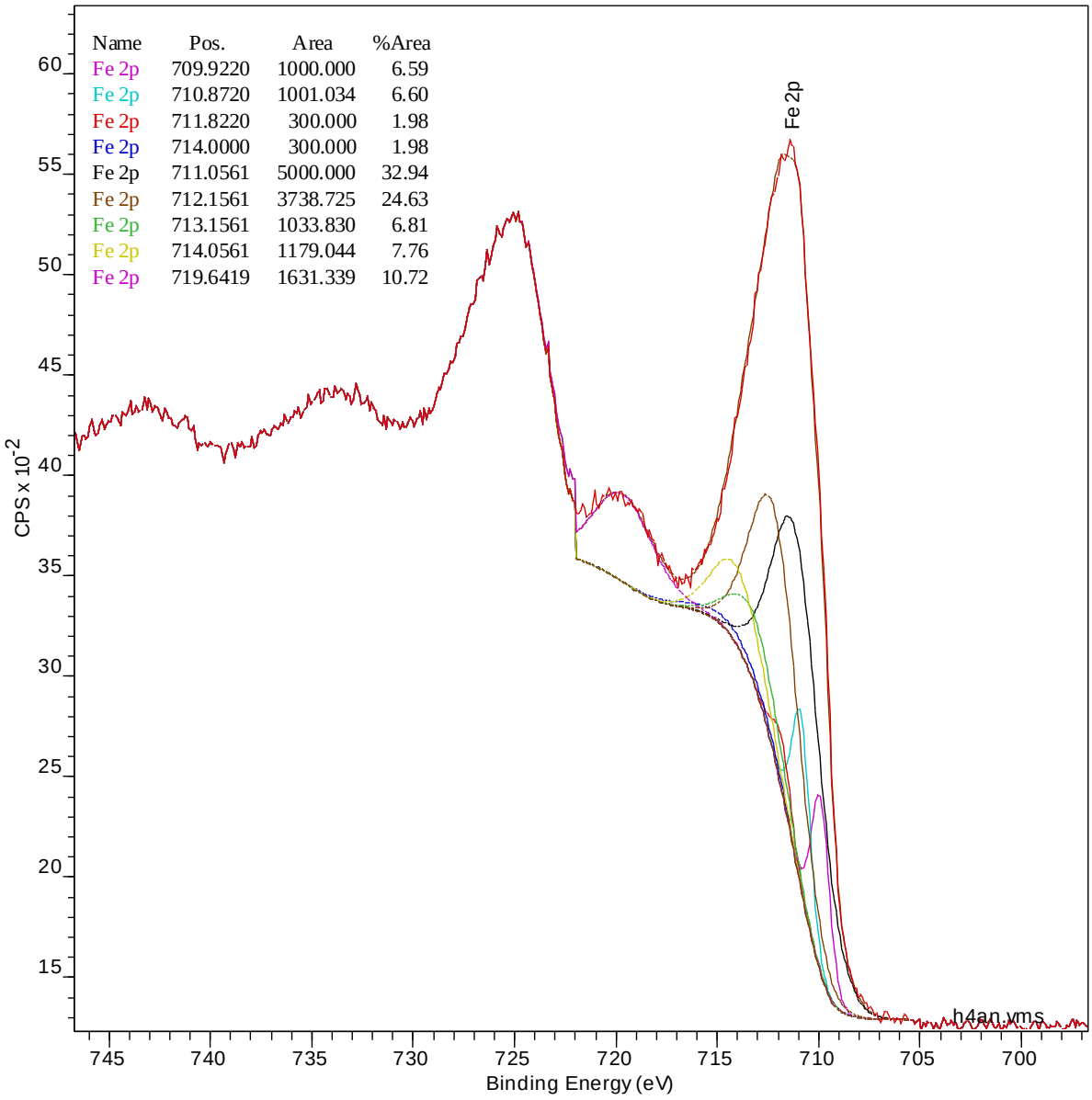

A5.1.8. Fitted peaks for Fe (2p) in hematite with benzoic acid in methanol.

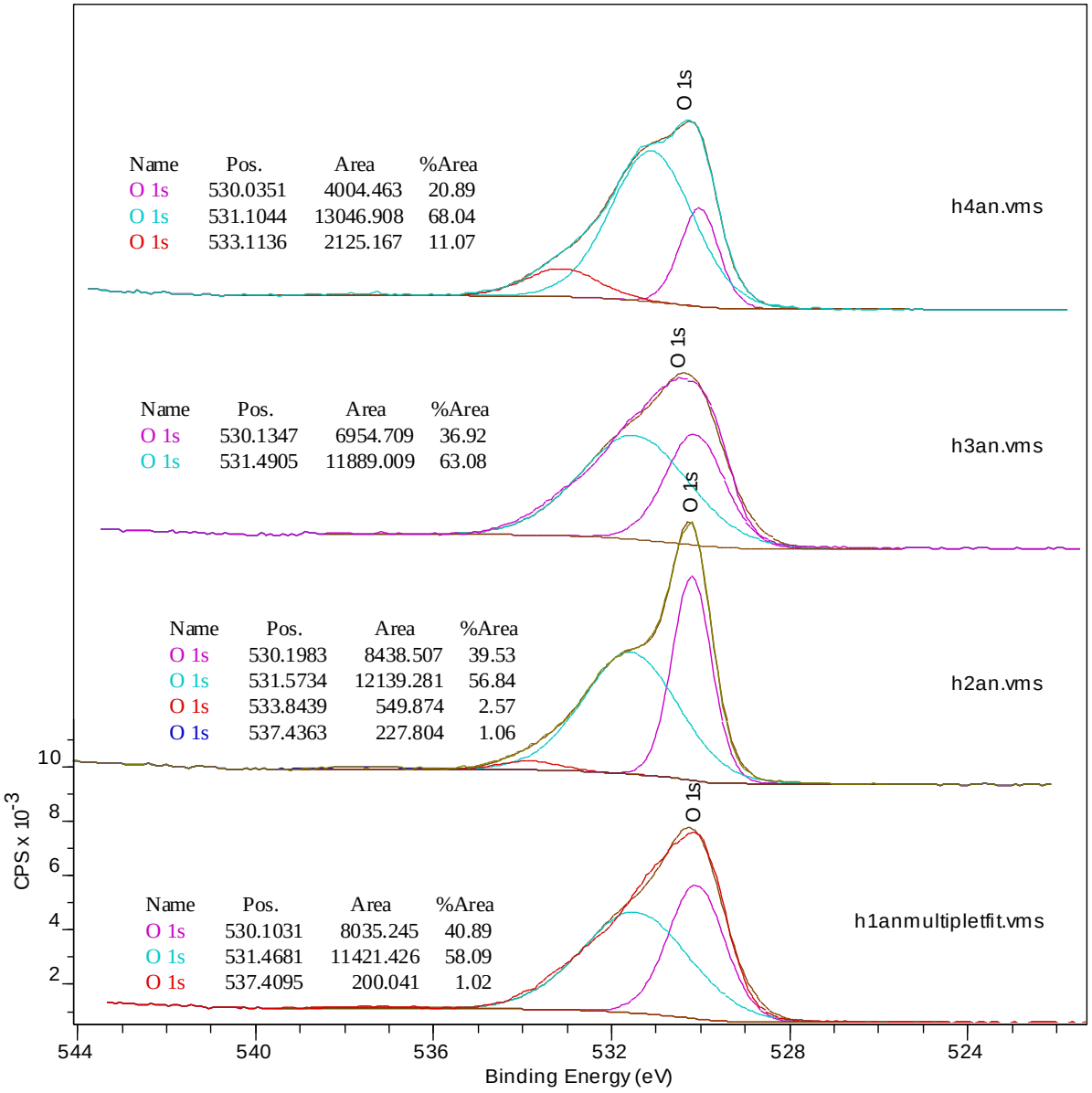

A5.1.9. Fitted peaks for O (1s) in hematite samples.

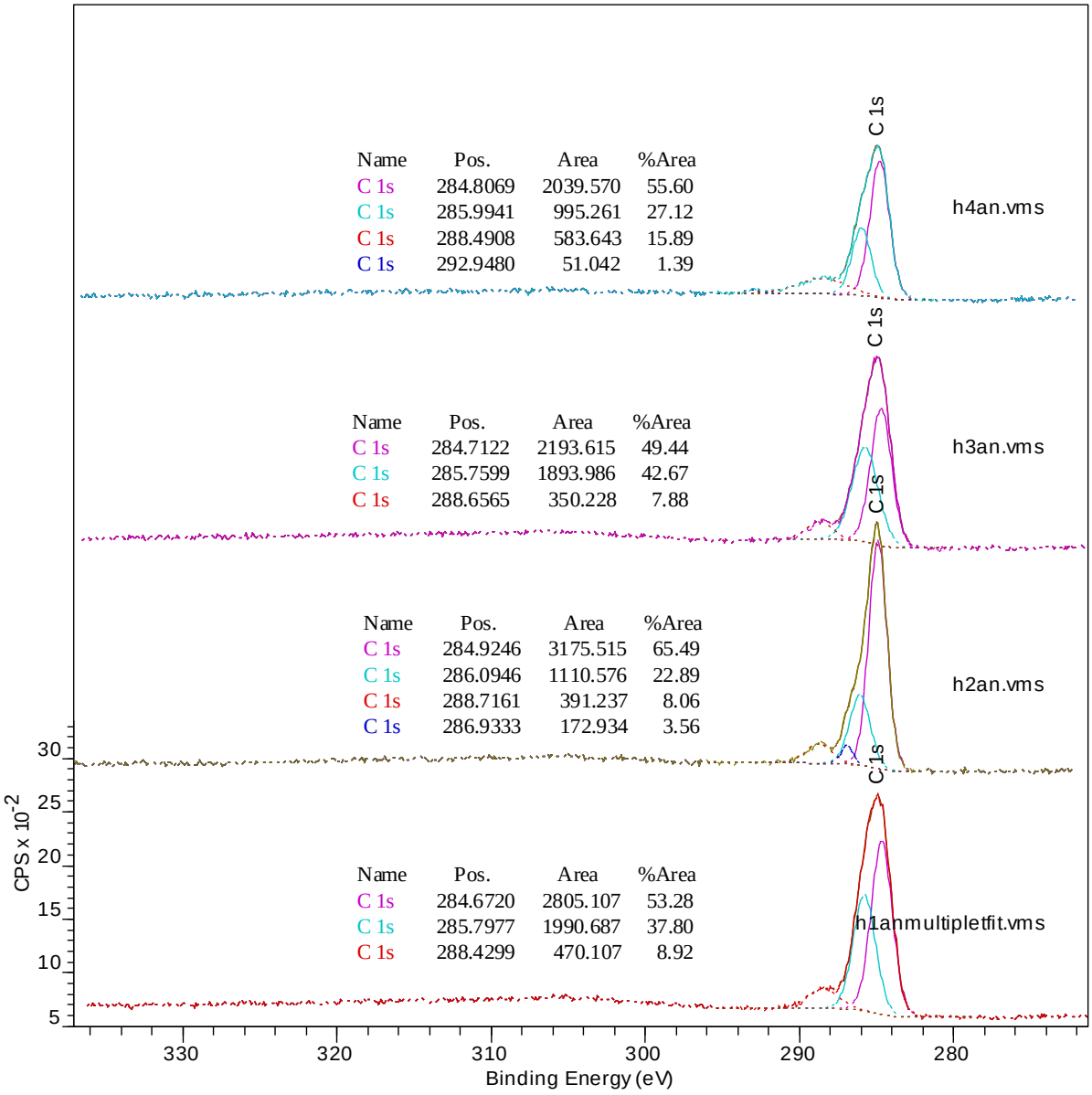

A5.1.10. Fitted peaks for C (1s) in hematite samples.

SILICA (QUARTZ) SAND

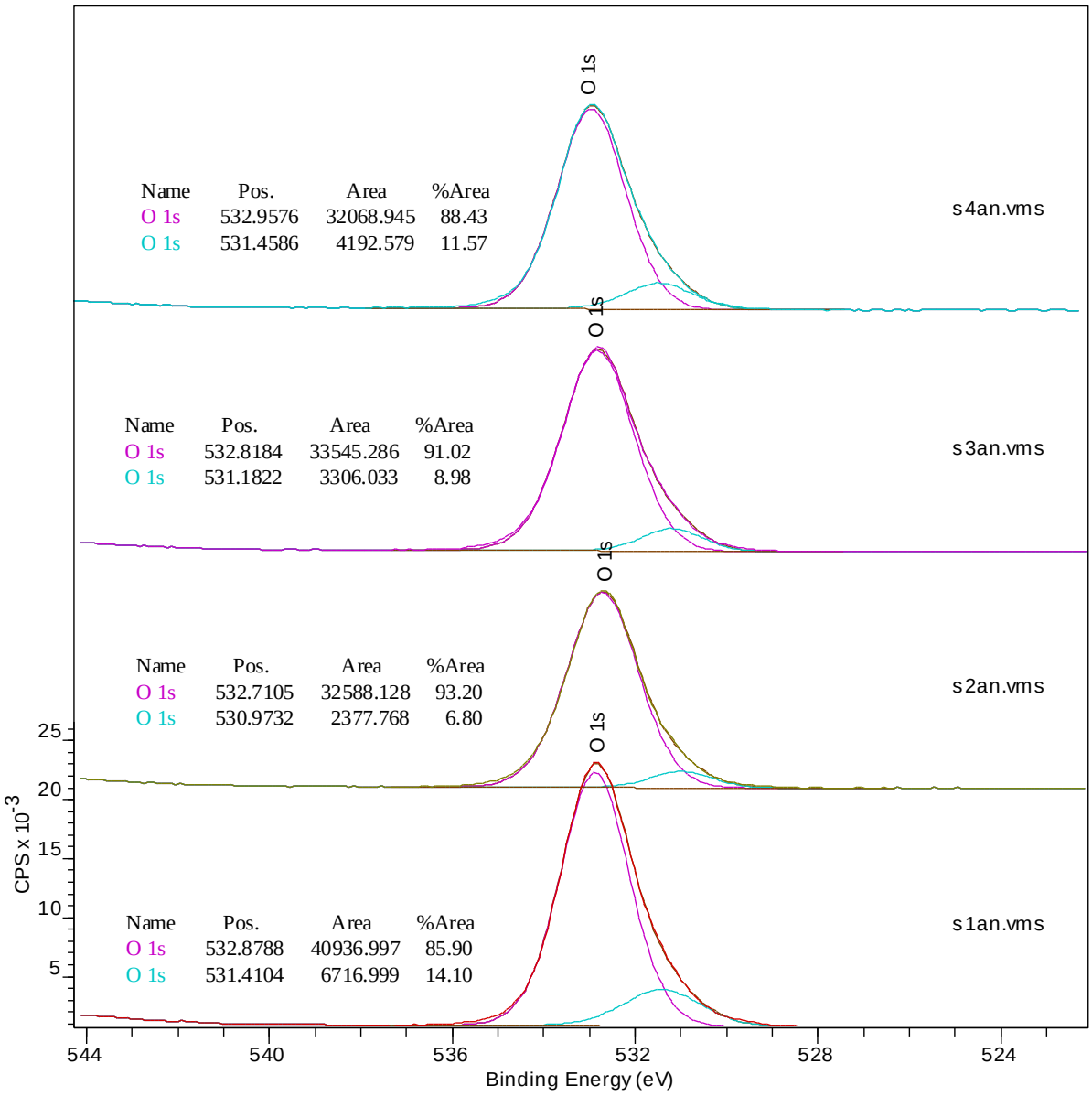

A5.1.11. Fitted peaks for O (1s) in silica sand samples.

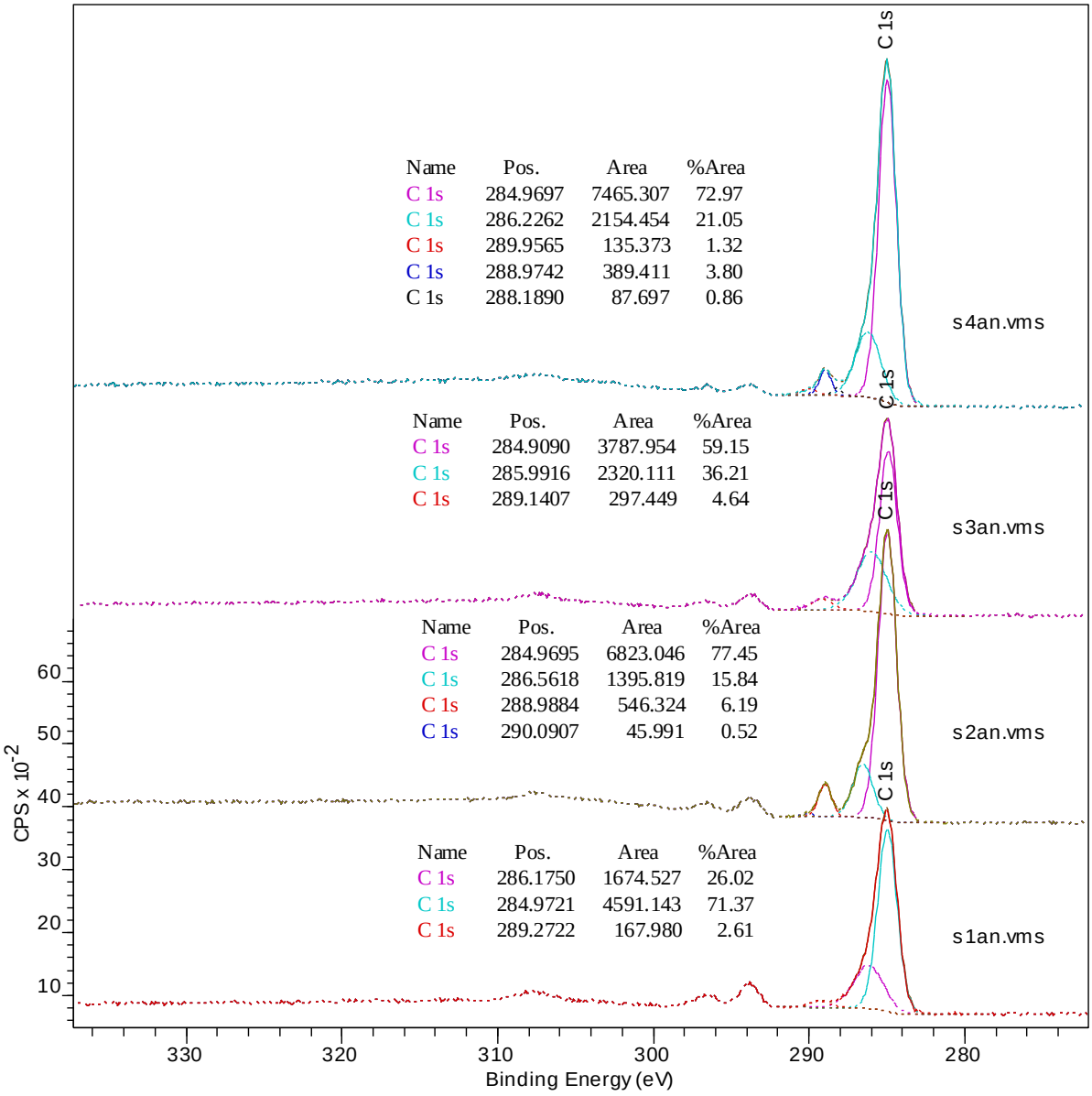

A5.1.12.. Fitted peaks for C (1s) in silica sand samples.

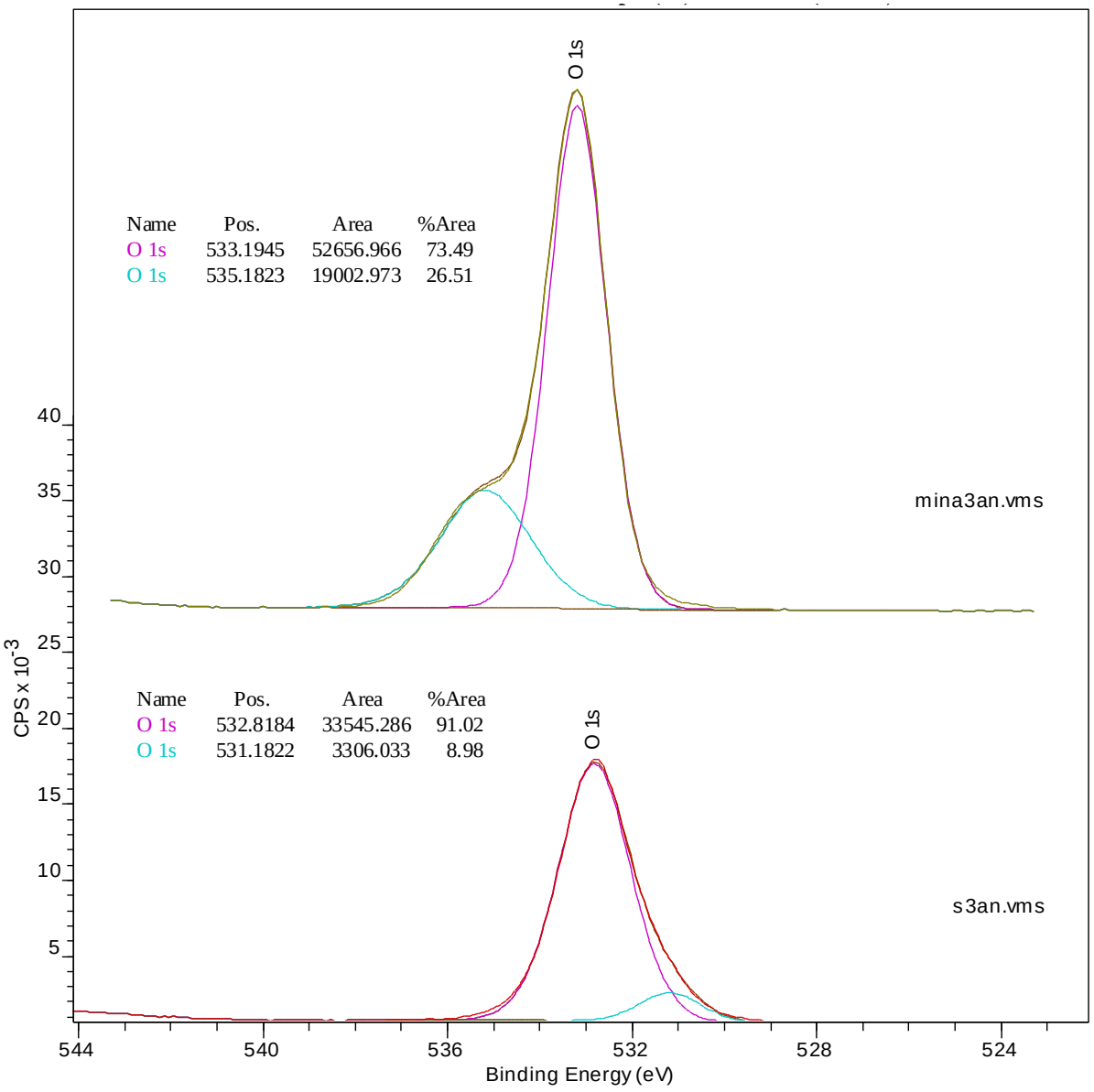

A5.1.13. Fitted peaks for O (1s) i9n silica for naphthalene and benzo[e]pyrene in methanol.

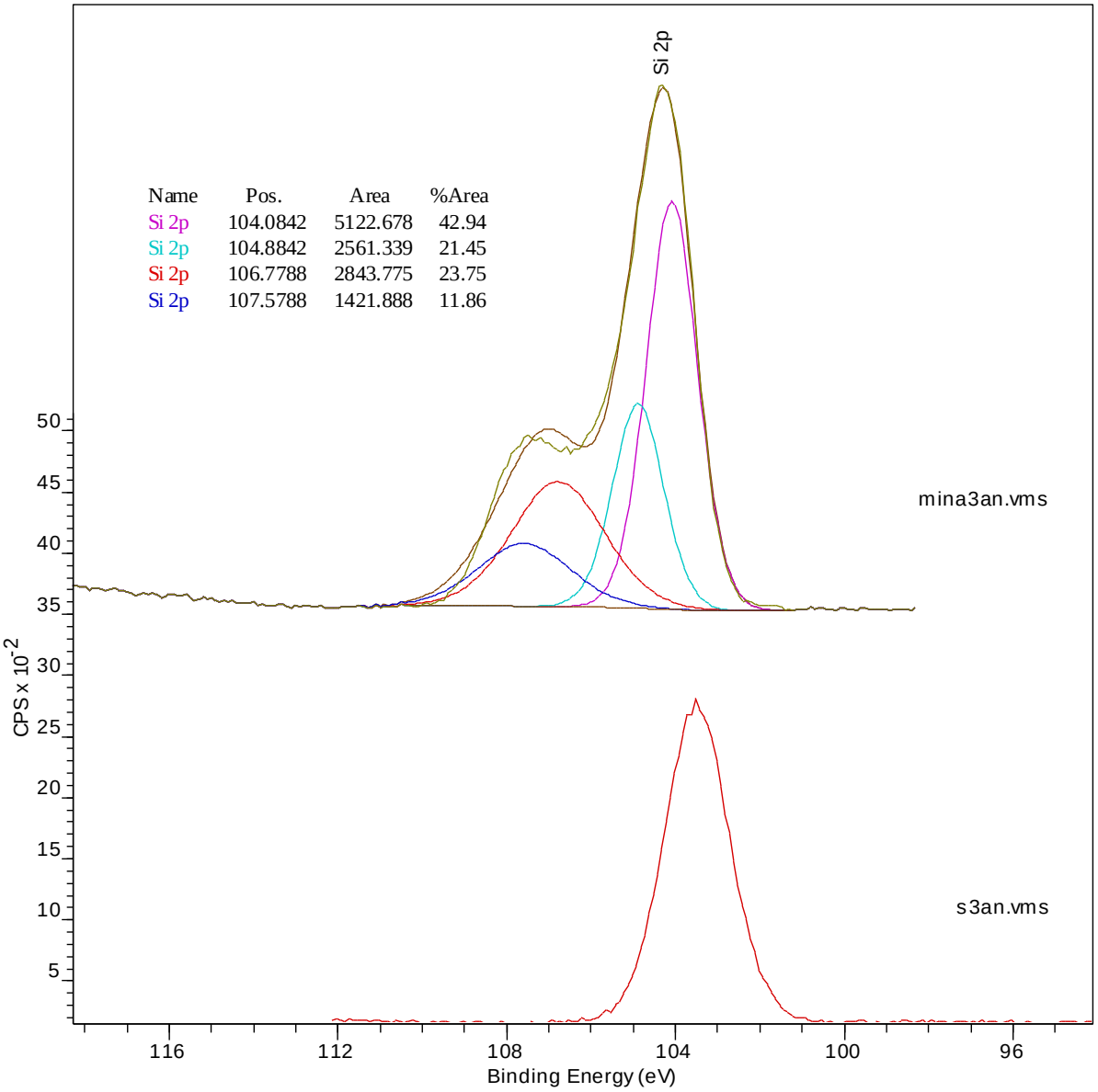

A5.1.14. Fitted peaks for Si (2p) in silica for benzo[e]pyrene in methanol.